Characterisation of nuclear actin family proteins and SNF2 ATPase chromatin remodellers during endodyogeny by *Toxoplasma gondii*

Matthew Gow

Dissertation an der Fakultät für Biologie der Ludwig-Maximilians-Universität München

Tag der Einreichung: 29. November 2023

Erstgutachter: Prof. Dr. Michael Boshart

Zweitgutachter: Prof. Dr. Markus Meissner

Tag der mündlichen Prüfung: 14. Mai 2024

Summary

Apicomplexans such as *Toxoplasma gondii* utilise temporally coordinated gene expression control the progress through both their cell- and life cycles. Whilst the roles and contributions of certain protein families towards gene expression control have been explored, most notably the ApiAP2 transcription factors, histone acetyltransferases, and a MORC chromatin remodeller, the roles of other nuclear protein families remain unexplored or minimally explored, such as nuclear actin family proteins and SNF2 chromatin remodellers. In this study, knockdown of the two *T. gondii* ISWI homologues, SNF2l and SNF2h, resulted in differing phenotypes, suggesting they have independent roles in regulating gene expression. The presence of nuclear actin filaments in *T. gondii* remains unexplored. Therefore, it was sought in introduce the actin Chromobody® to the *T. gondii* nucleus to enable visualisation of nuclear actin filaments. However, expression of actin Chromobody-mEmerald proved too toxic for the establishment of a stable line. For an unknown reason, *T. gondii* possess two homologues of *S. cerevisiae* ARP4, currently annotated as ALP2a and ARP4a. ARP4a has previously been shown to be required for nuclear segregation during *T. gondii* replication, though the mechanism leading to this phenotype is undefined. In this study, the phenotypic characterisation of inducible ALP2a and ARP4a knockdowns, including visualisation of the mitotic machinery, showed that both KDs resulted in nuclear mis-segregation phenotypes arising from an over-duplication of the centrosome with subsequent competition by mitotic spindles for kinetochore binding. Co-immunoprecipitation demonstrated that a coccidian-specific nuclear protein of unknown function, TGME49_205562, is a putative interaction partner common to both ALP2a and ARP4a, as well as demonstrating that only ARP4a, and not ALP2a, associates with conserved proteins from the Ino80, SWR1, and NuA4 chromatin modifying complexes.

Table of Contents

1 Introduction

1.1 The phylum Apicomplexa, its origins and significance

Species belonging to the phylum Apicomplexa are almost exclusively monocellular, obligate endoparasites. A diverse phylum, more than 6,000 apicomplexan species have been described and include the causative agents of several medically and veterinary significant diseases. Belonging to the clade Alveolata **(Figure 1.1.1)**, the closest relatives to apicomplexans are free-living protists such as Chromerida, Perkinsozoa, Dinoflagellata, and Cilliophora. The common alveolate ancestor species likely possessed a photosynthetic plastid organelle that was acquired from red algae (Rhodophyta) (Janouskovec *et al.*, 2010). This plastid is loosely conserved in moden day alveolates. In Apicomplexa, this plastid organelle is called the apicoplast and has lost its photosynthetic capabilities.

Apicomplexa comprises four subclasses **(Figure 1.1.1)**. Coccidia is a complicated subclass that is further broken down into the Eimeriorina, Sarcocystidae, and Adeleorina. Eimeriorina species are facultatively monoxenous, in that they can complete their life cycle in a single host. Sarcocystidae are cyst-forming coccidians that typically have a definitive host, where sexual reproduction occurs, and an intermediate host, where asexual reproduction occurs. Adeleorina species have invertebrate hosts and have either mono- or polyxenous hosts. Haematozoa, also known as Aconoidasida, parasitise the blood of vertebrate intermediate hosts but have invertebrate definitive hosts. Species of the Gregarinasina parasitise invertebrate hosts. The *Cryptosporidium* genus represents Cryptosporidiidae and inhabits the intestinal tract of a diverse range of hosts and represents an uncertain subclass that used to be considered part of Coccidia but is now thought to be phylogenetically closer to Gregarinasina (Ryan *et al.*, 2016).

As parasites, apicomplexans are often pathogenic and cause numerous diseases of significance. For human health, the most significant apicomplexans are *Plasmodium* spp., which caused an estimated 247 million cases of malaria and 619 thousand deaths in 2021 (*World malaria report*, 2022). Transmitted during the blood meal feeding by *Anopheles* spp. mosquitos, five species of *Plasmodium* cause malaria in humans: *P. falciparum*, *P. vivax*, *P. malariae*, *P. ovale*, and *P. knowlesi*. Parasitism by *Plasmodium* spp. is not limited to humans, however, with other *Plasmodium* species infecting reptiles, rodents, bats, primates, and birds (Baird, 2009). *Cryptosporidium* spp. cause an infection, known as cryptosporidiosis, in humans and livestock that is typified by gastroenteritis and diarrhoea and is of particular threat to immunocompromised individuals, with approximately 50 thousand fatalities per

Figure 1.1.1: Illustration showing the phylogeny of phylum Apicomplexa within the clade Alveolata.

Alveolata is found in the eukaryotic SAR supergroup (inset). Representative phyla and example species within Alveolata are shown as branches. Phyla and species are non-exhaustive. The alveolate common ancestor was photosynthetic and some alveolates continue to be photoheterotrophs, e.g., *C. velia*, and *V. brassicaformis*. The photosynthetic plastid organelle in Apicomplexa has lost is photosynthetic capabilities and is termed the apicoplast, and is present in all Apicomplexa except *Cryptosporidium* spp., who have lost their apicoplast. The phylum Apicomplexa consists of four subclasses. Apicomplexan subclasses are further broken down into orders. As the coccidian *T. gondii* is the focus of this study, only the orders of Coccidia are shown.

year (Wang *et al.*, 2018; Gerace, Lo Presti and Biondo, 2019). The diseases caused by Eimeriorina coccidians are often collectively referred to as coccidiosis, and it has a similar pathology to cryptosporidiosis, causing gastroenteritis and diarrhoea. Sarcocystidae coccidians cause different diseases depending on the infective agent, neosporosis (*Neospora* spp.), besnoitiosis (*Besnoitia* spp.), and toxoplasmosis (*Toxoplasma gondii*).

T. gondii, the species of focus for this study, has widespread seroprevalence in humans (Flegr *et al.*, 2014) and can infect nearly all nucleated cells from warm-blooded animals. Acute toxoplasmosis is threat to immunocompromised individuals, where an infection can lead to encephalitis and death. The first-time exposure of pregnant woman to *T. gondii* can result in congenital toxoplasmosis, which affects foetal development and can have severe health implications should the foetus make it to full term. It is estimated that 200 thousand cases of congenital toxoplasmosis occur annually (Torgerson and Mastroiacovo, 2013). *T. gondii* is the most common cause of retinochoroiditis, which can occur from infections contracted *in utero* or otherwise and results in vision loss (Maenz *et al.*, 2014). Current treatments for *T. gondii* infections involve some combination of spiramycin, pyrimethamine, sulphadiazine, and folinic acid (Konstantinovic *et al.*, 2019). Whilst drug resistance is a minimal, the current drugs against *T. gondii* cannot clear latent infections.

1.2 *Toxoplasma gondii* propagation: lifecycle, transmission, and structure

1.2.a Lifecycle

First described in two 1908 articles (Nicolle and Manceaux, 1908, 2009; Splendore, 1908, 2009), *T. gondii* has a bipartite lifecycle where it infects either definitive hosts or intermediate hosts (Frenkel, 1973) **(Figure 1.2.1).** The infective stages of the *T. gondii* lifecycle, sporulated oocysts and bradyzoite cysts, are infective to all host species, so transmission can occur from a definitive host to either a definitive or intermediate host, and *vice versa*.

Sexual reproduction by *T. gondii* is believed to only occur in felids, the definitive hosts. Note that felid means species belonging to the taxonomic family Felidae, and therefore includes both domesticated cats (*Felis catus*), wild cats (*Felis silvestris*), and big cats (lions, tigers, etc.). However, whilst oocyst shedding, which only occurs following sexual reproduction in a definitive host, in the faeces of domesticated cats is well documented, only tenuous evidence for oocyst shedding in the faeces of other felids exists. The detection of oocysts in lion faeces was reported (Bjork, Averbeck and Stromberg, 2000) but the animals were co-infected with numerous other coccidians so, without genetic confirmation, visual misidentification of the oocyst is a possibility. While oocyst contamination of ecosystems lacking the presence of *F. catus* remain high, it is unclear whether this is because of the presence of other *Felis* spp. or other felids (Bevins *et al.*, 2012). Oocysts have been found in panther (*Puma concolor*) faeces, for example (Aramini, Stephen and Dubey, 1998). Overall, there is a need to

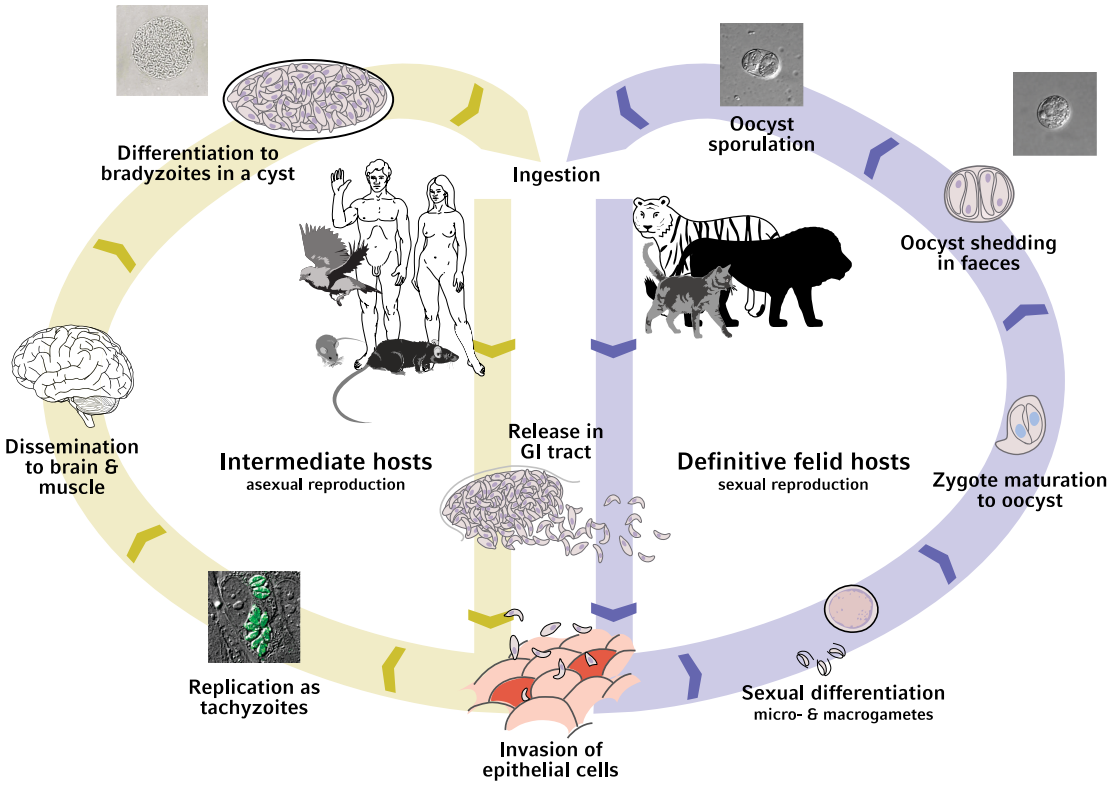

Figure 1.2.1: The lifecycle of *Toxoplasma gondii*.

T. gondii has polyxenous hosts, reproducing sexually in felids and asexually in warm-blooded animals. The ingestion of either a cyst or oocyst leads to infection of the gastrointestinal epithelium. In felids, the conversion of asexual *T. gondii* into male and female gametes is followed by fertilisation, meiosis, and oocyst formation. Oocysts are then shed into the environment through defecation. In intermediate hosts, *T. gondii* replicates asexually and disseminates through the body. *T. gondii* that infects brain and muscle cells develops into a dormant cyst that persists within the host. The carnivorous consumption of the host and the cysts completes the lifecycle. The figure and all artwork within were adapted in accordance with Creative Commons licences or are in public domain. Tachyzoite micrograph shows GFP-expressing tachyzoites (Hu *et al.*, 2006).

better define whether all or a limited number of felid species can serve as definitive hosts for *T. gondii* (Zhu, Shapiro and VanWormer, 2022).

Following ingestion of either a cyst or an oocyst by a felid, the *T. gondii* inside are released, invade the gastrointestinal epithelium, and replicate asexually by merogony. During merogony, the commitment to sexual reproduction may occur, with asexual merozoites differentiating to either male microgametes or female macrogametes. Fertilisation and zygote maturation also occurs in the felid gastrointestinal tract. This is the only point in the *T. gondii* lifecycle where the cells are diploid, all other stages are haploid. The zygote matures into an oocyst by developing an impervious oocyst wall that will allow it to survive the external environment and the zygote divides by meiosis. A further round of division called sporulation occurs creating a total of eight haploid sporozoites, and two sporocysts are visible within the one oocyst. The oocyst is then shed into the environment with the felid's faeces. Once shed, oocyst

viability will steadily decrease over time, and varies according to the specific environmental conditions, but viability of over a year has been reported (Frenkel, Ruiz and Chinchilla, 1975).

The initial progress of infection following ingestion of either a cyst or oocyst by an intermediate host is similar to that of definitive hosts in that the primary site of infection is the gastrointestinal epithelium. However, rather than asexual replication by merogony, *T. gondii* will instead replicate asexually as tachyzoites by endodyogeny. A detailed description of endodyogeny is given in section 1.3. Tachyzoites are able to disseminate through the host, either freely in the bloodstream or by hijacking migratory leukocytes (Bhandage and Barragan, 2019). Tachyzoites that enter brain or muscle cells are able to create a latent intracellular infection through the differentiation into bradyzoites, which are dormant and persist within a walled cyst. Through carnivorous predation of intermediate hosts, by either another intermediate host or a definitive host, the bradyzoite cysts are ingested and the lifecycle completed.

The replication and dissemination of tachyzoites is the acute phase of infection and causes clinical symptoms and pathology. The immune system of an immunocompetent individual is typically capable of resolving the acute infection. However, cysts cannot be cleared by the host's immune system, most likely because they reside in immune privileged tissues. Bradyzoites are capable of reactivating, reverting back to tachyzoites, an event that can result in morbidity and death through encephalitis.

1.2.b *T. gondii* strains and genome

Using PCR restriction fragment length polymorphisms, *T. gondii* isolates (strains) were placed in three haplotype groups, types I, II, and III (Howe and Sibley, 1995). The majority of *T. gondii* strains isolated are type II strains (Mondragon *et al.*, 1998). Subsequent analysis found a correlation between the three strain types and virulence (Saeij, Boyle and Boothroyd, 2005). Type II strains appear to be the most common strain isolated as they show the highest bradyzoite differentiation rate and therefore persist in infected individuals to a greater extent. The lower bradyzoite differentiation rate of type I strains means such strains have a higher rate of pathogenicity and are more associated with congenital toxoplasmosis. Type III strains are the least virulent *T. gondii* strains.

Table 1.2.1: The predominant haplotype grouping of *T. gondii*

Haplotype	Example strains	Virulence in mice
I	RH, GT1	High
II	Me49, Pru	Moderate
III	VEG	Low

Although heavy reference to the three haplotypes above is still made to the present day, it should be noted that rare divergent strains that do not conform to said haplotypes have been isolated. For example, rare strains isolated in South America have been designated haplotypes IV through X and are both highly virulent in mice and associated with ocular toxoplasmosis in humans (Calero-Bernal *et al.*, 2022).

The genomic reference strain for *T. gondii* is Me49, a type II strain. However, the majority of *T. gondii* research, including this study, is performed with the type I RH strain, due to its increased tractability for *in vitro* culture and genetic modification. The RH strain was isolated from the cerebral cortex of a 6-year-old boy during autopsy in 1937 (Sabin, 1941). The strain takes its name from the initials of the victim and through subsequent *in vitro* passaging has lost the ability to differentiate to bradyzoites and to reproduce sexually in felids (Frenkel, Dubey and Hoff, 1976; Dubey, 1977).

T. gondii possess a 66 Mbp genome that consists of 13 chromosomes. The first *T. gondii* next-generation sequencing assemblies, for the Me49 strain, gave *T. gondii* 14 chromosomes. This number was more recently revised to 13 chromosomes following HiC experiments and third generation sequencing with *de novo* genome assembly (Bunnik *et al.*, 2019; Xia *et al.*, 2021). It should be noted that the reference genome, the Me49 strain, has been neither re-sequenced with third generation sequencing nor revised and is still annotated as having 14 chromosomes. A fully annotated third generation sequencing genome for RH, the strain used in this study, with 13 chromosomes is available (termed RH-88 genome to avoid confusion with a previous RH genome). The genetic modifications designed as part of this study made reference to both Me49 and RH-88 genomes, which are available in the genomic database ToxoDB (Kissinger *et al.*, 2003).

1.2.c Lytic cycle

During the acute phase of infection, *T. gondii* tachyzoites infect nucleated host cells where they engage in repeated rounds of invasion, replication, and egress in a process known as the lytic cycle **(Figure 1.2.2).** Through use of their gliding motor, motile tachyzoites locate a host cell and attached to its surface. A brief reorientation phase ensues before the tachyzoite actively invades the host cell. The tachyzoite does not penetrate the plasma membrane of the host cell, instead creating an invagination of the host cell's plasma membrane that closes behind the tachyzoite. The tachyzoite now resides inside a parasitophorous vacuole composed of the host cell's plasma membrane. Through multiple rounds of replication by endodyogeny, the number of tachyzoites within the host cell will increase until

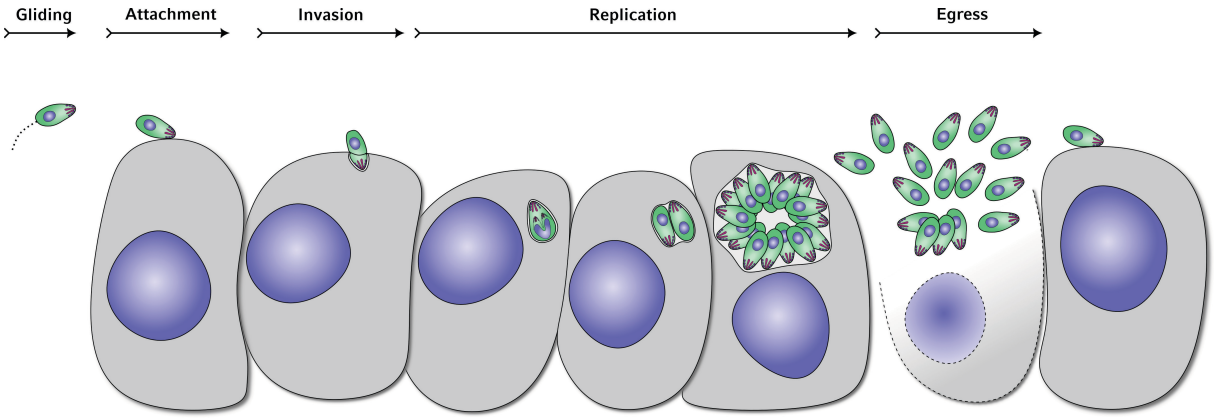

Figure 1.2.2: The lytic cycle of *T. gondii* tachyzoites.

Motile extracellular tachyzoites glide and attach to a host cell and invade, coming to reside in a parasitophorous vacuole. Through multiple rounds of endodyogeny, the tachyzoites replicate. At a point where the host cell can no longer sustain further tachyzoite replication, the tachyzoites lyse both the parasitophorous and plasma membranes to egress from the host cell, releasing the mature tachyzoites to invade another host cell and repeat the cycle.

the host cell can no longer support continued tachyzoite replication. At this point, the tachyzoites lyse both the parasitophorous vacuole and host's plasma membrane in order to egress, killing the host cell. The now free tachyzoites are mature and ready to invade another host cell, repeating the cycle. The replication of tachyzoites within a parasitophorous vacuole is near synchronous, but a culture of RH tachyzoites growing in multiple host cells will do so asynchronously, with one round of the lytic cycle lasting between 30 and 48 hours for this strain.

1.2.d Cellular structure of a *T. gondii* tachyzoite

T. gondii tachyzoites are elongated, crescent-shaped cells that are approximately 2 by 6 μm (Dubey, Lindsay and Speer, 1998) **(Figure 1.2.3)**. Most of the common eukaryotic organelles are present in tachyzoites. This includes a double membrane-enveloped nucleus, with nucleolus, surrounded by an endoplasmic reticulum, a Golgi, and a mitochondrion. The latter is a dynamic organelle whose morphology and size varies through the lytic cycle (Ovciarikova *et al.*, 2017).

1.2.d.i Cytoskeleton

A common feature of apicomplexans, including *T. gondii* tachyzoites, is a polarised cell structure with an apical complex used for the invasion of host cells (Koreny *et al.*, 2021). The apical complex of tachyzoites features a conoid composed of tubulin rings, the extrusion of which permits the secretion of secretory organelles to facilitate invasion of host cells (Haase, Dos Santos Pacheco and Soldati-Favre, 2022). The base of the conoid acts as a microtubule organising centre for the 22 evenly spaces

subpellicular microtubules that spiral two-thirds the length of the tachyzoite **(Figure 1.2.3c)**, acting as part of the tachyzoite's cytoskeleton and contributing to its shape. The other major component of the tachyzoite's cytoskeleton is the inner membrane complex (IMC). Situated between the plasma membrane and the subpellicular microtubules, the IMC is composed of many thin vesicles that are sutured together (Chen *et al.*, 2017). The constituent proteins found in the IMC varies according to position along the tachyzoite, and whether the IMC is mature or under assembly, with the IMC being critical for daughter cell assembly during endodyogeny (Pasquarelli *et al.*, 2023). Trafficking across the IMC is facilitated by an endocytic complex that localises to the IMC sutures (Koreny *et al.*, 2023). The IMC is connected to the subpellicular microtubules by intermediate filament-like alveolins (Tosetti *et*

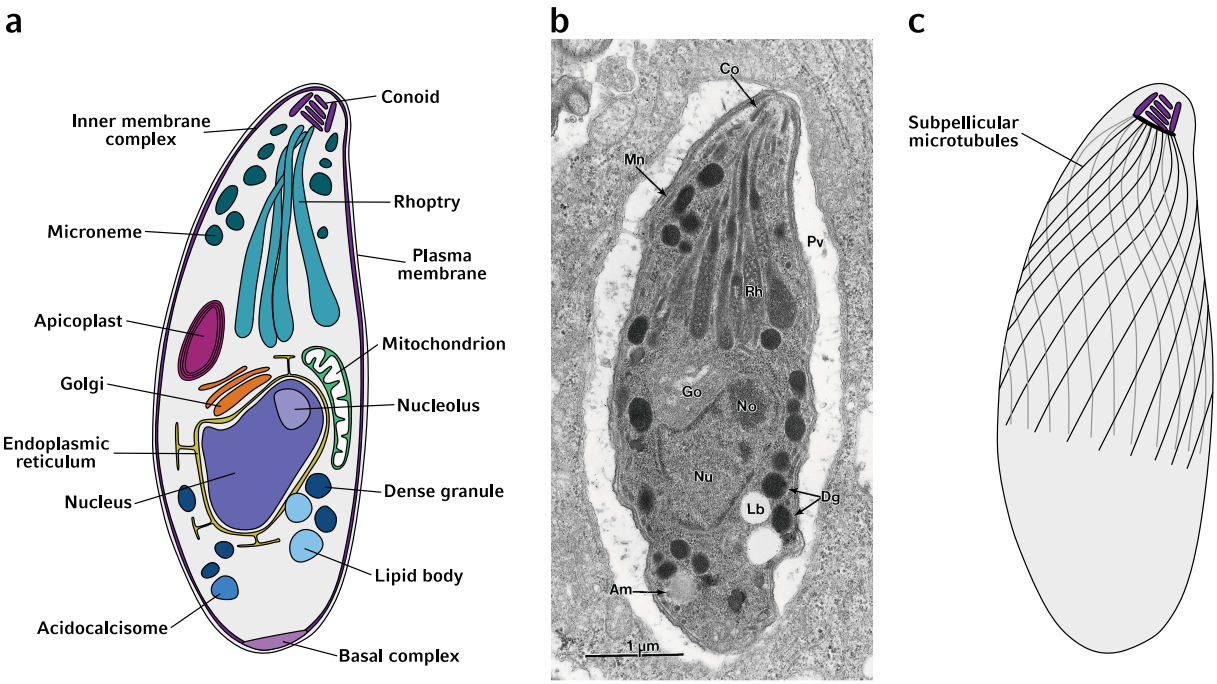

Figure 1.2.3: The structure of a *T. gondii* tachyzoite.

a. Illustration of organelle localisation within a tachyzoite. The apical pole features and apical complex that is formed of microtubules and includes the conoid. Behind the conoid are two types of secretory organelles, the micronemes and rhoptries. Another secretory organelle, the dense granules, are distributed throughout the cytoplasm. Typical eukaryotic organelles such as the nucleus, Golgi, endoplasmic reticulum, and mitochondrion are located in the lower half of the tachyzoite. Beneath the plasma membrane is the inner membrane complex (IMC), part of the cytoskeleton. The basal pole of the tachyzoite features the basal complex. Acidocalcisomes act as calcium storage organelles. Drawn using micrograph in b. from Dubey *et al.*, 1998 as a guide.

b. Transmission electron micrograph of an intracellular tachyzoite from Dubey *et al.*, 1998. Co, conoid; Mn, microneme; Pv, parasitophorous vacuole; Go, Golgi; No, nucleolus; Nu, nucleus; Dg, dense granules; Lb, lipid body; Am, amylopectin granule.

c. Distribution of the subpellicular microtubules that emanate from the apical complex. Tachyzoites have 22 subpellicular microtubules, which are located beneath the IMC and spiral two-thirds along the length of the tachyzoite.

al., 2020). At the basal pole of the tachyzoite is the basal complex whose function(s) are only partially understood but include cytokinesis during endodyogeny and intravacuolar trafficking (Gubbels *et al.*, 2022).

1.2.d.ii Secretory organelles

T. gondii tachyzoites possess lineage-specific secretory organelles that allow the attachment to, and invasion and manipulation of host cells. Immediately behind the apical complex are multiple micronemes and rhoptries. Secreted micronemal proteins typically lyse the parasitophorous vacuole and host cell plasma membrane (Kafsack *et al.*, 2009; Guerra *et al.*, 2018), act as adhesins (Sheiner *et al.*, 2010) and enable gliding motility, invasion, and egress (Alexander *et al.*, 2005; Carruthers and Tomley, 2008; Kessler *et al.*, 2008). Like micronemes, rhoptries are found immediately behind the apical complex but are much more elongated organelles. Rhoptries feature a bipartite composition with RON proteins localised to the apical end of the organelle (referred to as the rhoptry neck) and ROP proteins towards the bulbous basal end of the organelle (Bradley *et al.*, 2005). RON and ROP protein functions are diverse. For example, RON2 aids in stabilising the moving junction during invasion (Lamarque *et al.*, 2011; Tyler and Boothroyd, 2011) while ROP16 is a kinase secreted into the host cell's cytoplasm where it interferes with STAT3 and STAT6 signalling for the purpose of subverting the host's immune response (Saeij *et al.*, 2007). Distributed through the cytoplasm are another secretory organelle, the dense granules. GRA proteins within dense granules have roles in establishing and maintaining the parasitophorous vacuole as well as manipulating the host cell (Griffith, Pearce and Heaslip, 2022).

1.2.d.iii Apicoplast

Named after the phylum Apicomplexa to which it is specific, the apicoplast is a chloroplast-derived plastid-like organelle found in all apicomplexans with the notable exception of *Cryptosporidium* spp. Surrounded by four membranes, the apicoplast originated through secondary endosymbiosis of a red alga (taxonomic division Rhodophyta) that itself had a cyanobacterium-derived organelle obtained through primary endosymbiosis (Waller and McFadden, 2005; Lim and McFadden, 2010). Like the mitochondrion, the apicoplast is a DNA-containing organelle. The genome of the apicoplast is 35 kbp and is maintained as multiple copies (Matsuzaki *et al.*, 2001; Williamson *et al.*, 2001). However, unlike the mitochondrion, the apicoplast, along with the nucleus, is visible when using DNA makers such as DAPI and Hoechst with fluorescence microscopy. The apicoplast is not capable of photosynthesis but

is involved in metabolic pathways such as fatty acid and isoprenoid synthesis (Mazumdar *et al.*, 2006; Nair *et al.*, 2011).

1.3 Tachyzoite replication by endodyogeny

1.3.a Cell cycle

T. gondii tachyzoites, as well as some other coccidians, divide through endodyogeny, where two daughter cells are formed within a mother cell, with some mother cell components subsequently being broken down for recycling/scavenging (Nishi *et al.*, 2008; Anderson-White *et al.*, 2012; Verhoef, Meissner and Kooij, 2021) **(Figure 1.3.1)**. The cell cycle stages of endodyogeny are largely identical to that of other eukaryotes; after G_1 growth phase the cell enters S phase where DNA and organelle duplication begins, followed by the mitotic-like M phase, and finally cytokinesis in C phase. It has been suggested there is a G_2-like phase of the tachyzoite cell cycle, between S and M phase, due to an observed 1.8 N DNA content quantified by flow cytometry (Radke *et al.*, 2001). However, reproduction of the observed 1.8 N DNA content with similar experiments has produced differing results (Chen and Gubbels, 2013; Naumov *et al.*, 2017; Berry *et al.*, 2018). For nuclear segregation the core of the common eukaryotic mitotic machinery appears to be conserved in *T. gondii*, and the process of nuclear segregation is therefore often referred to as mitosis.

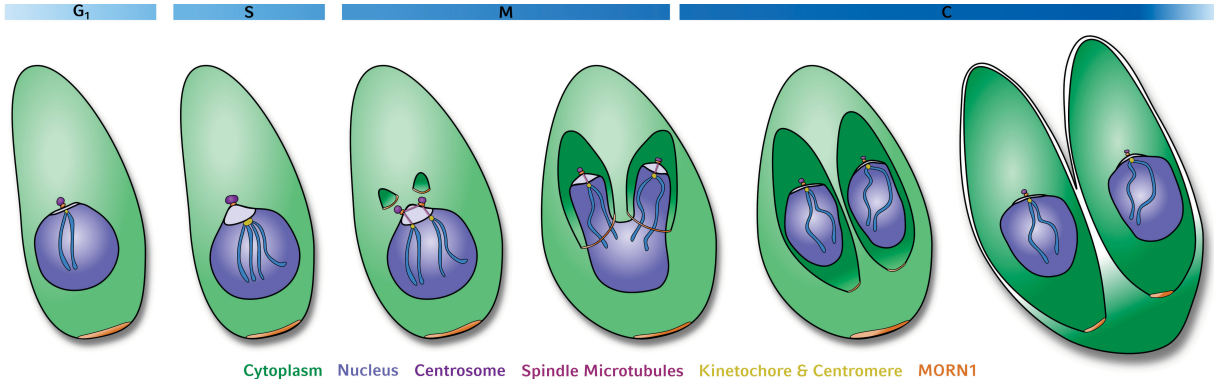

Figure 1.3.1: Overview of endodyogeny and the cell cycle

Endodyogeny begins with the transition from G_1 to S phase. During S phase the genome and centrosome duplicate in preparation for mitosis. With the onset of M phase two daughter cell IMCs begin to form, spindle microtubules attach to the nuclear DNA at their centromeres, and the centrosomes repel one another to begin the segregation of the nucleus. The segregating nucleus is enveloped by the elongating daughter IMCs, creating a bilobed nucleus. Through an unknown process, nuclear fission occurs following by completion of the daughter IMCs. In the last stage of endodyogeny, many of the remaining mother cell's components are broken down and recycled into the two daughter cells through their basal complexes (MORN1). Note that *T. gondii* chromosomes do not condense during mitosis and they are only depicted this way to demonstrate the segregation.

1.3.b Mitosis

As with model eukaryotes, *T. gondii* mitosis is coordinated by the centrosome. Normally situated at the apical side of the nucleus, beside the Golgi, *T. gondii*'s centrosome translocates around the nucleus in the early stages of S phase (Hartmann *et al.*, 2006; Nishi *et al.*, 2008). The purpose of this translocation is not yet known. Mitotic spindles originating at the centrosome polymerise, enter the nucleus at an electron dense, DNA-free region of the nucleus called the centrocone (Sheffield and Melton, 1968; Gubbels *et al.*, 2006) and attach to the kinetochores (Farrell and Gubbels, 2014; Brusini *et al.*, 2022). The centrocone is only visible in mitotic tachyzoites (Sheffield and Melton, 1968). With the attachment of the centrosomes to the chromosomes, nuclear segregation begins. Through an unknown mechanism, the two centrosomes become more spatially segregated and the two growing daughter cell inner membrane complexes (IMC) are extended and envelop the nucleus at the two centromeres, creating a bi-lobed, horseshoe-shaped nucleus. Before the completion of the daughter IMC, and the formation of the basal complex, the completion of nuclear segregation by fission of the two nuclear lobes occurs through an unknown process. Fission of the apicoplast and mitochondrion are DrpA and DrpC-dependent respectively, but neither dynamin is required for nuclear fission (van Dooren *et al.*, 2009; Heredero-Bermejo *et al.*, 2019; Melatti *et al.*, 2019).

1.3.c Centrosome

Apicomplexan centrosomes show significant divergence both from model eukaryotes and within the phylum. Like the spindle pole body of budding yeast (*Saccharomyces cerevisiae*), the *P. falciparum* centrosome does not feature a centriole, but it is not embedded in the nuclear membrane, like that of *S. cerevisiae* (Simon *et al.*, 2021) **(Figure 1.3.2a)**. The *T. gondii* centrosome, like animalian centrosomes, does feature a centriole, but it too is divergent. Human centrioles consist of nine triplets of microtubules arranged in a circle, referred to as a 9+0 layout, while *T. gondii* centrioles consist of nine singlets of microtubules arranged in a circle plus an additional central microtubule (9+1 layout) (Morrissette and Sibley, 2002) **(Figure 1.3.2a)**. Like the *T. gondii* centrosomal centriole, axonemes feature central microtubules, but as a doublet (9+2 layout). Such central doublets can also be found in the flagellum of *T. gondii* microgametes (Dubey, Lindsay and Speer, 1998).

Comparative genomics has identified numerous conserved or putative *T. gondii* centrosomal proteins (Morlon-Guyot *et al.*, 2017) but only a limited number have been functionally characterised to date. The first *T. gondii* centrosome marker characterised was centrin1 (Cen1) (Hu *et al.*, 2002).

Subsequently characterised centrosomal proteins showed varied co-localisation with Cen1, leading to the current bi-partite centrosome model, described as composed of an outer and inner core (Suvorova *et al.*, 2015) **(Figure 1.3.2)**. The centrosome outer core contains many evolutionary conserved centriole-associating proteins. The role of SAS-6 in centriole formation is likely conserved in *T. gondii*, with SAS-6 over-expression resulting in microtubule filament formation originating at the centrosome (de Leon *et al.*, 2013). Likewise conserved is the role of Sfi1 as a centrin-binding protein critical for centriole duplication (Suvorova *et al.*, 2015). Centrosome segregation in animals is proceeded by phosphorylation of CEP250 by Nek2 (Fry *et al.*, 1998; Mayor *et al.*, 2002). A conserved *T. gondii* homologue of CEP250 exhibits a dynamic localisation, being found in the centrosome outer core in non-mitotic tachyzoites, but localising as two distinct foci to both outer and inner cores following centrosome segregation (Suvorova *et al.*, 2015; Chen and Gubbels, 2019). The knockdown (KD) of CEP250 results in a loss of the close spatial association between the two centrosome cores in mitotic cells (Chen and Gubbels, 2019), indicating that the addition of CEP250 to the inner core is a critical step for tachyzoite mitosis. However, the KD of the *T. gondii* homologue of animalian Nek2, Nek1, does not interfere with the link between the two centrosome cores, instead inhibiting outer core segregation but not inner core segregation (Chen and Gubbels, 2019). Unfortunately, it is not known whether the addition of CEP250 to the centrosome inner core still proceeds following Nek1 KD. Additionally, a lineage-specific CEP250-like protein (CEP250L1) is localised exclusively to the inner core (Suvorova *et al.*, 2015). The KD of CEP250L1 results in the failure of nuclear segregation arising from the failure to assemble the mitotic spindles, illustrating the integral role of the centrosome inner core in mitosis (Tomasina *et al.*, 2022). However, despite the failure of mitosis, daughter cell assembly was unaffected, with daughter cells correctly inheriting centrosome outer cores, apicoplasts, and mitochondria.

The *T. gondii* centrosome functions as the central coordinator for both nuclear segregation via mitosis and daughter cell assembly. Following centrosome duplication, a polymer of striated fibre assemblins (SFA2 and 3) emerges from the centrosomes, the tip of which is the site of daughter cell conoid assembly (Francia *et al.*, 2012) **(Figure 1.3.2b)**. This SFA-mediated connection between the daughter conoid and centrosome persists until mitosis and daughter IMC elongation are complete, ensuring that the daughter inherits a nucleus. The KD of either SFA2 and SFA3 results in a failure to begin daughter cell assembly but does not impede mitosis, demonstrating that daughter cell assembly and mitosis are independent despite their shared coordination by the centrosome.

Centrosome segregation in animals is driven by a homodimer of the kinesin KIF11 (Blangy *et al.*, 1995; Kapitein *et al.*, 2005). The *T. gondii* genome contains 26 annotated kinesins but only one has been

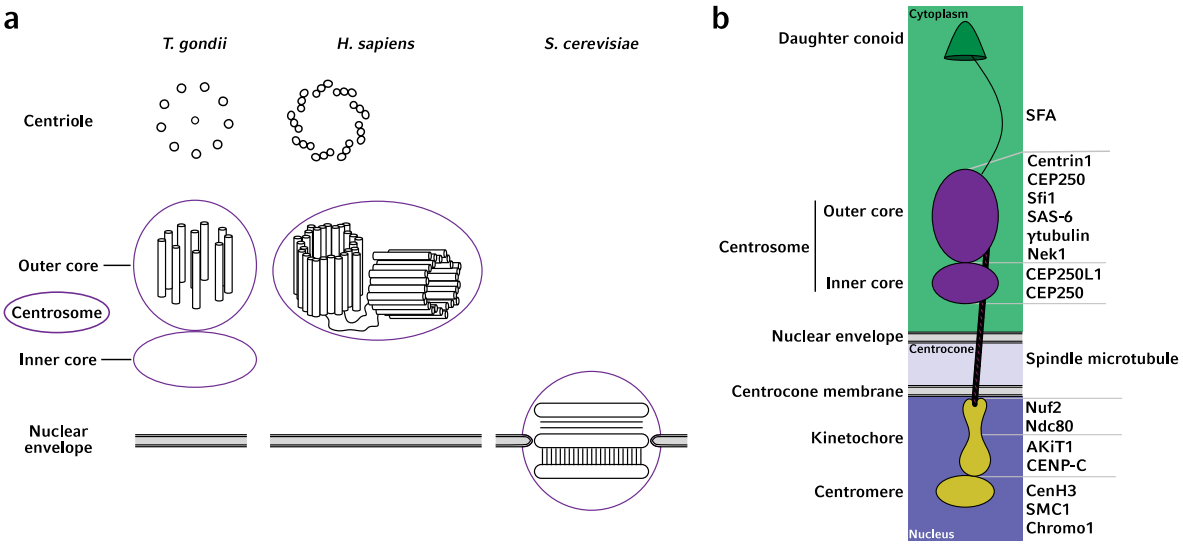

Figure 1.3.2: The *T. gondii* centrosome is the central coordinator of both daughter cell formation and mitosis.

a. Comparison of the *T. gondii* centrosome with the *H. sapiens* centrosome and *S. cerevisiae* spindle pole body. Like the *H. sapiens* centrosome, the *T. gondii* centrosome features a centriole. However, rather than nine triplet microtubules arranged in a circle, it is composed of nine singlet microtubules in a circle plus a central microtubule. The *T. gondii* centrosome is perinuclear and not integrated into the nuclear envelope. The *T. gondii* centrosome is also bi-partite, with the outer core featuring the centriole and the inner core, located towards the nucleus but still extra-nuclear, lacking a centriole.

b. Illustration of the arrangement of the centrosome and associated cellular components during endodyogeny, including representative proteins. The centrosome is connected to the developing daughter cell cytoskeleton via the SFA fibre. The centrosome is also connected to the nuclear chromosomes via mitotic spindles, which enter the nucleus at a DNA-free region of the nucleus called the centrocone.

characterised and was associated with the apical complex and not centrosomes (Leung *et al.*, 2017). The segregation of the two centrosome cores is not synchronous, with the outer core segregating before the inner core (Suvorova *et al.*, 2015). Whilst the mechanism that drives centrosome segregation remains to be elucidated, this pattern of segregation suggests that repulsion of the outer cores is active with the attached inner cores lagging behind. However, given that inner core segregation occurs independently of outer core segregation following Nek1 KD, it is more likely that both the outer core and inner core are actively repelled during centrosome segregation, albeit asynchronously.

1.3.d Mitotic machinery within the nucleus

During mitosis, the chromosomes of model eukaryotes condense to the point that the karyotype is visible, a process achieved through the phosphorylation of histone 3 tails (Wei *et al.*, 1998, 1999). Histone phosphorylation is a much rarer histone modification in *T. gondii* and no H3 tail residues have been found in a phosphorylated state (Nardelli *et al.*, 2013). Consequently, the chromosomes of

T. gondii do not condense prior to nuclear division and, therefore, no karyotype is visible (Nishi *et al.*, 2008; Brooks *et al.*, 2011). Instead, the centromeres of *T. gondii*'s 13 chromosomes are permanently fixed to kinetochores, which in turn are permanently anchored to a single location at the nuclear envelope (Brooks *et al.*, 2011; Farrell and Gubbels, 2014). This anchoring point has been speculated to be a nuclear pore complex and is located proximal to the centrosome (Francia *et al.*, 2020a)

Whilst the *T. gondii* mitotic spindles can be visualised by labelling α- and βtubulin, the conserved microtubule plus-end-binding protein EB1 has also been used as a mitotic spindle marker. However, while model eukaryotic EB1 is cytoplasmic and functions to promote elongation of all microtubules, not just mitotic spindles, (Nehlig *et al.*, 2017) *T. gondii* EB1 is a nuclear protein and its binding is specific to mitotic spindles (Chen *et al.*, 2015). However, *T. gondii* EB1 is not absolutely required for *in vitro* tachyzoite growth (Chen *et al.*, 2015) as microtubules are still able to polymerise in its absence.

Although it is permanently assembled in tachyzoites, the *T. gondii* kinetochore is minimally conserved **(Figure 1.3.2b)**. The two spindle microtubule-binding kinetochore subcomplexes, the Ndc80/Nuf2 and Ska complexes are conserved, and required for nuclear segregation by tachyzoites (Farrell and Gubbels, 2014; Brusini *et al.*, 2022). In contrast, the constitutive centromere-associated network (CCAN) kinetochore subcomplex is almost entirely not conserved, with only CENP-C being found in the *T. gondii* kinetochore. *H. sapiens* CENP-C (*S. cerevisiae* homologue Mif2) directly associates with the centromere and is required for the recruitment of other kinetochore proteins (Kato *et al.*, 2013; Klare *et al.*, 2015; Hara and Fukagawa, 2017). *T. gondii* CENP-C is essential for tachyzoites, with centrosome segregation failure following CENP-C KD (Brusini *et al.*, 2022). A novel family of Apicomplexa-specific kinetochore proteins have been described, termed AKiT proteins (Brusini *et al.*, 2022). *T. gondii* AKiT1 is required for proper nuclear segregation and its localisation to the kinetochore is CENP-C-dependent (Brusini *et al.*, 2022).

Like model eukaryotes, *T. gondii* chromosome centromeres are demarcated by the centromere-specific histone variant CenH3 (a.k.a. CENP-A) (Brooks *et al.*, 2011). The alignment of model eukaryote chromosomes during mitosis is aided by SMC-kleisin complexes (SMC: Structural Maintenance of Chromosome) (Muir *et al.*, 2020). SMC complexes only associate with chromosomes during mitosis and their dissociation immediately prior to anaphase is one of the tiggers required for chromosome segregation. A number of SMC proteins are conserved in *T. gondii*, however the characterisation of SMC1 showed that it is persistently associated with centromeres throughout the tachyzoite cell cycle (Francia *et al.*, 2020a), indicating its function is divergent from model eukaryotes. A chromo

domain-containing homologue of heterochromatin protein 1 (HP1) named Chromo1 is also found at *T. gondii* centromeres throughout the cell cycle except during nuclear segregation (Gissot *et al.*, 2012). However, its function is not known and it is not predicted to be essential for *in vitro* tachyzoite growth (Sidik *et al.*, 2016).

During this study the progress of *T. gondii* mitosis was visualised and tracked using the mitotic machinery marker proteins in Table 1.3.1.

Table 1.3.1: Summary of mitotic machinery marker proteins used in this study

Protein	Localisation	Function	Reference
Centrin 1	Centrosome outer core	Homologue of *H. sapiens* centrin 1	Hu *et al.*, 2002
Nuf2	Kinetochore	Connector between spindle microtubules and centromeric DNA	Farrell and Gubbels, 2014
EB1	Positive end of spindle microtubules	Non-essential promoter of spindle microtubule polymerisation	Chen *et al.*, 2015
CenH3	Centromere-specific histone variant	Demarcation of centromere, kinetochore recruitment	Brooks *et al.*, 2011

1.3.e Basal complex

One of the most enigmatic and dynamic proteins involved in endodyogeny is MORN1. First identified for containing a membrane occupation recognition nexus motif (MORN) (Takeshima *et al.*, 2000), MORN1 localises close to the centrosome during G_1 phase, duplicates with the centrosome and also localises as a ring to the elongating daughter IMCs, and finally to the basal complex at the completion of daughter IMC assembly (Gubbels *et al.*, 2006). Despite its localisation to different structures during endodyogeny, the phenotype associated with MORN1 KD is a failure of cytokinesis, with complete daughter cells formed that are fused by their basal poles due to a failure to assemble a basal complex (Lorestani *et al.*, 2010; Engelberg *et al.*, 2022).

1.3.f Control of endodyogeny

Like model eukaryotes, *T. gondii* utilises intracellular signal transduction pathways for the coordination of cell cycle progression and endodyogeny. However, the present understanding of the pathways is limited. For example, the catalytic targets of many signal transducers have not been identified.

Typically, progress through the cell cycle is controlled via cyclins and their dimerisation with cyclin-dependent kinases (CDK). In *T. gondii*, the dimerisation partners of cyclins are CDK-related kinases (Crks) (Alvarez and Suvorova, 2017). To date, the contribution of five cyclins and their Crks to endodyogeny and differentiation to bradyzoites has been characterised **(Table 1.3.2)** but other cyclins known to be required for tachyzoite growth have yet to be characterised (Alvarez and Suvorova, 2017). CDPK7 was identified as a substrate of both Crk4 and PRMT1 (Putative Arginine MethylTransferase 1) (El Bissati *et al.*, 2016; Hawkins *et al.*, 2023), which, given its described roles in mitosis, transcriptional regulation, and vesicular trafficking (Morlon-Guyot *et al.*, 2014; El Bissati *et al.*, 2016), indicates it to be a multifunctional kinase with roles in various signal transduction pathways.

Two further families of kinases, the aurora kinases and mitogen-activated kinases (Ark, MAPK), have members that have roles in coordinating mitosis **(Table 1.3.2)**. However, the proteins they phosphorylate have not been identified, so it is difficult to know how directly they act as mitosis coordinators.

In addition to mitosis, signal transduction enzymes also contribute to daughter cell formation and mother cell recycling during endodyogeny. The MAPK ERK7 (the MAPK family was originally called Extracellular signal-Regulated Kinase) is required for apical complex maturation (O'Shaughnessy *et al.*, 2020). Furthermore, one substrate of ERK7, a E3 ligase called CSAR1, localises to the vacuole's residual body and is required for mother cell recycling (O'Shaughnessy *et al.*, 2023). Likewise is the cytoplasmic kinase TKL4 required for mother cell recycling (Montano *et al.*, 2023) whilst the phosphatase PPKL is required for daughter cell assembly (Yang *et al.*, 2023).

Table 1.3.2: Signal transduction enzymes with characterised roles in endodyogeny

Protein	Localisation	Target	Null mutant phenotype	Reference
Crk1 & CycL	Nucleus		Nuclear mis-segregation	Alvarez and Suvorova, 2017
Crk2 & CycP2	Cytoplasm		Increased differentiation to bradyzoites	Naumov *et al.*, 2022
Crk2 & CycP5	Cytoplasm		Decreased differentiation to bradyzoites	Naumov *et al.*, 2022
Crk6 & Cyc1	Nucleus	Centromere	Centrosome over-duplication	Hawkins *et al.*, 2021
Crk4 & Cyc4	Cytoplasm	CDPK7, γtubulin complex, DNA replication complex	Duplicated but unsegregated centrosomes	Hawkins *et al.*, 2023, not peer reviewed

Protein	Localisation	Target	Null mutant phenotype	Reference
Ark1	Cytoplasm		No kinetochore segregation	Berry *et al.*, 2018
Ark3	Pericentrosomal & elongating daughter IMC		Disorganised vacuole	Berry *et al.*, 2016
CDPK7	Cytoplasm		Centrosome over-duplication, loss of kinetochore sequestration	Morlon-Guyot *et al.*, 2014
		Rab11a	Disrupted vesicular trafficking	Bansal *et al.*, 2021
MAPK-L1	Pericentrosomal		Centrosome over-duplication	Suvorova *et al.*, 2015
MAPK2	Cytoplasm		No centrosome duplication, incomplete DNA replication	Hu *et al.*, 2020
PRMT1	Pericentrosomal	CDPK7, RNA-binding proteins, ApiAP2 transcription factors	Centrosome over-duplication	El Bissati *et al.*, 2016; Yakubu *et al.*, 2017
ERK7	Apical pole	CSAR1	Immature apical complex	O'Shaughnessy *et al.*, 2023
TKL4	Cytoplasm	Tubulin, IMC, glideosome	Incomplete mother cell recycling	Montano *et al.*, 2023
PPKL	Daughter IMC, pericentrosomal	Microtubules	Incompletely assembled daughter IMC	Yang *et al.*, 2023, not peer reviewed

1.4 The regulation of gene expression in Apicomplexa

The use of differential gene expression is critical to the control and coordination of both the cell cycle and lifecycle progression in *T. gondii* and all other apicomplexans. This is principally achieved through the concerted efforts of transcriptional regulation, post-translational modifications of histones, and ATP-dependent chromatin remodelling. *T. gondii* organises its DNA into chromatin in the same manner as model eukaryotes **(Figure 1.4.1a)**. The DNA double helix is wound around an octamer of histones with each histone octamer and surrounding DNA making a nucleosome. Histones are composed of a globular region that forms the core of the nucleosome and an unfolded tail that is post-translationally modified to encode epigenetic signals. Nucleosomes only contain histones H2A, H2B, H3, and H4, including variants of each histone. Histone H1 is the linker histone that associates with DNA immediately adjacent to the nucleosome and functions to maintain chromatin stability. Chromatin can be remodelled for the purpose of exposing or hiding DNA motifs recognised by DNA-binding proteins such as transcription factors **(Figure 1.4.1b)**. This can involve nucleosome sliding, nucleosome

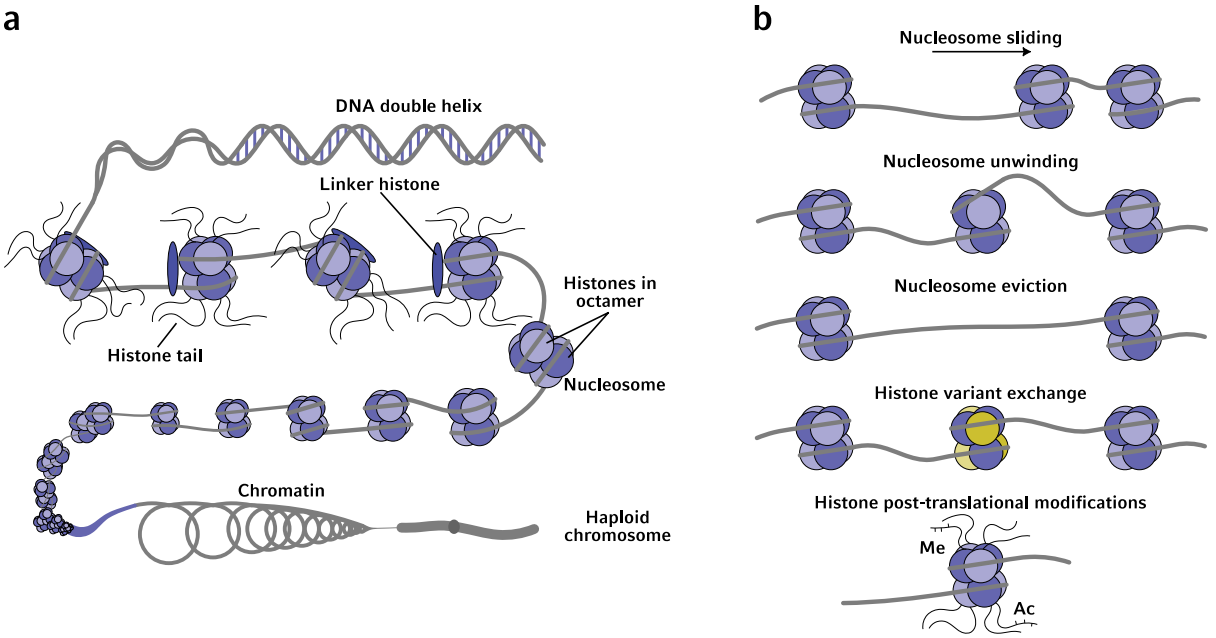

Figure 1.4.1: The organisation of DNA into chromatin and how chromatin can be modified.

a. The DNA double helix is wound around a histone octamer to form a nucleosome. Linker histones serve to improve chromatin stability. Nucleosomes are further wound around one another and compacted to form chromatin. In general, denser heterochromatin is transcriptionally silent while looser euchromatin is transcriptionally active. Inspired by illustration from National Human Genome Research Institute that is in the public domain.

b. Examples of how chromatin can be modified through the physical movement of nucleosomes by ATP-dependent chromatin remodellers, changing the histones variants within the nucleosome, and through post-translational modifications. Inspired and adapted from Xu et al., 2013.

unwinding, nucleosome eviction. Canonical histones can be exchanged for histone variants, which is used in the control of transcriptional regulation, chromatin compaction, chromatin localisation within the nucleus, and DNA damage repair. Through post-translational modifications, histone tails encode epigenetic information that is read by other nuclear proteins. In addition, post-translational modifications of histones close to their dyad (region that is in contact with DNA) can alter the affinity between DNA and nucleosome. For the purpose of controlling chromatin state, *T. gondii* and other apicomplexans utilise a mixture of conserved and lineage-specific mechanisms.

1.4.a Transcriptional regulation

Comparative genomics was used to probe apicomplexan genomes for transcription factor families that could regulate the complex lifecycles of the phylum. However, such approaches failed to identify known DNA-binding domains characteristic of transcription factors in other eukaryotes (Aravind *et al.*, 2003). Subsequent studies revealed several RNA polymerase II (RNAPII) complex subunits to be conserved in *T. gondii* and *P. falciparum*, as well as subset of general transcription factors (Callebaut *et al.*, 2005;

Meissner and Soldati, 2005), but nothing lineage-specific. By happenstance, another group, performing similar comparative genomics, noted an AT-hook on one *P. falciparum* nuclear protein (Balaji *et al.*, 2005). AT-hooks are found on many nuclear proteins and are far from exclusive to transcription factors. Arguing that DNA-binding domains are often found proximal to AT-hooks, the authors of this study were able to identify an amino acid sequence conserved within the Apicomplexa and sharing loose-homology to the AP2 (Apetala2)-integrase DNA-binding domain found in plant transcription factors. Termed the ApiAP2 proteins, these represent the only lineage-specific family of DNA-binding proteins found in the Apicomplexa, with many members now having been shown to behave as transcription factors (Painter, Campbell and Llinás, 2011; White, Radke and Radke, 2014). Note that AP2 transcription factors should not be confused with AP2 adaptor complex proteins that are involved in endocytosis. To limit the risk of confusion, the apicomplexan AP2 transcription factor family is herein referred to as ApiAP2, but the individual transcription factors themselves are referred to as AP2*xxxx*

T. gondii possess 67 ApiAP2 transcription factors, 23 of which are cell cycle variably expressed, 11 are bradyzoite specific, 27 are constitutively expressed, and 6 are not expressed in intermediate hosts (Behnke *et al.*, 2010). Unfortunately, the naming convention used for *T. gondii* ApiAP2 does not have an intuitive, functional basis, with *T. gondii* ApiAP2 factors named after the chromosome on which they are encoded and their relative position on said chromosome. For example, AP2X-9 is the 9th ApiAP2 found on chromosome 10. The functions of *T. gondii* ApiAP2 factors that have been characterised to date is given in **(Table 1.4.1)**.

The ApiAP2 are not the only transcription factors that *T. gondii* utilises for lifecycle control. Various proteins within the genome putatively contain Myb-like DNA binding domains. One such protein, BFD1, is required for the differentiation of tachyzoites to bradyzoites (Waldman *et al.*, 2020).

Table 1.4.1: Summary of characterised *T. gondii* ApiAP2 transcription factor functions

***T. gondii* ApiAP2**	**Function**	**Reference**
AP2IV-3	Activator of bradyzoite conversion	Hong, Radke and White, 2017
AP2IV-4	Bradyzoite gene-repressor expressed in tachyzoites	Radke *et al*., 2018
AP2X-5	Acts cooperatively with AP2XI-5	Lesage *et al*., 2018
AP2IX-4	Regulator of bradyzoite gene-expression	Huang *et al*., 2017
AP2IX-5	Activator of daughter cell assembly genes	Khelifa *et al*., 2021; Wang *et al*., 2021
AP2IX-9	Early bradyzoite repressor of bradyzoite conversion	Radke *et al.*, 2013
AP2X-5	Regulator of tachyzoite virulence and invasion gene-expression together with AP2XI-5	Lesage *et al.*, 2018
AP2XI-4	Regulator of bradyzoite gene-expression	Walker, Gissot, Croken, *et al*., 2013
AP2XI-5	Regulator of tachyzoite virulence and invasion gene-expression together with AP2X-5	Walker, Gissot, Huot, *et al*., 2013; Lesage *et al*., 2018
AP2XII-2	Global repressor	Srivastava, White and Sullivan, 2020; Srivastava *et al*., 2023
AP2XII-8	Promotes expression of ribosomal proteins	Lou *et al*., 2023, not peer reviewed

1.4.b Histones, histone variants, and their post-translational modifications

Referring to heritable traits that modulate gene expression without altering the DNA sequence, epigenetics typically involves alteration of chromatin structure, rendering genes more or less accessible to other DNA-binding proteins, such as transcription factors. Typical epigenetic methods employed by model eukaryotes include histone modifications, histone exchange, nucleosome positioning, non-coding RNA association, and sub-nuclear compartmentalisation.

1.4.b.i Histones

T. gondii possess a full complement of canonical histones and histone variants **(Table 1.4.2)**. The main H2B histone is the lineage-specific H2B.V, whilst two *H. sapiens* H2B paralogues (H2Ba and H2Bb) are mostly expressed in life cycle stages within definitive hosts. A direct homologue of *H. sapiens* H1, the inter-nucleosomal linker histone, does not exist in *T. gondii*. Instead, a H1-like protein, phylogenetically closer to bacterial and Kinetoplastida H1, has been described (Severo *et al.*, 2022), with the loss of H1 resulting in reduced chromatin compaction. Control of gene expression can be achieved through the exchange of canonical histones for histone variants. For example, H2A.Z and H2B.Z are found together

in nucleosomes deposited in the gene bodies and promoters of actively expressed genes (Bogado *et al.*, 2014; Nardelli *et al.*, 2022).

Table 1.4.2: *T. gondii* histones

***T. gondii* histone**	***H. sapiens* histone**	**Notes**
H1-like	H1	H1-like lacks mammalian H1 globular domain
H2A	H2A	
H2A.X	H2A.X	
H2A.Z	H2A.Z	
H2Ba	H2B	Oocysts
H2Bb		Sexual stages & sporulated oocysts
H2B.V (a.k.a. H2B.Z)		Most abundant H2B, unique to Apicomplexa
H3	H3	
H3.3	H3.3	
CenH3	CenH3 (a.k.a. CENP-A)	Centromere specific histone
H4	H4	

1.4.b.ii Histone post-translational modifications

The repertoire of *T. gondii* histone post-translational modifications is defined (Nardelli *et al.*, 2013). Overall, the acetylation and methylation of H3 and H4 tails is heavily conserved whilst the number phosphorylated residues are significantly diminished. However, there are disparities of detected histone post-translational modifications between different studies. For example, *P. falciparum* H4K31 has been shown to be both unmodified and modified by acetylation, methylation, and formylation (Nardelli *et al.*, 2013; Saraf *et al.*, 2016). Furthermore, the same H4K31 residue in *T. gondii* has been reported as methylated, succinylated, and formylated in one study but acetylated in another (Jeffers and Sullivan, 2012; Nardelli *et al.*, 2013). The possibility of undefined histone post-translational modifications is therefore an ever-present possibility. At present, only a limited number of histone post-translational modifications have been characterised, of which almost all are lysine methylation and acetylation **(Table 1.4.3)**. Whilst histone post-translational modifications are normally classified as having either an activating or repressing role in gene expression, the simultaneous presence of both activating and repressing markers has been described as holding genes in a poised status. For example, in Pru tachyzoites, some bradyzoite and sexual stage genes are marked with both the activating H3K14ac and the repressing H3K9me3 in what is believed to be a state of readiness for progression of the lifecycle (Sindikubwabo *et al.*, 2017).

Table 1.4.3: Summary of characterised *T. gondii* histone post-translational modifications

Histone post-translational modification	Genomic localisation	Characterisation	Putative writer & eraser enzymes	Reference
H3K4me1	Gene body	Lowered transcription	SET1	Sindikubwabo *et al.*, 2017
H3K4me3	Promoter & 5'UTR	Activation	SET1	Gissot *et al.*, 2007
H3K9ac	Promoter	Activation	GCN5b	Bhatti *et al.*, 2006; Gissot *et al.*, 2007
H3K9me2	Pericentromere	Silencing	SET3	Brooks *et al.*, 2011
H3K9me3	Promoter, gene body & pericentromere	Silencing	SET3	Brooks *et al.*, 2011; Sindikubwabo *et al.*, 2017
H3K14ac	Promoter & 5'UTR	Activation	GCN5b	Bhatti *et al.*, 2006; Gissot *et al.*, 2007
H3R17me	Promoter	Activation	CARM1	Saksouk *et al.*, 2005
H3K18ac	Promoter	Activation	GCN5a	Saksouk *et al.*, 2005
H4K20me1/2/3	Centromere & telomere heterochromatin	Inactivation	SET8	Sautel *et al.*, 2007
H4K31ac	Promoter & 5'UTR	Activation	GCN5b, HDAC3	Sindikubwabo *et al.*, 2017
H43K1me1	Gene body	Lowered transcription		Sindikubwabo *et al.*, 2017

1.4.b.iii Histone post-translational modification writers and erasers

The epigenetic state of chromatin is controlled by a repertoire of chromatin remodelling enzymes that are loosely grouped as writers, erasers, and readers. Writers and erasers add and remove chromatin post-translational modifications whilst readers are recruited to specific chromatin regions by such modifications. Such factors are highly conserved in *T. gondii* (Iyer *et al.*, 2008; Fleck, Nitz and Jeffers, 2021).

T. gondii possess two homologues of the histone acetyltransferase GCN5, termed GCN5a and GCN5b. Only GCN5b is required for *in vitro* tachyzoite growth (Bhatti *et al.*, 2006) but GCN5a is involved in stress response and therefore believed to contribute to the differentiation to bradyzoites (Naguleswaran *et al.*, 2010). The catalytic components of the NuA4 histone acetyltransferase complex are from the MYST family of enzymes. *T. gondii* has two MYST enzymes, MYST-A and MYST-B, the homologues of which are KAT5 in *H. sapiens* and ESA1 in *S. cerevisiae*. Both *T. gondii* MYST enzymes acetylate H4 tails (Smith *et al.*, 2005; Vonlaufen *et al.*, 2010). The removal of acetyl groups from histones is achieved by histone deacetylases (HDACs). In tachyzoites, HDAC3 deacetylates H4 tails and is a repressor of genes exclusively expressed in both bradyzoites and definitive host lifecycle stages (Bougdour *et al.*, 2009;

Antunes *et al.*, 2023). Histone methyltransferases are less well defined in *T. gondii*. PRMT1 is a major arginine methyltransferase most abundantly localised to the cytoplasm, and methylates a wealth of proteins including histones (Yakubu *et al.*, 2017). Despite the range of its substrates, PRMT1 is not essential for *in vitro* tachyzoite growth, with a KO only exhibiting slower growth (El Bissati *et al.*, 2016). Histone methyltransferases can function to both increase and decrease gene expression, as typified by SET1, which tri-methylates H3K4 in promoters to increase transcription but mono-methylates the same residue in gene bodies to reduce the transcription level (Gissot *et al.*, 2007; Sindikubwabo *et al.*, 2017) **(Table 1.4.3)**.

1.4.c ATP-dependent chromatin remodellers

1.4.c.i MORC

In repressing definitive host lifecycle stage-expressed genes, HDAC3 does not act alone but in concert with AP2XII-1, AP2XI-2, and MORC (Antunes *et al.*, 2023). MORC belongs to the microrchidia family of ATPase chromatin remodelling enzymes known to be found in Plantae and Animalia but not Fungi (Chutani *et al.*, 2022). *T. gondii* MORC is required for the recruitment of HDAC3 and subsequent silencing (Farhat *et al.*, 2020). However, MORC does not contain any known epigenetic reader domains so its recruitment to silenced loci is most likely dependent on other chromatin-associating proteins and not histone post-translational modifications. MORC directly interacts with a multitude of ApiAP2 transcription factors, which could possibly serve as the recruiters (Farhat *et al.*, 2020). Whether the MORC-interacting ApiAP2s share a common domain that facilitates an interaction with MORC, and what the nature of any chromatin remodelling by MORC is are both open questions.

1.4.c.ii SNF2 in model eukaryotes

Another family of ATPase chromatin remodellers that is more extensively conserved across eukaryotes is the SWI2/SNF2 family, hereafter referred to as SNF2 for simplicity. SNF2 is the catalytic component of the *S. cerevisiae* chromatin remodelling SWI/SNF complex (SWItching defective/Sucrose Non-Fermenting) (Haber and Garvik, 1977; Carlson, Osmond and Botstein, 1981). SNF2 chromatin remodellers are further categorised into four categories based on the conservation of their ATPase domain and distribution of other functional domains (Längst and Manelyte, 2015):

- The SWI/SNF family typically include a bromo domain for reading histone lysine acetylation and HSA (helicase-SANT) domain for recruiting actin family proteins.

- ISWI (Imitation SWItch) remodellers include HAND, SANT, and SLIDE domains that allow them to recognise nucleosomes.
- CHD (Chromo domain Helicase DNA-binding) remodellers feature chromo domains for reading histone lysine methylation.
- Ino80 (Inositol requiring 80) remodellers feature both a large insertion within their ATPase domain and a HSA domain.

SWI/SNF remodelling complexes have been shown to slide and evict nucleosomes (Wilson and Roberts, 2011). ISWI remodellers are the catalytic components of seven different chromatin remodelling complexes in *H. sapiens* with roles in nucleosome sliding, nucleosome remodelling, and the maintenance of nucleosome free regions (Goodwin and Picketts, 2018). Both *S. cerevisiae* and *H. sapiens* possess two ISWI remodellers, termed ISW1 and ISW2 in the former and SNF2h and SNF2l in the latter. The CHD subfamily of remodellers is the most diverse and divergent of the subfamilies, with mammals having nine CHD enzymes (Cardoso *et al.*, 2021). The Ino80 subfamily consists of two proteins, Ino80 and SWR1, which are responsible for the exchange of H2A for H2A.Z and *vice versa*, respectively (Mizuguchi *et al.*, 2004a; Papamichos-Chronakis *et al.*, 2011).

1.4.c.iii SNF2 in Apicomplexa

Chromatin accessibility studies have demonstrated that nucleosome remodelling is used by apicomplexans to regulate gene expression. The patterns of nucleosome coverage and positioning at transcriptional start sites are correlated with transcriptional changes in both *P. falciparum* and *T. gondii* (Kensche *et al.*, 2016; Toenhake *et al.*, 2018; Lou *et al.*, 2023). However, despite this and the fact that members of each SNF2 subfamily are known to be conserved in Apicomplexa (Watzlowik *et al.*, 2021), very few functional studies of apicomplexan SNF2 chromatin remodelling enzymes has taken place. An SWR1/Ino80 homologue was found to have higher transcription in bradyzoites than tachyzoites (Sullivan *et al.*, 2003). In *P. falciparum* a protein named ISWI was identified in association with actively expressed var genes whose knockdown led to global up- and down-regulation of gene expression, including down-regulation of var genes (Bryant *et al.*, 2020). Note that *P. falciparum* ISWI is a misnomer, as its ATPase domain is phylogenetically closer to the SWI/SNF subfamily and it lacks the HAND-SANT-SLIDE domain that is the hallmark of the ISWI remodeller subfamily. Characterisation of the only verifiably conserved *P. falciparum* ISWI subfamily member, Snf2L, showed that is a genome-wide regulator of nucleosome spacing at transcriptional start sites (Watzlowik *et al.*, in revision). However, no functional studies of *T. gondii* SNF2 chromatin modellers have been performed.

1.5 The actin family of proteins

1.5.a Actin

Belonging to the sugar kinase family of proteins, actin is abundantly found in the vast majority of eukaryotic cells (Hurley, 1996) and has a key role in a variety of cellular processes such as motility, vesicular trafficking, cell division, and as a component of the cytoskeleton (Pollard and Cooper, 2009; Olson and Nordheim, 2010). A key feature of actin, and other sugar kinase family proteins such as heat shock protein 70, is the presence of an ATP-binding pocket, which in actin is termed the actin fold (Kabsch and Holmes, 1995). The ATP-binding pocket functions as a ATPase, hydrolysing ATP to ADP and Pi and changing the structure of the molecule from a closed to an open conformation (Kudryashov and Reisler, 2013).

1.5.a.i Actin filaments

Actin exists in two forms, as a monomer referred to as globular actin (G-actin) and as a filamentous polymer (F-actin). The nucleation of F-actin requires three ATP-bound G-actin (Asakura, Taniguchi and Oosawa, 1963) with a filament rapidly polymerising following the addition of a fourth monomer. As an ATPase, each actin monomer within an F-actin filament hydrolyses its ATP to ADP and Pi, the latter of which is slowly lost from the filament (Carlier, 1990; Murakami *et al.*, 2010). Thus, the actin monomers within an F-actin filament exist in three states, ATP-bound at the +end, ADP-bound at the -end, and ADP+Pi bound in the middle. F-actin composed of ADP-bound monomers is less stable compared to that of ATP-bound monomers and so depolymerisation of the filament occurs at the ADP-bound -end (Korn, Carlier and Pantaloni, 1987). The process of F-actin polymerisation at the ATP-bound end and depolymerisation at the ADP-bound end is referred to as actin treadmilling. Actin treadmilling is essential for F-actin functions, especially within the context of cell motility (Bugyi and Carlier, 2010). The stability of an F-actin filament is further influenced by the family of actin binding proteins. For example, tropomyosins control filament length, the ARP2/3 complex facilitates F-actin branching, and formins bind to the +end and promote polymerisation.

Apicomplexan actin is highly divergent from that of other eukaryotes. For example, *S. cerevisiae* actin shares 87% amino acid identity with *H. sapiens* actin, but apicomplexan actins only ~80% (Dobrowolski, Niesman and Sibley, 1997). Unlike the actin of model eukaryotes, apicomplexan actins are only able for form short filaments *in vitro* (Schmitz *et al.*, 2005; Pospich *et al.*, 2017). Similar to the conserved role of F-actin in cell motility by model eukaryotes, *T. gondii* F-actin contributes to tachyzoite

gliding motility, with actin KO tachyzoites showing reduced and significantly impaired ability to attach to collagen (Whitelaw *et al.*, 2017). *T. gondii* F-actin is also critical for tachyzoite growth and replication. During endodyogeny, the inheritance of an apicoplast by each daughter tachyzoite is dependent of actin, formin 2, and myosin F (Andenmatten *et al.*, 2013a; Heaslip, Nelson and Warshaw, 2016; Stortz *et al.*, 2019; Tosetti *et al.*, 2019a). Tachyzoites establish an extensive F-actin network in the vacuole's residual body that is used for intravacuolar, intercellular communication and protein trafficking (Frénal *et al.*, 2017; Periz *et al.*, 2017, 2019).

1.5.a.ii Nuclear actin

Whilst model eukaryotes distribute the majority of actin to the cytoplasm, a small amount is imported into the nucleus by importin 9 (Dopie *et al.*, 2012). In recent years, the volume of evidence for the many roles of nuclear actin has grown. Despite this, specific mechanisms are often lacking and required further interrogation.

Observations of F-actin formation within the nucleus have linked it with various processes. A burst in nuclear F-actin polymerisation was found at the exit of mitosis into G_1 phase, without which chromosomes do not de-condense fully (Baarlink *et al.*, 2017). A similar burst in nuclear F-actin has been observed in CD4+ T cells that make cell-to-cell contact with B cells (Tsopoulidis *et al.*, 2019). Nuclear F-actin, along with the formin mDia2, restrict centromere movement to facilitate CenH3 deposition (Liu, Zhu and Mao, 2018). Moreover, F-actin has been demonstrated to enable the movement of DNA double strand breaks to the nuclear periphery, without which efficient DNA repair does not occur (Caridi *et al.*, 2018).

The roles of nuclear actin are not confined to F-actin though. G-actin has long been known to co-precipitate with RNA polymerases (Egly *et al.*, 1984), an association that has more recently been shown to include nuclear myosin 1 (Almuzzaini *et al.*, 2015, 2016). Whilst the transcriptional rate of RNA polymerases without associated actin is abrogated, the mechanism behind this has not been described. Nuclear G-actin also associated with several chromatin remodelling complexes. As stated, several the Ino80 and SWI/SNF subfamilies of SNF2 chromatin remodellers feature HSA domains that recruit actin family proteins, including ATP-bound G-actin (Eustermann *et al.*, 2018). In addition, nuclear G-actin is also associated with histone acetylation, being a component of the NuA4 histone acetyltransferase complex as well as by directly binding and inhibiting the activity of KAT14 (Viita *et al.*, 2019; Qu *et al.*, 2022).

Using the actin Chromobody®, it has recently been demonstrated that *Plasmodium berghei* nuclear F-actin has a role in DNA segregation as male gametes bud from their host erythrocyte (Hentzschel *et al.*, 2023). An ARP2/3-like complex composed of *P. berghei* actin-related proteins ALP5a and ALP5b, and accessory proteins ARPC1, ARPC2, and ARPC4 associates with the mitotic spindle microtubule organising centre and is required for the proper attachment of mitotic spindles to kinetochores. Beyond this no further characterisation of apicomplexan nuclear F-actin has taken place. However, given the presence of conserved chromatin remodelling complexes that, in model eukaryotes, include G-actin as a component, it would be of merit to further investigate the possible roles of nuclear F-actin in *T. gondii*.

1.5.b Actin-related proteins

Beyond F-actin-forming conventional actin proteins, the actin family of proteins also includes the actin-related proteins (ARPs). Unlike the highly conserved conventional actins, ARPs are only moderately conserved, typically presenting between 30 and 70% sequence homology compared to conventional actin (Oma and Harata, 2011). They do, however, retain actin's domain structure as well as the ATP-binding pocket. The naming convention of ARPs is based on the *Saccharomyces cerevisiae* ARPs, which were designated ARP1 through ARP10 based on descending homology to *S. cerevisiae* conventional actin (Poch and Winsor, 1997).

The functions of ARPs are diverse. ARP2 and 3 together form the ARP2/3 complex, responsible for binding to F-actin filaments to nucleate branching filaments (Pollard, 2007). ARP1 is part of the dynactin complex that interacts with microtubules and ensures correct orientation of the mitotic spindles during mitosis (Kahana *et al.*, 1998). Several ARPs localise to the nucleus, such as ARP4, ARP6, and ARP8, and are constituents of several chromatin modifying complexes, such as NuA4 histone acetyltransferase complex (Galarneau *et al.*, 2000), the SWR1 complex (Krogan *et al.*, 2003; Mizuguchi *et al.*, 2004b), and the INO80 complex (Shen *et al.*, 2000). Both ARP4 and ARP6 are widely conserved and distributed across eukaryotes (Muller *et al.*, 2005)

In apicomplexans, an initial comparative genomics study identified 10 and 9 putative ARPs in *T. gondii* and *P. falciparum* respectively (Gordon and Sibley, 2005). However, phylogenetic analysis suggested that for both species, only ARP1, ARP4, and ARP6 were conserved between these two apicomplexans and *S. cerevisiae* **(Table 1.5.1)**. As such, the authors elected to designate those proteins without a direct *S. cerevisiae* homologue as actin-like proteins (ALPs). However, it should be noted that neither the neighbour joining nor maximum parsimony phylogenetic trees presented by Gordon and Sibley were

well resolved, with the presence of multifurcating nodes suggesting ambiguity as to the trees' interpretation. In addition, there is a disparity between the gene names assigned by Gordon and Sibley, and the present genome annotation for *T. gondii* **(Table 1.5.1)**, with the basis behind the latter not apparent. All gene names stated hereafter will refer to the present genome annotation, not the gene names assigned by Gordon and Sibley.

Functional characterisation of apicomplexan ARPs is largely limited to three studies. A forward genetic screen to create *T. gondii* temperature-sensitive mutants led to the creation of an ARP4a mutant where, when cultured at 40°C, ARP4a mis-localised from the nucleus to the cytoplasm (Suvorova *et al.*, 2012). The absence of ARP4a in the nucleus resulted in a chromosome segregation phenotype, where DNA failed to segregate into daughter cells despite normal centrosome duplication and localisation. It was later shown that centromeres still clustered normally in the absence of nuclear ARP4a when visualised by the centromere-specific histone CenH3 (Francia *et al.*, 2020b). In *P. falciparum*, chromatin-associated ARP4 was largely localised to centromere boundaries and was associated with H2A.Z histone variant exchange and the H3K9ac histone modification (Liu *et al.*, 2020). Together these studies suggest that apicomplexan ARP4 has a strong role in centromere maintenance within the context of chromosomal segregation during replication. However, some apicomplexans, such as *T. gondii* but notably not *P. falciparum*, have two homologues of *S. cerevisiae* ARP4. In *T. gondii* these are currently annotated as ALP2a and ARP4a **(Table 1.5.1)**. Why *T. gondii* has two ARP4 proteins, and whether they have divergent functions, is an open question. As stated, an ARP2/3-like complex was recently described as having a critical role in nuclear segregation by *P. berghei* male gametes during budding from their host erythrocyte (Hentzschel *et al.*, 2023). Composed of a ALP5a and ALP5b heterodimer, and associated accessory proteins ARPC1, ARPC2, and ARPC4, this ARP2/3-like complex visually associated with the mitotic spindles. Co-immunoprecipitation showed that the complex interacts with AKiT7 of the kinetochore, and the visualisation of F-actin colocalised with the mitotic spindles suggests that the ARP2/3-like complex may nucleate F-actin formation in the nucleus during mitosis. The independent KOs of ARPC1, ARPC2, and ALP5b each resulted in the failure of male gametes to inherit a full complement of chromosomes. Moreover, this phenotype was phenocopied in male gametocytes treated with the F-actin depolymerising cytochalasin D. However, mitotic spindle segregation appeared to be unaffected by the KOs, indicating the role of the ARP2/3-like complex and nuclear F-actin is limited to the attachment of kinetochores to mitotic spindles. Using FoldSeek for the comparison of AlphaFold predicted protein structures (Varadi *et al.*, 2022; van Kempen *et al.*, 2023), the protein structures most similar to *P. berghei* ALP5a and ALP5b (PBANKA_0811800,

PBANKA_1007500) in *T. gondii* are ALP9a (TGCAST_234670, probability 1.0, E-value $1.12e^{-21}$) and ALP9b (TGVEG_269240, probability 1.0, E-value $4.94e^{-28}$), respectively. Note that this search was performed using all *T. gondii* strains because the availability of AlphaFold structural predictions varies between strains.

Table 1.5.1: Comparison of the ARPs in *S. cerevisiae* and *T. gondii*

S. cerevisiae	***T. gondii***				
	Gordon & Sibley, 2005	**Present annotation**	**Accession**	**Phenotype Score (Sidik et al., 2016)**	**Predicted Localisation (Barylyuk et al., 2020)**
ARP1	ARP1	ARP1	TGME49_248630	-1.82	Cytosol
	ALP1	ALP1	TGME49_219280	-2.53	Cytosol
ARP2					
ARP3					
	ALP2a	ALP3b	TGME49_248890	-4.54	Nucleus - chromatin
	ALP3	ALP4	TGME49_221410	-1.50	No data
ARP4	ARP4a	ARP4a	TGME49_253040	-4.16	Nucleus - chromatin
	ARP4b	ALP2a	TGME49_258050	-4.44	Nucleus - chromatin
ARP5					
ARP6	ARP6	ALP5		-5.04	No data
ARP7					
	ALP8	ALP7	TGME49_294850	-0.59	No data
ARP8					
ARP9					
	ALP9a	Actin-like family protein	TGME49_234670	-2.59	No data
	ALP9b	Actin-like family protein	TGME49_269240	-0.37	No data
ARP10					

1.5.c Visualising actin filaments

Due to its dynamic nature, the live visualisation of F-actin in living cells through fluorescence microscopy is the methodology of choice. The labelling of F-actin in fixed samples either through α-actin antibodies or epitope tagging of actin monomers is possible but only limited information from a fixed moment of F-actin can be gained. For the live visualisation of F-actin in model eukaryotes, a number of methodologies are available (Melak, Plessner and Grosse, 2017). Actin monomers can be tagged with fluorescent proteins, but this has the caveats of high background fluorescence and in interference of F-actin formation. Phalloidin, consisting of fluorescently labelled phallotoxin form the death cap mushroom (*Amanita phalloides*) is a highly specific F-actin marker, but is not fully cell

permeable and so more commonly used with fixed cells. LifeAct consists of a short peptide sequence from *S. cerevisiae* actin-binding protein 140, however it recognises both F- and G-actin. Another actin binding protein, utrophin from *H. sapiens*, has also been used for F-actin visualisation and has the advantage over LifeAct in that it does not bind G-actin, but it has been shown to artificially stabilise F-actin and affect actin dynamics. SiR-actin is a cell-permeable synthetic F-actin dye that is based on jasplakinolide from the marine sponge *Jaspis johnstoni*. As a drug, jasplakinolide binds and stabilises F-actin, properties that SiR-actin shares. The paratopes of camelid antibodies are made from a single peptide, unlike the paratopes of other mammals that are made from both heavy and light chain peptides folded together. This has allowed the V_HH domain of alpaca (*Vicugna pacos*) antibodies to be used as nanobodies termed Chromobodies®. Compared to other actin probes, the actin Chromobody® shows reduced interference of actin dynamics but has the caveats that it has some affinity for G-actin and that the fluorophore used is constitutively fluorescent.

The visualisation of apicomplexan F-actin has historically proven difficult due to the divergence of apicomplexan actins from other eukaryotic actins. Various antibodies have been raised against apicomplexan actins, which show anti-actin specificity when used for western blotting, do not work well for the visualisation of F-actin in fixed *T. gondii* samples by immunofluorescence assay (Whitelaw, 2017). Moreover, from the live F-actin labelling technologies described above, only the actin Chromobody® has the ability to bind to *T. gondii* F-actin (Periz *et al.*, 2017). As such, to date all fluorescence microscopy-based visualisation of *T. gondii* F-actin to characterise its functions has utilised the actin Chromobody®.

1.6 Reverse genetic technologies used in *T. gondii* research

1.6.a Genetic modification approaches

T. gondii is tractable to genetic modification. The transfection of expression plasmids in tachyzoites is long established and routine (Soldati and Boothroyd, 1993). Gene cassettes encoded on episomal plasmids are expressed, but the plasmids are not replicated, and so episomal expression is transient, lasting up to 72 hours. *T. gondii* is capable of both homologous recombination and non-homologous end joining for DNA repair. Thus homologous recombination can be exploited for targeted genetic modifications via double cross over (Donald and Roos, 1993), the efficiency of which is further improved in Δ*ku80* tachyzoites that are non-homologous end joining incompetent (Huynh and Carruthers, 2009).

When cloning constructs to be integrated into the *T. gondii* genome by homologous recombination, ligation-independent cloning (LIC) has been the historical method of choice over restriction enzyme-based cloning since it is scarless (Aslanidis and de Jong, 1990). More recently, however, the Cas9 nuclease has been used for the introduction of creating targeted double strand breaks that are subsequently repaired by homologous recombination using a provided, bespoke repair template (Shen *et al.*, 2017).

1.6.b Technologies for creating conditional null mutants

Various technologies for creating *T. gondii* conditional null mutants have been established **(Table 1.6.1)**. Conditional knockouts can be created through both the DiCre and splitCas9 systems (Andenmatten *et al.*, 2013a; Li *et al.*, 2022). Transcript knockdowns can be achieved using the TATi or U1 systems (Meissner, Schlüter and Soldati, 2002; Pieperhoff *et al.*, 2015).

For creating conditional KD mutants, this study made use of the auxin-inducible degron system (AID) (Nishimura *et al.*, 2009; Brown, Long and Sibley, 2018). AID makes use of the Tir1 (F-box transport inhibitor response 1) protein from rice (*Oryza sativa*) and IAA17 degron from *Arabidopsis thaliana* (referred to as the AID domain). The AID domain is fused to the protein of interest while the Tir1 is freely expressed in the cytoplasm. Upon the addition of auxin (indole-3-acetic acid, IAA), the Tir1 binds to the AID domain on the protein of interest and recruits the ubiquitin ligase complex. The E3 ubiquitin ligase ubiquitinates the AID domain with the AID domain and fused protein of interest subsequently degraded by the proteasome.

Table 1.6.1: The technologies utilised for creating *T. gondii* conditional KO and KD mutants

Technology	**TATi**	**DiCre**	**U1**	**splitCas9**	**AID**
Principle	Transcriptional silencing	Gene excision	mRNA degradation	Gene disruption	Protein degradation
Advantages	Reversible	Full KO	Fast Reversible	Minimal cloning	Fast Reversible
Disadvantages	Promoter exchange means altered expression level	Relies on natural protein turnover Inefficient excision	Not widely adopted	Relies on natural protein turnover Failure to repair double strand break results in apoptotic-like phenotype	Target protein might not tolerate AID domain Leakiness can cause partial KD without inducing

1.7 Aim of study

Apicomplexans including *T. gondii* rely on variable gene expression for both replication and lifecycle progression. Comparative genomics has demonstrated that the nucleus of *T. gondii* contains both conserved and novel, lineage-specific proteins. Whilst significant progress has been made in defining the roles of the ApiAP2 transcription factor family and histone post-translational modifications, the contributions of other nuclear factors remain to be explored. This study sought to improve our understanding of nuclear dynamics within the context of *T. gondii* tachyzoite replication through endodyogeny through the parallel functional characterisation of nuclear actin-related proteins, nuclear F-actin, and SNF2 chromatin remodellers.

The specific questions that this study aimed to answer were:

- Why does *T. gondii* encode two ARP4 homologues, ALP2a and ARP4a, and do they have divergent functions?
- What is the mechanism behind the previously described nuclear segregation phenotype described in an ARP4a null mutant?
- What are the roles of the other nuclear ARPs, ALP3b and ALP5?
- Is actin imported into the *T. gondii* nucleus and does it polymerise into F-actin?
- How do conserved SNF2 chromatin remodellers contribute to the growth of *T. gondii* tachyzoites?

2 Results

2.1 Adapting skip peptide technology to permit drug-selectable endogenous knock-ins with endogenous expression in *T. gondii*

For the purpose of visualising proteins within a cell, researchers often choose endogenous tagging, where an exogenous marker protein or peptide is used to tag the endogenous gene of interest. Epitope tags (haemagglutinin, myc, FLAG, etc.) are often utilised where no antibody against the target protein exists, whilst the fusion of a fluorescent protein (GFP, mCherry, etc.) with the protein of interest facilitates live-cell microscopy. Endogenous, C-terminal tagging of a gene of interest has the caveat that the endogenous 3'UTR (untranslated region) is supplanted by an exogenous 3'UTR **(Figure 2.1.1a)** (Roos *et al.*, 1997; Huynh and Carruthers, 2009)**,** potentially causing changes in expression levels. In *T. gondii*, various exogenous 3'UTRs have been used for this purpose, the most common being that of *T. gondii*'s *dhfr* and *sag1* gene. Whilst endogenous tagging can be achieved with WT *T. gondii*, the approach relies on homologous recombination and is most efficient when performed in Δ*ku80* transgenic strains, which are non-homologous end joining deficient (Huynh and Carruthers, 2009). To overcome and optimise endogenous tagging, it was decided to adapt a 2a self-cleaving peptide (Ryan, King and Thomas, 1991) (hereafter referred to as skip peptide) technology for use in creating *T. gondii* knock-ins. Utilised by various viruses, skip peptides are short amino acid sequences that cause ribosomes to skip a single peptide bond (Liu *et al.*, 2017). Thus, a single polycistronic mRNA molecule can encode for multiple proteins. Here, the T2A skip peptide from the *Thosea asigna virus* was used to polycistronically express drug resistance genes on the same transcript as the protein of interest, whilst maintaining the endogenous expression level of the protein of interest **(Figure 2.1.1b),** in a similar manner to selection-linked integration used for endogenous tagging in *P. falciparum* (Birnbaum *et al.*,

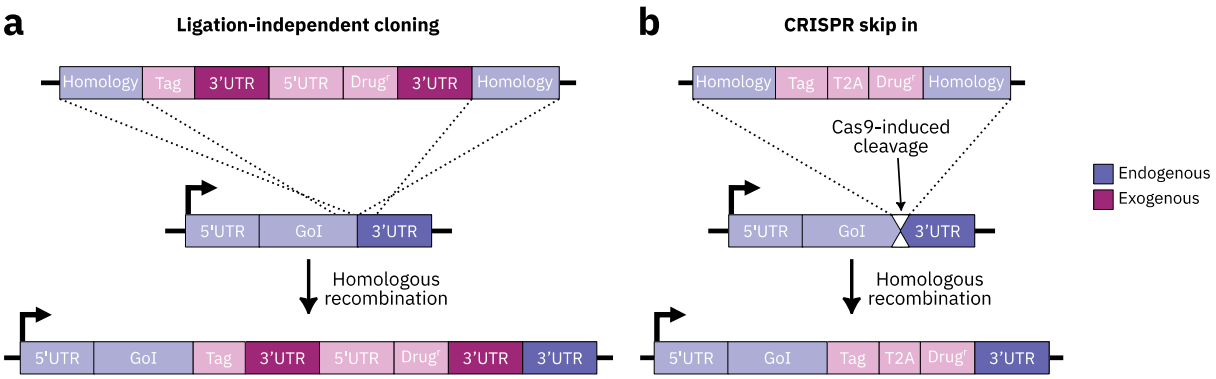

Figure 2.1.1: Comparison of historically used and newly adapted drug-selectable knock-in approaches. Ligation-independent cloning, where the endogenous 3'UTR is supplanted. Drug^r indicates drug resistance marker. 3'UTRs shown with deeper colour for emphasis. Both approaches are performed in Δ*ku80 T. gondii*.

2017).. Simultaneously, CRISPR/Cas9-based HiT (high-throughput tagging) was adopted (Smith *et al.*, 2022).

This approach, hereafter termed CRISPR-skip-in, works as follows **(Figure 2.1.1b)**:

1. In a Δ*ku80 T. gondii* strain, Cas9 and a sgRNA along with repair template DNA are transiently transfected into tachyzoites.
2. The sgRNA targets the Cas9 to a region proximal to the STOP codon of the gene of interest, where the latter cleaves the DNA to cause a double strand break.
3. The homologous recombination DNA repair mechanism detects homology regions on the repair template DNA and uses it as a template for repair the double strand break.
4. The gene of interest is now endogenously tagged and the drug resistance marker is expressed as a separate protein due to the T2A skip peptide.

One predicted shortcoming of CRISPR-skip-in was that the expression of the protein of interest might be too low to produce sufficient drug resistance marker to confer drug resistance. Therefore, three drug resistance markers that are typically utilised for knock-in tagging of endogenous proteins were tested:

- HXGPRT (hypoxanthine-guanine-phosphoribosyl transferase) (Donald and Roos, 1998)
- DHFR-TS (dihydrofolate reductase-thymidylate synthase) (Donald and Roos, 1993)
- CAT (chloramphenicol acetyltransferase) (Kim, Soldati and Boothroyd, 1993)

The endogenous HXGPRT expression could be used as an approximate reference of the required HXGPRT expression for use with CRISPR-skip-in. ~92% of *T. gondii* genes expressed in tachyzoites have lower mRNA expression compared to *hxgprt* **(Figure 2.1.2)** (Waldman *et al.*, 2020). It was therefore likely that a given target gene for endogenous tagging with CRISPR-skip-in using HXGPRT would express the HXGPRT at a level lower than that of WT *T. gondii*. The extent to which *hxgprt* expression could be lowered but still confer resistance to MPA was not known and had to be experimentally tested. Note that HXGPRT's use as a drug resistance marker for CRISPR-skip-in is therefore to Δ*hxgprt* transgenic *T. gondii* strains. The DHFR-TS resistance marker confers resistance to pyrimethamine, and the gene used in this approach was originally derived from the *T. gondii* gene. However, since *T. gondii* is susceptible to pyrimethamine, the gene was mutated to allow it to confer pyrimethamine resistance (Donald and Roos, 1993). Consequently, it was considered unlikely that the expression level of *dhfr* was representative of the required *dhfr-ts* required to confer pyrimethamine resistance, and that this would have to empirically determined through trial and error.

HXGPRT, DHFR, and CAT were all tested with CRISPR-skip-in, and all were successful to varying degrees. DHFR proved extremely efficacious when used with CRISPR-skip-in. Almost all knock-in attempts were successful, with the lowest expressed, successfully knocked-in gene (TGME49_205562) having a TPM (transcript per million) of 4.26, placing it in the lowest quartile of expressed transcripts **(Figure 2.1.2)**. The use of DHFR with CRISPR-skip-in was successful for all target genes, meaning the lower limit of *dhfr-ts* expression that confers pyrimethamine resistance remains to be determined. *hxgprt* has an endogenous mRNA expression of 243.01 TPM but using CRISPR-skip-in with continuous drug selection an expression of 62.75 TPM was sufficient to confer drug selection. Below this expression level, knocked-in *T. gondii* did not fatally succumb to drug selection, but their growth was severely retarded. However, once drug selection was removed following 10 days' treatment the tachyzoites growth returned to normal. With this time-limited drug selection, the knock-in of TGME49_205562 was also possible. In the six attempts at CRISPR-skip-in using CAT only one attempt was successful. This was because the CAT did not fully kill susceptible *T. gondii*, so drug-resistant but knock-in negative *T. gondii* were obtained. Moreover, in the single successful attempt, the pool of drug-resistant *T. gondii* was a heterogenous, with both WT and knocked-in *T. gondii* present. As such, CAT was not considered suitable for use with CRISPR-skip-in. It was therefore concluded that, at a minimum, endogenous tagging using CRISPR-skip-in with HXGPRT or DHFR is applicable to > 75% of *T. gondii* tachyzoite genes. Moreover, the anecdotal experience of the *hxgprt* transcript expression

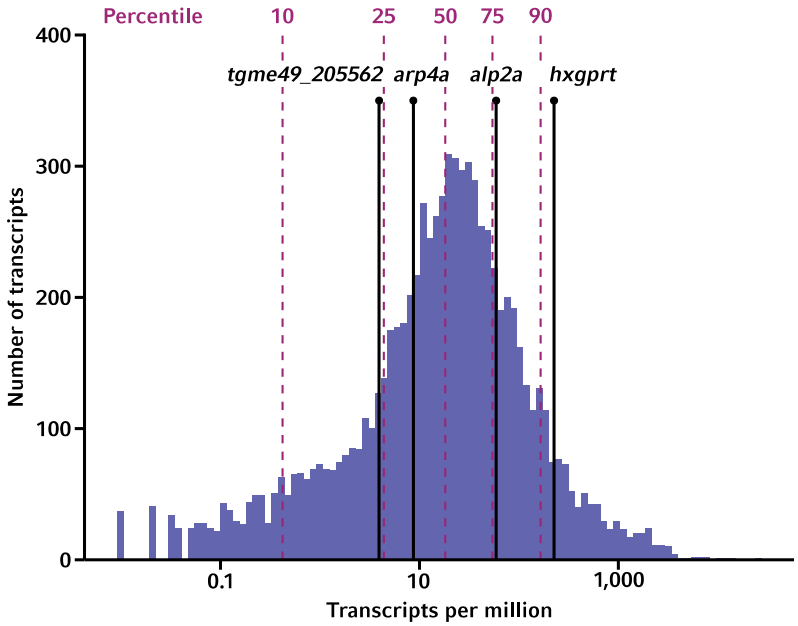

Figure 2.1.2: Transcript abundancy in *T. gondii* tachyzoites.

Histogram of RNAseq TPM values from Waldman *et al.*, 2020. Percentiles are represented with dashed magenta lines. Expression of *hxgprt* and other genes relative to this study that were tagged using CRISPR-skip-in are shown with horizontal black lines.

required for normal tachyzoite growth under MPA selection can be used as a reference for deciding the best MPA treatment strategy when using CRISPR-skip-in with HXGPRT.

2.2 Both ALP2a and ARP4a are required for *T. gondii* tachyzoite growth

2.2.a Generation of inducible knockdown strains for ALP2a and ARP4a

For the purpose of interrogating ALP2a and ARP4a function, it was decided to make use of the auxin-inducible degron (AID) system (Nishimura *et al.*, 2009; Brown, Long and Sibley, 2018) for creating protein knockdowns (KDs). Using CRISPR-skip-in, ALP2a and ARP4a were C-terminally tagged with *linker-mAID-3HA-T2A-hxgprt*. To confirm that the knock-ins were successful, genotyping PCRs were performed with primers that flanked the STOP codons of ALP2a and ARP4a **(Figure 2.2.1a)**. The expected shift in PCR product sizes confirmed the knock-in of the mAID construct **(Figure 2.2.1b)** and the strains are hereafter referred to as ALP2a iKD and ARP4a iKD. In parallel, ALP2a and ARP4a were separately tagged with *linker-3HA-T2A-hxgprt* to act as a control of normal expression, the integration of which was confirmed by genotyping PCRs as before **(Figure 2.2.1c)** and the strains termed ALP2a^{HA} and ARP4a^{HA}. To ensure that induction of the AID system with indole-3-acetic acid (IAA) led to the KD of ALP2a and ARP4a, quantitative western blotting was performed. In both cases, protein levels were undetectable or nearly undetectable from four hours after induction **(Figure 2.2.2)**. However, in the case of ALP2a, the mAID alone, without the addition of IAA, caused a ~75% reduction in protein levels when compared to ALP2a^{HA}. As discussed below, this mAID-associated reduction in ALP2a expression may account for a background phenotype seen in the strain without IAA treatment.

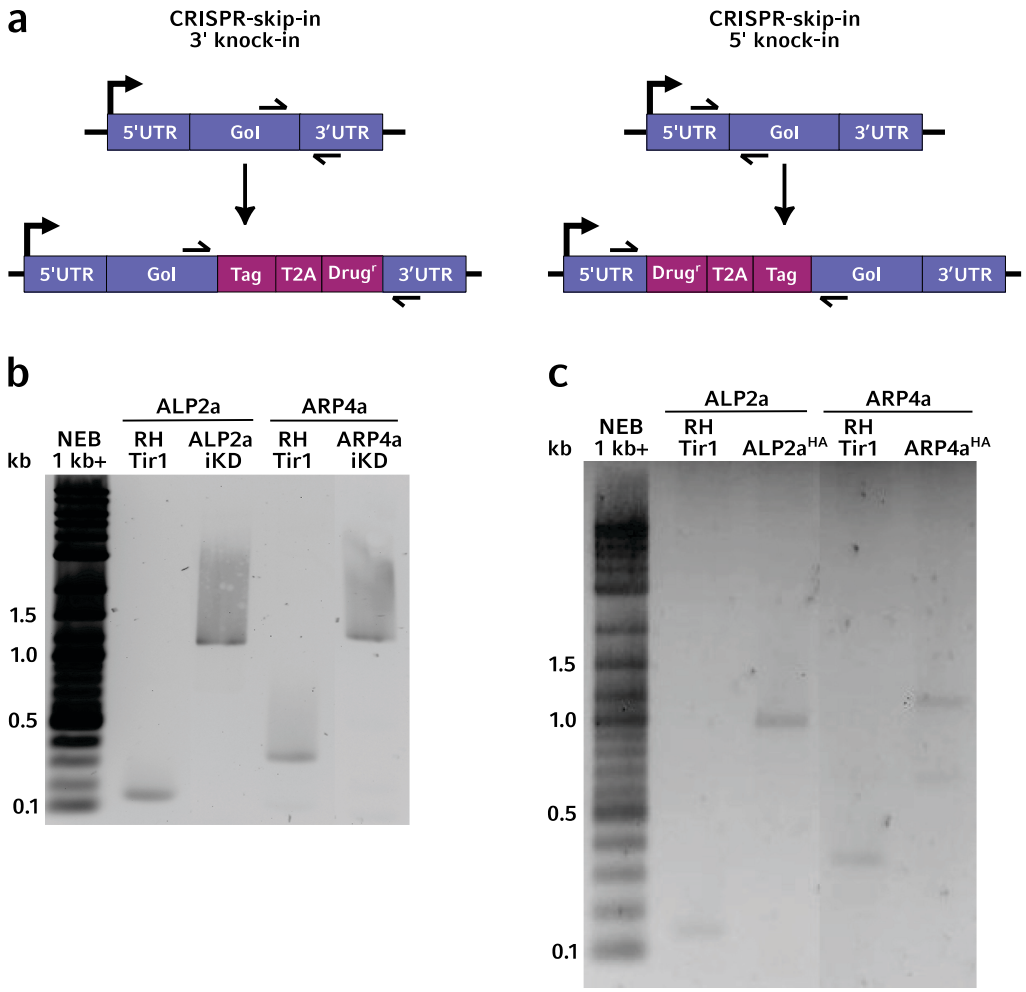

Figure 2.2.1: Genotyping to confirm CRISPR-skip-in knock-ins.

a. Diagrammatic overview of genotyping PCRs used throughout this study, showing PCR primer annealing sites, to confirm successful knock-ins following endogenous tagging with CRISPR-skip-in. Since CRISPR-skip-in was utilised for both 5‘ and 3‘ knock-ins during this study, the primer annealing sites for both approaches are shown.

b. Genotyping PCRs showing 3‘ integration of *linker-mAID-3HA-T2A-hxgprt* to create ALP2a iKD and ARP4a iKD strains. Expected ALP2a 3‘ amplicon sizes were 0.147 kb in WT (RH Tir1) and 1.3 kb in ALP2a iKD. Expected ARP4a 3‘ amplicon sizes were 0.37 kb in WT (RH Tir1) and 1.5 kb in ARP4a iKD.

c. Genotyping PCRs showing 3‘ integration of *linker-3HA-T2A-hxgprt* to create ALP2a^{HA} and ARP4a^{HA} strains. Expected ALP2a 3‘ amplicon sizes were 0.147 kb in WT (RH Tir1) and 1 kb in ALP2a^{HA}. Expected ARP4a 3‘ amplicon sizes were 0.37 kb in WT (RH Tir1) and 1.2 kb in ARP4a^{HA}.

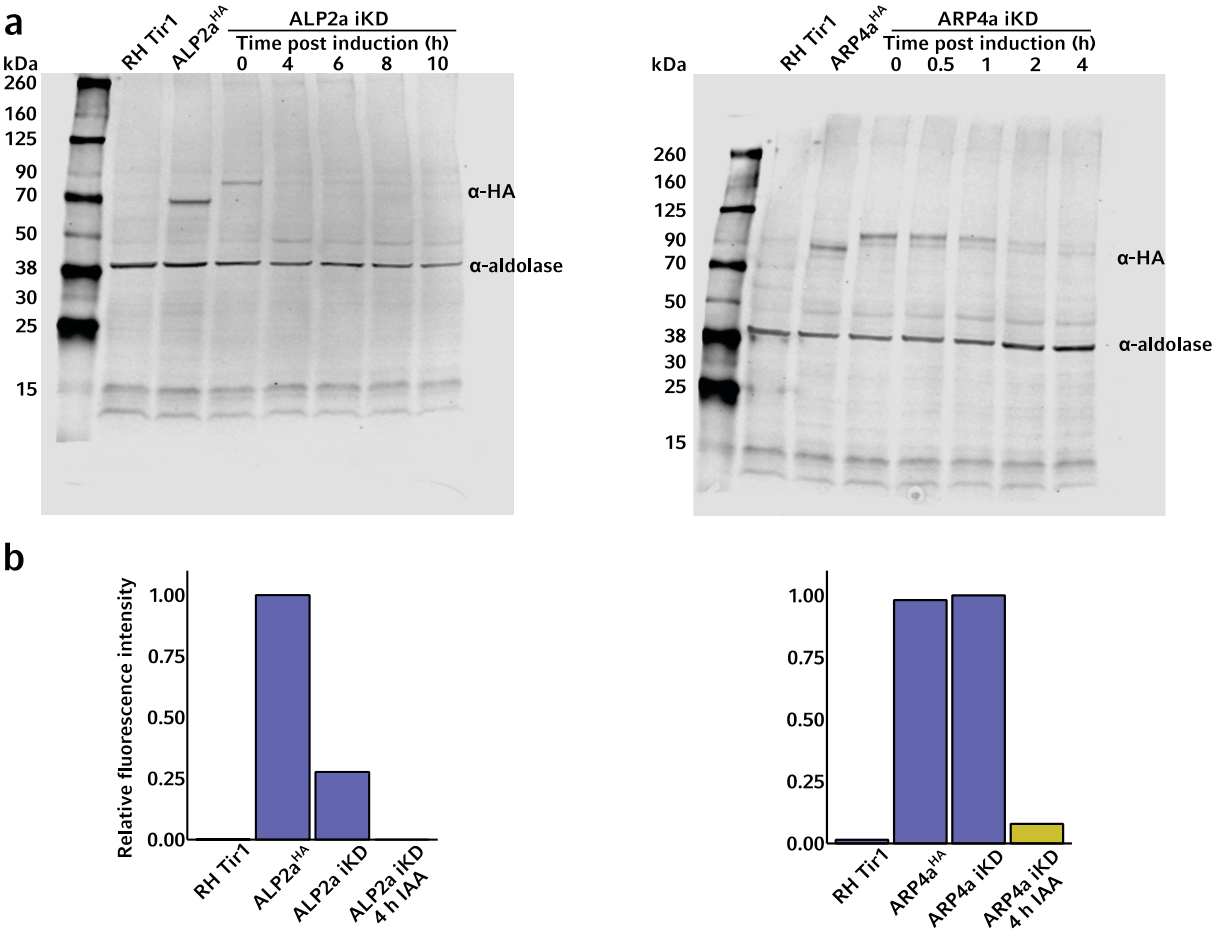

Figure 2.2.2: The knockdown of ALP2a and ARP4a following treatment with IAA.

a. Time course fluorescence western blots showing the effect of IAA treatment on ALP2a and ARP4a expression in the strains ALP2a iKD (left) and ARP4a iKD (right). 90 μg of protein was loaded per lane. Parental strain RH Tir1 included as control. Blots were probed with α-HA and, as a loading control, α-aldolase. Predicted protein molecular weights were 47 kDa aldolase, 73 kDa ALP2a^{HA}, 95 kDa ALP2a$^{mAID\text{-}3HA}$ (ALP2a iKD), 89 kDa ARP4a^{HA}, 112 kDa ARP4a$^{mAID\text{-}3HA}$ (ARP4a iKD).

b. Quantification of a-HA band fluorescence signal intensity from western blots in a. Signal intensities were normalised to α-aldolase band and plotted relative to the respective HA-tagged strains. For ARP4a, both bands of the double band were used for quantification.

2.2.b ALP2a and ARP4a are both indispensable for *T. gondii* tachyzoite growth

To investigate the effect of ALP2a and ARP4a KD on the growth of tachyzoite growth, plaque and replication assays were performed. *In vitro* growth assays showed that the KD of either ALP2a or ARP4a completely abrogated the formation of plaques in HFF monolayers **(Figure 2.2.3a),** indicating that the tachyzoites were unable to complete their lytic cycle. To compare the growth rate of tachyzoites during the first lytic cycle, the mean vacuole stage was quantified in replication assays between 4- and 30-hours post KD induction. Vacuole stage means the number of tachyzoites per vacuole as the tachyzoites replicate in a $\log_2$ exponential fashion. In the case of ALP2a iKD, comparing the growth of IAA-treated

to non-treated *T. gondii*, a retarded growth rate began at 10 h post IAA addition **(Figure 2.2.3b)**. To better define the nature of this growth retardation, the relative frequency of each individual vacuole stage was compared per time point. This highlighted an over-representation of 2 and 4 stage vacuoles and an under-representation of ≥ 16 stage vacuoles **(Figure 2.2.3c)**. In contrast, the KD of ARP4a did not result in a significantly altered growth rate during the 30 hours examined **(Figure 2.2.3b)**. However, significantly fewer vacuoles had reached ≥ 32 stage compared to non-KD tachyzoites **(Figure 2.2.3c)**. Therefore, it was concluded that no complete cell death occurred within the first 30 hours of the lytic cycle following either ALP2a KD or ARP4a KD and that the lack of plaque formation indicated either growth arrest or loss of viability between the end of the first lytic cycle and the beginning of the second.

To better understand the lack of plaque formation following ALP2a KD and ARP4a KD, tachyzoite and vacuole morphology were visually assessed through widefield fluorescence microscopy. In the case of ARP4a KD, this presented a nuclear mis-segregation phenotype, as previously reported in a ARP4a

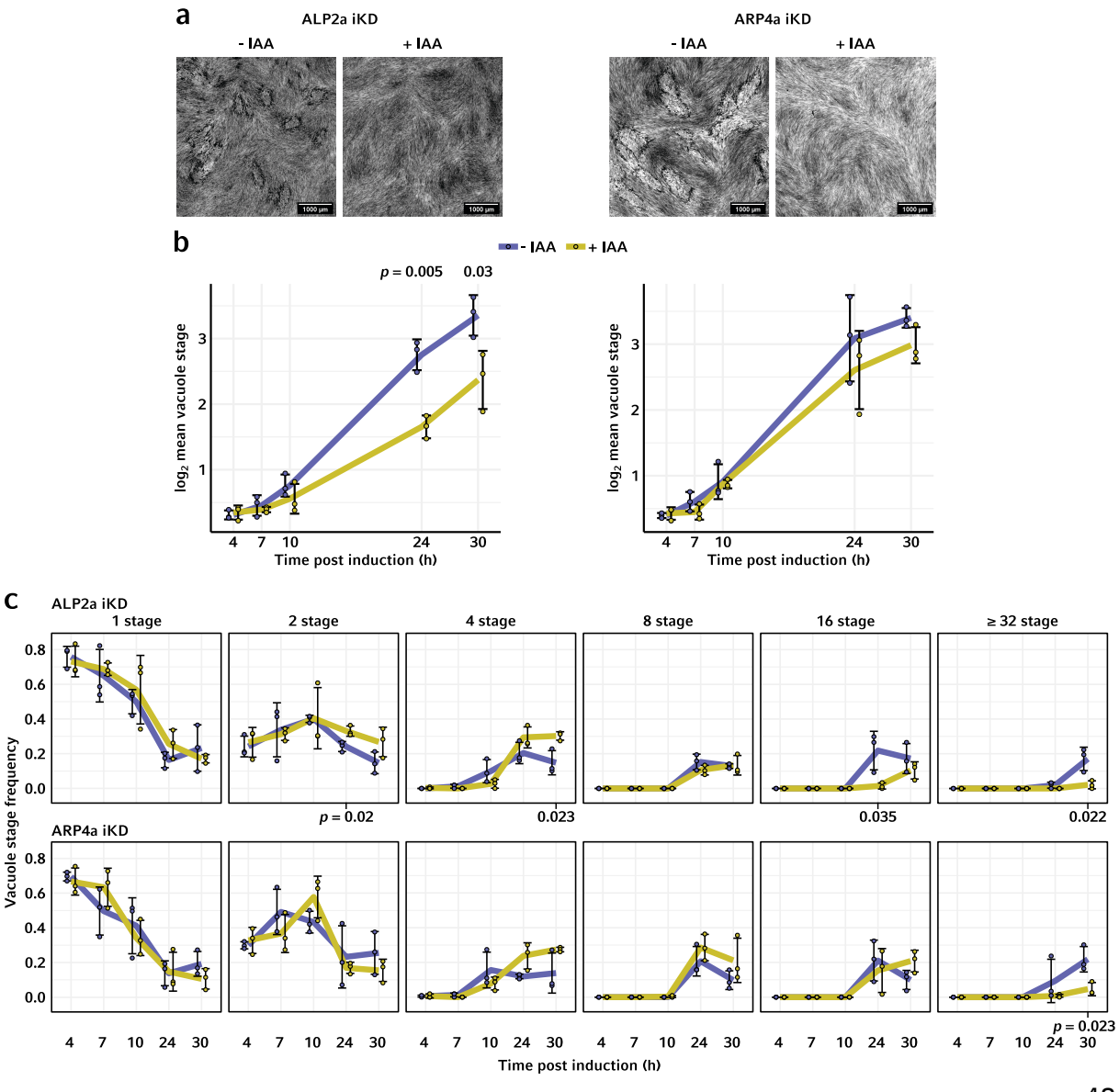

Figure 2.2.3: ALP2a and ARP4a KD are essential for multiple rounds of *T. gondii* tachyzoite lytic cycle.

a. Plaque formation by both ALP2a iKD and ARP4a iKD ± IAA following 7 days of culture. 1,000 tachyzoites per condition were inoculated onto HFFs. After 7 days of culture, cells were fixed with methanol, stained for DNA and protein, and imaged by brightfield microscopy.

b. Comparison of tachyzoite vacuole growth by ALP2a iKD and ARP4a iKD ± IAA during the first lytic cycle. Tachyzoites were allowed to invade HFFs for 1 hour in the absence of IAA before non-invaded tachyzoites were removed by washing and culture medium supplemented with ± 500 μM IAA. Assays were fixed between 4 and 30 hours and then cytoskeleton labelled by IFA using α-GAP45. The number of tachyzoites per vacuole was manually counted and used to calculate the mean vacuole stage (mean tachyzoites per vacuole) at each indicated time point. Error bars indicate standard deviation of three biological replicates. Result of Student's t-test shown where $p \leq 0.05$.

c. As b. but instead of mean vacuole stage, each panel represents a single vacuole stage with the data indicating the relative frequency of each vacuole stage per time point. Error bars indicate standard deviation of three biological replicates; result of Student's t-test shown where $p \leq 0.05$.

temperature-sensitive mutant (Suvorova *et al.*, 2012) **(Figure 2.2.4a)**, with daughter tachyzoites failing to inherit some or all nuclear DNA. ALP2a KD resulted in a similar phenotype, with irregularly shaped daughter tachyzoites formed and extracellular nuclei **(Figure 2.2.4a)**. However, for both ALP2a iKD and ARP4a iKD the presence of this nuclear mis-segregation phenotype was also found without KD induction of the KDs. In the case of ALP2a, it was unclear whether the presence of the phenotype in uninduced tachyzoites was a result of the ~75% reduction in ALP2a expression relative to the mAID-negative ALP2a^{HA} described above or another factor. Nuclear mis-segregation was evident from the first round of replication (7 hours post induction) with the severity of tachyzoite and vacuole disorganisation increase through the lytic cycle. The frequency of the nuclear mis-segregation phenotype was ~10-15% without IAA induction, rising to 50% and 80% with 30 hours of IAA treatment for ALP2a iKD and ARP4a iKD respectively **(Figure 2.2.4b)**.

2.2.c The expression of ALP2a and ARP4a are not co-dependent

That both ALP2a and ARP4a KDs resulted in highly similar nuclear mis-segregation phenotypes raised the question as to whether their own expression relies on that of the other. To investigate this possibility, co-tagged strains were created. Using CRISPR-skip-in, ARP4a was tagged with *linker-3FLAG-T2A-myc-DHFR* in the ALP2a iKD strain, and *vice versa*. The resulting strains were termed ALP2a iKD ARP4a^{FLAG} and ARP4a iKD ALP2a^{FLAG} and knock ins were confirmed by genotyping PCR **(Figure 2.2.5a)**. No stark change in ARP4a localisation was seen following ALP2a KD, nor with ALP2a after ARP4a KD **(Figure 2.2.5b)**. Quantification of the mean fluorescence signal per nucleus showed that ALP2a KD resulted in a small but significant decrease in mean fluorescence intensity of ARP4a **(Figure 2.2.5c)**. Contrastingly, ARP4a KD resulted in a small but significant increase in mean

fluorescence intensity of ALP2a **(Figure 2.2.5c)**. However, whether these small changes were biologically significant was not immediately apparent. Nevertheless, it was clear that the expression of neither ALP2a nor ARP4a was wholly dependent on the other.

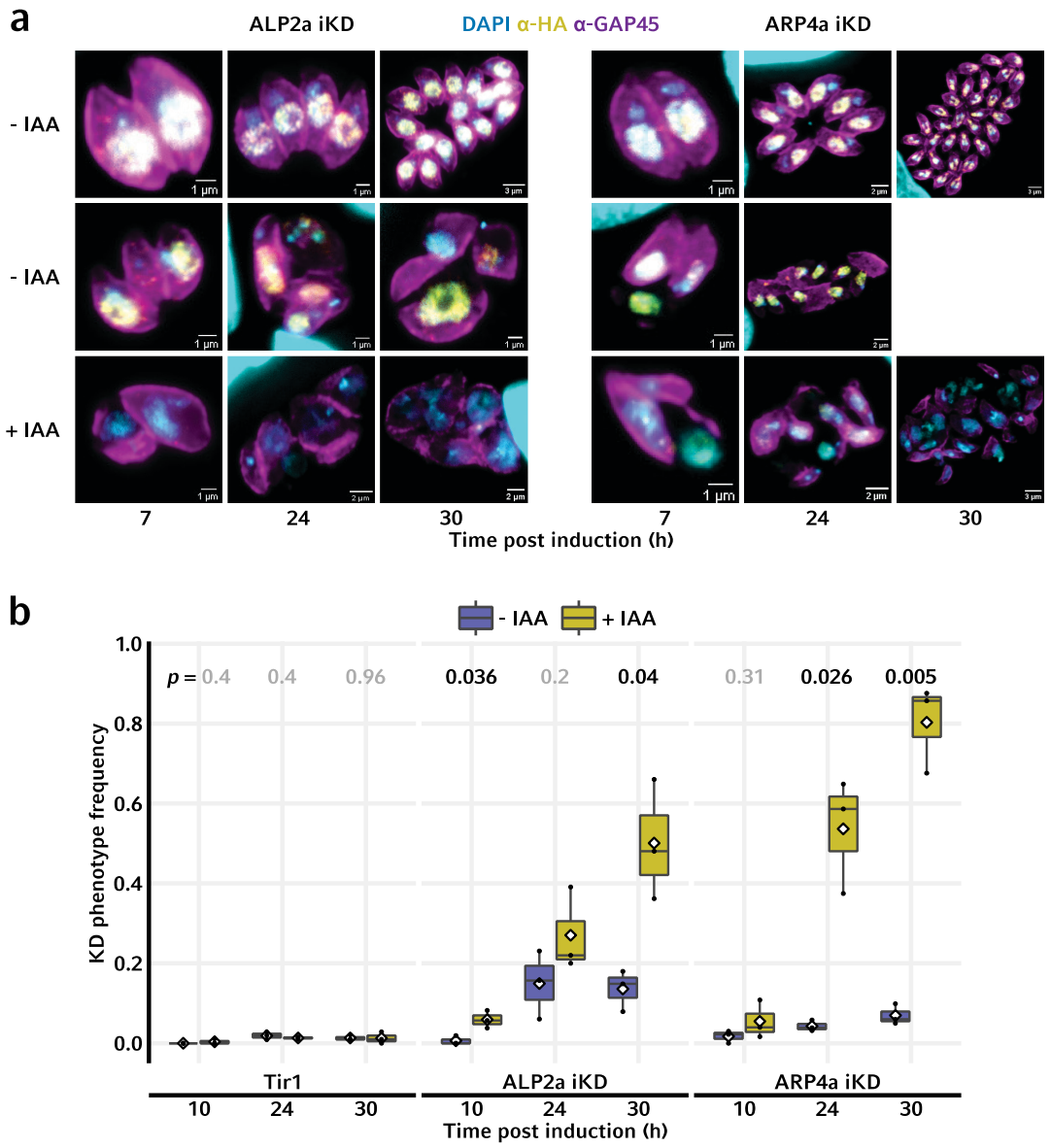

Figure 2.2.4: The KD of ALP2a and ARP4a both result in similar nuclear mis-segregation phenotypes.

a. Representative IFA widefield Z-max micrographs showing morphology of ALP2a iKD and ARP4a iKD vacuoles between 7- and 30-hours post induction. Tachyzoites were allowed to invade HFFs for 1 hour in the absence of IAA before non-invaded tachyzoites were removed by washing and culture medium supplemented with ± 500 μM IAA. Assays were fixed between 7 and 30 hours and labelled by IFA as indicated.

b. From a., the quantification of the number of vacuoles where ≥ 1 tachyzoite showed a nuclear mis-segregation phenotype for both ALP2a iKD and ARP4a iKD as well as parental RH Tir1 ± IAA treatment. Phenotype frequency was counted manually. Result of Welch's t-test shown.

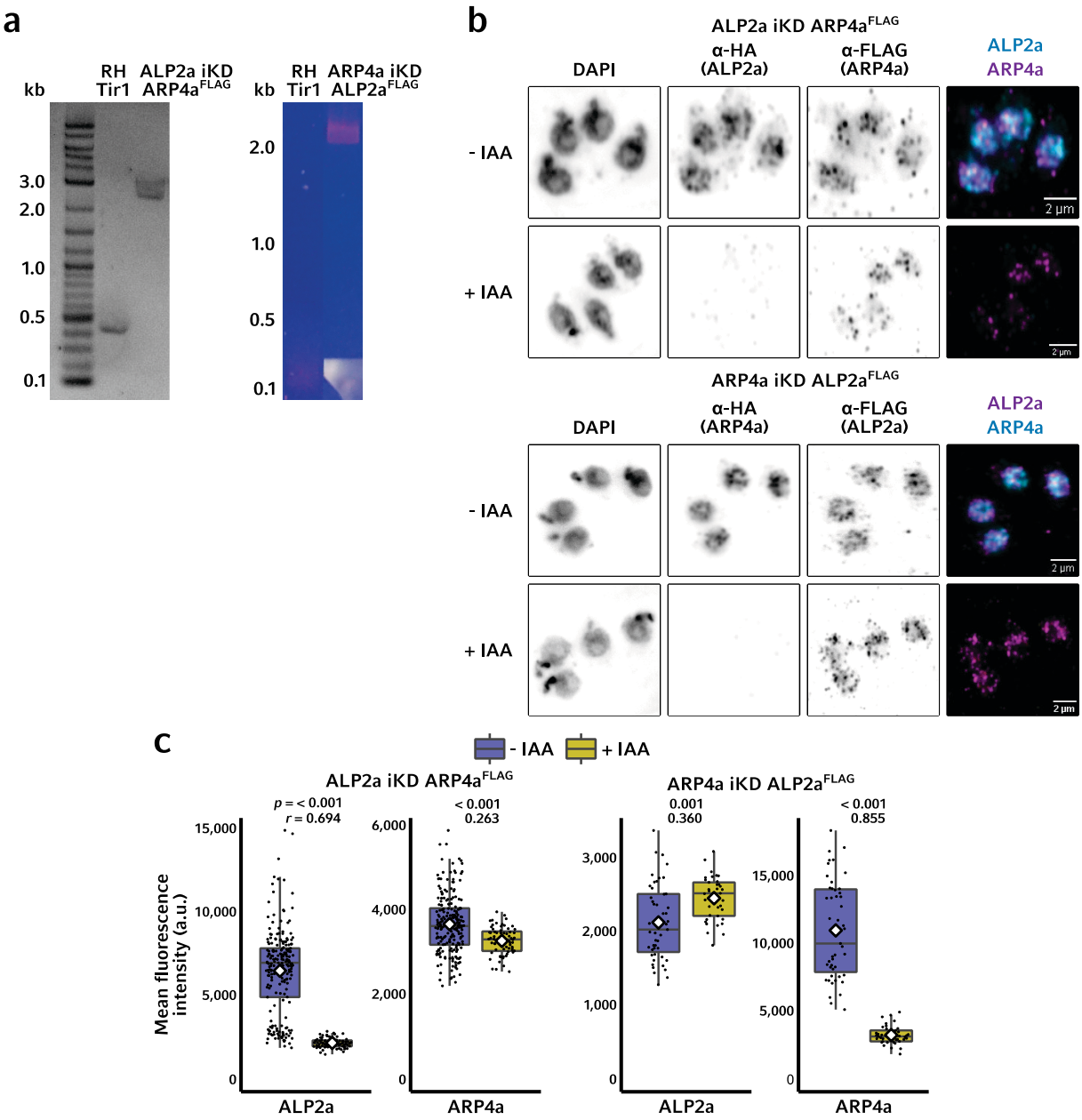

Figure 2.2.5: The KD of ALP2a or ARP4a has negligible impact on the expression of each other.

a. Genotyping PCRs showing 3‘ integration of *linker-3FLAG-T2A-dhfr* to create ALP2a iKD ARP4a^{FLAG} and ARP4a iKD ALP2a^{FLAG} strains. Expected ALP2a 3‘ amplicon sizes were 0.147 kb for WT (RH Tir1) and 2.2 kb for ALP2a^{FLAG}. Expected ARP4a 3‘ amplicon sizes were 0.37 kb for WT (RH Tir1) and 2.4 kb for ARP4a^{FLAG}.

b. Representative IFA widefield micrographs showing expression of ALP2a and ARP4a in co-tagged strains ± IAA. Tachyzoites were inoculated onto HFFs and cultured for 24 h ± 500 µM IAA before fixation and IFA labelling as indicated.

c. From b., quantification of ALP2a and ARP4a IFA mean fluorescence intensity per nucleus in co-tagged strains ± IAA treatment. Otsu’s thresholding was used to create a mask of the DAPI channel, with the MFI within the of α-HA and -FLAG channels within masks’ area quantified. Result of Wilcoxon rank sum test shown (*p* value) with effect size (*r* value).

2.3 Both ALP2a and ARP4a are required for the coordination of centrosome duplication during endodyogeny

2.3.a The nuclear mis-segregation phenotype following ALP2a KD and ARP4a KD does not arise from a failure of the mitotic spindle

To gain further insight into the mechanistic cause for nuclear mis-segregation following ALP2a KD and ARP4a KD it was decided to examine the spatial relationship and dynamics of components of the *T. gondii* mitotic machinery. The centrosome of *T. gondii* exhibits a dynamic localisation during replication. In S phase, prior to centrosome duplication, the centrosome translocates around the nucleus. In M phase, following centrosome duplication, the now two centrosomes repel one another to create sufficient separation for daughter cell IMC elongation. Prior to the commencement of centrosome segregation, the mitotic spindles have developed and attached to the kinetochores, establishing a physical link between the centrosomes, mitotic spindles, kinetochores, and the centromeres of the chromosomes **(Figure 2.3.1a)**. As such, the translocation of the centrosomes is mirrored by the attached mitotic machinery. Should the nuclear mis-segregation phenotypes following ALP2a KD and ARP4a KD have arisen from a failure of either mitotic spindle formation or attachment, it

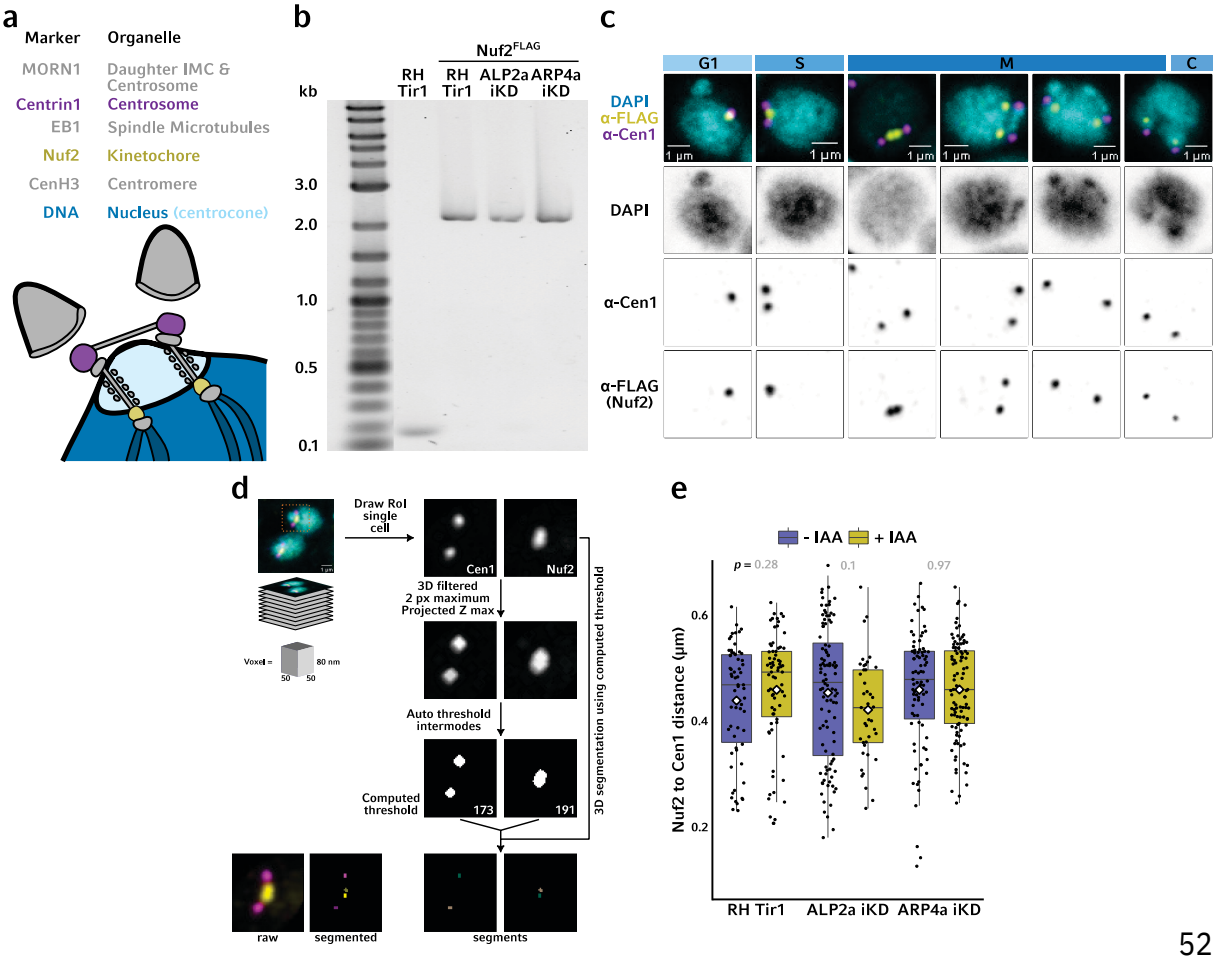

Figure 2.3.1: The spatial relationship between centrosomes and kinetochores is maintained following ALP2a KD and ARP4a KD.

a. Diagrammatic depiction of the mitotic machinery during normal *T. gondii* M phase. Duplication of centrosomes, DNA, and kinetochores has occurred as well as spindle attachment. The cytoskeleton of two daughter cells is elongating and centrosomes and the connected mitotic spindles, kinetochores, and DNA are segregating. Note that chromosomes do not condense during *T. gondii* mitosis and are only depicted this way for illustrative purposes.

b. Genotyping PCRs showing 3' integration of *linker-3FLAG-T2A-myc-dhfr* to create RH Tir1 Nuf2^{FLAG}, ALP2a iKD Nuf2^{FLAG}, and ARP4a iKD Nuf2^{FLAG}. Expected Nuf2 3' amplicon sizes were 0.14 kb for WT (RH Tir1) and 2.1 kb for Nuf2^{FLAG} strains.

c. Representative IFA confocal Z-sum micrographs depicting the spatial relationship between the centrosome (Cen1) and kinetochore (Nuf2) in RH Tir1 tachyzoites during the cell cycle. Tachyzoites were inoculated onto HFFs and cultured for 20 h before fixation and IFA labelling as indicated.

d. Image analysis workflow for segmentation to permit computation of spatial relationship between segmented Cen1 and Nuf2. From a Z-stack of confocal micrographs, RoIs around each tachyzoite's mitotic machinery was manually drawn. The channels of interest were filtered using a 2 pixel maximum 3D filter to improve contrast. Filtered micrographs were Z-max projected and thresholded using intermodes method. The resulting threshold pixel intensities were bespoke to each channel and RoI. The raw Z-stack micrographs were then 3D segmented using the computed threshold pixel intensity within a 3D iterative thresholding algorithm (3D ImageJ Suite). An iterative algorithm was used to produce conservative segments that would allow the detection of barely segregated foci as separate segments, as demonstrated in the Nuf2 example given.

e. Quantification of centroid-to-centroid distance of Nuf2 segments to their nearest Cen1 segment in tachyzoites with ≥ 2 centrosomes. Segmentation was performed as in d., and IFA as in c. with ± IAA. Result of Welch's t-test shown.

was hypothesised that the resulting loss of mirrored kinetochore movements would be detectable in changes of the distance between the centrosome and the kinetochore.

To test this hypothesis, CRISPR-skip-in was used to endogenously tag the kinetochore protein Nuf2 C-terminally with *linker-3FLAG-T2A-myc-dhfr*, creating RH Tir1 Nuf2^{FLAG}, ALP2a iKD Nuf2^{FLAG}, and ARP4a iKD Nuf2^{FLAG} **(Figure 2.3.1b)**. Visualisation of the centrosomes and kinetochores confirmed the aforementioned close spatial relationship between the two **(Figure 2.3.1c)**.

To enable the detection of subtle spatial changes in spatial relationship between centrosomes and kinetochores, which could indicate mitotic spindle problems, an automated image analysis workflow was established, whereby Cen1 and Nuf2 IFA signals were 3D segmented and the centroids of each segment used for 3D spatial measurements **(Figure 2.3.1d)**. Confocal imaging was used for this approach and the tachyzoites were heavily over sampled, with a voxel size of 50 × 50 × 80 nm for the purpose of accurate centroid approximation. Following either ALP2a or ARP4a KD , no change in the distance between the centrosome and kinetochore of mitotic tachyzoites was found **(Figure 2.3.1e)**,

indicating that the relationship between the centrosome and kinetochore is maintained and, therefore, mitotic spindle formation and attachment proceeded as normal despite the KDs.

2.3.b The KD of ALP2a and ARP4a both lead to over-duplication of the centrosome

In visualising the spatial relationship between the centrosome and kinetochore it was noticed that, following either ALP2a or ARP4a KD, a subpopulation of tachyzoites presented > 2 centrosomes **(Figure 2.3.2a),** suggesting centrosome over-duplication as another phenotype following ALP2a KD and ARP4a KD. In the given examples, note the left ALP2a KD tachyzoite has 4 centrosomes, likewise the ARP4a KD tachyzoite. Moreover, it was noted that tachyzoites with over-duplicated centrosomes displayed an unequal distribution of kinetochores between their centrosomes **(Figure 2.3.2a)**. For example, the left ALP2a KD tachyzoite has 4 centrosome foci and 3 kinetochore foci, with the latter consisting of 2 brighter foci and 1 dimmer focus. In the ARP4a KD example, 2 of the centrosome foci are localised with a very bright kinetochore focus whilst the remaining 2 centrosome foci are localised with a much dimmer kinetochore focus. Tachyzoites with over-duplicated centrosomes most often presented with 3 or 4 centrosomes **(Figure 2.3.2b)**.

For the purpose of correlating whether the described centrosome over-duplication phenotype following ALP2a KD and ARP4a KD with the nuclear mis-segregation phenotypes, the frequency of centrosome over-duplication was quantified through the lytic cycle **(Figure 2.3.2c)**. As with nuclear mis-segregation, centrosome over-duplication was present in a small population of ALP2a iKD and ARP4a iKD tachyzoites without IAA treatment (~ 10 and 5% respectively). However, the addition of IAA saw this frequency rise through the lytic cycle, peaking at ~ 40% following 30 hours of IAA treatment. The pattern of centrosome over-duplication phenotype frequency correlated with that of the nuclear mis-segregation phenotype **(Figure 2.2.4b)**, meaning that a link between the two phenotypes cannot be ruled out. However, the absolute frequencies of centrosome over-duplication were consistently lower than that of nuclear mis-segregation. The most likely explanation for this would be that every round of endodyogeny carried a probability of centrosome over-duplication that thereafter led to nuclear mis-segregation. The frequency of nuclear mis-segregation would therefore accumulate over several rounds of endodyogeny, ultimately resulting in the death of all tachyzoites within their parasitophorous vacuole.

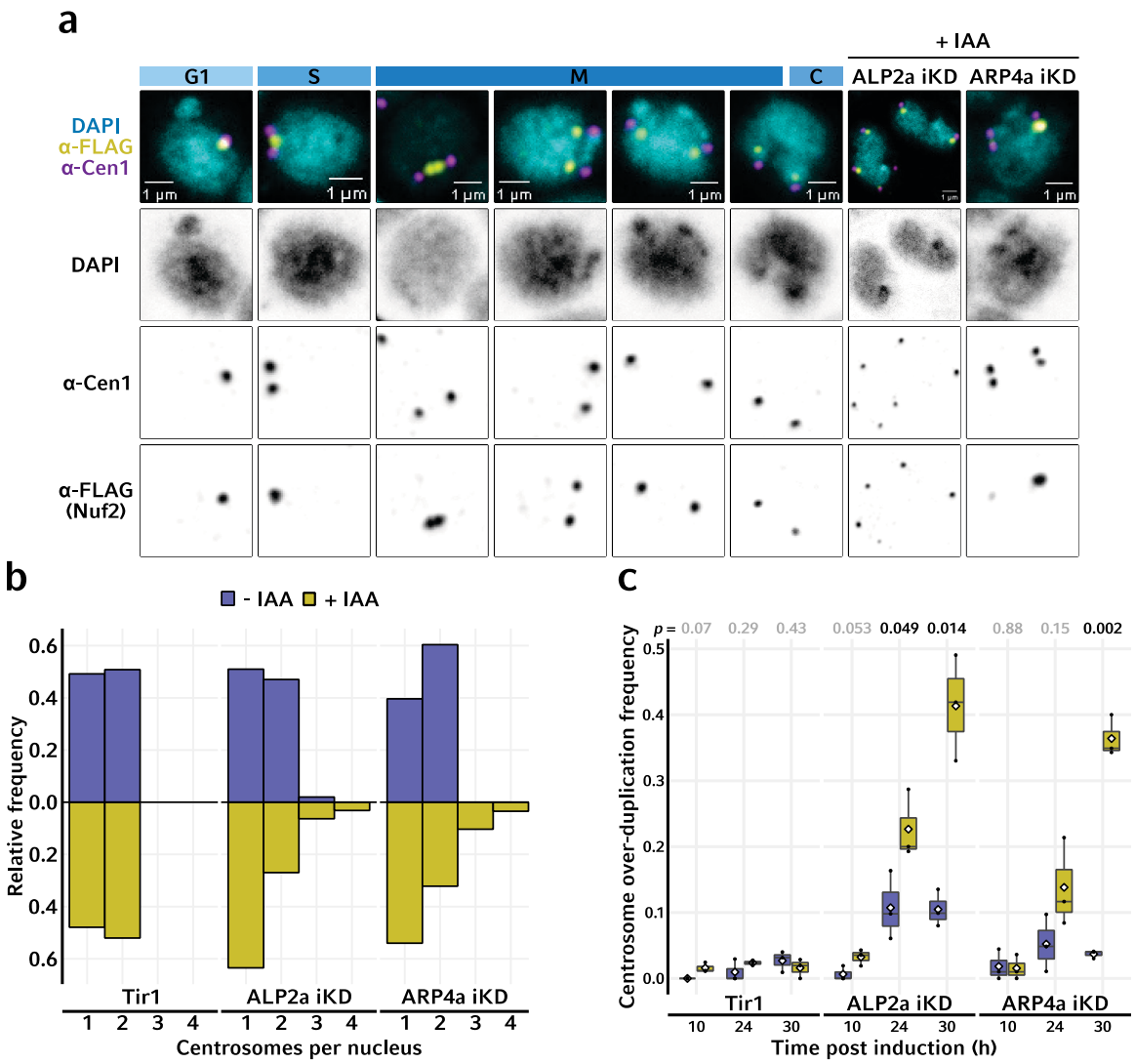

Figure 2.3.2: The KD of ALP2a and ARP4a both resulted in centrosome over-duplication.

a. As figure2.3.1c with the addition of ALP2a iKD and ARP4a iKD strains treated ± IAA for 20 h.

b. From a., quantification of the number of centrosomes per nucleus at 20 h ± IAA. Per nucleus, quantification was performed using find maxima function from 3D suite for ImageJ. Graph is representative as one of three biological replicates.

c. Time course quantification of centrosome over-duplication phenotype through the lytic cycle. Tachyzoites were inoculated and cultured for indicated times ± 500µM IAA before fixation and IFA labelling as in a. Shown is the relative number of vacuoles where centrosome over-duplication was evident in ≥ 1 tachyzoite. Quantification was manually performed. Result of Welch's t-test shown.

Kinetochores attach to nuclear DNA at the chromosomes' centromeres. Should centrosome over-duplication be the cause of nuclear mis-segregation, it would be expected that the centromeres would exhibit the same unequal distribution of foci between centrosomes in tachyzoites with over-duplicated centrosomes. The centromere-specific histone variant CenH3 was chosen as a marker for the visualisation of the centromeres **(Figure 2.3.3a)**. CenH3 was endogenously tagged N-terminally with *dhfr-myc-T2A-3FLAG-linker* using CRISPR-skip-in to create RH Tir1 ^{FLAG}CenH3, ALP2a iKD ^{FLAG}CenH3, and ARP4a iKD ^{FLAG}CenH3 **(Figure 2.3.3b)**. ^{FLAG}CenH3 yielded weaker signal compared to Nuf2^{FLAG} when visualised by IFA, but the dynamics of CenH3 localisation through the cell cycle mirrored that of Nuf2 **(Figure 2.3.3c)**. This was unexpected since each centromere contains significant CenH3 deposition, whereas each kinetochore only contains a single Nuf2 protein. A possible cause of this could have been poor antibody accessibility to the antigen. In ALP2a KD and ARP4a KD tachyzoites with centrosome over-duplication, the CenH3 foci became nigh impossible to distinguish from background signal **(Figure 2.3.3c)**. This could have indicated that the deposition of CenH3 at the centromeres was significantly reduced or completely lost following ALP2a KD and ARP4a KD **(Figure 2.3.3d, upper)**. However, given that Nuf2's presence in kinetochores is CenH3-dependent (Collins *et al.*, 2005), such an eventuality would likely have seen the loss of Nuf2 foci, which was not the case **(Figure 2.3.2a)**. As such, and alternatively, the loss of readily distinguishable CenH3 foci in tachyzoites with over-duplicated centrosomes may have arisen from the aforementioned weak signal intensity of ^{FLAG}CenH3. Were the centromeres to be unequally divided amongst the > 2 centrosomes, as seen with the kinetochores, the ^{FLAG}CenH3 fluorescence would have been divided over a larger volume, assuming unchanged centromere content **(Figure 2.3.3d, lower)**.

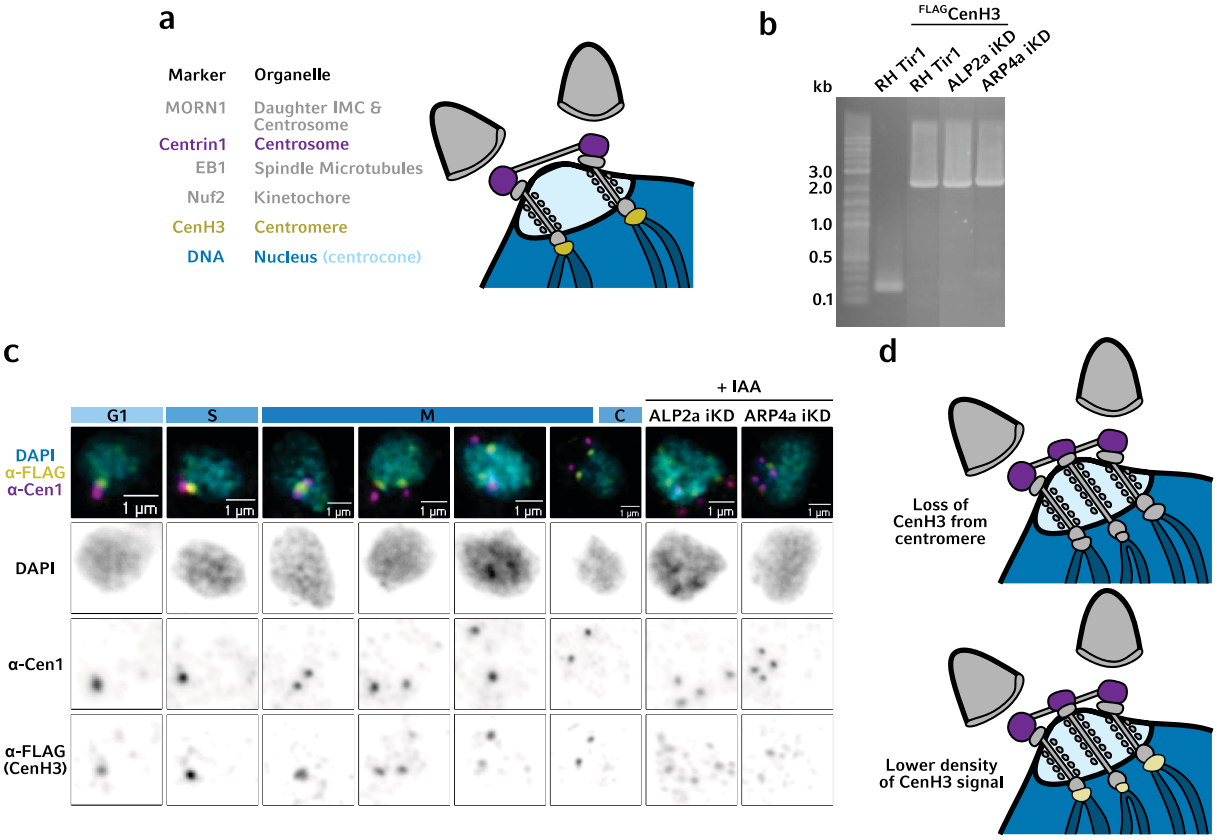

Figure 2.3.3: CenH3 occupancy at the centromeres is either lost or the centromeres are divided between the > 2 centrosomes in tachyzoites with over-duplicated centrosomes follow ALP2a or ARP4a KD.

a. Diagrammatic depiction of the mitotic machinery during normal *T. gondii* M phase. Duplication of centrosomes, DNA, and kinetochores has occurred as well as spindle attachment. The cytoskeleton of two daughter cells is elongating and centrosomes and the connected mitotic spindles, kinetochores, and DNA are segregating. Note that chromosomes do not condense during *T. gondii* mitosis and are only depicted this way for illustrative purposes.

b. Genotyping PCRs showing 5' integration of *dhfr-myc-T2A-3FLAG-linker* to create RH Tir1 ^{FLAG}CenH3, ALP2a iKD ^{FLAG}CenH3, and ARP4a iKD ^{FLAG}CenH3. Expected CenH3 5' amplicon sizes were 0.2 kb for WT (RH Tir1) and 2.2 kb for ^{FLAG}CenH3 strains.

c. Representative IFA confocal Z-sum micrographs showing the relationship between the centrosome (Cen1) and centromere (CenH3) during the tachyzoite cell cycle, as well as in ALP2a KD and ARP4a KD tachyzoites with over-duplicated centrosomes. Tachyzoites were inoculated onto HFFs and cultured ± 500 µM IAA for 20 h before fixation and IFA labelling as indicated.

d. Diagrammatic depiction of two possibilities that could explain the loss of detectable CenH3 foci in KD tachyzoites with over-duplicated centrosomes. Upper represents a scenario with intact mitotic machinery but the loss of CenH3 deposition (grey coloured) at the centromeres. Lower represents a scenario where CenH3 deposition is unaffected, but its fluorescence signal intensity is undetectable because the same number of centromeres, and therefore same amount of CenH3, is divided over a larger volume (pale yellow colour).

In the event of centrosome over-duplication, it was not immediately clear whether all centrosomes present were functional and capable of acting as microtubule organising centres for the assembly of mitotic spindles. To answer this, it was decided to visually check for mitotic spindle formation in KD tachyzoites with centrosome over-duplication. Whilst α-tubulin are often used for the visualisation of *T. gondii* microtubules, including the mitotic spindles, the intense staining of the subpellicular microtubules can conflate with the small and less discernible mitotic spindles. Therefore, the mitotic spindle binding protein EB1, which only localises to mitotic spindles, was selected to as a mitotic spindle marker **(Figure 2.3.4a)**. EB1 was C-terminally tagged with *linker-3FLAG-T2A-myc-dhfr* using CRISPR-skip-in **(Figure 2.3.4b)**. During interphase (G1 phase), EB1 was diffusely present in the nucleus but rapidly accumulated on the mitotic spindles following their polymerisation into the nucleus **(Figure 2.3.4c)**. In the case of ALP2a KD- and ARP4a KD-induced centrosome over-duplication, EB1 signal was present and emanating proximal to each centrosome **(Figure 2.3.4c)**, confirming that all centrosomes were functional and mitotic spindles from each had entered the nucleus.

Through the above examination of several components from the mitotic machinery it was concluded that the nuclear mis-segregation phenotype following ALP2a KD and ARP4a KD was not a result of a failure in the mitotic machinery. Instead, the data suggested that centrosome over-duplication was the most likely driving factor behind the nuclear mis-segregation phenotype. However, it remained to be determined whether other mitotic events, such as DNA replication, were affected by ALP2a KD and ARP4a KD.

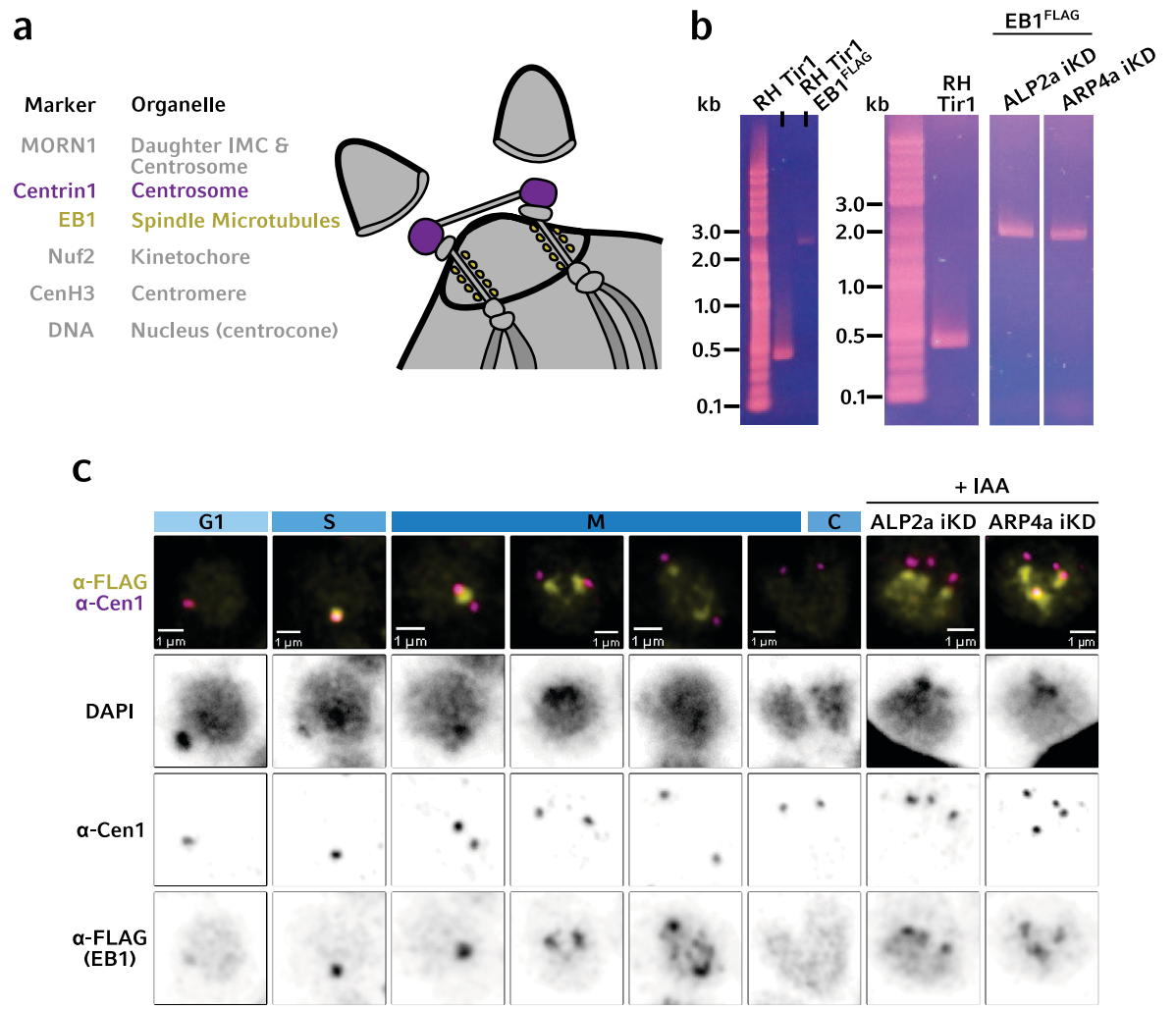

Figure 2.3.4: Over-duplicated centrosomes are viable, with mitotic spindles emanating from all centrosomes.

a. Diagrammatic depiction of the mitotic machinery during normal *T. gondii* M phase. Duplication of centrosomes, DNA, and kinetochores has occurred as well as spindle attachment. The cytoskeleton of two daughter cells is elongating and centrosomes and the connected mitotic spindles, kinetochores, and DNA are segregating. Note that chromosomes do not condense during *T. gondii* mitosis and are only depicted this way for illustrative purposes.

b. Genotyping PCRs showing 3' integration of *linker-3FLAG-T2A-myc-dhfr* to create RH Tir1 EB1^{FLAG}, ALP2a iKD EB1^{FLAG}, and ARP4a iKD EB1^{FLAG}. Expected EB1 3' amplicon band sizes were 0.45 bp for WT (RH Tir1) and 2.5 kb for EB1^{FLAG} strains.

c. Representative IFA confocal Z-sum micrographs showing the progress of mitotic spindle (EB1) formation from the centrosomes (Cen1) during tachyzoite mitosis, as well as in ALP2a KD and ARP4a KD tachyzoites with over-duplicated centrosomes. Tachyzoites were inoculated onto HFFs and cultured ± 500 µM IAA for 20 h before fixation and IFA labelling as indicated.

2.3.c Despite centrosome over-duplication, the remaining replication processes continue as normal.

The presence of over-duplicated centrosomes could have occurred within a single round of endodyogeny or indicate that multiple rounds of endodyogeny were initiated without completion of previous rounds. In the event of the former, only the centrosomes would duplicate more than once. Whilst the latter scenario would see over-duplication of not just the centrosomes but also, for example, DNA and kinetochores. To determine which scenario was at play following ALP2a KD and ARP4a KD, the sum fluorescence intensity of each Cen1, DAPI-labelled DNA, and ^{FLAG}Nuf2 was quantified from confocal IFA micrographs **(Figure 2.3.5a)**. Tachyzoites were grouped by whether then presented 1, 2, or ≥ 3 centrosome foci. For Cen1, the doubling of sum fluorescence intensity between tachyzoites with 1 and 2 centrosomes was clear. Since the aforementioned centrosome grouping was determined by number of foci, it required both centrosome duplication and segregation to have occurred before a change in group. Thus, centrosomes undergoing duplication prior to segregation would have increased protein content and consequently increased sum fluorescence intensity but would still be grouped as a single-centrosome tachyzoite. One is therefore to understand that tachyzoites grouped under 1 centrosome represent tachyzoites in both G_1 and S phases, exclusively and non-exclusively, respectively. This effect can be seen in a small S phase sub-population of single-centrosome tachyzoites **(Figure 2.3.5a; Cen1)**. The duplication of kinetochores and DNA content was also readily apparent in doubling of sum fluorescence intensity **(Figure 2.3.5a; Nuf2 and DAPI)**. However, tachyzoites with centrosome over-duplication did not present a further increase in either Nuf2 or DAPI sum fluorescence intensity.

For the purpose of statistically interrogating these sum fluorescence intensity observations, Gaussian mixture modelling was independently employed to determine the number of components (clusters) within the data. The pooled data from all strains and treatments was used for modelling. Based on known experimental variables such as unequal sample size and variable, binomial distributions, it was expected that a univariate model of unequal variance would best explain the data. However, for robustness, univariate models of equal and unequal variance were calculated. In the case of Cen1, the most likely model was a univariant model of unequal variance composed of 3 components (log-likelihood -4,678), whilst for Nuf2 and DAPI it was the sample model but with only 2 components (log-likelihoods -4,716 and -15,211, respectively) **(Figure 2.3.5b, c)**. This was in agreement with the earlier observation that only centrosomes showed an increase of sum fluorescence intensity of > 2-fold.

Moreover, when the individual data points from each model component were compared to the previous Cen1-foci groupings, there was a high degree of overlap **(Figure 2.3.5a)**. Therefore, it was concluded that centrosome over-duplication was happening within the context of a single round of endodyogeny and that the nuclear-localised endodyogeny processes of DNA and kinetochore replication were unaffected.

Whilst the sequence of mitotic events during endodyogeny are relatively well defined, less is known about the timing of said events. The quantification of mitotic machinery sum fluorescence intensity presented a novel opportunity to define the temporal sequence. As stated, there existed a S phase sub-population of tachyzoites with single centrosomes **(Figure 2.3.5a)**. A similar sub-population is present with regards to DAPI sum fluorescence intensity, indicating that centrosome duplication and DNA replication occur in concert with one another **(Figure 2.3.5a)**. Moreover, once centrosome segregation had occurred, the sum DAPI intensity continued to present a wide distribution, representing DNA content between 1- and 2-*n*. Therefore, DNA replication was not completed before centrosome segregation occurred. Note, the presented data are from different biological replicates and therefore a direct comparison between Cen1 and DAPI fluorescence intensity cannot be performed. Contrastingly, there was an absolute lack of any increase in Nuf2 fluorescence intensity in tachyzoites with single centrosomes, whilst those segregated centrosomes presented a binominal distribution of 1- and 2-*n* Nuf2 fluorescence intensities **(Figure 2.3.5a)**. Therefore, kinetochore duplication occurs after the onset of centrosome segregation and DNA replication. It cannot be determined from the data here, however, whether DNA replication was fully completed, or centromere replication completed before kinetochore replication.

2.3.d The nuclear mis-segregation phenotype following SLP1 KO is independent of ALP2a and ARP4a

The SUN domain-containing protein SLP1 (TGME49_250010) is a dynamically localised protein with nuclear and centrosomal proximity, the KO of which resulted in a nuclear segregation phenotype similar to that of the ALP2a KD and ARP4a KD phenotypes (Wagner *et al.*, 2023). It was therefore hypothesised that there may be a common mechanism to the phenotypes of SLP1 KO, ALP2a KD, and ARP4a KD. To investigate this, the dynamics of SLP1 were examined following ALP2a KD and ARP4a KD.

SLP1 was endogenously tagged C-terminally with *linker-3FLAG-T2A-myc-dhfr* using CRISPR-skip-in to create RH Tir1 SLP1^{FLAG}, ALP2a iKD SLP1^{FLAG}, and ARP4a iKD SLP1^{FLAG} **(Figure 2.3.6a)**. During G_1 phase,

SLP1 displayed a diffuse para-nuclear localisation **(Figure 2.3.6b)**. However, upon entering S phase, a focus of SLP1 appeared immediately adjacent to the centrosome. This SLP1 focus thereafter mimicked the centrosomes dynamics, duplicating after centrosome duplication and following the centrosome as it translocated around the nucleus, indicating a structural connection between the two. Once nuclear segregation began, SLP1 foci were rapidly lost. The dynamics of SLP1 were unaltered following either

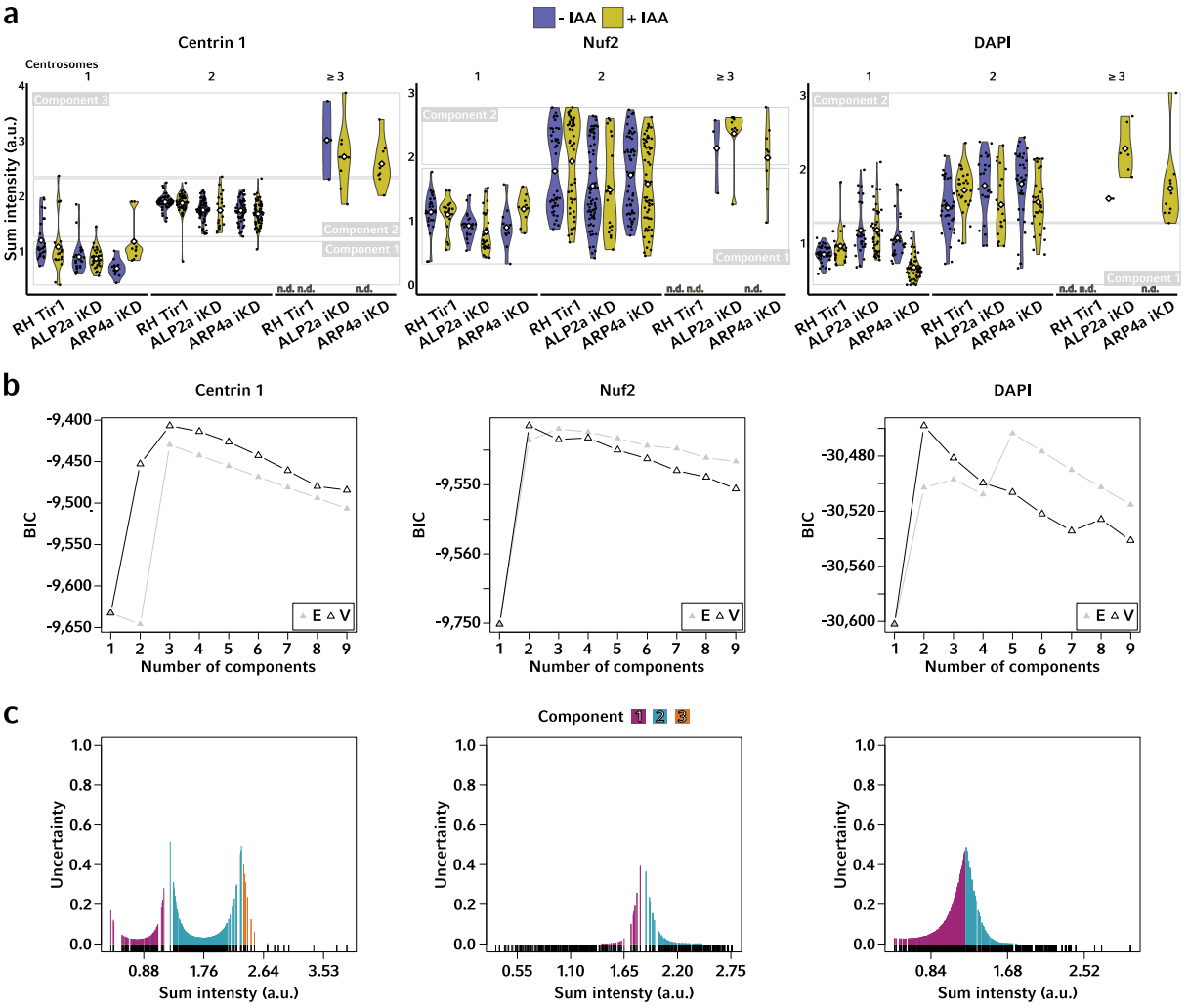

Figure 2.3.5: Centrosome over-duplication is unaccompanied by the over-duplication of neither DNA nor kinetochores.

a. Fluorescence signal quantification of the centrosome (Cen1), kinetochore (Nuf2), and DNA (DAPI) in non-mitotic (1 centrosome), mitotic (2 centrosomes), and mitotic with centrosome over-duplication (≥ 3 centrosomes) vacuoles. Normalised to mean of tachyzoites with 1 centrosome from all samples. Quantifications were taken from micrographs as in Figure 2.3.1c, segmented as per Figure 2.3.1d. Grey boxes indicate upper and lower limits of components identified from Gaussian mixture modelling.

b. Bayesian information criterion for Gaussian mixture models of 1 to 9 components using univariant equal variance (E) and univariant unequal variance (V) models. Models were fitted using pooled data of all strains and treatments from a.

c. The most probable component to which each fluorescence intensity data point from a. belongs and the uncertainty of this allocation.

ALP2a KD or ARP4a KD **(Figure 2.3.6b)**. In the case of centrosome over-duplication, SLP1 was inconsistent in mimicking the extra duplications, i.e., cells with 4 centrosomes and 2 SLP1 foci or 4 centrosomes and 3 SLP1 foci were seen. Due to this and SLP1's continued expression despite either ALP2a or ARP4a KD, a commonality between the between the SLP1 KO and the two ARP KDs was considered unlikely.

Since SLP1 foci displayed dynamic localisations that mirrored that of the centrosome, it was decided to use the aforementioned image analysis workflow **(Figure 2.3.1c)** to examine and measure the spatial relationship between SLP1 and the centrosome. In tachyzoites with only a single centrosome focus, the distance between each SLP1 focus and its nearest centrosome was ~200 nm **(Figure 2.3.7a)**. Following centrosome segregation, this distance doubled to ~400 nm. This result served as a good indication of the sensitivity of this analysis, clearly identifying a sub-diffraction limit change in relative distance between the two proteins. Since the SLP1 foci were proximal to the centrosome, and therefore the centrocone, it was posited that this increase in distance may be related to centrocone formation. Re-examination of published centrocone electron micrographs (Gubbels *et al.*, 2006) showed that the centrocone is approximately 269 nm in length **(Figure 2.3.7b)**. Since the centrocone is not visibly detectable in G_1, the development and protrusion of the centrocone could account for the ~ 200 nm measured increase in distance between SLP1 and the centrosomes. SUN domain-containing proteins

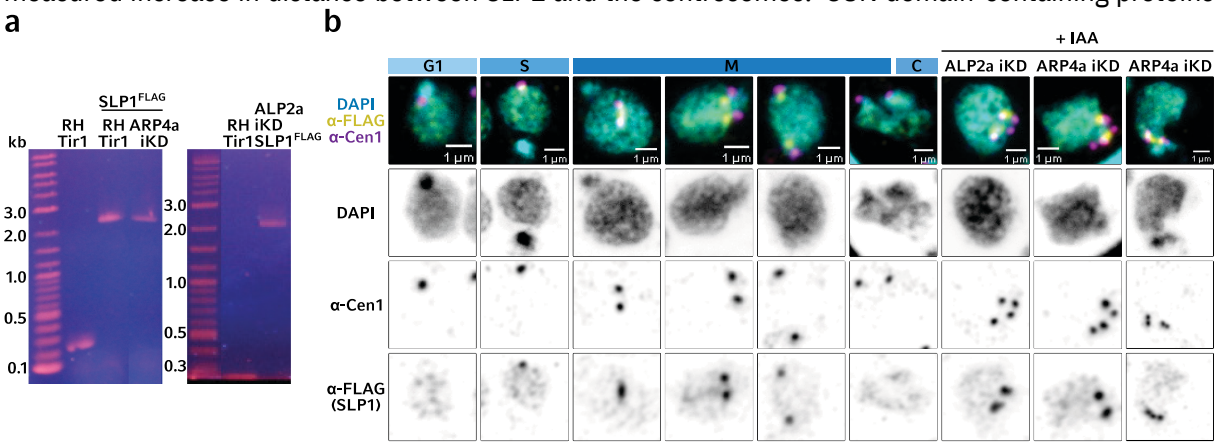

Figure 2.3.6: Dysregulation of SLP1 is not implicated in the nuclear mis-segregation phenotypes following ALP2a KD and ARP4a KD.

a. Genotyping PCRs showing 3' integration of *linker-3FLAG-T2A-myc-dhfr* to create RH Tir1 SLP1^{FLAG}, ALP2a iKD SLP1^{FLAG}, and ARP4a iKD SLP1^{FLAG}. Expected SLP1 3' amplicon band sizes were 0.21 bp for WT (RH Tir1) and 2.2 kb for SLP1^{FLAG} strains.

b. Representative IFA confocal Z-sum micrographs showing the dynamic localisation of SLP1 relative to the centrosomes (Cen1) during tachyzoite mitosis, as well as in ALP2a KD and ARP4a KD tachyzoites with over-duplicated centrosomes. Tachyzoites were inoculated onto HFFs and cultured ± 500 µM IAA for 20 h before fixation and IFA labelling as indicated.

are typically transmembrane proteins that span the outer nuclear membrane. Should SLP1 instead associate with the centrocone membrane, that segregates the DNA-free centrocone from the rest of the nucleus, its distance to the centrosome would be determined by the length of the centrocone **(Figure 2.3.7c)**. The data presented here is, however, not sufficient to draw a firm conclusion and further work is required to more accurately determine SLP1's precise localisation.

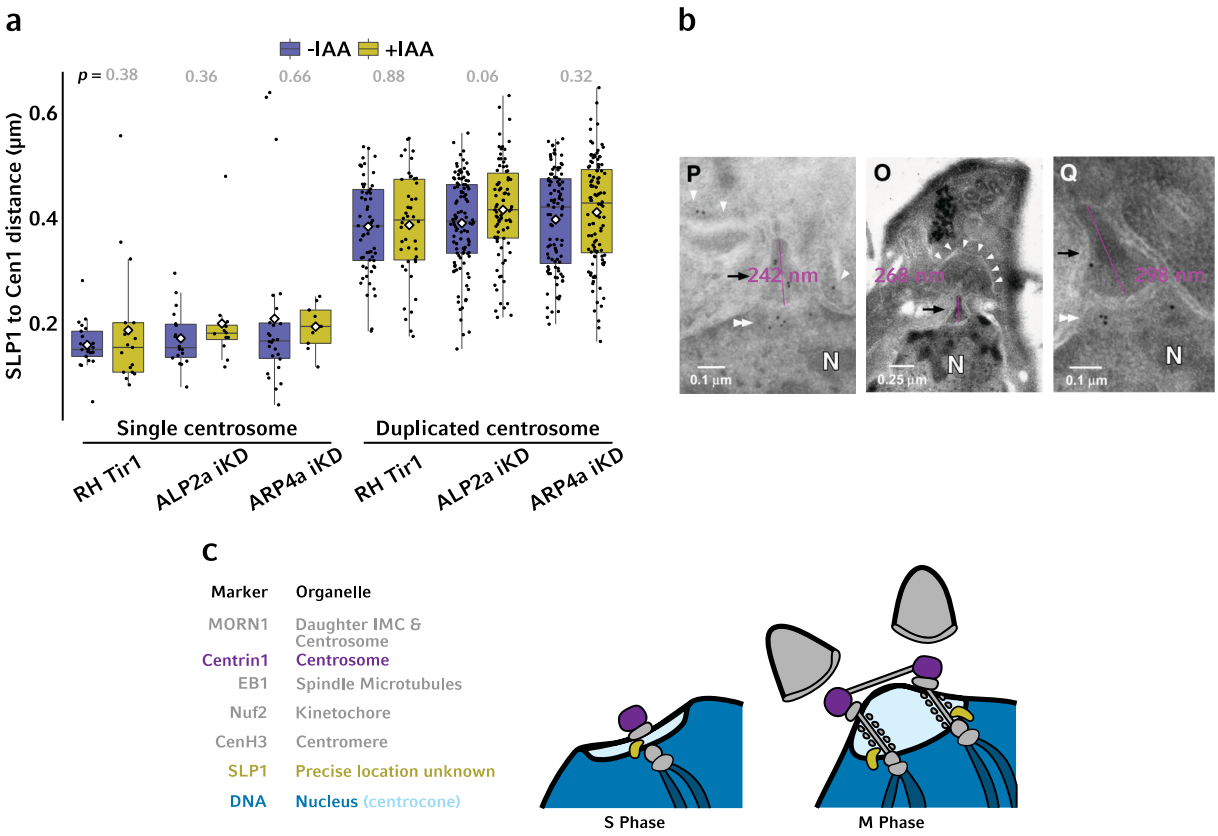

Figure 2.3.7: SLP1 may localise to the intra-nuclear membrane that segregates the centrocone from the remaining nucleus.

a. Quantification of centroid-to-centroid distance of SLP1 segments to their nearest Cen1 segment. Segmentation was performed as in Figure 2.3.1d., and IFA as in Figure 2.3.6b. Tachyzoites were grouped on whether they possessed 1 or 2 centrosomes, determined by the number of Cen1 maxima per tachyzoite. Result of Welch's t-test shown.

b. Measurements of centrocone length using electron micrographs taken from Gubbels et al., 2006. Using ImageJ, the micrographs pixel scale was determined using the embedded scale bars and a region of interest (magenta lines) drawn to approximate the length of each centrocone.

c. Diagrammatic depictions of a possible SLP1 localisation that would explain the ~ 200 nm increase in SLP1 to nearest centrosome distance shown in a. Were SLP1 integrated into the centrocone membrane, the latter's 200 nm protrusion during M phase would separate see the distance between SLP1 and the centrosomes increase.

2.3.e ALP2a KD and ARP4a KD resulted in impaired MAPK-L1 up-regulation during mitosis.

Centrosome over-duplication phenotypes have been described previously in *T. gondii*. Notably in null mutants of Ark1 (Berry *et al.*, 2018), Cyc1, Crk6 (Hawkins *et al.*, 2021), Cep530 (Courjol and Gissot, 2018), and MAPK-L1 (Suvorova *et al.*, 2015), which are all associated with centrosome over-duplication phenotypes, are variably expressed through the cell cycle of *T. gondii*, peaking in either S or M phase (Behnke *et al.*, 2010) **(Figure 2.3.8a)**. As two nuclear proteins, it was considered improbable that ALP2a an ARP4a directly regulate centrosome duplication, and that an indirect link remained to be elucidated. In explanation of a link between the centrosome, ALP2a, and ARP4a, it was hypothesised that ALP2a KD and ARP4a KD could have result in the dysregulation of gene expression, and that this in turn could end in the failure to up-regulate the aforementioned genes as the tachyzoites progress through the cell cycle.

To explore the possibility of a failure to up-regulate cell cycle variably expressed genes, MAPK-L1 was endogenously tagged with *linker-3FLAG-T2A-myc-dhfr* using CRISPR-skip-in **(Figure 2.3.8b)**. MAPK-L1 protein levels were previously reported to peak at the S to M phase transition, and to localise proximal to the centrosome (Suvorova *et al.*, 2015). Here, visualisation of MAPK-L1 confirmed the cyclical nature of protein expression, but the centrosomal localisation was not reproducible. Instead, MAPK-L1 was diffusely present in the cytoplasm **(Figure 2.3.8c)**. Following ALP2a KD and ARP4a KD, MAPK-L1 expression was still visible in mitotic tachyzoites **(Figure 2.3.8c)**. As such, the sum fluorescence intensity per vacuole as quantified and this showed that ALP2a KD and ARP4a KD both resulted in a lesser MAPK-L1 signal increase between mitotic and non-mitotic cells **(Figure 2.3.8d)**. In the control Tir1 with IAA treatment, an increase in MAPK-L1 signal of 2.11× was measured, with this dropping to 1.4× for ALP2a iKD +IAA and 1.66× for ARP4a iKD + IAA. To aid in the distinction of what MAPK-L1 signal intensities constituted normal G_1 expression, and likewise mitotic expression, Gaussian mixture modelling was used to determine the borders of the components from the model that best fitted the data. Using the pooled data from all conditions, the best model was univariant with unequal variance and composed of 2 components **(Figure 2.3.8e, f)** (model log-likelihood -5,007.705). Comparing the 2 Gaussian mixture modelling components with the MAPK-L1 signal intensities split between mitotic and non-mitotic tachyzoites, a reasonable correlation was found. MAPK-L1 signal intensities in non-mitotic cells almost entirely belonged to component 1, whilst most Tir1 MAPK-L1 signal intensities from mitotic cells belonged to component 2 **(Figure 2.3.8d)**. Significantly, the mean MAPK-L1 signal intensity of ALP2a KD and ARP4a KD vacuoles was in component 1, reinforcing the aforementioned

lower increases in MAPK-L1 signal. Together the data suggested that both ALP2a KD and ARP4a KD resulted in an impaired ability to up-regulate MAPK-L1 expression and that this may in part explain the centrosome over-duplication phenotypes. However, this impairment in up-regulated expression was not absolute and so additional factors in phenotype development could not be ruled out. Moreover, the observed effect could be an indirect, downstream consequence of ALP2a KD and ARP4a KD, rather than a more immediate effect.

Figure 2.3.8: MAPK-L1 up-regulation is impaired following ALP2a KD and ARP4a KD.

a. Microarray RNA quantification through the cell cycle of genes whose disruption has previously been reported to cause centrosome over-duplication. Data taken from Behnke *et al*., 2010.

b. Genotyping PCRs confirming the 3' integration of *linker-3FLAG-T2A-myc-dhfr* to create RH Tir1 MAPK-L1^{FLAG}, ALP2a iKD MAPK-L1^{FLAG}, and ARP4a iKD MAPK-L1^{FLAG}. Expected 3' MAPK-L1 amplicons were 0.3 bp for WT (RH Tir1) and 2.3 kb for MAPK-L1^{FLAG} strains.

c. Representative widefield Z-max micrographs showing MAPK-L1 expression in mitotic (≥ 2 centrosome) and non-mitotic tachyzoites (1 centrosome). Tachyzoites were inoculated onto HFFs and cultured for 20 h ± 500 μM IAA before fixation and IFA labelling as indicated. Mitotic vs non-mitotic grouping was automatedly determined by the number of Cen1 maxima per tachyzoite. For mitotic KD tachyzoites (+IAA), examples with over-duplicated centrosomes (> 2) are given.

d. Sum fluorescence intensity of MAPK-L1 per vacuole from c. Per vacuole, Z-stacks were sum intensity projected and Otsu's thresholding was used to create a mask of MAPK-L1 channel, the sum signal intensity of which was measured. Result of Welch's t-test with Benjamini-Hochberg adjustment shown. Fluorescence intensity values are shown relative to the mean fluorescence intensity of non-mitotic tachyzoites (1 centrosome) from all strains. Grey boxes indicate upper and lower limits of components identified from Gaussian mixture modelling.

e. Bayesian information criterion for Gaussian mixture models of 1 to 9 components using univariant equal variance (E) and univariant unequal variance (V) models.

f. The most probably component to which each MAPK-L1 fluorescence intensity data point in d. belongs and the uncertainty of this allocation.

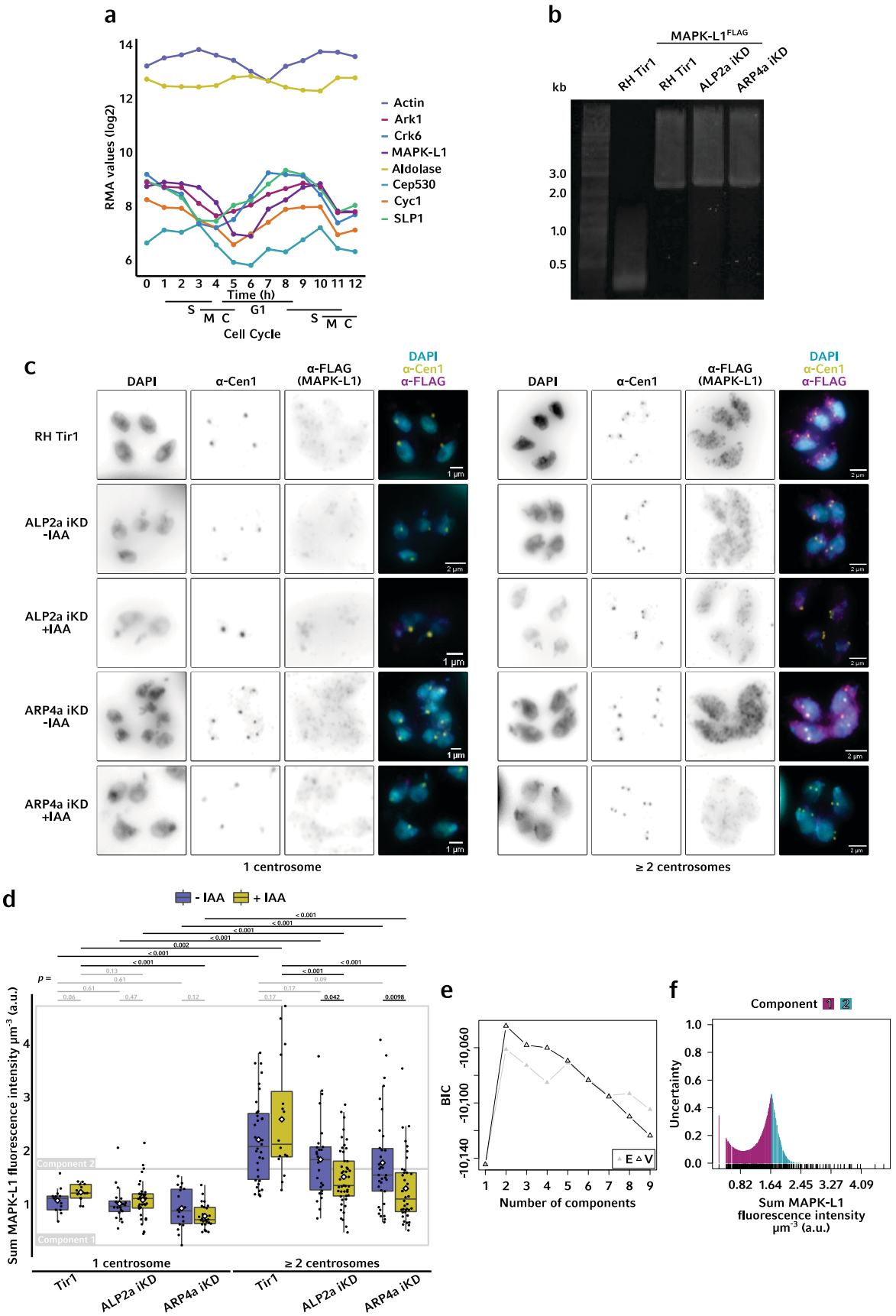
a
RMA values (log2)
Time (h)
Cell Cycle
S
M
C
G1
Actin
Ark1
Crk6
MAPK-L1
Aldolase
Cep530
Cyc1
SLP1
b
MAPK-L1FLAG
kb
RH Tir1
RH Tir1
ALP2a iKD
ARP4a iKD
3.0
2.0
1.0
0.5
c
DAPI
α-Cen1
α-FLAG (MAPK-L1)
DAPI α-Cen1 α-FLAG
RH Tir1
ALP2a iKD -IAA
ALP2a iKD +IAA
ARP4a iKD -IAA
ARP4a iKD +IAA
1 centrosome
≥ 2 centrosomes
d
- IAA
+ IAA
p =
Sum MAPK-L1 fluorescence intensity µm-3 (a.u.)
Component 2
Component 1
1 centrosome
≥ 2 centrosomes
Tir1
ALP2a iKD
ARP4a iKD
e
BIC
Number of components
E
V
f
Component
Uncertainty
Sum MAPK-L1 fluorescence intensity µm-3 (a.u.)

To summarise, the data highlights a sequence of events that ultimately lead to the nuclear mis-segregation phenotypes following ALP2a KD and ARP4a KD. During S phase, there is a non-zero probability that centrosome over-duplication will occur, and more than 2 sets of mitotic spindles enter the nucleus. Competition for kinetochore binding ensues, and kinetochore mis-segregation occurs, with an unequal distribution of kinetochores, and therefore chromosomes, between the too-numerous centrosomes. Though an impaired ability to up-regulate MAPK-L1 expression was implicated, it was clear that the possibility of other indirect links between the centrosome and the two ARPs needed to be explored.

2.4 The interaction partners of ALP2a and ARP4a

2.4.a ARP4a is the evolutionary conserved ARP4 orthologue whilst ALP2a is a lineage-specific paralogue

For the purposes of elucidating a potential indirect link between the centrosome and both ALP2a and ARP4a it was sought to identify ALP2a and ARP4a's interaction partners through co-immunoprecipitation (CoIP). The immunoprecipitation of ALP2a and ARP4a was confirmed by western blot **(Figure 2.4.1a)** before co-precipitating proteins identified by mass spectrometry.

ARP4a co-precipitated with several evolutionary conserved components from all three of the chromatin-modifying complexes in which *S. cerevisiae* ARP4 is found **(Figure 2.4.1b).** In addition to these known chromatin modifying-associated proteins, five proteins of unknown function co-precipitated with ARP4a (TGME49_225000, 235420, 214740, 205562, 287970) **(Figure 2.4.1b, Figure 2.4.2b)**.

In contrast to ARP4a, far fewer proteins co-precipitated with ALP2a with only ROP35, RPS4, and TGME49_205562 identified **(Figure 2.4.1c)**. As a rhoptry protein, ROP35 was determined to be a false positive contaminant. Likewise, ribosomal proteins are frequent contaminants of CoIP results, and RPS4 was considered unlikely to be a genuine ALP2a interaction partner. Thus, the only putative ALP2a interaction partner identified was TGME49_205562. TGME49_205562 also co-precipitated with ARP4a **(Figure 2.4.1b)**, creating the prospect that it may be an interaction partner common to both. That neither ALP2a nor ARP4a co-precipitated with one another further suggests that they function independently from one another and that their putative interaction with TGME49_205562 may be mutually exclusive.

Since ARP4a co-precipitated with conserved components of the Ino80, SWR1, and NuA4 complexes, the degree to which each complex is conserved in *T. gondii* was examined via reciprocal BLAST searches. In the case of each complex, clear but limited conservation was found **(Figure 2.4.2a)**. For the Ino80 group (which consists of the Ino80 and SWR1 complexes), reciprocal BLAST searches of both ScINO80 and ScSWR1 core proteins identified TgINO80, with no direct homologue of ScSWR1.

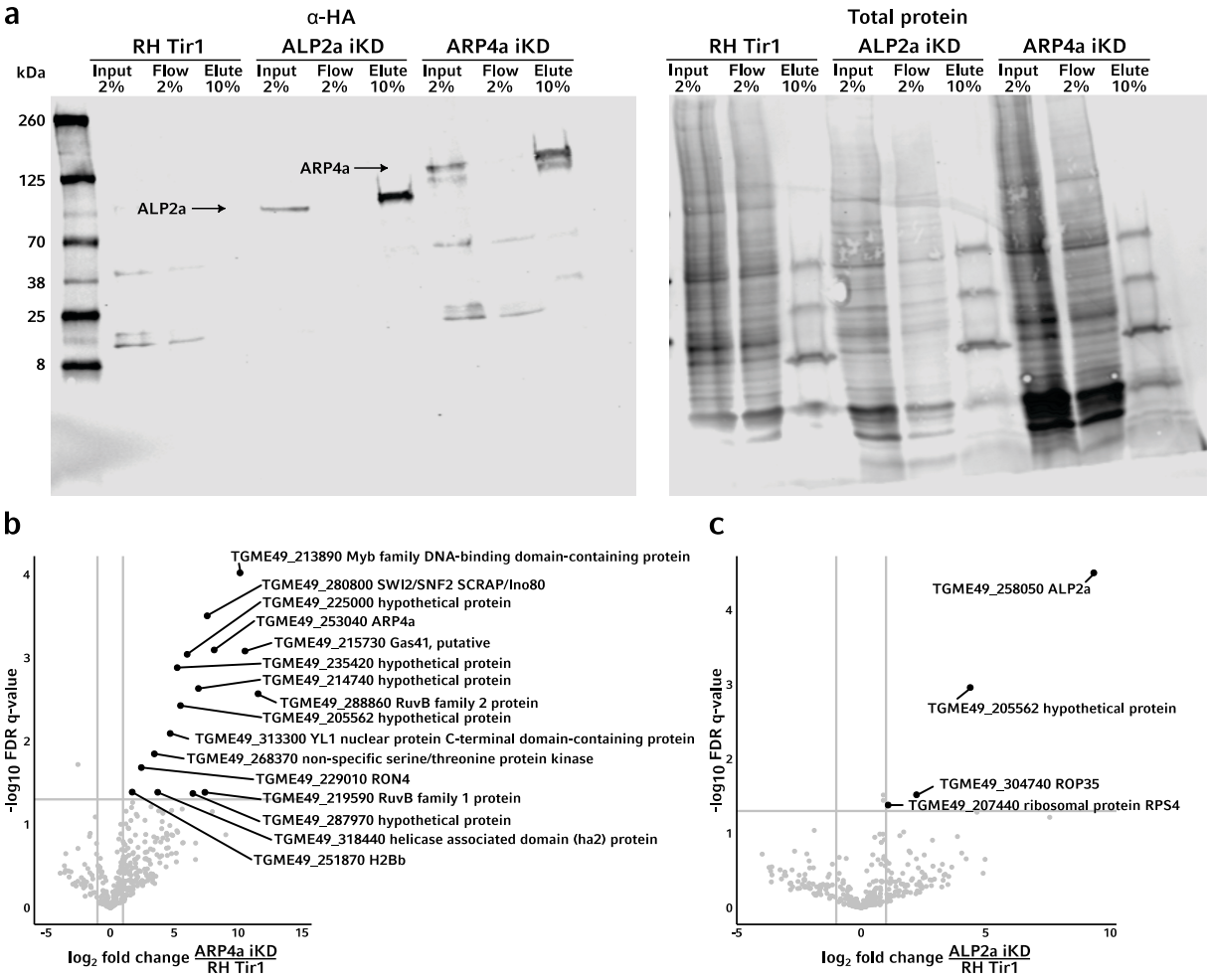

Figure 2.4.1: The interaction partners of ALP2a and ARP4a as identified through CoIP.

a. Western blot confirming enrichment of both ALP2a and ARP4a following immuno-precipitation. The nuclei of 1×10^9 intracellular tachyzoites from indicated strains were extracted and lysed. Nuclear lysates were incubated with α-HA magnetic beads overnight before magnetised beads were washed six times. Input represents nuclear lysate, flow the final wash, and elute the proteins that were SDS-extracted from the washed beads. Percentages indicate relative amount of sample loaded. Total protein was labelled with Revert (LI-COR) and western blotted with α-HA. Predicted protein molecular weights were 95 kDa for ALP2a$^{mAID\text{-}3HA}$ (ALP2a iKD) and 112 kDa for ARP4a$^{mAID\text{-}3HA}$ (ARP4a iKD).

b. Volcano plot showing the putative interactors of ARP4a as identified by mass spectrometry following triplicate anti-HA CoIPs with ARP4a as bait. CoIPs performed as described in a. Vertical cut-offs indicate $\log_2$ fold changes of -1 and 1; horizontal cut-off indicates FDR 0.05. All proteins with ≥ 1 $\log_2$ fold change and FDR ≥ 0.05 are labelled.

c. As b. but with ALP2a as bait protein.

Additional BLAST searches in model species indicated this to be a trait common to alveolates (e.g., *Tetrahymena thermophilia*), whereas other protists (e.g., *Trypanosoma brucei* and *Leishmania major*) were found to possess homologues of both ScINO80 and ScSWR1 (data not shown). Together, the absence of a clear SWR1 homologue on *T. gondii*, the homologous presence of Ino80 and SWR1 complex components, both in the *T. gondii* genome and in the ARP4a CoIP, raises the possibility that

a

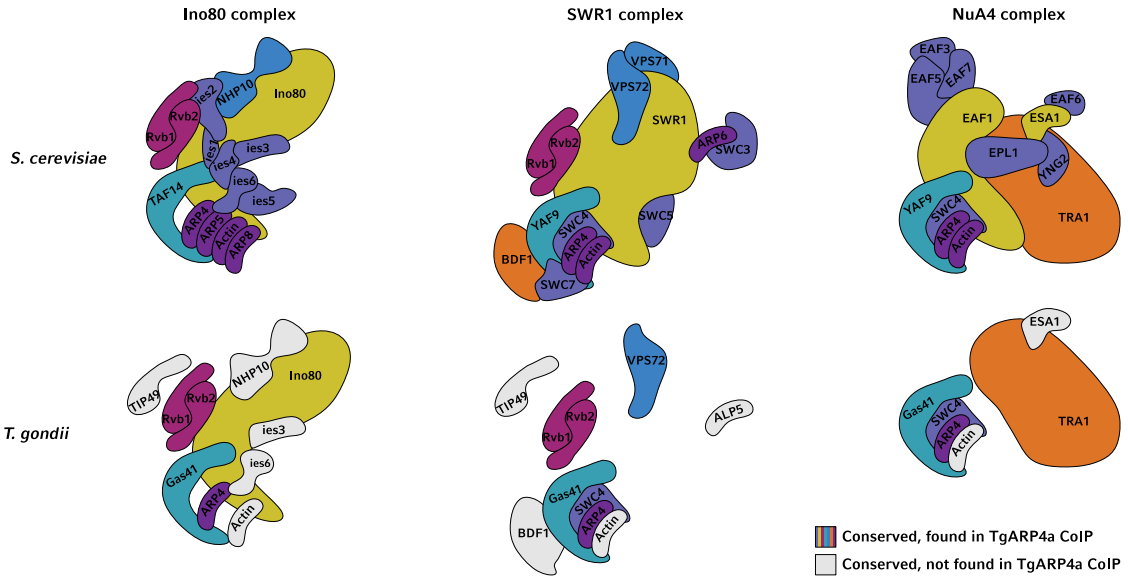

b

Gene ID	Annotation	Conserved homologue	Molecular weight (kDa)	Phenotype score	Predicted localisation
TGME49_253040	actin-related protein ARP4a	ARP4	77		Nucleus - chromatin
TGME49_213890	Myb family DNA-binding domain-containing protein	SWC4	118	-2.72	Nucleus - chromatin
TGME49_280800	SWI2/SNF2 SRCAP/Ino80	Ino80 & SWR1	317	-4.32	Nucleus - chromatin
TGME49_215730	Gas41, putative	TAF14 & YAF9	55	-2.73	Nucleus - chromatin
TGME49_288860	RuvB family 2 protein	Rvb2	55	-4.09	Nucleus - non-chromatin / chromatin
TGME49_313300	YL1 nuclear protein C-terminal domain containing protein	VPS72	82	-1.07	n.d.
TGME49_268370	non-specific serine/threonine protein kinase	TRA1	905	-3.56	Nucleus - chromatin
TGME49_219590	RuvB family 1 protein	Rvb1	53	-4.12	Cytosol / Nucleus - chromatin
TGME49_251870	histone H2Bb	H2Bb	13	1.72	
TGME49_318440	helicase associated domain (ha2) protein		237	-0.24	Nucleus - non-chromatin
TGME49_225000	hypothetical protein		155	-5.36	Nucleus - chromatin
TGME49_235420	hypothetical protein		423	-4.80	Nucleus - chromatin
TGME49_214740	hypothetical protein		166	-1.04	Nucleus - non-chromatin / chromatin
TGME49_205562	hypothetical protein		627	-3.33	n.d.
TGME49_287970	hypothetical protein		250	-4.59	n.d.
TGME49_229010	rhoptry neck protein RON4		107		Rhoptries

Conserved Ino80/SWR1/NuA4 complex component | Protein of unknown function

Figure 2.4.2: The conservation of chromatin modifying complexes to which ARP4 associates.

a. Illustrative reconstruction of the three *S. cerevisiae* chromatin-modifying complexes to which ScARP4 is a component. From reciprocal BLAST searches, the degree of each complex's conservation in *T. gondii* is shown, and whether *T. gondii* homologues co-precipitated with TgARP4a.

b. Table of ARP4a CoIP enrich proteins from Figure 2.4.1a. Conserved homologues were identified by reciprocal BLAST search against *S. cerevisiae*. Phenotype score indicates essentiality to tachyzoites (Sidik *et al.*, 2016); localisation prediction from HyperLOPIT dataset (Barylyuk *et al.*, 2020).

T. gondii and other alveolates use INO80 as a shared core component for both Ino80 and SWR1 complexes.

The presence of conserved components from each of the Ino80, SWR1, and NuA4 complexes, albeit limited in number, indicates that the complexes and their functions in H2A.Z and histone acetylation are likely conserved. By extension, that some but not all of the complexes' sub-components co-precipitated with ARP4a **(Figure 2.4.2b)** further implies a degree of conservation in ARP4a's function in *T. gondii*. This, together with the dearth of ALP2a co-precipitating proteins, indicates that ARP4a is the orthologue of *S. cerevisiae* ARP4, whilst ALP2a is an apicomplexan-specific paralogue.

2.4.b Comparative genomics of ARP4a interaction partners with unknown functions

Five proteins of unknown function co-precipitated with ARP4a. In an attempt to assign any putative function, the five proteins were analysed with HHpred, which performs pairwise comparisons of protein alignments using hidden Markov models to detect weakly conserved sequence and structural homology (Hildebrand *et al.*, 2009). Statistically likely homologies were only detected for two candidates, TGME49_225000 and TGME49_235420.

A ~100 amino acid region of TGME49_225000 showed high similarity to a region of *S. cerevisiae* EPL1 **(Figure 2.4.3a)**. EPL1 (enhancer of polycomb-like 1) is a component of the *S. cerevisiae* NuA4 complex (Boudreault *et al.*, 2003) **(Figure 2.4.2a)** for which no clear homologue is identifiable in the *T. gondii* genome. The HHpred-identified homologous region corresponds to parts of the EPcA-I and EPcA-II domains of EPL1 **(Figure 2.4.3b)**. the EPcA-II domain is an α-helix that forms a four-helix bundle together with YNG2 and ESA1, whilst the EPcA-I domain associates with a globular domain of ESA1 to form a catalytic core (Xu *et al.*, 2016) **(Figure 2.4.3c)**. Using the HHpred alignment, a structural prediction of the aligned region from TGME49_225000 was created using MODELLER (Sali *et al.*, 1995) **(Figure 2.4.3c)**. The resulting structure showed similarity to that of EPL1, with two α-helices connected by a disordered region, but with a notable difference in the conformation of the EPcA-II α-helix. It is therefore possible that TGME49_225000 is a minimally conserved homologue of *S. cerevisiae* EPL1 or a non-homologous protein that serves a similar role within the putative *T. gondii* NuA4 complex.

HHpred also identified a ~70 amino acid region of TGME49_235420 that shows similarity to *H. sapiens* SRCAP **(Figure 2.4.3d)**. *H. sapiens* SRCAP is the homologue of *S. cerevisiae* SWR1, members of the Ino80 family of chromatin remodellers. The region of homology identified aligns to the HSA domain of SRCAP, responsible for the recruitment of actin family proteins, increasing the likelihood that

TGME49_235420 is a genuine ARP4a interaction partner **(Figure 2.4.3e)**. Other Ino80 family proteins, *H. sapiens* INO80, *S. cerevisiae* INO80, or SWR1, were not among the HHpred results, indicating that TGME49_235420's putative HSA domain is minimally conserved. No structural model of SRCAP's HSA domain exists, predicted or empirically determined, for a comparison of protein folding. SNF2 chromatin remodellers typically show high conservation of the ATPase domains but no homology to any ATPase was found by HHpred. It is therefore not clear whether TGME49_235420, like other HSA domain-containing proteins, could function as the core ATPase of a large protein complex.

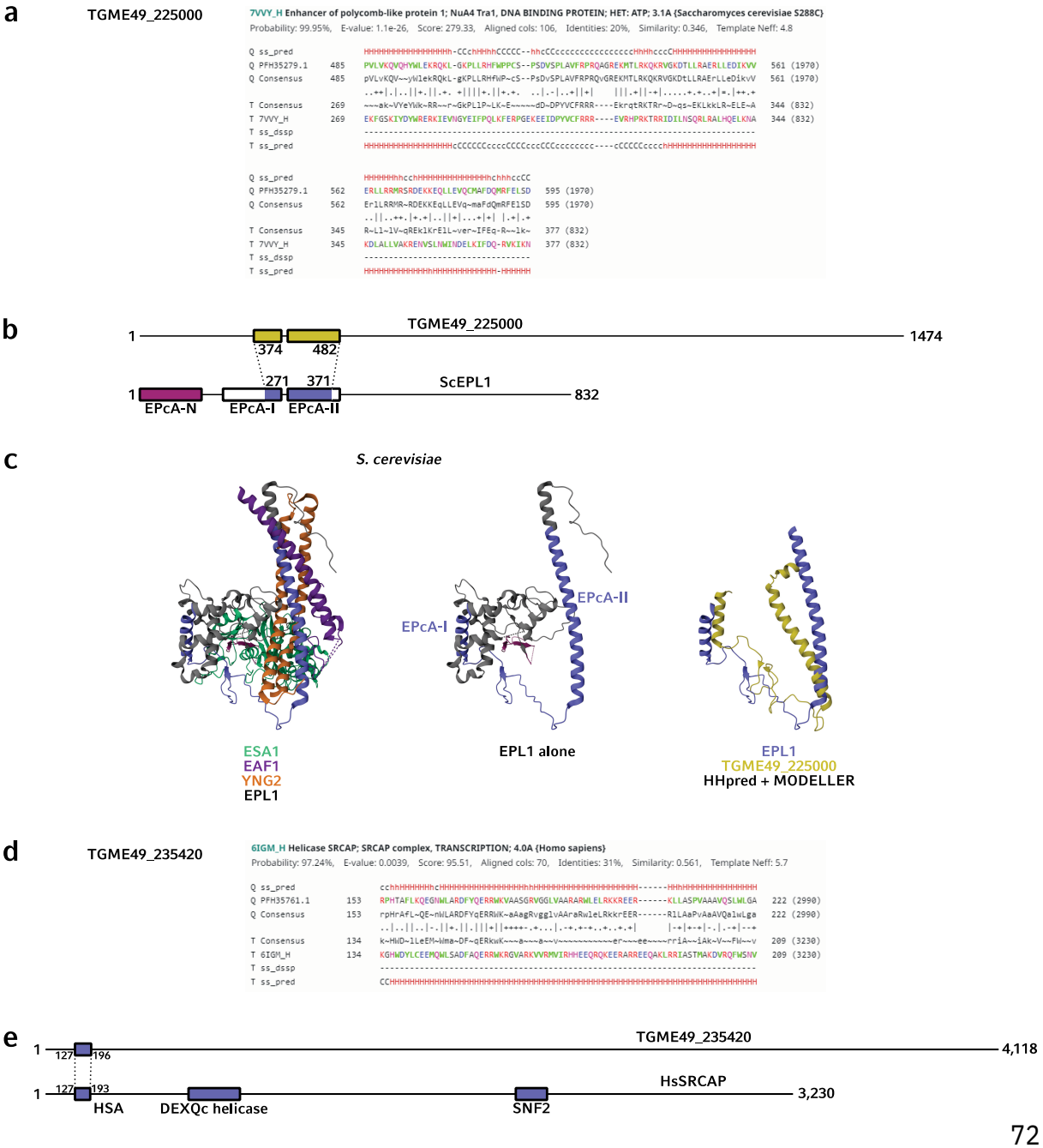

Figure 2.4.3: HHpred domain prediction for ARP4a interaction partners with no known homology.

a. HHpred result of TGME49_225000 showing predicted homology to *S. cerevisiae* EPL1. The amino acid sequence of TGME49_225000 and orthologues, as defined by OrthoDB group OG6_132978, were aligned using ClustalΩ and used in a HHpred search against *S. cerevisiae*, *H. sapiens*, and *T. thermophilia* proteins.

b. Diagramatic representation of the domain architecture of *S. cerevisiae* EPL1 with dashed lines indicating region of homology identified by HHpred.

c. Left and middle: Protein Data Bank model 5J9U (Xu *et al.*, 2016) showing the subcomplex formed by *S. cerevisiae* ESA1, EAF1, YNG2, and EPL1 within the NuA4 complex. The EPcA-II domain of EPL1 forms an α-helix that bundles with three other α-helices of the subcomplex to provide structural support. The EPcA-I domain of EPL1 associates with the catalytic, globular domain of ESA1. The EPcA-N domain, most of which is missing in model 5J9U, associates with the nucleosome. Right: the HHpred-aligned region of TGME49_225000 was folded using MODELLER with the HHpred-aligned region of EPL1 acting as a template. The two folded peptides were superposed using Mol*, yielding a root-mean-square deviation of 10.83.

d. HHpred result of TGME49_235420 showing predicted homology to *H. sapiens* SRCAP. The amino acid sequence of TGME49_235420 and orthologues, as defined by OrthoDB group OG6_111998, were aligned using ClustalΩ and used in a HHpred search against *S. cerevisiae*, *H. sapiens*, and *T. thermophilia* proteins.

e. Diagramatic representation of the domain architecture of *H. sapiens* SRCAP with dashed lines indicating region of homology identified by HHpred.

2.4.c TGME49_205562 is a coccidian-specific nuclear protein

As a putative mutual interaction partner of both ALP2a and ARP4a, TGME49_205562 was further characterised. A 627 kDa protein, TGME49_205562 is a coccidian-specific protein with strong amino acid sequence conservation amongst *T. gondii* strains, and more sequence divergence across coccidia **(Figure 2.4.4a)**. TGME49_205562 was previously identified in mass spectrometry experiments, being present in the cytosolic and membrane fractions of fractionated *T. gondii* (Dybas *et al.*, 2008) and the phosphoproteome (Dybas *et al.*, 2008). Despite its large size, TGME49_205562 had very few predicted domains, with only the PANTHER proteomic database (release 17.0) predicting any domains. However, notwithstanding the aforementioned strong sequence conservation, PANTHER predicted a myriad of different domains between the analysed *T. gondii* strains **(Figure 2.4.4b)**. Despite the absence of the F-actin-interacting WASp (Wiskott-Aldrich Syndrome protein) in the *T. gondii* proteome, a WASp interacting protein-related domain was predicted for all sequences, albeit at differing positions within the proteins. In all but two *T. gondii* strains (ME49 and VAND) the proteins were predicted to be NYN domain-containing proteins; ribonucleases conserved across Prokaryota and Eukaryota (Anantharaman and Aravind, 2006). However, the veracity of these domain predictions was doubted given their lack of consistency.

With ARP4a and ALP2a's nuclear localisation, were TGME49_205562 a genuine interaction partner it would likely be similarly localised. However, TGME49_205562 since was previously identified in both cytoplasmic and membrane subcellular protein fractions (Dybas *et al.*, 2008). TGME49_205562 was not, however, predicted to possess any transmembrane domains. Moreover, soluble nuclear proteins are commonly trafficked to the nucleus from the cytoplasm and are therefore a frequent contaminant of cytoplasmic protein fractions. To infer the likelihood of TGME49_205562's nuclear localisation, its nuclear localisation score, as predicted by NucPred (Brameier, Krings and MacCallum, 2007), was

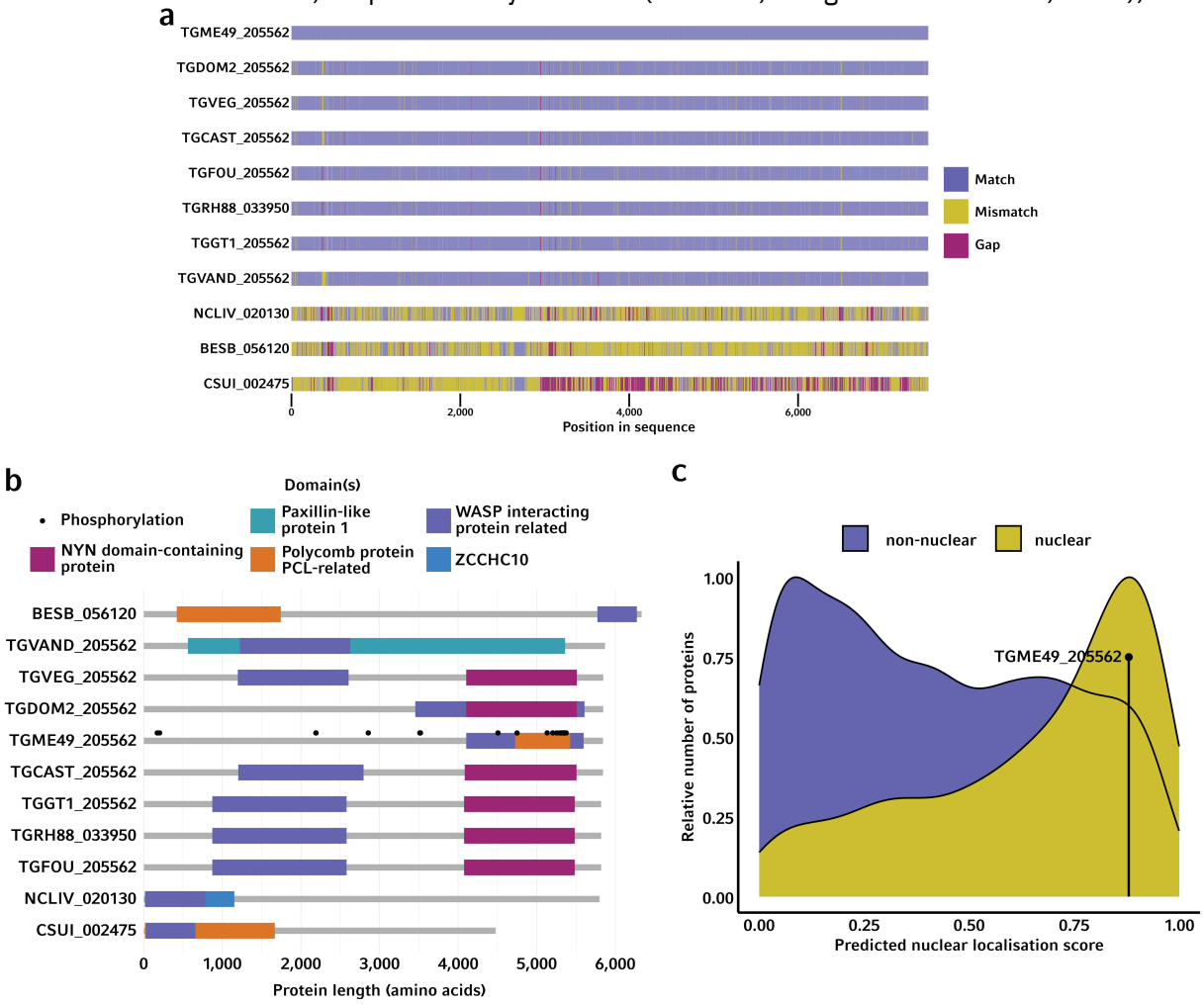

Figure 2.4.4: Bioinformatic prediction of TGME49_205562 function and localisation.

a. Amino acid sequence alignment of TGME49_205562 with a selection of homologues in other *T. gondii* strains and coccidian species. Sequences were aligned using MUSCLE *msa* package for R. Matches, mismatches, and gaps are relative to TGME49_205562 sequence.

b. PANTHER domain predictions of the proteins from a. PANTHER proteomic database release 17.0.

c. Predicted nuclear localisation score for TGME49_205562. All *T. gondii* ME49 protein sequences were processed with NucPred to predict whether they localise to the nucleus. Proteins were then filtered for those with highly probable HyperLOPIT localisations ($p > 0.9$). Remaining proteins were then grouped as nuclear when HyperLOPIT localisation was either "nucleus – chromatin", "nucleus non-chromatin", or "nucleolus", or grouped as non-nuclear otherwise. TGME49_205562's NucPred score indicated by horizontal black line.

compared to known nuclear and non-nuclear proteins **(Figure 2.4.4c)**. Filtering and grouping proteins as either nuclear or non-nuclear based on HyperLOPIT localisation probabilities (Barylyuk *et al.*, 2020) demonstrated that known nuclear proteins obtained much higher NucPred scores compared to known non-nuclear proteins. A score of 0.88 for TGME49_205562 was similar to the majority of known nuclear proteins, but also a minority of non-nuclear proteins. Thus TGME49_205562's nuclear localisation was considered more probable than improbable.

To confirm this likely nuclear localisation, TGME49_205562 was N-terminally tagged with a triple FLAG epitope tag (C-terminal knock-ins proved unviable) using CRISPR-skip-in **(Figure 2.4.5a)**. IFA visualisation of TGME49_205562 provided a punctate nuclear localisation, which was unaltered following the KD of either ALP2a or ARP4a **(Figure 2.4.5b)**. To evaluate whether TGME49_205562 could act as the link between centrosomes and either ALP2a or ARP4a, TGME49_205562's co-localisation with the centrosome was visualised. No clear co-localisation between TGME49_205562 and the centrosome was found in either parental RH Tir1 *T. gondii* or ALP2a KD and ARP4a KD tachyzoites with centrosome over-duplication **(Figure 2.4.5c)**. However, due to the fluorescence intensity of the nuclear-localised TGME49_205562, weaker or more transient interactions cannot be excluded. Further investigations such as live cell microscopy and co-precipitation would be necessary to conclusively prove whether TGME49_205562 interacts with the centrosome. Thus, it was concluded that TGME49_205562 is a coccidian-specific nuclear protein but that its function as a link between centrosomes and either ALP2a or ARP4a is not proven.

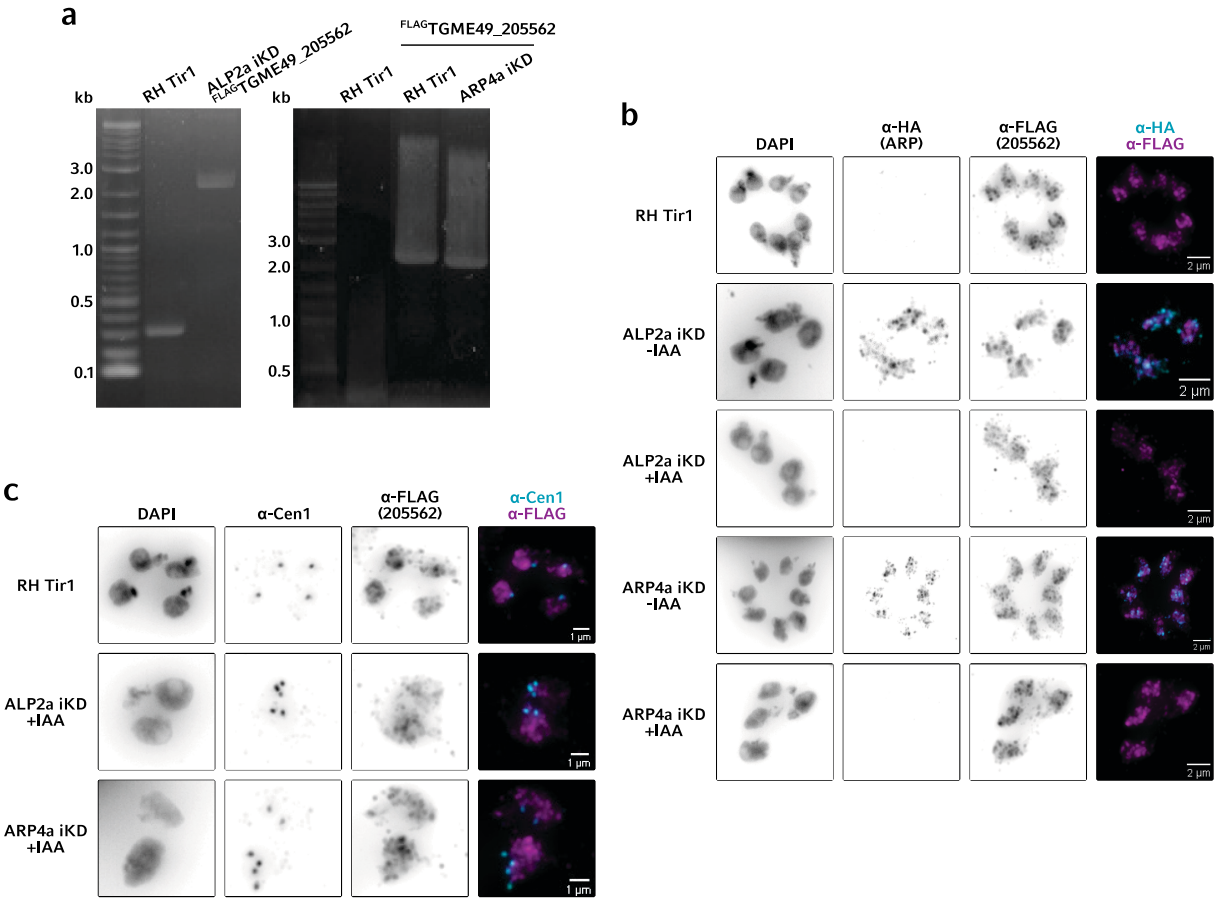

Figure 2.4.5: The co-localisation of TGME49_205562 with both ALP2a and ARP4a, as well as the centrosome

a. Genotyping PCRs confirming 5' integration of *dhfr-myc-T2A-3FLAG-linker* to create RH Tir1 FLAGTGME49_205562, ALP2a iKD FLAGTGME49_205562, and ARP4a iKD FLAGTGME49_205562. Expected 5' TGME49_205562 amplicons were 0.3 kb for WT (RH Tir1) and 2.3 kb for FLAGTGME49_205562 strains.

b. Representative Z-max widefield micrographs showing the co-localisation of ALP2a and ARP4a with TGME49_205562. Tachyzoites were inoculated into HFFs and cultured for 24 h ± 500 μM IAA before fixation and IFA labelling as indicated.

c. Representative Z-max widefield micrographs showing the lack of co-localisation between centrin 1 and TGME49_205562. Tachyzoites were inoculated into HFFs and cultured for 24 h ± 500 μM IAA before fixation and IFA labelling as indicated. KD examples shown include tachyzoites with over-duplicated centrosomes.

2.4.d Attempt to create an inducible KD of TGME49_205562

Should a null mutant of TGME49_205562 have the same phenotype as ALP2a KD and ARP4a KD this would strengthen the evidence of the protein-protein interaction between TGME49_205562 and the two ARPs. It was therefore sought to create an inducible KD strain using CRISPR-skip-in, in the same manner as had been achieved for ALP2a and ARP4a. The successful N-terminal knock-in of *hxgprt-T2A-mAID-3HA-linker* was confirmed by PCR **(Figure 2.4.6a)**. However, despite the earlier visualisation of FLAG-tagged TGME49_205562, no signal was detectable by IFA in this HA-tagged strain **(Figure 2.4.6b)**. The induction of the AID KD system resulted in no defects in tachyzoite morphology **(Figure 2.4.6b)** or altered growth rate **(Figure 2.4.6c)**. Attempts to create a stable TGME49_205562 KO using Cas9 disruption failed (data not shown).

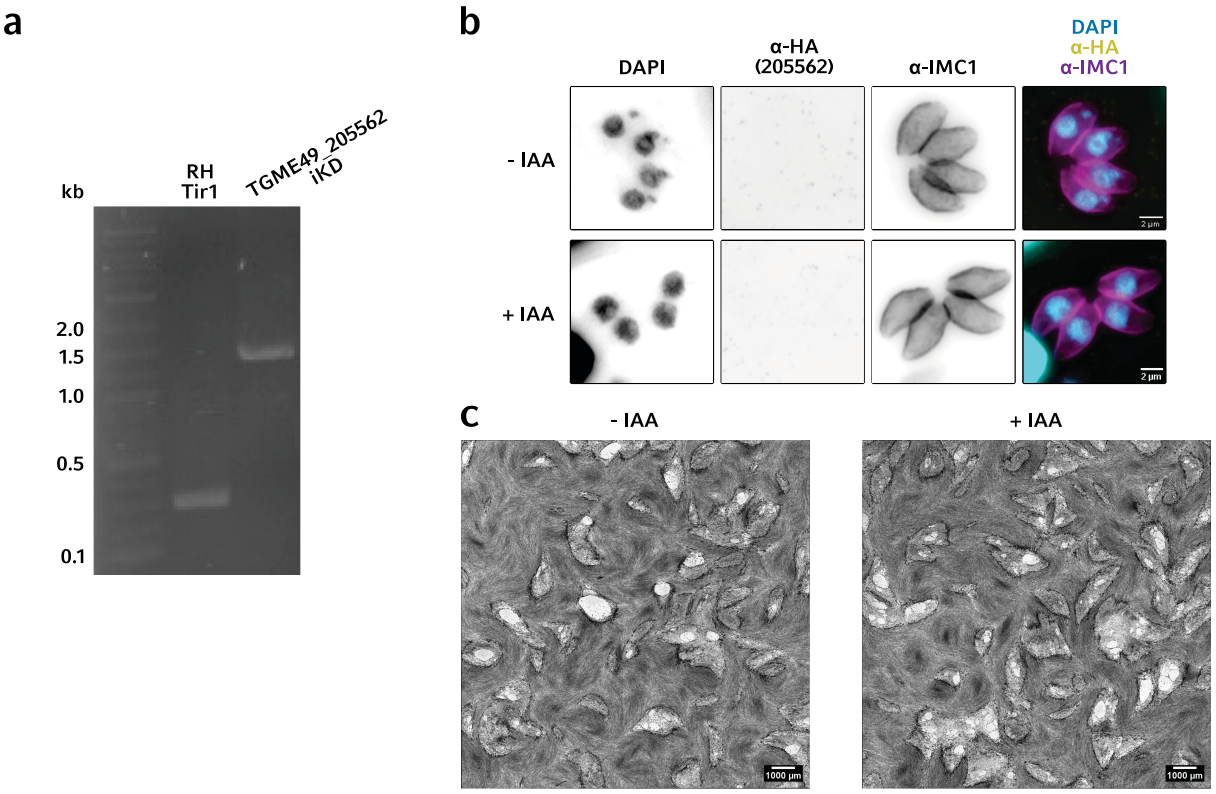

Figure 2.4.6: An inducible KD strain of TGME49_205562 showed no evidence of expression.

a. Genotyping PCRs confirming the 5' integration of *hxgprt-T2A-3HA-mAID-linker* to create TGME49_205562 iKD. Expected 5' TGME49_205562 amplicons were 0.3 kb for WT (RH Tir1) and 1.4 kb for TGME49_205562 iKD.

b. Representative IFA Z-max widefield micrographs showing lack of detectable TGME49_205562 expression in TGME49_205562 iKD strain. Tachyzoites were inoculated onto HFFs and cultured for 24 h ± 500 μM IAA before fixation IFA labelling as indicated. α-HA channel was contrasted to highlight background fluorescence.

c. Plaque formation by both TGME49_205562 iKD ± IAA following 7 days of culture. 1,000 tachyzoites per condition were inoculated onto HFFs. After 7 days of culture, cells were fixed with methanol, stained for DNA and protein, and imaged by brightfield microscopy.

2.5 Attempt to create inducible KDs of other putative *T. gondii* nuclear ARPs

2.5.a Creating an inducible ALP5 KD strain

T. gondii ALP5 (TGME49_257710), previously known as ARP6, was previously identified as a homologue of *S. cerevisiae* ARP6, another nuclear ARP known to associate with the *S. cerevisiae* Ino80 and SWR1 complexes. For the purpose of interrogating ALP5's function in *T. gondii* tachyzoites, it was attempted to create an inducible KD strain using CRISPR-skip-in. The C-terminal knock-in of *linker-3HA-mAID-T2A-hxgprt* was confirmed by PCR **(Figure 2.5.1a)**. However, like TGME49_205562, no signal from ALP5 was detected neither by IFA **(Figure 2.5.1b)** nor western blot **(Figure 2.5.1c)**. Likewise, induction of the AID KD caused no defects in tachyzoite morphology **(Figure 2.5.1b)** or altered growth rate **(Figure 2.5.1d)**.

2.5.b Creating an inducible ALP3b KD strain

T. gondii ALP3b (TGME49_248890) was previously indicated to be an apicomplexan-specific ARP (Gordon and Sibley, 2005) and was predicted to localise to the nucleus (Barylyuk *et al.*, 2020). It was therefore decided to create a null mutant of ALP3b for the purpose of characterising this potentially unusual ARP. However, despite repeated attempts at C-terminal knock-ins of the *linker-3HA-mAID-T2A-hxgprt* construct using CRISPR-skip-in, no tachyzoites ever survived drug selection.

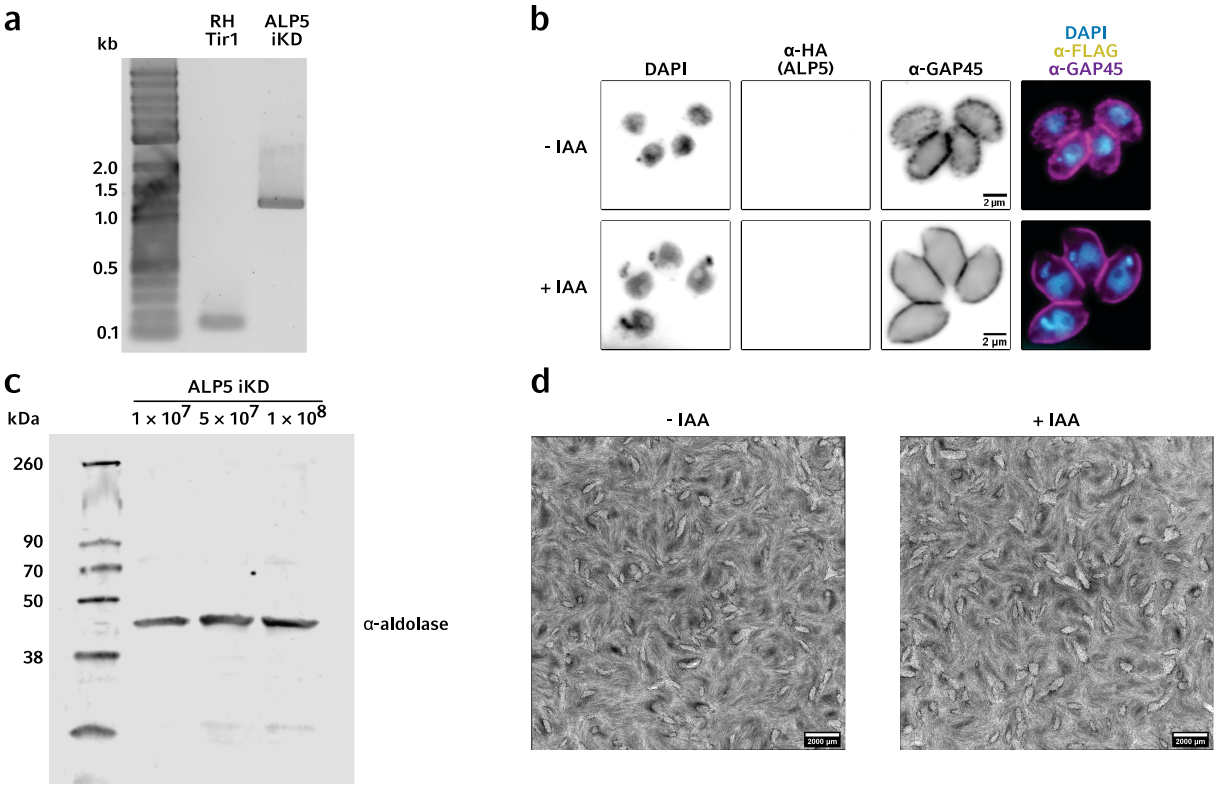

Figure 2.5.1: An inducible KD strain of ALP5 showed no evidence of expression.

a. Genotyping PCR confirming 3' integration of ALP5 with *linker-mAID-3HA-T2A-hxgprt* to create ALP5 iKD. Expected ALP5 3' amplicon sizes were 0.15 kb for WT (RH Tir1) and 1.3 kb for ALP5 iKD.

b. Representative IFA Z-max widefield micrographs showing no detectable expression of ALP5 in ALP5 iKD. Tachyzoites were inoculated onto HFFs and cultured for 24 h ± 500 µM IAA before fixation and IFA labelling as indicated.

c. Western blot showing lack of detectable ALP5 expression in ALP5 iKD. Whole cell lysate from indicated number of intracellular tachyzoites was loaded. Blots were probed with α-HA and α-aldolase. Predicted protein molecular sizes were 47 kDa for aldolase, 66 kDa for WT ALP5, and 82 kDa for ALP5$^{mAID-3HA}$.

d. Plaque formation by ALP5 iKD ± 500 µM IAA following 7 days of culture. 1,000 tachyzoites per condition were inoculated onto HFFs. After 7 days of culture, cells were fixed with methanol, stained for DNA and protein, and imaged by brightfield microscopy.

2.6 Characterisation of null mutants of SNF2 ATPase chromatin remodellers

Since nuclear ARPs most commonly function as part of ATP-dependent chromatin remodelling complexes, the study of *T. gondii* nuclear ARPs was complemented by the parallel investigation of multiple SNF2 chromatin remodellers. Of the SNF2 ATP-dependent chromatin remodellers targeted, knock-ins were obtained for SNF2l, SNF2h, CHD1, and Ino80.

2.6.a Attempt to create an INO80 null mutant

As the putative core component of the ARP4a-containing Ino80 complex, it was sought to create a null mutant of the INO80 core protein. Whilst C-terminal knock-in of INO80 with *3HA-FLAG* was possible **(Figure 2.6.1a)** and INO80 expression visible by IFA **(Figure 2.6.1b)**, repeated attempts at C-terminal knock-ins of INO80 with mAID failed.

2.6.b Generation of SNF2l inducible knockdown strain

CRISPR-skip-in was used to C-terminally knock-in SNF2l (TGME49_321440) with *linker-3HA--mAID-T2A-hxgprt* for the purpose of creating an inducible knockdown strain, creating the strain termed SNF2l iKD **(Figure 2.6.2a)**. Western blotting confirmed that, upon the addition of IAA, SNF2l protein levels were knocked down after 1 hour **(Figure 2.6.2b)**. To determine whether SNF2l was essential for tachyzoite growth, plaque assays were performed. The KD of SNF2l completely abrogated the formation of plaques **(Figure 2.6.2c)**, indicating that tachyzoites were unable to complete a full lytic

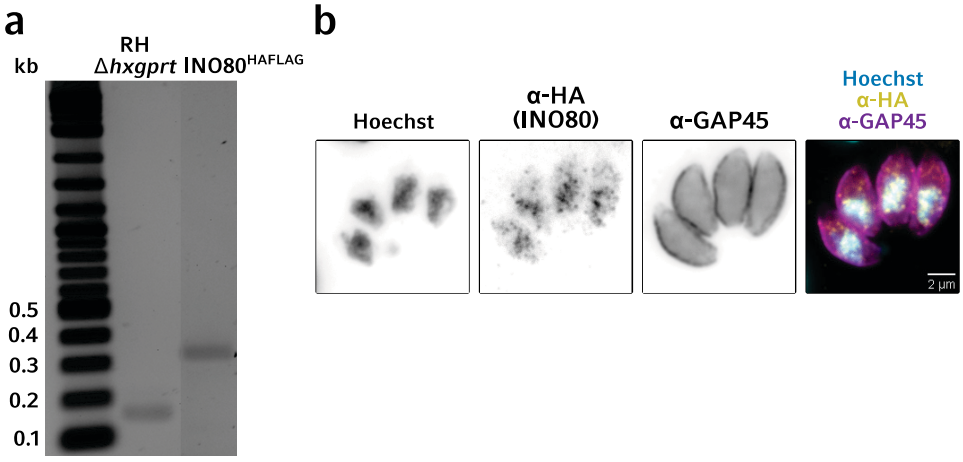

Figure 2.6.1: The visualised expression of INO80.

a. Genotyping PCR confirming 3' integration in INO80 with *linker-3HA-FLAG*. Expected INO80 3' amplicon sizes were 0.16 kb for WT (RHΔ*hxgprt*) and 0.33 kb for INO80^{HAFLAG}.

b. Widefield IFA Z-max micrograph showing the expression of INO80 in INO80^{HAFLAG} strain. Tachyzoites were inoculated onto HFFs are cultured for 24 h before fixation and IFA labelling as indicated.

cycle without the expression of SNF2l. This was confirmed through the visualisation and quantification of tachyzoite vacuole growth during the lytic cycle. Visually, it was found that SNF2l KD tachyzoites presented an intact cytoskeleton but with an additional, atypical, bulbous posterior structure **(Figure 2.6.2d)**. The quantification of tachyzoite growth through mean vacuole stage showed that SNF2l KD tachyzoites grew relatively normal until 10 hours post IAA addition, at which point growth slowed in comparison to non-induced SNF2l iKD, before complete growth arrest occurred at 24 hours post IAA addition **(Figure 2.6.2e)**. Growth arrested vacuoles consisted of 1- and 2-stage vacuoles **(Figure 2.6.2f)**. Therefore, SNF2l is critical for the replication of *T. gondii* tachyzoites through endodyogeny, and not just the lytic cycle.

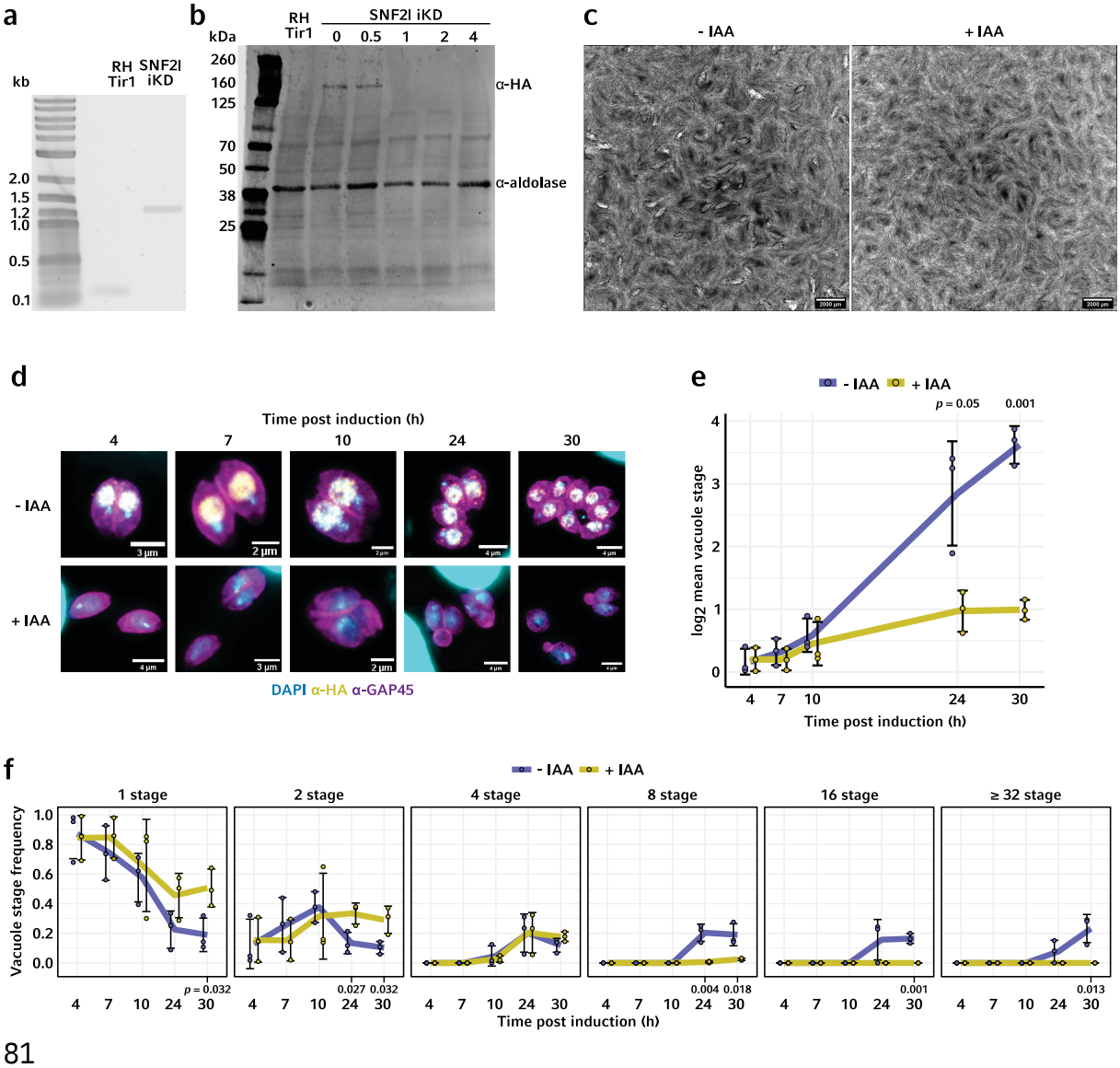

Figure 2.6.2: The KD of SNF2l resulted in the growth arrest of *T. gondii* tachyzoites.

a. Genotyping PCR confirming 3' integration of SNF2l with *linker-mAID-3HA-T2A-hxgprt* to create SNF2l iKD. Expected SNF2l 3' amplicons were 0.2 kb for WT (RH Tir1) and 1.4 kb for SNF2l iKD.

b. Time course fluorescence western blot showing the effect of IAA treatment on SNF2l expression in SNF2l iKD. 50 μg of protein was loaded per lane. Parental strain RH Tir1 included as control. Blots were probed with α-HA and, as a loading control, α-aldolase. Predicted protein molecular weights were 47 kDa aldolase, 155 kDa SNF2l$^{mAID\text{-}3HA}$ (SNF2l iKD).

c. Plaque formation of SNF2l iKD after 7 days ± 500 μM IAA. 1,000 tachyzoites per condition were inoculated onto HFFs. After 7 days of culture, cells were fixed with methanol, stained for DNA and protein, and imaged by brightfield microscopy.

d. Representative IFA widefield Z-max micrographs showing morphology of SNF2l iKD vacuoles between 4- and 30-hours post induction. Tachyzoites were allowed to invade HFFs for 1 hour in the absence of IAA before non-invaded tachyzoites were removed by washing and culture medium supplemented with ± 500 μM IAA. Assays were fixed between 4 and 30 hours and labelled by IFA as indicated.

e. Comparison of tachyzoite vacuole growth by SNF2l iKD ± IAA during the first lytic cycle. Assay performed as in d. The number of tachyzoites per vacuole was manually counted and used to calculate the mean vacuole stage (mean tachyzoites per vacuole) at each indicated time point. Error bars indicate standard deviation of three biological replicates. Result of Student's t-test shown where $p \leq 0.05$.

f. As e. but instead of mean vacuole stage, each panel represents a single vacuole stage with the data indicating the relative frequency of each vacuole stage per time point. Error bars indicate standard deviation of three biological replicates; result of Student's t-test shown where $p \leq 0.05$.

2.6.c Generation of SNF2h inducible knockdown strain

In the same manner as SNF2l, SNF2h (TGME49_273870) was C-terminally knocked-in with *linker-3HA-mAID-T2A-hxgprt* to create SNF2h iKD **(Figure 2.6.3a)**. Again, the essentially of SNF2h to tachyzoite growth was determined through plaque assay, with SNF2h KD resulting in completely abrogated plaque formation **(Figure 2.6.3b)**. Visualising the tachyzoites through the lytic cycle, morphological defects became apparent from 24 hours post IAA addition. Irregular cytoskeletal shape, extracellular nuclei, and other gross failed replication phenotypes were present **(Figure 2.6.3c)**. Reciprocally, the quantification of mean vacuole stage highlighted a normal growth rate until 10 hours post IAA addition, whereafter growth continued until the last time point of 30 hours, but at a retarded rate **(Figure 2.6.3d)**. Unlike with SNF2l KD, complete growth arrest did not occur within the 30 hours examined. At this final time point, the retarded growth rate resulted in an over-representation of 4 stage vacuoles and under-representation of ≥ 32 stage vacuoles, when compared to non-induced SNF2h iKD **(Figure 2.6.3e)**. It was therefore concluded that the two ISWIs, SNF2l and SNF2h, have differing but equally essential roles during the lytic cycle.

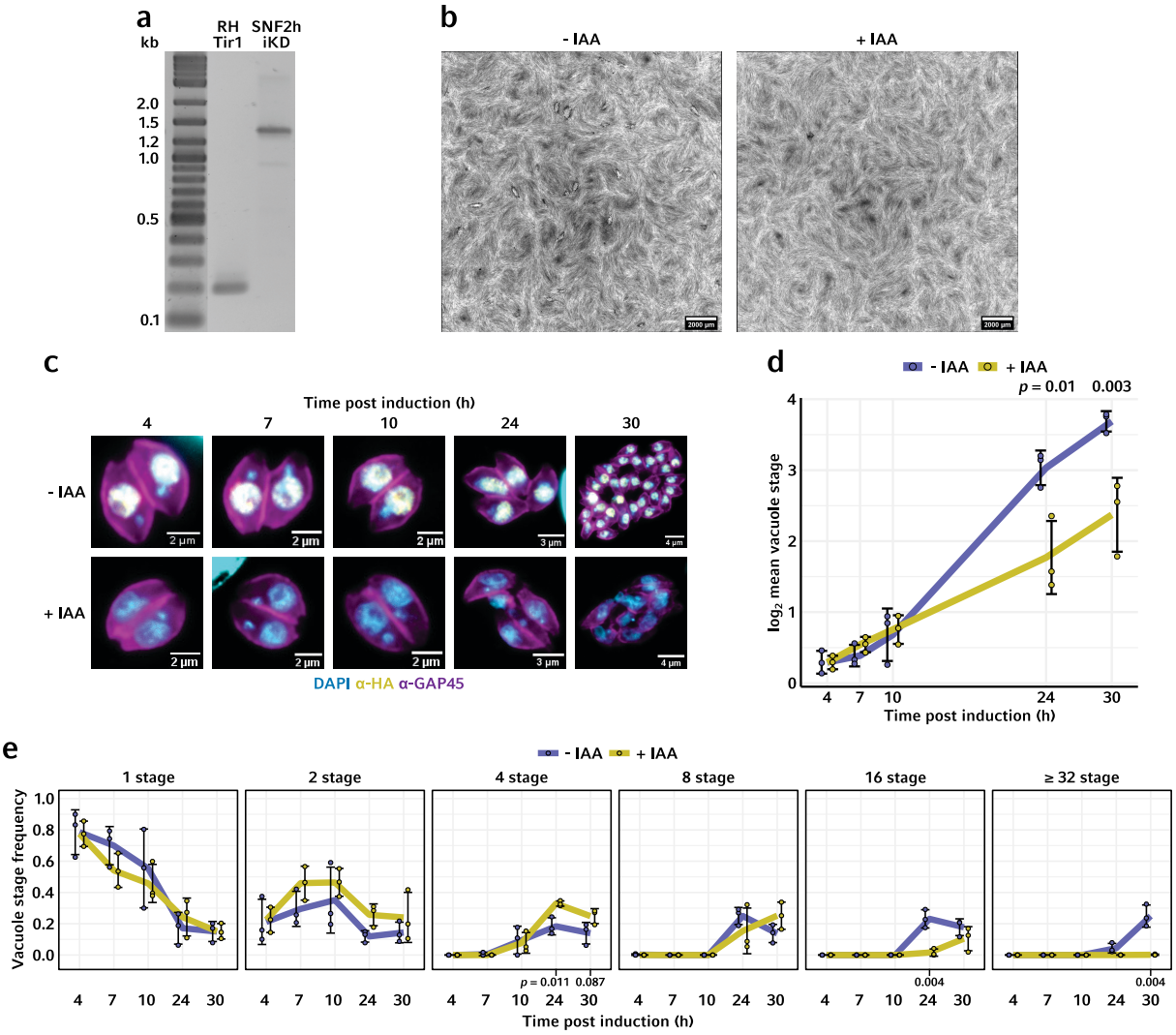

Figure 2.6.3: The KD of SNF2h resulted in growth retardation and death of *T. gondii* tachyzoites.

a. Genotyping PCR confirming 3' integration of SNF2l with *linker-mAID-3HA-T2A-hxgprt* to create SNF2l iKD. Expected SNF2l 3' amplicons were 0.2 kb for WT (RH Tir1) and 1.4 kb for SNF2l iKD.

b. Plaque formation of SNF2l iKD after 7 days ± 500 μM IAA. 1,000 tachyzoites per condition were inoculated onto HFFs. After 7 days of culture, cells were fixed with methanol, stained for DNA and protein, and imaged by brightfield microscopy.

c. Representative IFA widefield Z-max micrographs showing morphology of SNF2l iKD vacuoles between 4- and 30-hours post induction. Tachyzoites were allowed to invade HFFs for 1 hour in the absence of IAA before non-invaded tachyzoites were removed by washing and culture medium supplemented with ± 500 μM IAA. Assays were fixed between 4 and 30 hours and labelled by IFA as indicated.

d. Comparison of tachyzoite vacuole growth by SNF2l iKD ± IAA during the first lytic cycle. Assay performed as in c. The number of tachyzoites per vacuole was manually counted and used to calculate the mean vacuole stage (mean tachyzoites per vacuole) at each indicated time point. Error bars indicate standard deviation of three biological replicates. Result of Student's t-test shown where $p \leq 0.05$.

e. As d. but instead of mean vacuole stage, each panel represents a single vacuole stage with the data indicating the relative frequency of each vacuole stage per time point. Error bars indicate standard deviation of three biological replicates; result of Student's t-test shown where $p \leq 0.05$.

2.6.d Generation of CHD1 inducible knockdown strain

A CHD1 (TGME49_258240) inducible knockdown strain was created using CRISPR-skip-in to knock-in *linker-3HA-mAID-T2A-hxgprt* C-terminally, creating CHD1 iKD **(Figure 2.6.4a)**. However, inducing the KD through IAA addition did not result in any change in the growth rate of tachyzoites, as seen determined by plaque formation **(Figure 2.6.4b)**. The visualisation of CHD1 iKD ± IAA treatment indicated that IAA addition did lead to CHD1 KD, with the loss of IFA signal **(Figure 2.6.4c)**. Though, in line with the normal growth rate of CHD1 iKD + IAA, no morphological defects were seen with CHD1 KD vacuoles **(Figure 2.6.4c)**. CHD1 expression is therefore not required for the *in vitro* culture of *T. gondii* tachyzoites.

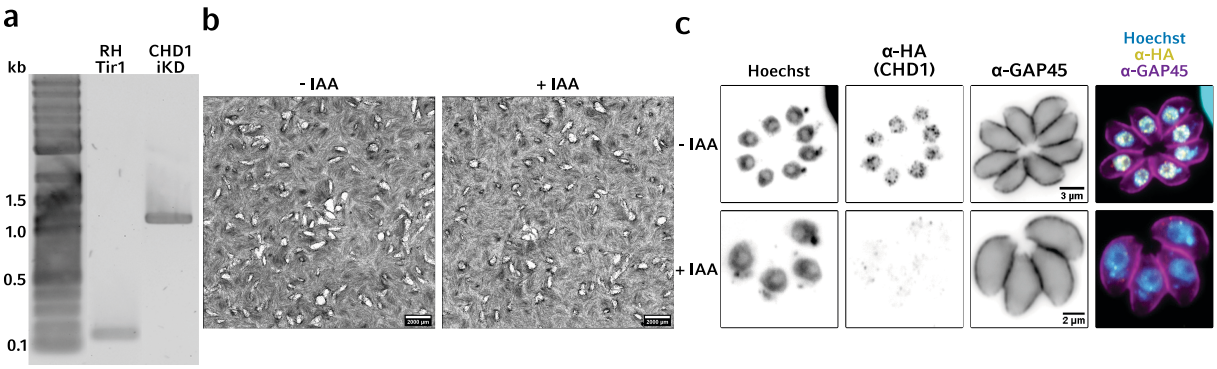

Figure 2.6.4: CHD1 expression is dispensable for *T. gondii* tachyzoite growth.

a. Genotyping PCR confirming CHD1 endogenous 3' tagging with *linker-mAID-3HA-T2A-hxgprt* to create CHD1 iKD. Expected CHD1 3' amplicon sizes were 0.19 kb for WT (RH Tir1) and 1.3 kb for CHD1 iKD.

b. Plaque formation of CHD1 iKD after 7 days ± IAA. 1,000 tachyzoites per condition were inoculated onto HFFs. After 7 days of culture, cells were fixed with methanol, stained for DNA and protein, and imaged by brightfield microscopy.

c. Representative IFA widefield Z-max micrographs showing knockdown of CHD1 in CHD1 iKD. Tachyzoites were inoculated onto HFFs and cultured for 24 h ± 500 μM IAA before fixation and IFA labelling as indicated.

2.7 Using the actin Chromobody® to visualise nuclear F-actin in *T. gondii*

2.7.a Cloning of nuclear actin Chromobody® plasmids

Multiple plasmids intended to aid in the visualisation of nuclear F-actin were created. The explanations for their creation are detailed in the coming sections, but a summary of their cloning is as follows.

To introduce the actin Chromobody®-mEmerald (CbEm) to the nucleus of *T. gondii*, twin SV40 nuclear localisation signals (NLS) were added to the *pDHFR-Chromobody-mEmerald* plasmid **(Figure 2.7.1a)** (Periz *et al.*, 2017) after the mEmerald by site-directed mutagenesis PCR **(Figure 2.7.1b)**. To permit the isolation of stable lines expressing the construct by drug selection, a HXGPRT cassette was added by traditional restriction enzyme cloning **(Figure 2.7.1c)**. For tighter nuclear expression, two additional NLS were added before the actin Chromobody® by site-directed mutagenesis PCR **(Figure 2.7.1d)**. To express the nuclear actin Chromobody® polycistronically with the drug resistance marker HXGPRT, Gibson assembly was used to add T2A-HXGPRT in frame with the existing frame **(Figure 2.7.1e)**.

2.7.b Expressing nuclear actin Chromobody® in *T. gondii* tachyzoites

To create stable lines expressing the CbEm in the *T. gondii* nucleus, vectors CbEm^{NLS} **(Figure 2.7.1c)** and ^{NLS}CbEm^{NLS} **(Figure 2.7.1d)** were integrated into the genome of RHΔ*hxgprt T. gondii* using restriction enzyme-mediated integration (Black *et al.*, 1995). Following the establishment of MPA-resistant *T. gondii* pools, successful integration and expression of the constructions was assessed by microscopy. However, it was found the pools were only 0.8 and 0.3% positive for CbEm^{NLS} and ^{NLS}CbEm^{NLS}, respectively. Therefore, the pools were subjected to further purification via FACS, with one event per well being sorted into 96-well plates to create clonal lines. Following one week's outgrowth, the CbEm expression of six clones per strain was monitored for four cell culture passages **(Figure 2.7.2a)**. For both strains, CbEm^{NLS} and ^{NLS}CbEm^{NLS}, some clones had either lost the CbEm expression completely or progressively lost expression during the four passages **(Figure 2.7.2a, yellow lines)**. No clones showed 100% expression of CbEm. The clones with the highest number of CbEm-positive vacuoles were selected for further characterisation **(Figure 2.7.2a, blue lines)**. The CbEm localisation of the clones was found to be predominantly nuclear **(Figure 2.7.2b)**.

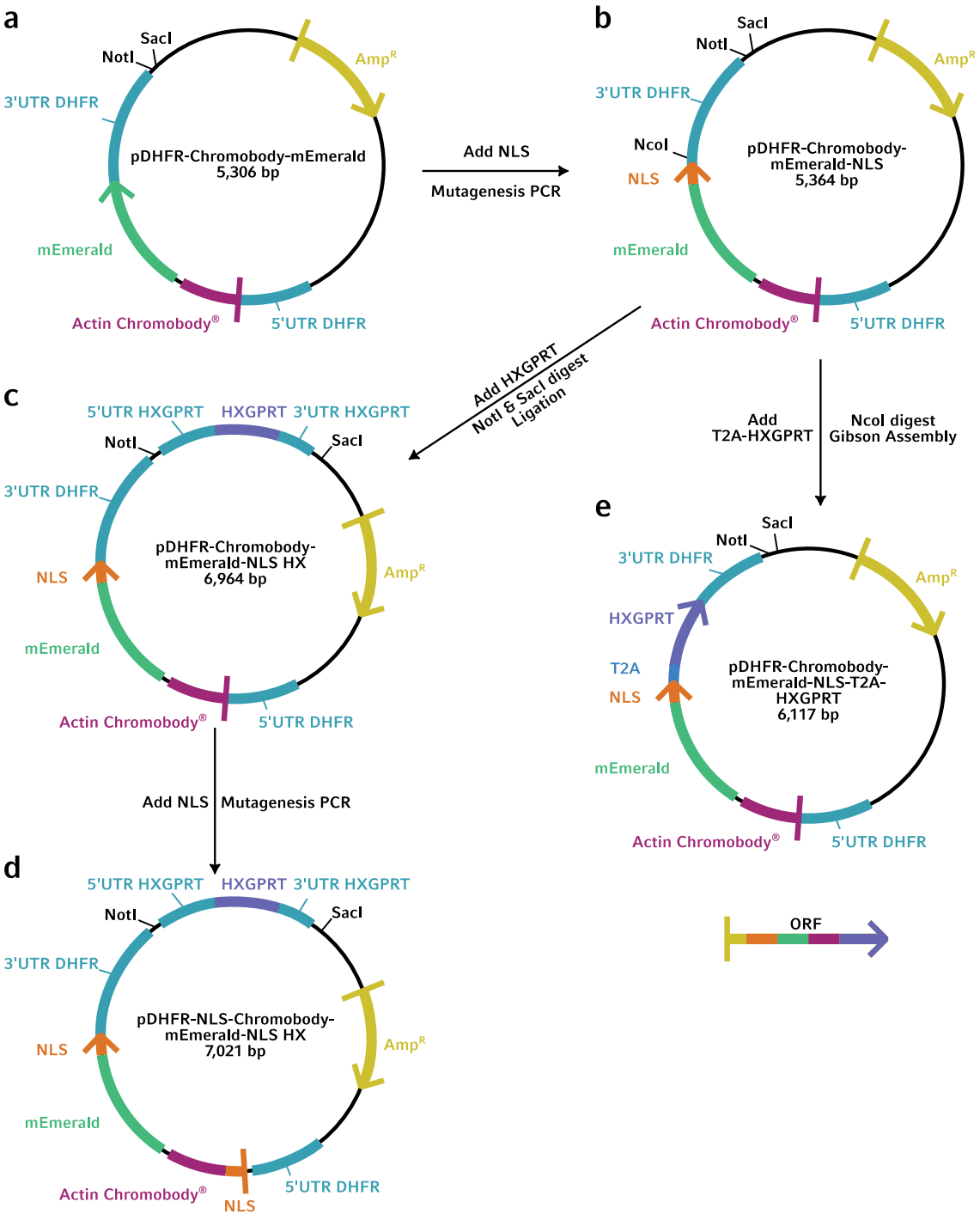

Figure 2.7.1: Overview of cloning steps to create nuclear actin Chromobody® expression plasmids.

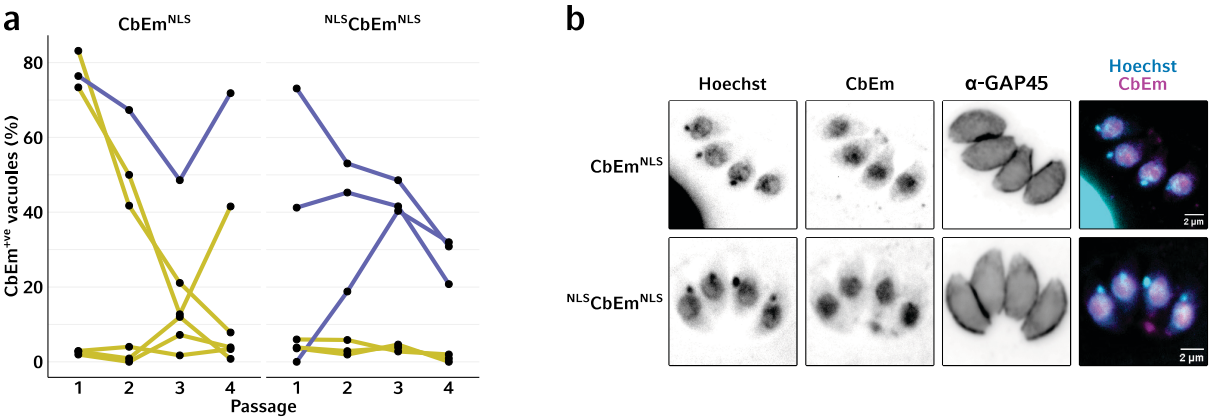

Figure 2.7.2: The generation of stable lines expressing CbEm^{NLS} and ^{NLS}CbEm^{NLS}.

a. Number of CbEm positive vacuoles through four cell culture passages for six FACS-generated clonal strains. Relative number of CbEm^{+ve} vacuoles was quantified manually via widefield microscopy. At each passage, tachyzoites from each clonal strain were inoculated onto HFFs and cultured for 24 h before fixation and IFA labelling with α-GAP45. Blue lines indicate strains selected for subsequent experiments; yellow lines indicate strains that were discarded.

b. Widefield Z-max micrographs showing the localisation of CbEm^{NLS} and ^{NLS}CbEm^{NLS} in clonal lines of a. Assay performed as in a.

Since the mEmerald of CbEm^{NLS} and ^{NLS}CbEm^{NLS} was constitutively fluorescent, regardless of whether it was F-actin bound, the ability of the CbEm to bind F-actin was assessed via treatment with jasplakinolide, an F-actin stabiliser and polymerisation enhancer. Treatment of the CbEm^{NLS} clone with 50 nM jasplakinolide resulted in condensation of the CbEm signal, indicating that, in this clone, F-actin formation in the nucleus is possible and that the CbEm^{NLS} construct has retained its ability to selectively bind to F-actin **(Figure 2.7.3a)**. This condensation of the CbEm signal presented itself as three localisations: condensates in the nucleus, condensates in the vacuole's residual body with reduced nuclear CbEm expression, and a mix of the two localisations **(Figure 2.7.3a)**. Treatment of the CbEm^{NLS} clone with 200 nM jasplakinolide resulted in strong nuclear F-actin bundles, although toxic side effects of the treatment were, overall, more apparent **(Figure 2.7.3b)**. For each of the three ^{NLS}CbEm^{NLS} clones, treatment with jasplakinolide did not lead to condensation of the CbEm signal, using either 50 nM **(Figure 2.7.3c)** or 200 nM jasplakinolide **(Figure 2.7.3d)**, suggesting that this construct was not capable of binding to F-actin.

All clones examined continued to progressively lose CbEm expression, in terms of both CbEm expression intensity and number of CbEm-expressing tachyzoites within the lines. Near or total loss of expression transpired with four to six weeks (estimated).

Despite progressively losing their CbEm expression, the CbEm^{NLS} and ^{NLS}CbEm^{NLS} clones maintained their resistance to mycophenolic acid (MPA) treatment, suggesting a silencing of the CbEm cassette but not the independently expressed HXGPRT cassette occurred. To overcome this shortcoming, the expression of the HXGPRT selection marker was coupled to the expression of the CbEm^{NLS} construct by means of a T2A skip peptide, so that CbEm^{NLS} and HXGPRT could be expressed polycistronically

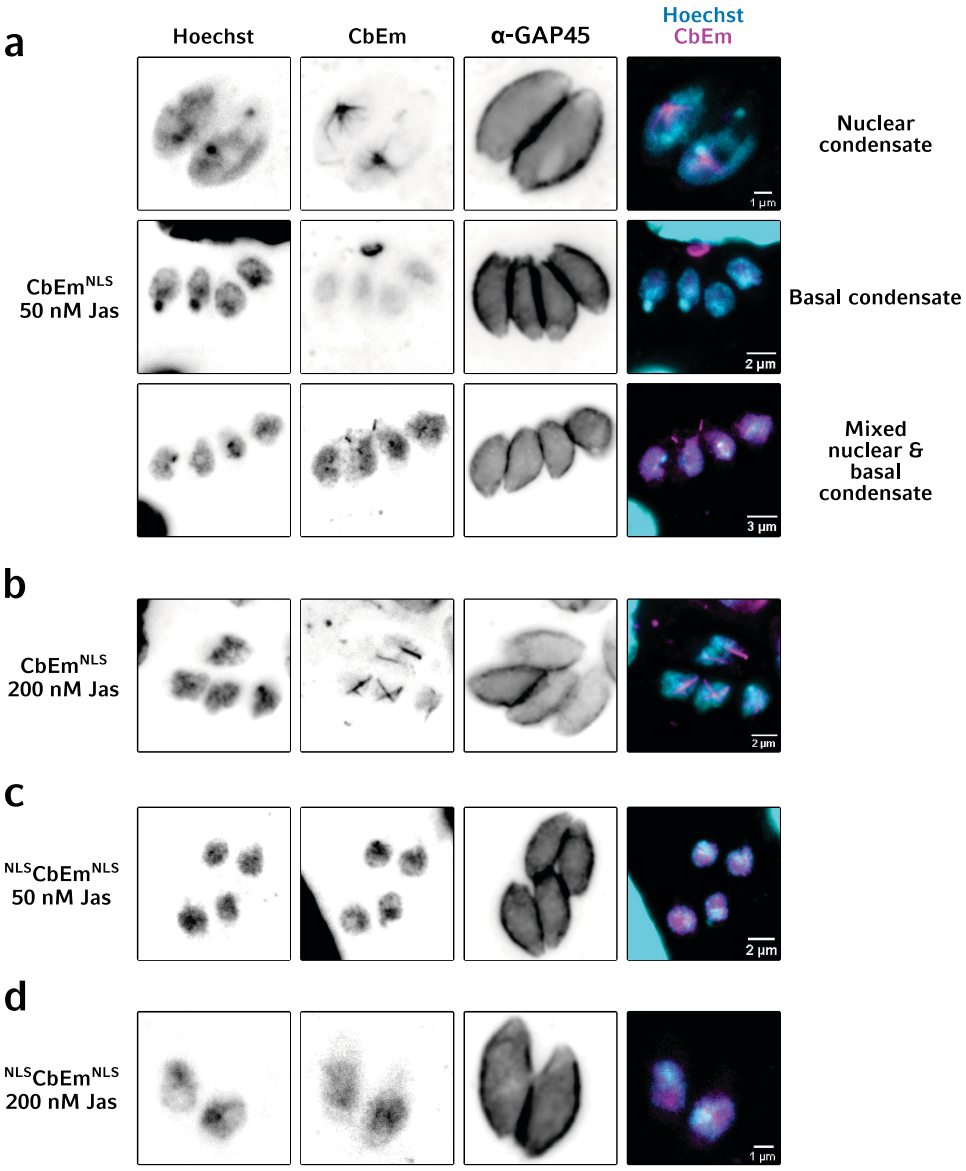

Figure 2.7.3: The effect of jasplakinolide on the localisation of CbEm^{NLS} and ^{NLS}CbEm^{NLS}.

a. Widefield Z-max micrographs showing the range of CbEm^{NLS} localisations after treatment with 50 nM jasplakinolide. Tachyzoites were inoculated onto HFFs and cultured for 24 h before the culture medium was supplemented with 50 nM jasplakinolide for a further 30 min. Following PFA fixation, IFA labelling proceeded as indicated.

b. As a., but with 200 nM jasplakinolide treatment for 30 min.

c. As a., but with ^{NLS}CbEm^{NLS}.

d. As c., but with 200 nM jasplakinolide treatment for 30 min.

(Figure 2.7.1e). Following transfection of this vector and four weeks' of MPA selection, a drug-resistance pool was formed. However, despite the continuous MPA treatment, this pool showed no CbEm expression **(Figure 2.7.4)**.

Since the generation of a stable CbEm^{NLS} did not prove possible, the extent to which transient assays could be used to visualise nuclear F-actin was explored. Whilst transient expression of the CbEm^{NLS} led to higher nuclear CbEm signal intensity, the higher expression also resulted in significant CbEm^{NLS} expression in the vacuole's residual body **(Figure 2.7.5)**. To determine whether nuclear F-actin filaments were present in *T. gondii*, STED microscopy was used with RHΔ*hxgprt* transiently expressing CbEm^{NLS}. This revealed several filamentous structures that could be F-actin **(Figure 2.7.5, insets)**. However, it cannot be definitively concluded whether these structures were intra- or para-nuclear.

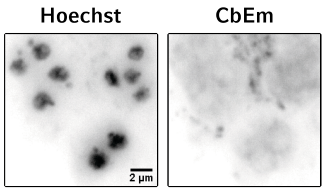

Figure 2.7.4: No CbEm^{NLS} expression in drug-resistant pool following transfection of CbEm^{NLS}-T2A-*hxgprt*.

Tachyzoites that were MPA-resistant following transfection of CbEm^{NLS}-T2A-*hxgprt* were inoculated onto HFFs and cultured for 24 h before PFA fixation, labelling with Hoechst, and visual examination of CbEm expression by widefield microscopy.

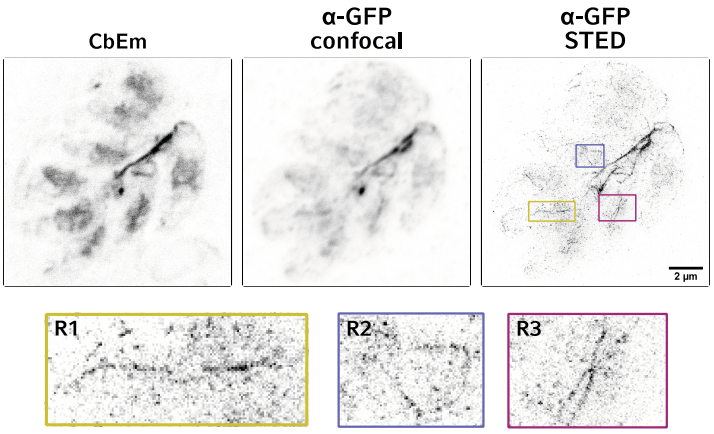

Figure 2.7.5: Filamentous CbEm^{NLS} structures visualised with STED microscopy with transiently expressed CbEm^{NLS}.

RHΔ*hxgprt* tachyzoites were transfected with *pDHFR-Chromobody-mEmerald-NLS* (Figure 2.7.1b), inoculated onto HFFs and cultured for 24 h before PFA fixation. IFA labelling with α-GFP was used to facilitate STED imaging, with the native CbEm fluorescence and α-GFP channel fluorescence spectrally segregated. Micrographs were generated using a STEDYCON (Abberior) operating in both confocal and STED imaging modes.

3 Discussion

3.1 The niche of CRISPR-skip-in as a reverse genetic tool for *T. gondii* research

CRISPR-skip-in is largely a fusion of existing genetic engineering approaches utilised in both *T. gondii* and wider research. Combining the drug resistance-driven LIC, the specificity of Cas9-based HiT, and the polycistronic expression of skip peptides, CRISPR-skip-in was highly efficacious in the generation of knock-in *T. gondii* strains when utilised with HXGPRT or DHFR drug selection. Existing *T. gondii* knock-in strategies like LIC and HiT both supplant the endogenous 3'UTR of the gene of interest. Whilst they are non-protein-encoding, 3'UTRs are a factor in the control of gene expression by means of mRNA localisation, stability, translation, and recruitment of post-transcriptional modification complexes (Mayr, 2019). In *T. gondii*, the modification of- and replacement of endogenous 3'UTRs has been shown to alter the gene product's expression level (Pieperhoff *et al.*, 2015; Farhat *et al.*, 2021). Whether any changes in protein expression following 3'UTR replacement are deleterious will vary by the gene targeted and by the nature of the changes made. However, since over- and under-expression of proteins can both cause deleterious effects, as seen with *T. gondii* Rab proteins (Kremer *et al.*, 2013), it is generally advisable to maintain endogenous expression where possible. Thus, as the first *T. gondii* knock-in approach to combine drug selection whilst maintaining endogenous expression levels, CRISPR-skip-in has clear advantages over the aforementioned approaches. In addition, CRISPR-skip-in proved successful for both N- and C-terminal knock-ins, further increasing the likelihood that CRISPR-skip-in can be successfully applied to endogenously tag a given gene.

A caveat of CRISPR-skip-in, however, is that it is only suitable for knock-ins within protein-coding sequences. Since the drug resistance marker must be translated along with the protein of interest, the sequence to be knocked-in must be inserted proximal to either the ATG or STOP codons, as well as in the same open reading frame as the gene of interest. This means that CRISPR-skip-in is not ideally suited for the employment of technologies that require genetic modifications to be made outside of an open reading frame, such as TATi and DiCre, which require promoter exchange and the knock-in of loxP within UTRs, respectively (Meissner, Schlüter and Soldati, 2002; Andenmatten *et al.*, 2013b). Using CRISPR-skip-in, promoter exchange would not be possible, only supplanting the endogenous promoter by knocking in the TATi promoter between the endogenous promoter and the ORF of the gene of interest. This would carry the risk that the still present endogenous promoter can still function to regulate expression of the gene of interest. LoxP knock-in using CRISPR-skip-in is theoretically

possible, with a *loxP-ATG-drug^r-T2A-* construct for 5' loxP knock-in, and *-T2A-drug^r-STOP-loxP* for 3' loxP knock-in. However, this would require the use of two different drug markers. Since only HXGPRT and DHFR proved sufficiently successful with CRISPR-skip-in, further drug selection-based genetic modifications would be limited to non-CRISPR-skip-in approaches following the loxP insertions. In addition, CRISPR-skip-in is not suitable for internal knock-ins, since the protein of interest would be truncated by the drug resistance marker.

In two cases, CRISPR-skip-in appeared to work at the DNA level but without detectable expression of the protein of interest. By genotyping PCR, ALP5 was successfully tagged C-terminally and TGME49_205562 N-terminally. In both cases, the mAID domain was part of the tagging construct. Whilst a clear explanation for these instances is not immediately available, it seems more likely that this a problem specific to the mAID domain rather than the CRISPR-skip-in approach. Non-mAID CRISPR-skip-in N-terminal knock-ins of TGME49_205562 were successful, highlighting the viability of the approach. Moreover, both strains, ALP5 iKD and TGME49_205562 iKD, were MPA-resistant, indicating that the *hxgprt* was being transcribed and translated. Skip peptides, including T2A, do not act as ribosomal entry sites. Therefore, in the case of ALP5 iKD, the ALP5-3HA-mAID cistron must be translated before the HXGPRT cistron, or else no HXGPRT expression would occur. Thus, the MPA-resistance infers ALP5 expression. In the case of ALP2a iKD, the fusion of the mAID domain to ALP2a alone resulted in a ~ 70% reduction in protein levels. Whilst this effect was not seen with ARP4a, indicating that the mAID-fusion-associated partial KD is not consistent between different proteins, it is plausible that a similar partial KD led to the inability to detect ALP5 and TGME49_205562 expression when fused with mAID.

The use of skip peptides is not scarless, insofar that the peptide remains fused to the gene products after translation. All characterised skip peptides end with a glycine and a proline. T2A's amino acid sequence is EGRGSLLTCGDVEENPGP. During translation, the peptide bond between the C-terminal glycine and proline is omitted. As such, the entire T2A peptide sequence except the final proline is fused to the N-terminal cistron's gene product, and the proline likewise to the C-terminal's. It is conceivable that these residual amino acids could interfere with the protein of interest's function or folding, and therefore the protein's expression levels. However, in the case of TGME49_205562, which was N-terminally endogenously tagged, the addition of a lone N-terminal proline is unlikely to significantly affect the protein.

A known shortcoming of skip peptides is incomplete cleavage. For example, T2A has been demonstrated to only result in separate proteins in 60 – 90% of translated protein, depending on cell type used for expression (Kim *et al.*, 2011). The efficiency of T2A in *T. gondii* has not been quantified. However, some knock-ins used in this study made use of myc-fused DHFR. Visualisation of the ^{myc}DHFR and Nuf2^{FLAG} localisation, for example, by microscopy showed the DHFR to be exclusively cytoplasmic (data not shown), indicating that T2A efficiency is good in *T. gondii*. However, quantitative western blotting would be required to more reliably determine the efficiency of T2A cleavage.

As a potential further improvement on CRISPR-skip-in, it is postulated that the requirement for skip peptide drug marker expression could be dispensed with. MPA kills *hxgprt*$^{-}$ *T. gondii* within three days (Weiss and Kim, 2020). Without the inclusion of an episomal-maintenance-sequence (Black and Boothroyd, 1998), *T. gondii* cannot replicate episomal DNA, with transfected plasmid DNA and their gene products typically lost within 3 – 5 days (Soldati and Boothroyd, 1993). Were a *hxgprt* cassette added to the Cas9 vector used for HiT and CRISPR-skip-in, the 3 – 5 days' expression of episomal *hxgprt* would be long enough to kill the non-transfected tachyzoites with MPA. In a Δ*ku80* strain, the surviving Cas9-positive tachyzoites would have to either repair their Cas9-induced double strand break using the co-transfected knock-in repair template or die. This approach, if viable, would utilise the advantages of drug selection-based knock-ins but in a scarless way, since the drug resistance marker is lost after a few days. Numerous knock-ins could therefore be performed successively, and not just the two to which CRISPR-skip-in is limited. Moreover, this approach would, unlike CRISPR-skip-in, not be limited to knock-ins within coding regions at the ATG and STOP codons but could be used genome wide. However, whilst CRISPR-skip-in positively selects for the desired integration event, this approach would only select for transient expression of the Cas9 without any positive selection for the desired genetic modification outcome. Consequently, this approach carries the risk that the Cas9 plasmid may be integrated into the genome through a method such a micro homology-mediated end joining, with or without the parallel knock-in of the gene of interest.

3.2 Mechanism and coordination of nuclear segregation

3.2.a The integral role of centrosome duplication in replication

As the central coordinator of cell division, it is to be expected that the centrosome and its duplication are pivotal to the progress of *T. gondii* endodyogeny. Concordantly, a multitude of null mutants have previously been reported to result in centrosome over-duplication **(Table 3.2.1)**. Knocking down the

aurora kinase Ark1 resulted in centrosome over-duplication (Berry *et al.*, 2018). In contrast to ALP2a and ARP4a KDs, however, Ark1 KD also inhibited kinetochore and centromere segregation. It is therefore unclear whether this centrosome over-duplication resulted directly from Ark1's KD or indirectly as a result of multiple cell cycle rounds proceeding without nuclear segregation from the preceding round. Note that two different *T. gondii* genes have been referred to as Ark1. The centrosome over-duplication-associated Ark1 is TGME49_210280 (Berry *et al.*, 2018). TGME49_203010 is a different gene that has been named both Ark1 (Suvorova *et al.*, 2015) and Ark3 (Berry *et al.*, 2016). The cyclin Cyc1 and Cdk-related kinase Crk6 are interaction partners localised to the nucleus (Hawkins *et al.*, 2021). The KD of either Cyc1 or Crk6 resulted in the over-duplication of both inner and outer centrosome cores (Hawkins *et al.*, 2021). Knocking down the centrosome protein Cep530 resulted in a similar nuclear mis-segregation phenotype to both ALP2a and ARP4a KDs (Courjol and Gissot, 2018). Likewise, the KD of Cep250 resulted in over-duplication of the centrosome's outer core, its dissociation from the inner core, and nuclear mis-segregation (Chen and Gubbels, 2019). The knockdown of Crk4 too resulted in the over-duplication of centrosomes, but contrastingly also caused apicoplast segregation defects (Alvarez and Suvorova, 2017), the latter not being seen following either ALP2a or ARP4a KD. A stable KO of PRMT1, which localises close to the centrosome, is viable but has mis-regulated replication, which included over-duplicated centrosomes (El Bissati *et al.*, 2016). A null mutant of MAPK-L1 also resulted in centrosome over-duplication (Suvorova *et al.*, 2015). Since MAPK-L1 is dynamically expressed through the cell cycle, peaking during the S/M phase transition, following centrosome duplication, it was considered a putative repressor of centrosome duplication that functions as an "off switch".

Table 3.2.1: *T. gondii* genes whose disruption is reported to cause centrosome over-duplication

Protein	Localisation	Null mutant phenotype	Notes
Crk6 & Cyc1	Nucleus	Centrosome over-duplication	
Ark1	Cytoplasm	No kinetochore segregation	May represent repeated cell cycle rounds without nuclear segregation
CDPK7	Cytoplasm	Centrosome over-duplication, loss of kinetochore sequestration	
MAPK-L1	Pericentrosomal	Centrosome over-duplication	Cell cycle regulated
PRMT1	Pericentrosomal	Centrosome over-duplication	Disrupted transcriptome across whole cell cycle
Cep530	Centrosome	Centrosome over-duplication and nuclear mis-segregation	
Cep250	Centrosome	Centrosome outer core over-duplication, loss of connection between inner and outer cores	

As two nuclear proteins, it is unlikely that either ALP2a or ARP4a directly regulate or influence centrosome duplication. Of the above proteins, all except Cyc1 and Crk6 have either a centrosomal or cytoplasmic localisation and therefore a potential direct role in centrosome duplication. Like ALP2a and ARP4a, Cyc1 and Crk6 are nuclear proteins, whose KDs presented centrosome over-duplication and nuclear mis-segregation phenotypes (Hawkins *et al.*, 2021). Crk6 co-precipitated with Cyc1, the centromeric histone CenH3, and the kinetochore recruiting CENP-C, indicating a role in kinetochore and centromere biology. This raises the possibility of an unknown feedback loop that exists between the *T. gondii* kinetochores and centrosomes during centrosome duplication. With the association of *P. falciparum* ARP4 to centromeres (Liu *et al.*, 2020), a role for *T. gondii* ALP2a or ARP4a in this feedback loop is worthy of consideration. However, the biological rationale behind such a system, should it exist, is not immediately apparent. Despite the association of the Cyc1/Crk6 complex to kinetochores, both proteins exhibited a diffuse nuclear localisation during mitosis, rather than just a kinetochore localisation. It is therefore possible that, in contrast to the above feedback loop hypothesis, Cyc1 and Crk6 have further roles within the nucleus. In support of this, the majority of proteins with altered phosphorylation states following Cyc1 KD were nuclear proteins and nucleic acid binding proteins (Hawkins *et al.*, 2021). This does not appear to have been a direct result of increased Crk6 activity following Cyc1 KD, since the list of predicted nuclear Crk6 substrates was limited to just CENP-C. Moreover, unlike Cyc1 and Crk6 KD, the KD of CENP-C did not affect kinetochore segregation (Brusini *et al.*, 2022). This indicates that the Cyc1 KD and Crk6 KD phenotypes may be the result of more general, global changes within the nucleus. The present study did not investigate whether the nuclear phosporylome was altered following ALP2a KD and ARP4a KD. The similar phenotypes of ALP2a, ARP4a, Cyc1, and Crk6 KDs together with the shared indications of global changes within the nucleus suggest that centrosome over-duplication may be a common response to nuclear dysregulation during endodyogeny.

Due to the high degree of evolutionary divergence between endodyogeny and mitosis, it was questioned how specific such centrosome over-duplication phenotypes are to *T. gondii*. In *S. cerevisiae*, spindle pole body duplication is triggered by the release of Cdc14 from sequestration in the nucleolus, with the mis-regulation of this sequestration also leading to spindle pole body over-duplication (Avena *et al.*, 2014). In *H. sapiens*, centrosome duplication is driven by polo-like kinase 4 (Plk4), the over-expression of which resulted in centrosome over-duplication (Habedanck *et al.*, 2005). Plk4 expression is, in part, transcriptomically controlled, being inactive during G_1 phase (Uchiumi, Longo and Ferris, 1997), demonstrating the direct influence transcription can have over centrosome duplication. Moreover, and

of relevance to *T. gondii* ARP4a, the siRNA KD of INO80 in HeLa cells also resulted in centriole over-duplication (Cao *et al.*, 2015). Given the gross transcriptional changes that occur within the nucleus through the cell cycle, the emerging picture is that nuclear dysregulation in eukaryotes at critical junctures of mitosis often manifests itself in centrosome over-duplication phenotypes.

3.2.b ARP4 and the kinetochore

It has been suggested that *S. cerevisiae* ARP4 is required for kinetochore assembly. A temperature-sensitive S23A/D159A ARP4 mutant (ScARP4^{TS}) arrested in metaphase, was more sensitive to the microtubule depolymerising agent benomyl, and saw reduced ChIPseq enrichment of centromeres by various kinetochore proteins (Ogiwara *et al.*, 2007). In contrast, the present study did not see any growth arrest during the first 30 hours post ALP2a KD and ARP4a KD. Indeed, cytokinesis proceeded, and, based on Nuf2 fluorescence intensity measurements, kinetochore duplication was unaffected. Similarly, growth arrest was also not reported in the first 4 erythrocytic cycles post *P. falciparum* ARP4 KD (Liu *et al.*, 2020).

Both S23 and D159 are within *S. cerevisiae* ARP4's ATP-binding pocket (Kabsch and Holmes, 1995; Berman *et al.*, 2000; Fenn *et al.*, 2011; Sehnal *et al.*, 2021) **(Figure 3.2.1)**, and neither is in the HSA binding region (I458 - L468, subdomain 1) (Cao *et al.*, 2016). S23 is not conserved in *T. gondii* or *P. falciparum*, but D159 is **(Figure 3.2.1a, b)**. The *T. gondii* ARP4a temperature-sensitive mutant, which mis-localises to the cytoplasm, possess a I621T mutation, a site that is conserved in *P. falciparum* ARP4, but not *S. cerevisiae* ARP4, where multiple sequence alignments indicate it is equivalent to V389 **(Figure 3.2.1c)**. Given the requirement of ATP-binding by actin family proteins and the strong phenotype of ScARP4^{TS}, it could be implied that ScARP4^{TS} is a non-functional null mutant, permitting direct comparison of the ScARP4^{TS} and *T. gondii* ALP2a KD / ARP4a KD phenotypes. Therefore, it could be that the kinetochore assembly function is not conserved in apicomplexan ARP4 family proteins.

Alternatively, the claim that *S. cerevisiae* is required for kinetochore assembly could be an over-interpretation. As well as exhibiting increased sensitivity to benomyl, ScARP4^{TS} was also more sensitive to hydroxyurea treatment, a ribonucleotide reductase inhibitor that prevents the production of deoxyribonucleotides (Ogiwara *et al.*, 2007), suggesting ScARP4^{TS} was generally stressed and more susceptible to additional stress factors. Moreover, that ScARP4^{TS} saw lower centromere ChIPseq enrichment by kinetochores does not necessarily mean ARP4 is required for kinetochore assembly, as this assumes that the kinetochore proteins were readily available for assembly. Furthermore, ScARP4's

localisation to centromeres, as determined by ChIP, was mirrored by INO80 and, to a lesser extent, SWR1 (Ogiwara *et al.*, 2007), signifying that free ARP4 was unlikely to be involved in kinetochore assembly. Instead, it seems more likely that the well conserved roles of ARP4 is H2A.Z exchange across the genome may account for the metaphase arrest of ScARP4^{TS}.

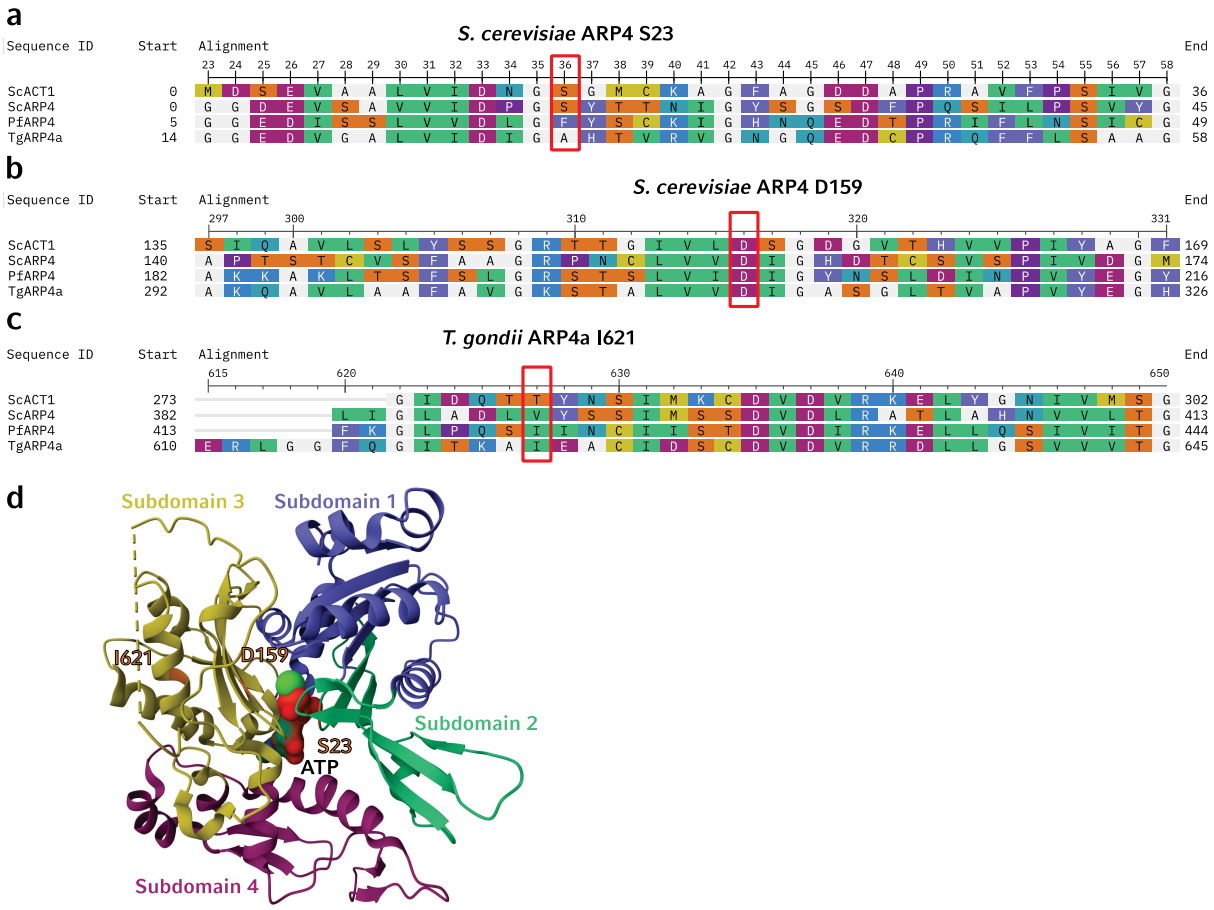

Figure 3.2.1: The localisation of amino acids in *S. cerevisiae* ARP4 and *T. gondii* ARP4a that have been shown to be essential through temperature-sensitive mutants.

a-c. Multiple sequence alignments of *S. cerevisiae* actin, ARP4, *P. falciparum* ARP4, and *T. gondii* ARP4a. Amino acid residues that are mutated in temperature-sensitive mutants are indicated by red boxes. *S. cerevisiae* ARP4^{TS} possess S23A **(a)** and D159A **(b)** mutations. *T. gondii* ARP4a^{TS} possess a I621T mutation **(c)**. Sequences were aligned using MUSCLE and plotted using NCBI's Multiple Sequence Alignment Viewer, with adjustments in Inkscape. RasMol amino acid colouring was used. Start and End indicates start and end sequence positions for each individual protein of the amino acids shown (minus gaps). Alignment indicates the amino acid position within the alignment (plus gaps).

d. 3D structure of *S. cerevisiae* ARP4 whilst bound to ATP, as defined by Fenn *et al.*, 2011. Structure was retrieved from the Protein Data Bank (Berman *et al.*, 2000) and annotated using Mol* (Sehnal *et al.*, 2021). ATP molecule is shown in the centre of the protein. ARP4^{TS} site mutations are shown in orange. Equivalent *T. gondii* ARP4a I621 site mutated in ARP4a^{TS} (*S. cerevisiae* ARP4 V389) also shown in orange.

3.3 The *T. gondii* nuclear ARP repertoire

3.3.a Two ARP4 homologues

Although rare, the presence of two ARP4 homologues in the *T. gondii* genome is not unique. Within Apicomplexa, ARP4aARP4aARP4a homologues are widely distributed in Coccidia and Piroplasmida (e.g. *Theileria* spp.) (Gordon and Sibley, 2005). Since thARP4as no ALP2a homologue in Haemospororida (e.g. *Plasmodium* spp.), it is not clear whether the presence of Coccidia anARP4aoplasmida ALP2a homologues arose from two independent evolutionary events, one per taxonomical order, or from a single event in an ancestral apicomplexan species, with the gene thereafter becoming lost in Haemospororida.

Although *S. cerevisiae* is often the reference organism in ARP homology and naming conventions, this does not mean it is representative of the actin family proteins of all yeasts. Two yeast species, *Schizosaccharomyces pombe* and *Yarrowia lipolytica*, possess two ARP4 homologues (Muller *et al.*, 2005). The *S. cerevisiae* ARP4 homologue in *S. pombe* is termed ALP5 and, like *S. cerevisiae* ARP4, it is a component of the Ino80, SWR1, and NuA4 complexes (Minoda *et al.*, 2005; Hogan *et al.*, 2010; Hou *et al.*, 2010). Contrastingly, the other ARP4 homologue in *S. pombe*, ARP42, is a component of the SWI/SNF and RSC complexes (Monahan *et al.*, 2008), both complexes with roles in nucleosome positioning (Krietenstein *et al.*, 2016; Nagai *et al.*, 2017; Klein-Brill *et al.*, 2019). The functions of the two *Y. lipolytica* ARP4 proteins remains to be identified.

The *H. sapiens* homologue of *S. cerevisiae* ARP4 is actARP4ake protein 6a (ACTL6a), which was historically referred to as Baf53a. HoweveARP4a *sapiens*ARP4aess an ACTL6a paralogue, ACTL6b (historically Baf53b), which is also nuclear localised (Harata, MoARP4aki and Mizuno, 1999). While ACTLARP4a expressed in all nucleated cells, ACTL6b expression is limited to neuronal cells where it associates with the neuronal-specific nBAF chromatin remodelling complex (Olave *et al.*, 2002; Euskirchen, Auerbach and Snyder, 2012), which has roles in neural development and dendritic outgrowth (Alfert, Moreno and Kerl, 2019). In line with this specific function, ACTL6b homologues are distributed throughout and exclusive to the kingdom Animalia.

The apicoplast organelle, a defining feature present in most Apicomplexa spp., most likely arose from an endosymbiotic event that saw a red alga (Rhodophyta) species engulfed by a species ancestral to apicomplexans: the chromalveolate hypothesis (Cavalier-Smith, 1999). Species united in sharing red algae-inherited plastids have been grouped under the infrakingdom Halvaria (Cavalier-Smith, 2010;

Strassert *et al.*, 2021). Like *T. gondii*, red algae species appear to have two ARP4 homologues (Goodson, Kelley and Brawley, 2021). Whilst it was clear that the ARP4 gene duplication occurred early in red algae evolution, it is not clear whether this duplication was lineage-specific or has wider implications for the evolution of ARP4 homologues across Eukaryota. The lack of any functional characterisation of red algae ARP4 proteins further compounds the difficulty in drawing conclusions from their presence. The transfer of genes from plastid to nuclear genomes has been well documented. For example, approximately 480 genes of the *P. falciparum* nuclear genome originated in, and transferred from, the apicoplast genome (Gardner *et al.*, 2002; Foth and McFadden, 2003; Ralph *et al.*, 2004). The possibility that *T. gondii* inherited ALP2a via endosymbiotic gene transfer from red algae cannot therefore be ruled out. Moreover, were this hypothesis true, it could be expected, but not guaranteed, that Chromerida, as the closest known relative to Apicomplexa whose plastid remains photosynthetic, would likewise possess two ARP4 homologues. *Chromera velia* does, indeed, possess two ARP4 homologues (Cvel_13588 and Cvel_13747). Further circumstantial support for this hypothesis comes from diatoms. Diatoms, most recently described as a diverse phylum within the clade Stramenopiles (Adl *et al.*, 2019), have both a halvarian, red alga-derived plastid (Dorrell and Bowler, 2017) and two ARP4 homologues within their genomes (Aumeier, Polinski and Menzel, 2015). Further phylogenetic resARP4a studies to determine whether *T. gondii* ALP2a arose in an ancestral apicomplexan species or red algae is therefore warranted.

At a minimum, the duplication of ARP4 genes has occurred at least three times: once in Animalia, once in yeast, and once in red algae. Although the requirement and function of two ARP4 homologues in many species remains to be defined, most notably in Halvaria, within species where the homologues have been functionally characterised a clear divergence in function is present. Despite their similar ARP4aARP4a, the interaction partners of *T. gondii* ALP2a and ARP4a were, with the exception of TGME49_205562, vastly different, suggesting a limited at best functional overlap. Together with the lackAARP4a4auncAARP4a4al redundancy, the emerging picture is that the ALP2a KD and ARP4a KD phenotypes arise through one of three mechanisms:

1. An interdependent mechanism that relies on their shared interaction with TGME49_205562.
2. Independent mechanisms that converge at a later downstream point.
3. Independent mechanisms that never converge but coincidentally result in similar phenotypes.

The extent to which points 2 and 3 aARP4ave could be true wARP4aARP4aARP4aable through the creation of a double KD strain, where both ALP2a and ARP4a are KD at the same time. In the event of

mechanism 2, the convergence would represent a bottleneck in phenotype formation and therefore no increased rate of either nuclear mis-segregation or centrosome over-duplication would be seen. Conversely, mechanism 3 would likely ARP4ARP4a the increased frequency of both phenotypes. AltARP4augh no gross changes in ALP2a or ARP4a fluorescence intensity were witnessed following the KD of the other, this does not necessarily rule out some degree of interdependence as unchanged protein expression cannoARP4aARP4a unchanged proARP4ain-protein interactions.

The extent of the interconnectivity between ALP2a and ARP4a, as well as their KD phenotypes, wouldARP4aARP4aore apparent with the employment of genomics-based approaches. ChIPseq would illustrate whether ALP2a and ARP4a localise to the same genomic regions. ARP4aARP4ae, coupling ChIPseq data with RNAseq-identified transcriptomic changes would aid in defining the functions ALP2a and ARP4a at specific genomic loci.

3.3.b The outstanding question of ALP5 and ALP3b essentiality

Despite PCR and sequencing confirmation that ALP5 iKD was created as intended, no expression of ALP5 was detected. The expression of ALP5 protein has previously been detected in tachyzoites through mass spectrometry (Treeck *et al.*, 2011; Krishna *et al.*, 2015). Moreover, ALP5 transcript is more abundant than that of ARP4a (Waldman *et al.*, 2020). The inability to detect ALP5 was therefore unexpected. Neither IFA nor western blotting are as sensitive as mass spectrometry. It could therefore be that ALP5 protein expression is very low and undetectable byARP4aae means. Alternatively, the addition of the mAID domain to ALP5 could have lowered its expression, as was seen in the case of ALP2a iKD. Direct assessment of ALP5 protein expression would therefore be better served through endogenous tagging without the mAID domain. However, ALP5 is predicted to be highly essential to tachyzoite growth, with a phenotype score of -5.04 ARP4adik *et al.*, 2016). As such, even with sub-detectable protein expression, it would still be expected thaARP4anduction of ALP5 iARP4a with IAA would negatively affect tachyzoite growth, which was not the case. In explanation, either the addition of IAA did not lead to the KD of ALP5, or the predicted essentiality of ALP5 was wrong. The latter eventuallARP4aARP4a proven through the creation of a stable ALP5 KO strain.

The inability to generate an ALP3b iKD strain may indicate that ALP3b, unlike ALP2a and ARP4a, is refractory to C-terminal tagging. However, it is also possible that the currently annotated gene model is wrong and that this caused the failure of ALP3b knock-ins using CRISPR-skip-in. The cloning approach used in this study was designed with the gene model present in ToxoDB release 47, which

sees ALP3b comprised of 4 exons. In release 50, community annotations of the *T. gondii* genome were made possible, prompting a review of the genome annotation. A proposed alternative gene model for ALP3b (TGME49_248890-t26_1-00001) possess a fifth exon **(Figure 3.3.1)**. Were this proposed five exon gene model to be accurate, this would fully explain the inability to create a ALP3b iKD strain, since the location targeting for C-terminal knock-in would be intronic. Consequently, the *hxgprt* drug resistance marker would not be expressed, and all tachyzoites woulARP4aARP4ato MPA treatment. A renewed atteARP4ao create an ALP3b iKD strain, using the five exon gene model, is therefore warranted.

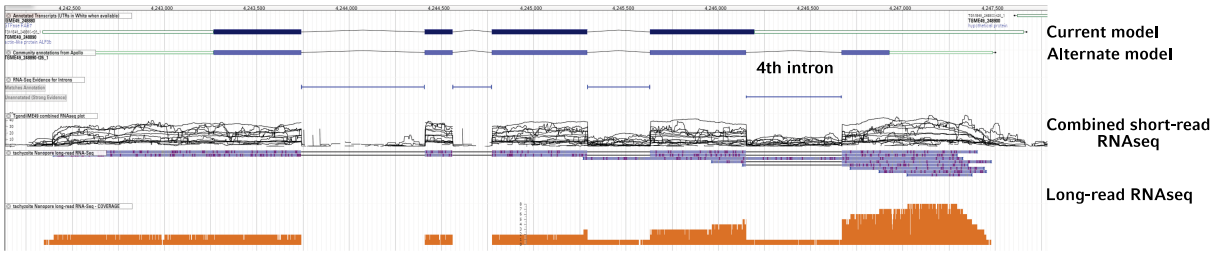

Figure 3.3.1: The ALP3b locus

The current model of ALP3b has 4 exons and 3 introns. However, RNAseq evidence, from both short-read Illumina sequencing and long-read Nanopore sequencing, suggests and alternate gene model with 5 exons and 4 introns. Data is from ToxoDB and was visualised with JBrowse genome browser.

3.4 The interactomes of ARP4a and ALP2a are divergent but may still intersect

3.4.a ARP4a and histone variant exchange

In model eukaryotes, the two Ino80 family chromatin remodelling complexes Ino80 and SWR1 directly regulate the deposition of the histone 2A variant H2A.Z (Eustermann *et al.*, 2018; Giaimo *et al.*, 2019), with Ino80 exchanging H2A.Z-containing canonical H2A nucleosomes (Papamichos-Chronakis *et al.*, 2011) and SWR1 *vice versa* (Mizuguchi *et al.*, 2004a). Given the number of conserved Ino80 and SWR1 complex components that co-precipitated with ARP4a, it is likely that ARP4a's role in histone variant exchange is conserved. The roles of H2A.Z are extensive and diverse, encompassing its deposition in promoters and nucleosome-free regions at transcriptional start sites, its roles in nucleosome positioning and DNA methylation, as well as double strand break DNA repair (Giaimo *et al.*, 2019). Within the context of gene expression, H2A.Z is associated with both activation and repression.

In *T. gondii*, active gene expression is typified by the presence of H3K4me3 in the promoter region (Gissot *et al.*, 2007) along with H2A.Z and H2B.Z histone variants (Nardelli *et al.*, 2022). In contrast, non-expressed genes lack H3K4me3, and H2A.Z/H2B.Z occupancy is not confined to the promoter but

is found across the majority of the gene body (Nardelli *et al.*, 2022), demonstrating the extent of H2A.Z's role in *T. gondii* gene expression regulation. This pattern of H2A.Z occupancy extends to genes that are variably expressed through the cell cycle. G_1-expressed genes exhibited low H2A.Z occupancy at peak expression, with occupancy rising as the tachyzoites progress through the cell cycle (Nardelli *et al.*, 2022). S- and M-expressed genes, meanwhile, showed a dichotomy of low and high H2A.Z occupancy, indicative of the genes' short expression windows (Nardelli *et al.*, 2022). Together with the diminished ability of ARP4a KD tachyzoites to up-regulate MAPK-L1, it therefore seems likely that H2A.Z deposition is a significant factor in *T. gondii* gene expression regulation, and that ARP4a remains a critical component of the Ino80 and SWR1 histone variant exchange complexes. However, follow-up experiments such as time-resolved ChIPseq are required before definitive conclusions can be drawn.

In *P. falciparum*, ChIPseq experiments showed that ARP4 localised, non-exclusively, to the centromere and that the KD of ARP4 resulted in the depletion of H2A.Z from the centromere (Liu *et al.*, 2020). Contrastingly, H2A.Z is not enriched at the centromeres of *T. gondii* (Nardelli *et al.*, 2022). In the present study, kinetochore duplication was unaffected by ARP4a KD, which suggests that centromeric chromatin was also unaffected by the KD of ARP4a. This difference in H2A.Z deposition between *T. gondii* and *P. falciparum* serves as another example highlighting different gene expression regulatory mechanisms between the two apicomplexan species (Sindikubwabo *et al.*, 2017).

It is unlikely that ALP2a also has a direct role in H2A.Z variant exchange since it did not co-precipitate with any of the conserved Ino80 and SWR1 complex components. Instead, the only likely ALP2a interaction partner was TGME49_205562, which likewise co-precipitated with ARP4a.

3.4.b TGME49_205562

Through endogenous tagging, TGME49_205562 was confirmed as a coccidian-specific nuclear protein, and therefore may be a genuine interactor of both ALP2a and ARP4a. The likelihood of this interaction could be strengthened through the reciprocal co-precipitation of ALP2a and ARP4a with TGME49_205562 used as bait. Due to the similar phenotypes of ALP2a KD and ARP4a KD, TGME49_205562 is a promising a promising candidate for linking the two KDs and the shared centrosome over-duplication phenotype. However, the failure to detect any expression in the TGME49_205562 iKD strain, and the lack of any phenotype when IAA treated, means the extent to which TGME49_205562 is involved in the development of the ALP2a KD and ARP4a KD phenotypes remains untested. However, the inability to create a stable TGME49_205562 KO using Cas9 disruption

of the gene would suggest that the gene is essential for tachyzoite growth. The use of other technologies, such as DiCre, to create either a KD or KO of TGME49_205562 is therefore warranted.

The expression of TGME49_205562 within the nucleus was both higher and more widely distributed in comparison to ALP2a and ARP4a. However, TGME49_205562 was not freely distributed within the nucleus, being absent from the nucleolus, not showing full co-localisation with nuclear DNA, and showing a varying density across its localisations. This pattern of localisation within the nucleus is typical of chromatin-associating proteins, particularly those that do not have genome-wide functions. The higher expression of TGME49_205562 may indicate that its function is not exclusively reliant on association with ALP2a and ARP4a, or that it functions within multiple protein complexes.

Although TGME49_205562 is a large protein (predicted 630 kDa), no reliable functional domains have been predicted for the protein. In the course of this study, no potential homologies were detected using HHpred. No AlphaFold (Varadi *et al.*, 2022) structural prediction exists for TGME49_205562. The genome annotation of the *T. gondii* COUG strain is weaker than that of Me49 and its orthologue of TGME49_205562 is erroneously split into two separate genes, TGCOUG_205562A and TGCOUG_205562B. AlphaFold has a structural prediction for TGCOUG_205562B (A0A2G8Y542) but it is unreliable, with most residues having very low model confidence scores (mean pLDDT 38.25) and large sections of the protein unfolded. Foldseek (van Kempen *et al.*, 2023) has not detected any similarity between TGCOUG_205562B's AlphaFold model and any other protein structures within the AlphaFold database. The inability of comparative genomics to assign a putative function to the protein is not unexpected, given that the protein is phylogenetically confined to just Coccidia. Thus, even speculation as to TGME49_205562's function is impossible, and it is likely that the protein's function will have to be empirically determined. Identifying TGME49_205562's interaction partners would significantly aid in assigning putative functions to the protein.

Post-translational modifications (PTM) of proteins are an intricate and important means by which protein function and subcellular localisation can be controlled. Serine and threonine *O*-fucosylation was reported on sixty-nine nuclear membrane associated proteins (Bandini *et al.*, 2016). Similarly, serine phosphorylation can be used to control both nuclear entry and exit (Nardozzi, Lott and Cingolani, 2010). The amino acid sequence of TGME49_205562 possesses multiple serine rich regions, which have already been shown to be phosphorylated (Treeck et al., 2011). Whilst there is insufficient data to infer a purpose for TGME49_205562's serine phosphorylation, it is a promising avenue through which its function could be further investigated.

3.5 The diverse functions of ATPase chromatin remodellers in *T. gondii*

3.5.a ISWIs

In model eukaryotes, the two ISWI chromatin remodellers, SNF2l and SNF2h in *H. sapiens*, function in highly similar mechanistic and catalytic ways but have roles in a myriad of genome organisation events. This diversification of roles stems from the number of different ISWI-containing complexes that can be formed depending on the sub-components recruited (Längst and Manelyte, 2015; Goodwin and Picketts, 2018). The differing phenotypes found in this study following *T. gondii* SNF2l KD and SNF2h KD suggests that this diversification of function is retained by the *T. gondii* ISWIs.

As global regulators of nucleosome spacing, pleiotropic effects were one anticipated outcome following SNF2l KD and SNF2h KD. This seems likely to be the case following SNF2h KD, where tachyzoites continued to grow through the first lytic cycle, albeit in disorganised and aberrant vacuoles, but were ultimately unviable. *P. falciparum* only encodes a single ISWI family chromatin remodeller, SNF2l, which is a global regulator of nucleosome spacing at transcriptional start sites (Watzlowik *et al*., in revision). In doing so, *P. falciparum* SNF2l is a critical component of the just-in-time transcriptional regulation pattern utilised during progression through the cell cycle and erythrocytic cycle, as well as, presumptively, lifecycle progression. Following *P. falciparum* SNF2l KO, the transcriptome became increasingly dysregulated from 45 h post DiCre induction, at the end of the first erythrocytic cycle, with growth arrest occurring at approximately 55 h post DiCre induction, at the beginning of the second erythrocytic cycle. The abrupt nature of this growth arrest is more similar to that of *T. gondii* SNF2l than SNF2h, possibly indicating conserved function between the two SNF2l orthologues. In the future, RNAseq, ChIPseq, and MNase-seq investigations like that of Watzlowik and colleagues would elucidate the functional niches of *T. gondii* SNF2l and SNF2h.

Pleiotropic effects following SNF2l KD cannot be ruled out, but the observed complete growth arrest may itself be specific. The bulbous posterior structure visualised with α-GAP45 labelling in growth arrested SNF2l KD tachyzoites is reminiscent of the localisation of mother cell cytoskeletal components being recycled into the daughter cells that occurs during the emergence of the daughter cells (Goldman, Carver and Sulzer, 1958; Ouologuem and Roos, 2014; Attias, Miranda and De Souza, 2019). Although incompletely understood, this recycling occurs after mitochondrial inheritance, the last organelle to be inherited, and is believed to be integral to the formation of the residual body (Gubbels *et al.*, 2022). It

would therefore be of merit to determine whether growth arrested SNF2l KD tachyzoites show complete or incomplete mitochondrial inheritance to better time resolve the point of growth arrest.

The translocation of proteins from the residual body into tachyzoites is dependent on F-actin and formin 3 (Periz *et al.*, 2017; Tosetti *et al.*, 2019b). Moreover, two myosins, MyoI and MyoJ, localise to the residual body and basal complex, respectively (Frénal *et al.*, 2017). However, the accumulation of non-recycled components in the residual body has not been described in null mutants of these proteins. Recently, the KO of the residual body-localising ubiquitin ligase CSAR1 was shown to result in the accumulation of non-recycled mother cell tubulin within the residual body (O'Shaughnessy *et al.*, 2023). CSAR1 is cyclically expressed through the cell cycle, peaking at the S to M phase transition (Behnke *et al.*, 2010). It is therefore possible that one outcome of SNF2l KD is the disruption of CSAR1 expression with subsequent accumulation of mother cell IMC in the residual body. However, unlike SNF2l KD, CSAR1 KO tachyzoites did not completely growth arrest, only replicating at a slightly reduced rate during the first lytic cycle and only establishing small plaques in a growth assay (O'Shaughnessy *et al.*, 2023), supporting the presence of pleiotropic effects following SNF2l KD.

Regardless, further interrogation of the SNF2l KD growth arrest phenotype would represent an opportunity to better understand the cytoskeletal recycling during the disassembly of mother cells in late endodyogeny.

3.5.b CHD1

Although strongly expressed in the nucleus, the KD of CHD1 had no strong effect on tachyzoite growth. However, as a KD, the presence of residual protein below detection threshold cannot be ruled out. Whilst CHD1 has previously been predicted to be non-essential for *in vitro* tachyzoite growth (Sidik *et al.*, 2016), with a genome-wide Cas9 essentiality score of -0.87, a stable KO strain would be required to definitively conclude that CHD1 is non-essential for tachyzoites. As a chromo domain-containing protein, it would be expected that CHD1 recognises methylated lysine residues in histones. Histone lysine methylation does not have a common purpose, and can serve in both the activation and repression of gene expression, depending on the location of the methylated lysine in the histone and the location of the histone relative to the gene body (Black, Van Rechem and Whetstine, 2012). In model eukaryotes, CHD1 is a component of the SAGA and SLIK complexes that promote RNA polymerase II recruitment and transcriptional elongation (Pray-Grant *et al.*, 2005; Grant, Winston and Berger, 2021). Additionally, CHD1, in conjunction with nucleosome-sliding ISWI chromatin

remodellers, has a role in the maintenance of nucleosome spacing (Gkikopoulos *et al.*, 2011). The use of histone lysine methylation in the control of gene expression is conserved in *T. gondii*, with, for example, H4K31me1 along gene bodies being correlated with transcriptional silencing (Sindikubwabo *et al.*, 2017). Moreover, the requirement of the *T. gondii* ISWIs SNF2l and SNF2h was clearly demonstrated in the iKD strains produced and characterised in this study. Therefore, whilst the gene expression control mechanisms in which model eukaryote CHD1 plays a role are conserved in *T. gondii*, the role of CHD1 is not conserved. It is not immediately apparent why tachyzoites express CHD1 when it is dispensable. The control of gene expression in Apicomplexa has been described as a just-in-time mechanism where gene products are only produced during the timeframes in which they are required (Llinás and DeRisi, 2004; Radke *et al.*, 2005). Whilst not a universal principle for the expression of all apicomplexan genes, were the just-in-time principle to hold true for CHD1, this may indicate that the expression of CHD1 in tachyzoites is in expectation of future events such as transition to another lifecycle stage. No up-regulation of CHD1 was measured in tachyzoites that convert to bradyzoites (Waldman *et al.*, 2020), but this does not rule out a role for CHD1 in the conversion to bradyzoites. Whilst Waldman and colleagues (2020) screened for candidates involved in the conversion to bradyzoites, CHD1 was not among the candidates tested. The function of CHD1, therefore, remains to be elucidated.

3.6 The viability of using the actin Chromobody® to investigate *T. gondii* nuclear F-actin

Despite having previously been adapted for the purpose of visualising nuclear F-actin in *in vitro* cultured mammalian cell lines (Plessner *et al.*, 2015), the present study experienced difficulty in expressing the actin Chromobody® in the *T. gondii* nucleus. Although stable lines expressing CbEm^{NLS} and ^{NLS}CbEm^{NLS} were successfully generated, they rapidly lost expression within a number of weeks. This would suggest that are deleterious effects associated with the presence of CbEm in the nucleus that resulted in the positive selection for tachyzoites that reduced their CbEm expression.

All molecular tools used to visualise F-actin carry disadvantages (Melak, Plessner and Grosse, 2017). One disadvantage of the actin Chromobody® is that it does not exclusively bind to F-actin, showing an affinity for G-actin as well (Krippner *et al.*, 2020). Since G-actin is required in both the cytoplasm and nucleus, a control mechanism to regulate its distribution must exist. In mammalian cells, G-actin is chaperoned into the nucleus by importin 9 (Dopie *et al.*, 2012), a homologue of which is absent in *T. gondii*. Nevertheless, the G-actin binding capacity, together with the NLS present on CbEm^{NLS} and ^{NLS}CbEm^{NLS}, could cause the CbEm to act as an indirect nuclear importer for G-actin. Were this the case,

it would be foreseeable that the nuclear concentration of G-actin would increase. Had it not been for the aforementioned expression problems, it was the intention of this project to control for such an eventuality through cell fractionation and quantitative western blotting. Whether an increase in nuclear G-actin concentration could cause the deleterious effects responsible for the loss of $CbEm^{NLS}$ expression is unknown, but it is notable that the simultaneous fusion of the actin Chromobody® to both a NLS and NES (nuclear export signal) has been employed to counter any nuclear G-actin accumulation caused by actin Chromobody® expression in the nucleus (Plessner *et al.*, 2015).

Whilst several antibodies have been raised that are specific to apicomplexan actins, their use in *T. gondii* IFAs did not highlight the residual body F-actin network seen using the actin Chromobody® (Periz *et al.*, 2017; Whitelaw, 2017). Instead, their staining patterns were largely cytoplasmic and diffuse, which may indicate a greater affinity for F-actin than G-actin. The actin Chromobody® is more specific for F-actin than G-actin and since chromobodies consist of an antigen-binding V_HH domain from camelid antibodies (Bannas, Hambach and Koch-Nolte, 2017), the binding of chromobodies to their target is functionally identical to that of antibodies. For this reason, recombinant chromobodies and other nanobodies can be used to label fixed and permeabilised cells in the same manner as regular antibodies (Ma *et al.*, 2017; Li *et al.*, 2019). Therefore, the validation and quantification of normal nuclear F-actin abundance could be hypothetically achieved through the labelling of fixed and permeabilised tachyzoites with recombinant actin Chromobody®. This would no doubt require the optimisation of fixation, to prevent F-actin depolymerisation during fixation, and labelling, and comes with the caveat that all F-actin would be labelled, in both *T. gondii* and its host cell. Nevertheless, the approach would represent a novel chance to visualise *T. gondii* F-actin, both inside and outside the nucleus, without the risk of F-actin stabilising artefacts caused by expression of the actin Chromobody® in live cells.

When expressed cytoplasmically in *T. gondii*, the actin Chromobody® highlighted an extensive F-actin network in the vacuole's residual body, linking all the tachyzoites of the vacuole (Periz *et al.*, 2017). Despite the addition of NLS sequences, both $CbEm^{NLS}$ and $^{NLS}CbEm^{NLS}$ still exhibited a degree of localisation to the residual body, more pronouncedly in the former than the latter. This could be explained by the aforementioned affinity of the actin Chromobody® for both G-actin and F-actin functioning to hold the Chromobody® in the cytoplasm (later to make its way to the residual body) in opposition to the chaperone proteins that would escort $CbEm^{NLS}$ and $^{NLS}CbEm^{NLS}$ to the nucleus. This potential three-way conflict could be another factor that ultimately led to the loss of $CbEm^{NLS}$ and $^{NLS}CbEm^{NLS}$ expression.

The lack of a response by ^{NLS}CbEm^{NLS}-expressing tachyzoites to jasplakinolide treatment suggested that the Chromobody® was no longer capable of binding F-actin because of its N-terminal NLS. This was an unexpected result as the actin Chromobody® retained its F-actin-binding ability when fused N-terminally with YFP (Rocchetti, Hawes and Kriechbaumer, 2014). Due to the vastly difference peptide sizes, it would be expected that any steric hinderance caused by N-terminal fusions would be more significant with YFP than with an NLS. Alternatively, this result could be explained by the actin Chromobody® having different binding affinities for mammalian F-actin versus *T. gondii* F-actin. In this scenario, N-terminal fusions to the actin Chromobody® universally lower its affinity for F-actin, with the affinity for F-actin lowered below a threshold required for binding in the case of *T. gondii* F-actin alone.

The nucleus achieves subnuclear compartmentalisation of proteins and nucleic acids without the need for lipid membranes through the use of liquid-liquid phase separation (A and Weber, 2019; Lee, Strom and Brangwynne, 2022). In the context of proteins, the factors controlling liquid-liquid phase separation are numerous, but one strong factor is the presence of intrinsically disordered regions (IDRs) in the amino acid sequences (Boeynaems *et al.*, 2018; Gao *et al.*, 2021). As a fusion of two non-nuclear proteins that lack IDRs, it would be understandable if the presence of CbEm in the nucleus were to disrupt the normal nuclear homeostasis of liquid-liquid phase separation and therefore cause genome-wide deleterious effects. Despite the potentially reduced F-actin binding affinity of ^{NLS}CbEm^{NLS}, both CbEm^{NLS} and ^{NLS}CbEm^{NLS} lost expression at equally rapid rates. It therefore seems more likely that this loss of expression was caused by their disruptive presence in the nucleus than by any deleterious effects on nuclear actin, without completely ruling out the latter instance.

3.7 Closing Perspective

The control of gene expression in *T. gondii* is a juxtaposition of evolutionary conservation and divergence. Many nuclear factors found in other eukaryotes are likewise found in *T. gondii*, but, in its evolution towards parasitism, *T. gondii* has also evolved unique, divergent proteins for the purpose of regulating its genome. Historically, the major focus of *T. gondii* gene expression research has focused on the lineage-specific ApiAP2 transcription factor family. This study sought to broaden the understanding of nuclear events during *T. gondii* endodyogeny through the parallel interrogation of both conserved (e.g. ISWI chromatin remodellers) and divergent factors (e.g. ALP2a).

Despite the similar phenotypes following ALP2a KD and ARP4a KD, this study was unable to describe a shared mechanism that led to said phenotypes. Instead, the evidence presented points in the direction

of the phenotypes arising from general nuclear perturbance following the KDs. This exemplifies how care should be taken in interpreting the specificity of phenotypes in the null mutants of nuclear factors. Nevertheless, this study identified and characterised a previously unknown consequence of ARP4a disruption, centrosome over-duplication, that mechanistically explains the previously known phenotype, nuclear mis-segregation. In doing so, this study acts as further evidence of an "off switch" required to limit centrosome duplication to a single duplication, and that the nucleus is involved in this mechanism. Thus, the coordination between nucleus and centrosome during endodyogeny has been underlined. Further genomic and proteomic approaches are required to better define the nature of this coordination, and whether it is a direct or indirect consequence of other mitotic events.

The trend of contrasting evolutionary divergence and conservation was further highlighted through the identification of ALP2a and ARP4a interaction partners. The shared interaction of ALP2a and ARP4a with TGME49_205562 makes the latter the most probable, though not guaranteed, candidate to explain similar KD phenotypes of ALP2a KD and ARP4a KD. Being conserved only to coccidian apicomplexans, comparative genomics analysis, both by this study and others, has been unable to assign a putative function to TGME49_205562. Characterisation of TGME49_205562's function, and its interaction with ALP2a and ARP4a, will therefore have to be determined in future studies. In addition to TGME49_205562, ARP4a's interaction partners indicated a degree of conservation in the components of all three *S. cerevisiae* ARP4-containing chromatin modifying complexes: Ino80, SWR1, and NuA4. However, several proteins of unknown function were also identified. Most notably, TGME49_225000, which may serve a similar function to that of *S. cerevisiae* EPL1 within the NuA4 complex, and TGME49_235420, which has a putative HSA domain to facilitate interaction with actin family proteins but otherwise no identifiable functional domains. Additional biochemistry and genomics studies will be required to further interrogate the composition and function of the ARP4a-containing chromatin modifying complexes.

4 Materials and Methods

4.1 Equipment

Table 4.1.1: Equipment used in this study

Machine	Manufacturer
4D-Nucleofector™	Lonza
-86°C ULT freezer	Haier Biomedical
Agarose gel electrophoresis	Bio-Rad & Peqlab (Avantor)
Analytical balance	Satorius, KERN
Centrifuge 5810R & 5910 & 524R	Eppendorf
Centrifuge Pico™ 21	Thermo Fisher Scientific
Centrifuge Mikro 200R	Hettich
Dynamag™-2 magnet	Thermo Fisher Scientific
FACSAria™ III	BD Biosciences
FastGene blue/green LED transilluminator	Nippon Genetics
Fridge	Siemens & Bosch
Genius dry bath incubator	Major Science
ThermoMixer® C & ThermoMixer® Comfort	Eppendorf
UM300 incubator	Memmert
Hercell™ 240i incubator	Thermo Fisher Scientific
Innova™ 4200 incubator	New Brunswick Scientific
HERAsafe HS15 laminar flow hood	Thermo Heraeus
ENVAIReco® Comfort Plus laminar flow hood	ENVAIReco
3D STED microscope	Abberior Instruments
Axiovert A1 microscope	Zeiss
Primovert microscope	Zeiss
DMi8 microscope	Leica Microsystems
Microwave	Sharp
NanoDrop® ND-1000	Thermo Fisher Scientific
Neubauer haemocytometer	Carl Roth
Odyssey CLx	Li-Cor Biosciences
pH meter	Mettler Toledo
Accujet® pro pipette	BrandTech
ErgoOne pipettes	StarLab
P93D printer	Mitsubishi
SB2 rotator	Stuart
MiniProtean SDS-PAGE & blotting	BioRad
Titertek shaker	Flow Laboratories
Mastercycler Pro thermal cycler	Eppendorf
Vacuum pump	A. Hartenstein
Vortex	Scientific Industries, Bender & Hobein GmbH
WB-12 water bath	Phoenix Instruments

4.2 Computer software

Table 4.2.1: Computer software and online resources used in this study

Software	Source
Adobe Acrobat Reader	Adobe Systems Inc.
ApE Plasmid Editor v3.1.2	Davis and Jorgensen, 2022
Basic Local Alignment search tool (BLAST)	National Institute for Biotechnology Information (NCBI) https://blast.ncbi.nlm.nih.gov/blast/Blast.cgi
Clustal Omega & MUSCLE	EMBL-EBI Madeira *et al.*, 2022 https://www.ebi.ac.uk/Tools/msa/
Eukaryotic Pathogen sgRNA Design Tool (EuPaGDT)	Peng and Tarleton, 2015 http://grna.ctegd.uga.edu/
Gimp v2.10.34	https://www.gimp.org/
FIJI ImageJ v1.54f	Schindelin *et al.*, 2012 https://imagej.net/software/fiji/
3D ImageJ Suite	Ollion *et al.*, 2013 https://imagej.net/plugins/3d-imagej-suite/
Inkscape v1.3	https://inkscape.org/
Imspector v16.3.14274	Abberior Instruments
JBrowse genome browser	Diesh *et al.*, 2023
LasX v3.4.2.183668	Leica Microsystems
Image Studio v4.0	Li-Cor Biosystems
MaxQuant v2.0.1.0	Max Planck Institute for Biochemistry Tyanova, Temu and Cox, 2016
Mendeley Desktop v1.19.8	Mendeley Ltd
Max Planck Institute Bioinformatic Toolkit	Gabler *et al.*, 2020 https://toolkit.tuebingen.mpg.de/
HHpred v57c8707149031cc9f8edceba362c71a3762bdbf8	Hildebrand *et al.*, 2009; Zimmermann *et al.*, 2018 https://toolkit.tuebingen.mpg.de/tools/hhpred
MODELLER v10.0	Sali *et al.*, 1995 https://toolkit.tuebingen.mpg.de/tools/modeller
Mol*	Sehnal *et al.*, 2021
NucPred	Brameier, Krings and MacCallum, 2007 https://nucpred.bioinfo.se/nucpred/
Protein Data Bank	Berman *et al.*, 2000 https://www.rcsb.org/
VEuPathDB & ToxoDB	Amos *et al.*, 2022 Kissinger *et al.*, 2003 https://toxodb.org/toxo/app
Windows 10 Education v22H2	Microsoft
Office 365 Apps for Enterprise v2308	Microsoft
R v4.0.3 Bunny-Wunnies Freak Out	R Core Team https://www.R-project.org/

Software	Source
RStudio v2022.12.0+353 Elspeth Gernanium	Posit Software https://posit.co/products/open-source/rstudio/
ggplot2 v3.4.0	Wickham, 2009
dplyr v1.0.10	Wickham H, François R, Henry L, Müller K, 2022 https://dplyr.tidyverse.org/
stringr v1.5.0	Wickham, 2022 https://stringr.tidyverse.org/
mclust v6.0.0	Scrucca *et al.*, 2016
msa v1.22.0	(Palme, Hochreiter and Bodenhofer, 2015)
RColorBrewer v1.1-3	Neuwirth, 2022 https://cran.r-project.org/package=RColorBrewer
rstatix v0.7.2	Kassambara, 2023 https://CRAN.R-project.org/package=rstatix
tidyr v1.2.1	Wickham & Girlich, 2022 https://tidyr.tidyverse.org/
data.table v1.14.6	Dowle & Srinivasan, 2022

4.3 Consumables and reagents

4.3.a Consumables

Table 4.3.1: Consumables used in this study

Product	Source
Eppendorf tubes	Eppendorf
Cryovials, Falcon tubes, TPP cell culture vessels	Faust
Microscopy coverslips	A. Hartenstein
Microscopy slides, Parafilm	Carl Roth
Serological pipettes, aspirating pipettes	Sarstedt
3 µm filter membranes, Amersham™ Protran® 0.45 µm nitrocellulose, Whatman® cellulose chromatography paper	Merck
Needles, gloves, syringes	SMS Medipool
Micropipette tips	StarLab
PCR tubes, Petri dishes, reagent reservoirs	Avantor

4.3.b Kits

Table 4.3.2: Commercial kits used in this study

Kit	Manufacturer
ExtractMe Genomic DNA kit, ExtractMe Plasmid Mini kit, ExtractMe DNA clean-up & Gel-out kit	Blirt

Plasmid plus midi kit	Qiagen
P3 primary cell XL nucleofection kit	Lonza

4.3.c Buffers & Solutions

Table 4.3.3: Self-prepared buffers and solutions used in this study

Solution	**Composition**
LB medium	10 g L^{-1} tryptone, 5 g L^{-1} yeast extract, 10 g L^{-1} NaCl, 50 mg mL^{-1} ampicillin
LB agar	1.5% agar w/v in LB medium
Tfb II	10 mM MOPS, 10 mM RbCl, 75 mM $CaCl_2$-H_2O_2, 15% glycerol v/v
Complete DMEM	500 mL DMEM (Merck D6546), 10% FBS v/v (Merck F2442), 4 mM L-glutamine (Merck G7513), 20 μg mL^{-1} gentamicin (Merck G1397)
1× Freezing medium	25% FBS, 10% DMSO, 65% complete DMEM
IFA blocking buffer 1	3% BSA w/v 300 nM DAPI
IFA blocking buffer 2	1% milk (Marvel) w/v 300 nM DAPI
IFA blocking & permeabilisation buffer 1	3% BSA w/v 0.2% Triton Tx-100 v/v 300 nM DAPI
IFA blocking & permeabilisation buffer 2	1% milk w/v 0.2% Triton Tx-100 v/v 300 nM DAPI
DNA oligo annealing buffer	10 mM Tris base pH7.5, 50 nM NaCl, 1 mM EDTA
SDS lysis buffer	2% SDS w/v, 50 mM Tris-HCl pH8.1, 200 mM EDTA, 1× protease inhibitors (Pearce A32955)
Swelling buffer	20 mM HEPES pH7.9, 10 mM KCl, 100 μM EDTA, 100 μM EGTA, 1mM DTT, 1× protease inhibitors (Pierce A32955)
RIPA50	50 mM NaCl, 50 mM Tris-HCl pH7.4, 1 mM EDTA, 1× protease inhibitors (Pierce A32955)
4× OrangeG protein loading dye	125 mM Tris-HCl pH6.5, 50% glycerol v/v, 4% SDS w/v, 0.2% OrangeG w/v
SDS-PAGE running buffer	250 mM Tris base, 1.92 M glycine, 1% SDS w/v
Bjerrum Schafer-Nielson buffer	48 mM Tris base, 39 mM glycine, 20% methanol v/v
Tris-buffered saline (TBS)	152 mM Tris-HCl, 46 mM Tris base, 1.5 M NaCl
TBS-T	1× TBS, 0.2% Tween-20 v/v
Ponceau S	0.1% w/v Ponceau S, 5% v/v glacial acetic acid
Western blocking buffer	1× TBS, 5% milk (Marvel)

Table 4.3.4: Commercial reagents used in this study

Product	**Source**
Trypsin EDTA	Biochrom L2143
4-20% Mini-PROTEAN TGX gels	BioRad 4561093
GelRed	VWR 41003
Agarose	Hartenstein CA47

Product	Source
Chameleon Duo ladder	Li-Cor 928-60000
DAPI	Thermo Fisher Scientific D1306
Hoechst	Thermo Fisher Scientific 62249
Hemacolor®	Merck 111661
Acetic acid	Carl Roth 3738.4
Ampicillin sodium salt	Merck A9518
Anti-HA magnetic beads	Thermo Fisher Scientific 88836
Benzonase	Merck E1014
Chloramphenicol	Merck C3175
DMEM high glucose	Merck D6546
DMSO	Carl Roth 4720.4
Ethanol	Carl Roth T171.4
FBS	Merck F2442
Fluoromount G	Biozol SBA-0100-01
Gentamycin	Merck G1397
HCl	Merck H1758
IGEPAL CA-630	Merck I8896
Immersion oil Leica	Thorlabs MOIL-10LF
Immersion oil Zeiss 518F	Jülich 444970-9000-000
IPTG	Merck 16758
Isopropanol	Carl Roth 9866.1
L-glutamine	Merck G7513
Lens tissue	Thorlabs MC-50E
Methanol	Carl Roth 0082.2
Methanol HPLC grade	Carl Roth HN41.1
NaCl	Merck S7653
OrangeG	Merck O3756
Dulbecco's PBS	Merck D8537
20% paraformaldehyde	Electron Microscopy Science 15713
pGEM T-easy	Promega A1360
Ponceau S	Carl Roth 5938.2
Pierce protease inhibitors EDTA-free	Thermo Fisher Scientific A32955
Pyrimethamine	Merck 46706
Revert total protein strain	Li-Cor 926-11010
SDS	Carl Roth 0183.2
Sodium acetate	Merck S2889
Sodium deoxycholate	Merck D6750
TAE	Carl Roth CL86.2
Tris-HCl	Merck T6791
Tris base	Merck T6791
Tween-20	Merck P9416
Triton Tx-100	Carl Roth 3051.3
X-Gal	Merck 3117073001
Mycophenolic acid	Merck M3536
Xanthine	Merck X3627
IAA	Merck 45533

Product	Source
rCutSmart	NEB B6004
AgeI-HF	NEB R3552
BamHI-HF	NEB R3136
BsaI-HFv2	NEB R3733
NcoI-HF	NEB R3193
NdeI	NEB R0111
NheI-HF	NEB R3131
NotI-HF	NEB R3189
DpnI	NEB R0176
HincII	NEB R0103
HindIII-HF	NEB R3104
KpnI-HF	NEB R3142
PvuI-HF	NEB R3150
SacI-HF	NEB R3156
XhoI	NEB R0146
XmaI	NEB R0180
1 kb+ DNA ladder	NEB N0550
dNTPs	NEB N0447
Q5 HF DNA polymerase	NEB E0555
Q5 site directed mutagenesis kit	NEB E5520
Quick load purple	NEB B7025
T4 DNA ligase	NEB M0202
Taq DNA polymerase with ThermoPol buffer	NEB M0267

4.3.d Antibodies

Table 4.3.5: Antibodies used in this study

Antibody	Dilution	Source
Aldolase	$3{,}000^{-1}$ WB	David Sibley
Centrin mouse	200^{-1} IFA	Millipore 04-1624
Centrin rabbit	$1{,}000^{-1}$ IFA	Abcam ab11257
FLAG M2	200^{-1} IFA	Merck F1804
FLAG rabbit	400^{-1} IFA	Merck F7425
GAP45	$10{,}000^{-1}$ IFA	Dominique Soldati
GFP mouse	500^{-1} IFA	Roche 11841460001
HA rabbit	$1{,}000^{-1}$ IFA	Cell Signal Tech 3724
HA rat	500^{-1} IFA, $1{,}000^{-1}$ WB	Roche 1187431001
6His	500^{-1} IFA	Thermo Fisher Scientific MA1-21315
IMC1	$1{,}000^{-1}$ IFA	Gary Ward 45.36 PAB5806
Alexa Fluor 488 donkey α-mouse	$2{,}000^{-1}$ IFA	Thermo Fisher Scientific A21202
Alexa Fluor 488 donkey α-rat	$2{,}000^{-1}$ IFA	Thermo Fisher Scientific A21208
Alexa Fluor 488 donkey α-rabbit	$2{,}000^{-1}$ IFA	Thermo Fisher Scientific A21206
Alexa Fluor 594 donkey α-mouse	$2{,}000^{-1}$ IFA	Thermo Fisher Scientific A21203
Alexa Fluor 594 donkey α-rabbit	$2{,}000^{-1}$ IFA	Thermo Fisher Scientific A21207

Antibody	Dilution	Source
Alexa Fluor 647 donkey α-mouse	$2{,}000^{-1}$ IFA	Thermo Fisher Scientific A31571
Alexa Fluor 647 donkey α-rabbit	$2{,}000^{-1}$ IFA	Thermo Fisher Scientific A31573
IRDye 680RD goat α-mouse	$10{,}000^{-1}$ WB	Li-Cor 926-68070
IRDye 680RD goat α-rabbit	$10{,}000^{-1}$ WB	Li-Cor 926-68071
IRDye 800CW goat α-mouse	$10{,}000^{-1}$ WB	Li-Cor 926-32210
IRDye 800CW goat α-rabbit	$10{,}000^{-1}$ WB	Li-Cor 926-32211

4.3.e DNA oligos

Table 4.3.6: ssDNA oligos used in this study

Oligo	Internal #	Target gene	Sequence
gR348 Fw	6740	ALP3b	aagttAAGGAAAGGGGGAAACGCTGg
gR348 Rv	6741	ALP3b	aaaacCAGCGTTTCCCCCTTTCCTTa
3' tag repair Fw	6815	ALP3b	AGGAGGAGGTAACACAGAGAGAGATGAGAGACAAGGAAA GGGGGAAACGCgctaaaattggaagtggagg
3' tag repair Rv	6816	ALP3b	CCAGTGTGTGCCGTTTCACTTCCTTCGCTTCAGTCCTCG CATTTCCTCAGataacttcgtataatgtatgctatacg
3' tag genotype Fw	6872	ALP3b	CGTCGAAGCCGTCAGAGAAT
3' tag genotype Rv	6873	ALP3b	GTGTGTGCCGTTTCACTTCC
gR352 Fw	6744	ARP4a	aagttCAGGCGGCGAACGACGCTCCg
gR352 Rv	6745	ARP4a	aaaacGGAGCGTCGTTCGCCGCCTGa
3' tag repair Fw	6818	ARP4a	AAAGAGAATTCGAGCAACACGGCGTCGACATCATCAACC GCCGGTGTCGGgctaaaattggaagtggagg
3' tag repair Rv	6819	ARP4a	CCTCGCCTGCGCCTTTCTGGATTCTGCTCTCCTCGAAGC CTCCACCTGGAataacttcgtataatgtatgctatacg
3' tag genotype Fw	6876	ARP4a	ATCATCAACCGCCGGTGTC
3' tag genotype Rv	6877	ARP4a	TTTTGCTTCGTCTGCCTTCC
gR354 Fw	6748	ALP2a	aagttAGAGTTCGCCTGGAGTGGGGg
gR354 Rv	6749	ALP2a	aaaacCCCCACTCCAGGCGAACTCTa
3' tag repair Fw	6822	ALP2a	GGGAGGAGTACGACGAGCACGGTCCGTCCATCGTCGAAC GAAAATGCTACgctaaaattggaagtggagg
3' tag repair Rv	6823	ALP2a	AGGTATGTACCGAGCACTTGCGAGGCTTTTTCCAGAGTT CGCCTGGAGTGataacttcgtataatgtatgctatacg
3' tag genotype Fw	6880	ALP2a	ATGTCTGCTTTCCAGTCGCT
3' tag genotype Rv	6881	ALP2a	TGCGAGGCTTTTTCCAGAGT
gR356 Fw	6752	ALP5	aagttGAACGGTTGCGAACCAAGCGg
gR356 Rv	6753	ALP5	aaaacCGCTTGGTTCGCAACCGTTCa
3' tag repair Fw	6825	ALP5	GCTCCAATGGCAAACACACAGGTCGAGGTGCTCTGGACG GAGGCCTTTACgctaaaattggaagtggagg
3' tag repair Rv	6826	ALP5	TTCGACTTCTGTGCCCGGTGCCTCCCTAGTTCTCTACCT TGTCTCCCCGCataacttcgtataatgtatgctatacg
3' tag genotype Fw	6884	ALP5	CTGTCGCTCCAATGGCAAAC

Oligo	Internal #	Target gene	Sequence
3' tag genotype Rv	6885	ALP5	ACTTTCGACTTCTGTGCCCG
gR501 Fw	8017	CenH3	AAGTTAATGGCTCGCATCAAGACGAG
gR501 Rv	8018	CenH3	AAAACTCGTCTTGATGCGAGCCATTA
gR501 repair primer DHFR-FLAG Fw	8019	CenH3	TGTATTTTCTGGCAGCAGCGGTTCGTTTTTCGTGGCAGA TGCACCCCAATATGCAGAAACCGGTGTGTC
gR501 repair primer Rv	8020	CenH3	GGCCGCGAGCCAGGTCCTGCTCTGCGCGCAGGCGTCGTC TTGATGCGAGCTCCGCCACTTCCAATTTTAGC
CenH3 5' genotype Fw	8022	CenH3	TGAAAGCACCACAAGGAGCG
CenH3 5' genotype Rv	8023	CenH3	TTCGACCGTGAGATGGGGGT
gR466 Fw	7564	Nuf2	AAGTTGCCGAGTAGAGCACCGATCTG
gR466 Rv	7565	Nuf2	AAAACAGATCGGTGCTCTACTCGGCA
3' tag repair Fw	7566	Nuf2	CAAGGGAGCCCAGAGAAGACGGCGACTTTCCAATGTATA GTCACGCCGAGGCTAAAATTGGAAGTGGAGG
3' tag repair Rv	7567	Nuf2	GCCAAAGTTCTCCGAGTGTCCGTACACCGGAAACTTTCT CCATGCCAAGAATAACTTCGTATAATGTATGCTATACG
3' tag genotype Fw	7615	Nuf2	AGCGAGAACGAGAATCCGAC
3' tag genotype Rv	7616	Nuf2	CGAGTGTCCGTACACCGGAA
fw gR127	5211	SLP1	AAGTTgtttctgggcatgcCTAGTTGG
rv gR127	5212	SLP1	AAAACCAACTAGgcatgcccagaaacA
SLP1 homology C-Tagging LoxPfw	5213	SLP1	GCCTGAGAGTCCACGGCGAGAAGGCGGTGCTGAAGTCCA CCACCCTCAACGCTAAAATTGGAAGTGGAGG
SLP1 homology C-Tagging LoxPrv	5214	SLP1	agcatgtgcgactgctttgctttctttgcctacgtttct gggcatgcCTAATAACTTCGTATAATGTATGCTATACG
SLP1 internal fw	5227	SLP1	CTGAAGGAGAAGCCGGTACG
SLP1 3UTR rv	5226	SLP1	gcagttgggcattccatttcg
fw gR498	7914	EB1	AAGTTACACCGGGGCGTGCGCAGACG
rv gR498	7915	EB1	AAAACGTCTGCGCACGCCCCGGTGTA
primer homology fw gR498	7916	EB1	GAGAGGAATGCGAAAGAGACCTTCTGGCAGGAAAGCGCC GAGCGCCGGTCTGtGCtCGgCCgGGaGTgGAaACgGCaG AaCCtATGCTcCAgGCTAAAATTGGAAGTGGAGG
primer homology rv gR498	7917	EB1	TCGCTTCATTGAAGCATCGGCTCAGCTGTCTCGACACCG GGGCGTGCGCAATAACTTCGTATAATGTATGCTATACG
EB1 genotyping Fw	8060	EB1	ACGAACCGACAAGACAGGCG
EB1 genotyping Rv	8061	EB1	TCGCAGAATGTTGCCGCAGA
gR524 Fw	8065	TGME49_205562	AAGTTGCTTGGATCCCCCGCCATTGTG
gR524 Rv 205562 n-term	8066	TGME49_205562	AAAACACAATGGCGGGGGATCCAAGCA

Oligo	Internal #	Target gene	Sequence
Repair primer gR524 DHFR Fw	8067	TGME49_205562	gagcgccagactctacgatctctcctccacggtctgccgctttccctacaATGCAGAAACCGGTGTGTCTG
Repair primer gR524 HX Fw	8159	TGME49_205562	gagcgccagactctacgatctctcctccacggtctgccgctttccctacaATGGCGTCCAAACCCATTG
Repair primer gR524 Rv	8068	TGME49_205562	GAAGATCCGGTCTCCTCGCGCCGGGTTTGCGCTTCGCTTGGATCCCCCGCTCCGCCACTTCCAATTTTAGC
Genotype 205562 n-term Fw	8069	TGME49_205562	gacccagaggcgaatctcag
Genotype 205562 n-term Rv	8070	TGME49_205562	GGAGAAAAAGAGGTCGGGGG
gR526 Fw 205562 internal2	8078	TGME49_205562	AAGTTAAAACAGTTTCTGCAGGACGG
gR526 Rv 205562 internal2	8079	TGME49_205562	AAAACCGTCCTGCAGAAACTGTTTTA
Genotype gR526 Fw	8083	TGME49_205562	GGATGGGCTGAGGGAGATAA
Genotype gR526 Rv	8084	TGME49_205562	ACGGTTTTGGGGTGTATGGC
gR531 Fw	8126	MAPK-L1	AAGTTGAAGGGAACAAGCTTTCTCCG
gR531 Rv	8127	MAPK-L1	AAAACGGAGAAAGCTTGTTCCCTTCA
Repair MAPK-L1 c-term tag primer Fw	8128	MAPK-L1	AGTTTCTGCTTCTGAGGCAACAGCAGCTGCAGCATGGCCAGCAGCAGCTGGCTAAAATTGGAAGTGGAGG
Repair MAPK-L1 c-term tag primer Rv	8129	MAPK-L1	TTGTTGTAGATACTTCCACAGTTTGAGATGCTTGAAGGGAACAAGCTTTCATAACTTCGTATAATGTATGCTATACG
Genotype MAPK-L1 3'end Fw	8130	MAPK-L1	AAGAATCCGGGCGATCTGAG
Genotype MAPK-L1 3'end Rv	8131	MAPK-L1	GGAATCCCCGCTTCCAAACT
gR261 Fw	5839	CHD1	aagttGCTCCAGCTGAGCACAGTGGg
gR261 Rv	5840	CHD1	aaaacCCACTGTGCTCAGCTGGAGCa
TGME49_258240 3' tag repair Fw	5841	CHD1	TCAGTGCAACTCCAGCCTTTGGCAATATCTCGAACGTCGCCCGCTCCAGCgctaaaattggaagtggagg

Oligo	Internal #	Target gene	Sequence
CHD1 3' tag repair Rv	5842	CHD1	AACACGGTGGACACACGGATATGGAGATACGAAATGCCTGAGATCCACCAataacttcgtataatgtatgctatacg
CHD1 3' tag genotype Fw	5843	CHD1	TCGGCTACTGTCGCCCT
CHD1 3' tag genotype Rv	5844	CHD1	TCCCTTTCAGAAGTTTCGCCA
gR263 Fw	5851	SNF2h	aagttACACGGCAAACTGGTTGCGTg
gR263 Rv	5852	SNF2h	aaaacACGCAACCAGTTTGCCGTGTa
SNF2h 3' tag repair Fw	5853	SNF2h	GAGAGAAAGAAGAGGAAAAGGACGGTGATGAACACGGCAAACTGGTTGCGgctaaaattggaagtggagg
SNF2h 3' tag repair Rv	5854	SNF2h	ttgcacctcggttgaaggccacaaagaaggattctcgacctccgcCTACGataacttcgtataatgtatgctatacg
SNF2h 3' tag genotype Fw	5855	SNF2h	GACATGAGGGCGACGAAAAC
SNF2h 3' tag genotype Rv	5856	SNF2h	TGGACTGAAAAAGAAAGACCATCT
gR271 Fw	5902	SNF2l	aagttatgcgcgaaagcaaaaaagtg
gR271 Rv	5903	SNF2l	aaaacacttttttgctttcgcgcata
SNF2l 3' tag repair Fw	5904	SNF2l	CCGCGAGCGGTCGAGCCAAGCGTCTTCGCAGCACAGCCTGGGCTGCAGCCgctaaaattggaagtggagg
SNF2l 3' tag repair Rv	5905	SNF2l	cgagtccggtgcctctctctaacggaacactacagaactcccatccaactataacttcgtataatgtatgctatacg
SNF2l 3' tag genotype Fw	5906	SNF2l	GTTTAGGGACTAACGCCGGG
SNF2l 3' tag genotype Rv	5907	SNF2l	CTTCCGCCAGAACAGACCAT
gR267 Fw	5878	Ino80	aagttAAGAGGACGATGAATAGcacg
gR267 Rv	5879	Ino80	aaaacgtgCTATTCATCGTCCTCTTa
Ino80 3' tag repair Fw	5880	Ino80	GGCCCGCGCTGTGGGAGAGTGAGATCGAGTCCACAGAAGAGGACGATGAAgctaaaattggaagtggagg
Ino80 3' tag repair Rv	5881	Ino80	gacttctcccgttgaagtctttcgcttctcttcgtacaccagtgCTATTCataacttcgtataatgtatgctatacg
Ino80 3' tag genotype Fw	5882	Ino80	ACGAAGACAGGCAGAGTGAAT
Ino80 3' tag genotype Rv	5883	Ino80	CACATGGACTTCTCCCGTTG
CbEm NdeI Fw	6492	n.a.	catatgCCCAAGAAAAAACGCAAG
CbEm NdeI Rv	6493	n.a.	CTTGTACAGCTCGTCCATG
SacI 3UTR DHFR Rv	6568	n.a.	gttGAGCTCCGCGGCTTATTTAGTTAAGGGA
NotI 5UTR DHFR Fw	6569	n.a.	catGCGGCCGCGAAGATCCGATCTTGCTGCT
Q5muta +5'NLS CbEm Fw	6554	n.a.	taagaaaaagcggaaagtggacagttctGCTCAGGTGCAGCTGGTG
Q5muta +5'NLS CbEm Rv	6555	n.a.	ggatcttccaccttgcgtttttcttgggCATGCTAGCGGATCTGACAAC

Oligo	Internal #	Target gene	Sequence
CbEmNLS + NcoI Q5muta Fw	7133	n.a.	GAAAGTGGACccatggTAACTTAAGTAAACAGAAGC
CbEmNLS + NcoI Q5muta Rv	7134	n.a.	CGCTTTTTCTTAGGATCTTC
T2A-HX Fw	7135	n.a.	aagatcctaagaaaaagcggaaagtggaccCAGAAGGTAGAGGTTCAC
T2A-HX Rv	7136	n.a.	agacgggcagcttctgtttacttaagttaccatggCTTCTCGAACTTTTTGCG
17 ΔmAID Fw	7928	n.a.	TACCCGTACGACGTCCCG
17 ΔmAID Rv	7929	n.a.	TCCGCCACTTCCAATTTTAGC
17 I6his Fw	7930	n.a.	catcaccacTAACGTATAGCATACATTATAC
17 I6his Rv	7931	n.a.	gtgatgatgCTTCTCGAACTTTTTGCG

4.3.f dsDNA fragments

dhfr-myc-T2A-3FLAG

ATGCAGAAACCGGTGTGTCTGGTCGTCGCGATGACCCCCAAGAGGGGCATCGGCATCAACAACGGCCT
CCCGTGGCCCCACTTGACCACAGATTTCAAACACTTTCGTCGTGTGACAAAAACGACGCCCGAAGAAG
CCAGTCGCCTGAACGGGTGGCTTCCCAGGAAATTTGCAAAGACGGGCGACTCTGGACTTCCCTCTCCA
TCAGTCGGCAAGAGATTCAACGCCGTTGTCATGGGACGGAAAAACTGGGAAAGCATGCCTCGAAAGTT
TAGACCCCTCGTGGACAGATTGAACATCGTCGTTTCCTCTTCCCTCAAAGAAGAAGACATTGCGGCGG
AGAAGCCTCAAGCTGAAGGCCAGCAGCGCGTCCGAGTCTGTGCTTCACTCCCAGCAGCTCTCAGCCTT
CTGGAGGAAGAGTACAAGGATTCTGTCGACCAGATTTTTGTCGTGGGAGGAGCGGGACTGTACGAGGC
AGCGCTGTCTCTGGGCGTTGCCTCTCACCTGTACATCACGCGTGTAGCCCGCGAGTTTCCGTGCGACG
TTTTCTTCCCTGCGTTCCCCGGAGATGACATTCTTTCAAACAAATCAACTGCTGCGCAGGCTGCAGCT
CCTGCCGAGTCTGTGTTCGTTCCCTTTTGTCCGGAGCTCGGAAGAGAGAAGGACAATGAAGCGACGTA
TCGACCCATCTTCATTTCCAAGACCTTCTCAGACAACGGGGTACCCTACGACTTTGTGGTTCTCGAGA
AGAGAAGGAAGACTGACGACGCAGCCACTGCGGAACCGAGCAACGCAATGAGCTCCTTGACGTCCACG
AGGGAGACAACTCCCGTGCACGGGTTGCAGGCTCCTTCTTCGGCCGCAGCCATTGCCCCGGTGTTGGC
GTGGATGGACGAAGAAGACCGGAAAAAACGCGAGCAAAAGGAACTGATTCGGGCCGTTCCGCATGTTC
ACTTTAGAGGCCATGAAGAATTCCAGTACCTTGATCTCATTGCCGACATTATTAACAATGGAAGGACA
ATGGATGACCGAACGGGCGTTGGTGTCATCTCCAAATTCGGCTGCACTATGCGCTACTCGCTGGATCA
GGCCTTTCCACTTCTCACCACAAAGCGTGTGTTCTGGAAAGGGGTCCTCGAAGAGTTGCTGTGGTTCA
TTCGCGGCGACACGAACGCAAACCATCTTTCTGAGAAGGGCGTGAAGATCTGGGACAAGAATGTGACA
CGCGAGTTCCTCGATTCGCGCAATCTCCCCCACCGAGAGGTCGGAGACATCGGCCCGGGCTACGGCTT
CCAGTGGAGACACTTCGGCGCGGCATACAAAGACATGCACACAGACTACACAGGGCAGGGCGTCGACC
AGCTGAAGAATGTGATCCAGATGCTGAGAACGAATCCAACAGATCGTCGCATGCTCATGACTGCCTGG
AATCCTGCAGCGCTGGACGAAATGGCGCTGCCGCCTTGTCACTTGTTGTGCCAGTTCTACGTGAACGA
CCAGAAGGAGCTGTCGTGCATCATGTATCAGCGGTCGTGCGATGTCGGCCTCGGCGTCCCCTTCAACA
TCGCTTCCTATTCGCTTTTGACGCTCATGGTTGCACACGTCTGCAACCTAAAACCTAAGGAGTTCATT
CACTTCATGGGGAACACGCATGTCTACACGAACCATGTCGAGGCTTTAAAAGAGCAGCTGCGGAGAGA
ACCGAGGCCGTTCCCCATTGTGAACATCCTCAACAAGGAACGCATCAAGGAAATCGACGATTTCACCG
CCGAGGATTTTGAGGTCGTGGGCTACGTCCCGCACGGACGAATCCAGATGGAGATGGCTGTCGAGCAG
AAGCTGATCTCTGAGGAGGACCTGGAAGGTAGAGGTTCACTTCTTACATGTGGTGATGTTGAAGAAAA
TCCAGGTCCAGATTACAAGGATCACGACGGGGATTACAAAGACCATGACATCGACTACAAGGACGACG
ACGATAAGGCTAAAATTGGAAGTGGCGGA

3FLAG-T2A-*cat*

GCTAAAATTGGAAGTGGCGGAGATTACAAGGATCACGACGGGGATTACAAAGACCATGACATCGACTA
CAAGGACGACGACGATAAGGAAGGTAGAGGTTCACTTCTTACATGTGGTGATGTTGAAGAAAATCCAG
GTCCAggatccATGCATGAGAAAAAAATCACTGGATATACCACCGTTGATATATCCCAATGGCATCGT
AAAGAACATTTTGAGGCATTTCAGTCAGTTGCTCAATGTACCTATAACCAGACCGTTCAGCTGGATAT

TACGGCCTTTTTAAAGACCGTAAAGAAAAATAAGCACAAGTTTTATCCGGCCTTTATTCACATTCTTG
CCCGCCTGATGAATGCTCATCCGGAATTCCGTATGGCAATGAAAGACGGTGAGCTGGTGATATGGGAT
AGTGTTCACCCTTGTTACACCGTTTTCCATGAGCAAACTGAAACGTTTTCATCGCTCTGGAGTGAATA
CCACGACGATTTCCGGCAGTTTCTACACATATATTCGCAAGATGTGGCGTGTTACGGTGAAAACCTGG
CCTATTTCCCTAAAGGGTTTATTGAGAATATGTTTTTCGTCTCAGCCAATCCCTGGGTGAGTTTCACC
AGTTTTGATTTAAACGTGGCCAATATGGACAACTTCTTCGCCCCCGTTTTCACCATGGGCAAATATTA
TACGCAAGGCGACAAGGTGCTGATGCCGCTGGCGATTCAGGTTCATCATGCCGTTTGTGATGGCTTCC
ATGTCGGCAGAATGCTTAATGAATTACAACAGTACTGCGATGAGTGGCAGGGCGGGGCTTAATTAACG
TATAGCATACATTATACGAAGTTAT

3FLAG-T2A-*dhfr*

GCTAAAATTGGAAGTGGCGGAGATTACAAGGATCACGACGGGGATTACAAAGACCATGACATCGACTA
CAAGGACGACGACGATAAGGAAGGTAGAGGTTCACTTCTTACATGTGGTGATGTTGAAGAAAATCCAG
GTCCAggatccATGCAGAAACCGGTGTGTCTGGTCGTCGCGATGACCCCCAAGAGGGGCATCGGCATC
AACAACGGCCTCCCGTGGCCCCACTTGACCACAGATTTCAAACACTTTCGTCGTGTGACAAAAACGAC
GCCCGAAGAAGCCAGTCGCCTGAACGGGTGGCTTCCCAGGAAATTTGCAAAGACGGGCGACTCTGGAC
TTCCCTCTCCATCAGTCGGCAAGAGATTCAACGCCGTTGTCATGGGACGGAAAAACTGGGAAAGCATG
CCTCGAAAGTTTAGACCCCTCGTGGACAGATTGAACATCGTCGTTTCCTCTTCCCTCAAAGAAGAAGA
CATTGCGGCGGAGAAGCCTCAAGCTGAAGGCCAGCAGCGCGTCCGAGTCTGTGCTTCACTCCCAGCAG
CTCTCAGCCTTCTGGAGGAAGAGTACAAGGATTCTGTCGACCAGATTTTTGTCGTGGGAGGAGCGGGA
CTGTACGAGGCAGCGCTGTCTCTGGGCGTTGCCTCTCACCTGTACATCACGCGTGTAGCCCGCGAGTT
TCCGTGCGACGTTTTCTTCCCTGCGTTCCCCGGAGATGACATTCTTTCAAACAAATCAACTGCTGCGC
AGGCTGCAGCTCCTGCCGAGTCTGTGTTCGTTCCCTTTTGTCCGGAGCTCGGAAGAGAGAAGGACAAT
GAAGCGACGTATCGACCCATCTTCATTTCCAAGACCTTCTCAGACAACGGGGTACCCTACGACTTTGT
GGTTCTCGAGAAGAGAAGGAAGACTGACGACGCAGCCACTGCGGAACCGAGCAACGCAATGAGCTCCT
TGACGTCCACGAGGGAGACAACTCCCGTGCACGGGTTGCAGGCTCCTTCTTCGGCCGCAGCCATTGCC
CCGGTGTTGGCGTGGATGGACGAAGAAGACCGGAAAAAACGCGAGCAAAAGGAACTGATTCGGGCCGT
TCCGCATGTTCACTTTAGAGGCCATGAAGAATTCCAGTACCTTGATCTCATTGCCGACATTATTAACA
ATGGAAGGACAATGGATGACCGAACGGGCGTTGGTGTCATCTCCAAATTCGGCTGCACTATGCGCTAC
TCGCTGGATCAGGCCTTTCCACTTCTCACCACAAAGCGTGTGTTCTGGAAAGGGGTCCTCGAAGAGTT
GCTGTGGTTCATTCGCGGCGACACGAACGCAAACCATCTTTCTGAGAAGGGCGTGAAGATCTGGGACA
AGAATGTGACACGCGAGTTCCTCGATTCGCGCAATCTCCCCCACCGAGAGGTCGGAGACATCGGCCCG
GGCTACGGCTTCCAGTGGAGACACTTCGGCGCGGCATACAAAGACATGCACACAGACTACACAGGGCA
GGGCGTCGACCAGCTGAAGAATGTGATCCAGATGCTGAGAACGAATCCAACAGATCGTCGCATGCTCA
TGACTGCCTGGAATCCTGCAGCGCTGGACGAAATGGCGCTGCCGCCTTGTCACTTGTTGTGCCAGTTC
TACGTGAACGACCAGAAGGAGCTGTCGTGCATCATGTATCAGCGGTCGTGCGATGTCGGCCTCGGCGT
CCCCTTCAACATCGCTTCCTATTCGCTTTTGACGCTCATGGTTGCACACGTCTGCAACCTAAAACCTA
AGGAGTTCATTCACTTCATGGGGAACACGCATGTCTACACGAACCATGTCGAGGCTTTAAAAGAGCAG
CTGCGGAGAGAACCGAGGCCGTTCCCCATTGTGAACATCCTCAACAAGGAACGCATCAAGGAAATCGA
CGATTTCACCGCCGAGGATTTTGAGGTCGTGGGCTACGTCCCGCACGGACGAATCCAGATGGAGATGG
CTGTCTAGTTAATTAACGTATAGCATACATTATACGAAGTTAT

hxgprt-T2A-3HA-mAID

ATGGCGTCCAAACCCATTGAAGACTACGGCAAGGGCAAGGGCCGTATTGAGCCCATGTATATCCCCGA
CAACACCTTCTACAACGCTGATGACTTTCTTGTGCCCCCCCACTGCAAGCCCTACATTGACAAAATCC
TCCTCCCTGGTGGATTGGTCAAGGACAGAGTTGAGAAGTTGGCGTATGACATCCACAGAACTTACTTC
GGCGAGGAGTTGCACATCATTTGCATCCTGAAAGGCTCTCGCGGCTTCTTCAACCTTCTGATCGACTA
CCTTGCCACCATACAGAAGTACAGTGGTCGTGAGTCCAGCGTGCCCCCCTTCTTCGAGCACTATGTCC
GCCTGAAGTCCTACCAGAACGACAACAGCACAGGCCAGCTCACCGTCTTGAGCGACGACTTGTCAATC
TTTCGCGACAAGCACGTTCTGATTGTTGAGGACATCGTCGACACCGGTTTCACCCTCACCGAGTTCGG
TGAGCGCCTGAAAGCCGTCGGTCCCAAGTCGATGAGAATCGCCACCCTCGTCGAGAAGCGCACAGATC
GCTCCAACAGCTTGAAGGGCGACTTCGTCGGCTTCAGCATTGAAGACGTCTGGATCGTTGGTTGCTGC
TACGACTTCAACGAGATGTTCCGCGACTTCGACCACGTCGCCGTCCTGAGCGACGCCGCTCGCAAAAA
GTTCGAGAAGGAAGGTAGAGGTTCACTTCTTACATGTGGTGATGTTGAAGAAAATCCAGGTCCATACC
CGTACGACGTCCCGGACTACGCTGGCTATCCCTATGATGTGCCCGATTATGCGTATCCTTACGATGTT
CCAGATTATGCCTACAAGCCTAGGATGGTGAGCGCTAGCAAGGGCTCGGGCTCGACCCAGCTGGAGAA
GAGCGCGTGTCCTAAAGATCCCGCTAAGCCGCCTGCCAAGGCCCAGGTGGTTGGCTGGCCCCCGGTTA
GGAGTTACCGCAAGAACGTGATGGTCTCTTGCCAGAAGTCTAGTGGTGGCCCTGAGGCGGCGGCATTC

GTTAAAGTCTCCATGGACGGAGCGCCGTACCTGCGAAAGATTGATTTGCGAATGTATAAAAGTGGCGG
CGGCGGCTCTGCTAAAATTGGAAGTGGCGGA

mAID-3HA-T2A-*hxgprt*

GCTAAAATTGGAAGTGGCGGATACAAGCCTAGGATGGTGAGCGCTAGCAAGGGCTCGGGCTCGACCCA
GCTGGAGAAGAGCGCGTGTCCTAAAGATCCCGCTAAGCCGCCTGCCAAGGCCCAGGTGGTTGGCTGGC
CCCCGGTTAGGAGTTACCGCAAGAACGTGATGGTCTCTTGCCAGAAGTCTAGTGGTGGCCCTGAGGCG
GCGGCATTCGTTAAAGTCTCCATGGACGGAGCGCCGTACCTGCGAAAGATTGATTTGCGAATGTATAA
AAGTGGCGGCGGCGGCTCTTACCCGTACGACGTCCCGGACTACGCTGGCTATCCCTATGATGTGCCCG
ATTATGCGTATCCTTACGATGTTCCAGATTATGCCGAAGGTAGAGGTTCACTTCTTACATGTGGTGAT
GTTGAAGAAAATCCAGGTCCAATGGCGTCCAAACCCATTGAAGACTACGGCAAGGGCAAGGGCCGTAT
TGAGCCCATGTATATCCCCGACAACACCTTCTACAACGCTGATGACTTTCTTGTGCCCCCCCACTGCA
AGCCCTACATTGACAAAATCCTCCTCCCTGGTGGATTGGTCAAGGACAGAGTTGAGAAGTTGGCGTAT
GACATCCACAGAACTTACTTCGGCGAGGAGTTGCACATCATTTGCATCCTGAAAGGCTCTCGCGGCTT
CTTCAACCTTCTGATCGACTACCTTGCCACCATACAGAAGTACAGTGGTCGTGAGTCCAGCGTGCCCC
CCTTCTTCGAGCACTATGTCCGCCTGAAGTCCTACCAGAACGACAACAGCACAGGCCAGCTCACCGTC
TTGAGCGACGACTTGTCAATCTTTCGCGACAAGCACGTTCTGATTGTTGAGGACATCGTCGACACCGG
TTTCACCCTCACCGAGTTCGGTGAGCGCCTGAAAGCCGTCGGTCCCAAGTCGATGAGAATCGCCACCC
TCGTCGAGAAGCGCACAGATCGCTCCAACAGCTTGAAGGGCGACTTCGTCGGCTTCAGCATTGAAGAC
GTCTGGATCGTTGGTTGCTGCTACGACTTCAACGAGATGTTCCGCGACTTCGACCACGTCGCCGTCCT
GAGCGACGCCGCTCGCAAAAAGTTCGAGAAGTAACGTATAGCATACATTATACGAAGTTAT

4.3.g Plasmids

Table 4.3.7: Plasmids used during this study

Plasmid	**Genotype**	**Internal designation**	**Origin**
Cas9_YFP	pTUB1-Cas9-HA-NLS-eYFP-NLS / pU6-ccdb-tracrRNA	pG474	Curt-Varesano *et al.*, 2016
Cas9_YFP gR348	As Cas9_YFP, BsaI digested, sgRNA inserted		This study
Cas9_YFP gR352	As Cas9_YFP, BsaI digested, sgRNA inserted		This study
Cas9_YFP gR354	As Cas9_YFP, BsaI digested, sgRNA inserted		This study
Cas9_YFP gR356	As Cas9_YFP, BsaI digested, sgRNA inserted		This study
Cas9_YFP gR501	As Cas9_YFP, BsaI digested, sgRNA inserted		This study
Cas9_YFP gR466	As Cas9_YFP, BsaI digested, sgRNA inserted		This study
Cas9_YFP gR127	As Cas9_YFP, BsaI digested, sgRNA inserted	pG1070	Wagner *et al.*, 2023
Cas9_YFP gR498	As Cas9_YFP, BsaI digested, sgRNA inserted		This study
Cas9_YFP gR524	As Cas9_YFP, BsaI digested, sgRNA inserted		This study
Cas9_YFP gR526	As Cas9_YFP, BsaI digested, sgRNA inserted		This study
Cas9_YFP gR531	As Cas9_YFP, BsaI digested, sgRNA inserted		This study

Plasmid	Genotype	Internal designation	Origin
Cas9_YFP gR261	As Cas9_YFP, BsaI digested, sgRNA inserted		This study
Cas9_YFP gR263	As Cas9_YFP, BsaI digested, sgRNA inserted		This study
Cas9_YFP gR271	As Cas9_YFP, BsaI digested, sgRNA inserted		This study
Cas9_YFP gR267	As Cas9_YFP, BsaI digested, sgRNA inserted		This study
CbEm	pDHFR-Chromobody-mEmerald	pG694	Periz *et al.*, 2017
$CbEm^{NLS}$ nosel	pDHFR-Chromobody-mEmerald-NLS		This study
$CbEm^{NLS}$	pDHFR-Chromobody-mEmerald-NLS *hxgprt*		This study
$^{NLS}CbEm^{NLS}$	pDHFR-NLS-Chromobody-mEmerald-NLS *hxgprt*		This study
$CbEm^{NLS}$ T2A HX	pDHFR-Chromobody-mEmerald-NLS-T2A-*hxgprt*		This study
pGEM 3FLAG-T2A-CAT		Tagging template 22	This study
pGEM 3FLAG-T2A-*dhfr*		Tagging template 21	This study
pGEM 3HA-T2A-*hxgprt*			This study
pGEM 3HA-T2A-*hxgprt*-6His		Tagging template 24	This study
pGEM *dhfr*-myc-T2A-3FLAG		Tagging template 23	This study
pGEM *hxgprt*-T2A-3HA-mAID			This study
pGEM mAID-3HA-T2A-*hxgprt*		Tagging template 17	This study

4.3.h Cell strains

Table 4.3.8: Non-*T. gondii* cell strains used in this study

Strain	Source
DH5α *E. coli*	NEB C2987I
Human foreskin fibroblasts	ATCC SCRC-1041

Table 4.3.9: *T. gondii* strains used in this study

Strain	Full Genotype	Internal #	Source / Parent
RH Δ*hxgprt*	RH Δ*hxgprt*	MG1	
RH Tir1	RH Δ*hxgprt* Δ*ku80* Δ*uprt tir1-ty*	MM462	Farhat *et al.*, 2020

Strain	Full Genotype	Internal #	Source / Parent
Ino80^{HAFLAG}	RH Δ*hxgprt ku80::dhfr frb_cre2-T2A-cat-T2A-fkbp_cre1 ino80-3HA-FLAG*	MM431	Parent RH Δ*ku80* DiCre (Hunt *et al.*, 2019)
CbEm^{NLS}	RH CbEm^{NLS} *hxgprt*	MM458	MG1
SNF2l iKD	RH Δ*ku80* Δ*uprt tir1-ty snf2l-mAID-3HA-T2A-hxgprt*	MM506	MM462
SNF2h iKD	RH Δ*ku80* Δ*uprt tir1-ty snf2h-mAID-3HA-T2A-hxgprt*	MM590	MM462
ALP2a iKD	RH Δ*ku80* Δ*uprt tir1-ty alp2a-mAID-3HA-T2A-hxgprt*	MM596	MM462
ARP4a iKD	RH Δ*ku80* Δ*uprt tir1-ty arp4a-mAID-3HA-T2A-hxgprt*	MM597	MM462
CHD1 iKD	RH Δ*ku80* Δ*uprt tir1-ty chd1-mAID-3HA-T2A-hxgprt*	MM604	MM462
ALP5 iKD	RH Δ*ku80* Δ*uprt tir1-ty alp5-mAID-3HA-T2A-hxgprt*	MM605	MM462
ARP4a iKD ALP2a^{FLAG}	RH Δ*ku80* Δ*uprt tir1-ty arp4a-mAID-3HA-T2A-hxgprt alp2a-3FLAG-T2A-dhfr*	MM695	MM597
Tir1 Nuf2^{FLAG}	RH Δ*ku80* Δ*uprt tir1-ty nuf2-3FLAG-T2A-dhfr*	MM701	MM462
ALP2a iKD Nuf2^{FLAG}	RH Δ*ku80* Δ*uprt tir1-ty alp2a-mAID-3HA-T2A-hxgprt nuf2-3FLAG-T2A-dhfr*	MM702	MM596
ARP4a iKD Nuf2^{FLAG}	RH Δ*ku80* Δ*uprt tir1-ty arp4a-mAID-3HA-T2A-hxgprt nuf2-3flag-T2A-dhfr*	MM703	MM597
ALP2a iKD ARP4a^{FLAG}	RH Δ*ku80* Δ*uprt tir1-ty alp2a-mAID-3HA-T2A-hxgprt nuf2-3flag-T2A-dhfr*	MM708	MM596
Tir1 SLP1^{FLAG}	RH Δ*ku80* Δ*uprt tir1-ty slp1-3FLAG-T2A-dhfr*	MM723	MM462
ALP2a iKD SLP1^{FLAG}	RH Δ*ku80* Δ*uprt tir1-ty alp2a-mAID-3HA-T2A-hxgprt slp1-3FLAG-T2A-dhfr*	MM724	MM596
ARP4a iKD SLP1^{FLAG}	RH Δ*ku80* Δ*uprt tir1-ty arp4a-mAID-3HA-T2A-hxgprt slp1-3FLAG-T2A-dhfr*	MM725	MM597
Tir1 EB1^{FLAG}	RH Δ*ku80* Δ*uprt tir1-ty eb1-3FLAG-T2A-dhfr*	MM789	MM462
ALP2a iKD EB1^{FLAG}	RH Δ*ku80* Δ*uprt tir1-ty alp2a-mAID-3HA-T2A-hxgprt eb1-3FLAG-T2A-dhfr*	MM790	MM596
ARP4a iKD EB1^{FLAG}	RH Δ*ku80* Δ*uprt tir1-ty arp4a-mAID-3HA-T2A-hxgprt eb1-3FLAG-T2A-dhfr*	MM791	MM597

Strain	Full Genotype	Internal #	Source / Parent
ALP2a^{HA}	RH Δ*ku80* Δ*uprt tir1-ty alp2a-3HA-T2A-hxgprt*	MM798	MM462
ARP4a^{HA}	RH Δ*ku80* Δ*uprt tir1-ty arp4a-3HA-T2A-hxgprt*	MM799	MM462
Tir1 ^{FLAG}CenH3	RH Δ*ku80* Δ*uprt tir1-ty dhfr-myc-T2A-3flag-cenh3*	MM814	MM462
ALP2a iKD ^{FLAG}CenH3	RH Δ*ku80* Δ*uprt tir1-ty alp2a-mAID-3HA-T2A-hxgprt dhfr-myc-T2A-3flag-cenh3*	MM815	MM596
ARP4a iKD ^{FLAG}CenH3	RH Δ*ku80* Δ*uprt tir1-ty arp4a-mAID-3HA-T2A-hxgprt dhfr-myc-T2A-3flag-cenh3*	MM816	MM597
Tir1 ^{FLAG}TGME49_205562	RH Δ*ku80* Δ*uprt tir1-ty dhfr-myc-T2A-3flag-TGME49_205562*	MM837	MM462
ALP2a iKD ^{FLAG}TGME49_205562	RH Δ*ku80* Δ*uprt tir1-ty alp2a-mAID-3HA-T2A-hxgprt dhfr-myc-T2A-3flag-TGME49_205562*	MM823	MM596
ARP4a iKD ^{FLAG}TGME49_205562	RH Δ*ku80* Δ*uprt tir1-ty arp4a-mAID-3HA-T2A-hxgprt dhfr-myc-T2A-3flag-TGME49_205562*	MM838	MM597
Tir1 MAPK-L1^{FLAG}	RH Δ*ku80* Δ*uprt tir1-ty mapkl1-3flag-T2A-dhfr*	MM839	MM462
ALP2a iKD MAPK-L1^{FLAG}	RH Δ*ku80* Δ*uprt tir1-ty alp2a-mAID-3HA-T2A-hxgprt mapkl1-3flag-T2A-dhfr*	MM840	MM596
ARP4a iKD MAPK-L1^{FLAG}	RH Δ*ku80* Δ*uprt tir1-ty arp4a-mAID-3HA-T2A-hxgprt mapkl1-3flag-T2A-dhfr*	MM841	MM597
TGME49_205562 iKD	RH Δ*ku80* Δ*uprt tir1-ty hxgprt-T2A-mAID-3HA-TGME49_205562*	MM845	MM462

4.4 Bacterial methods

Bacteria grown on LB agar plates were incubated at 37°C for between 14 and 18 hours. Single bacterial colonies were picked and incubated in LB medium at 37°C for between 14 and 18 hours with shaking. For transformation of plasmid DNA, 50 μL DH5α chemical competent bacteria in Tfb II buffer were thawed on ice and incubated with 1-10 μL plasmid for 20 min before a 30 s, 42°C heat shock. After 2 min recover on ice, transformed bacteria were plated onto LB agar and incubated as described above. Following ligation into pGEM, bacterial transformations were cultured on LB agar with topically supplemented 100 μL of 100 mM IPTG and 20 μL of 122 mM X-Gal.

4.5 Molecular cloning

4.5.a Polymerase chain reaction

PCRs were performed using with Q5 DNA polymerase (NEB) or Taq DNA polymerase with ThermoPol buffer (NEB) using manufacturer's protocols. Annealing temperatures were determined by NEB's Tm calculator. Typically, 35-40 cycles were performed.

4.5.b Agarose gel electrophoresis

DNA electrophoresis was performed in TAE agarose gels containing 0.8-2% w/v agarose with 12 V cm^{-1}. DNA was stained with $10{,}000^{-1}$ GelRed in TAE for 20 min post electrophoresis before visualisation with a UV transilluminator.

4.5.c DNA restriction digestion

Restriction digests were performed per manufacturer's protocol. Analytical digests were performed using 20 units of each enzyme and 20 min reaction incubation. For the digestion of plasmid DNA to be transfected into *T. gondii*, 20 ng of plasmid was digested with 400 units of enzyme overnight. For the digestion of plasmids to subsequently be ligated, 2 μg of plasmid was digested with 200 units of each enzyme for 2 hours. Restriction digests were purified with ExtractMe DNA clean-up kit (Blirt) with or without proceeding gel electrophoresis.

4.5.d Cas9 sgRNA plasmid cloning

Complementary sgRNA ssDNA oligos were synthesised (Thermo Fisher Scientific or Integrated DNA Technologies) and 2 μL of 10 μM oligos hybridised in 20 μL DNA oligo annealing buffer in a thermocycler. Thermal cycle was 98°C 10 min 1% ramp to 20°C. 5 μL of hybridised sgRNAs were then ligated into 50 ng of Cas9-eYFP plasmid using T4 DNA ligase (NEB) according to manufacturer's protocol. Ligations were incubated overnight at room temperature. Following ligation, ligated plasmid was transformed as described above.

4.5.e Plasmid ligation

For the creation of CbEm plasmids, inserts were ligated into linearised plasmid using T4 DNA ligase (NEB) per manufacturer's protocol. 50 ng of plasmid backbone and 5:1 insert to backbone was used. Ligations were incubated overnight at room temperature before transformation.

4.5.f Cas9 repair PCR template plasmids

A library of plasmids was created to be used as standard PCR templates when PCR amplifying repair DNA to be used with CRISPR-skip-in. dsDNA constructs containing the PCR template were synthesised (Integrated DNA Technologies, gBlock), a-tailed using Taq DNA polymerase (NEB) following NEB's protocol, and ligated into pGEM T-easy (Promega) following manufacturer's protocol.

4.5.g Plasmid extraction from bacteria

Mini preps were performed with 4 mL of bacterial culture using ExtractMe plasmid mini kit (Blirt) per manufacturer's protocol. Midi preps were performed with 50 mL of bacterial culture using Plasmid plus midi kit (Qiagen) per manufacturer's protocol.

4.5.h Genomic DNA isolation from *T. gondii*

gDNA was extracted from ~ 500 μL of freshly egressed *T. gondii* tachyzoites using ExtractMe genomic DNA kit (Blirt) per manufacturer's protocol.

4.6 Cell culture

4.6.a HFF and *T. gondii* culture

Human foreskin fibroblasts were cultured in complete DMEM at 37°C 5% CO_2. For passaging, HFFs were washing with PBS, incubated with 0.05% w/v trypsin 10 min 37°C, and resuspended in complete DMEM at desired concentration.

T. gondii tachyzoites were cultured in HFF monolayers in identical conditions to HFF culture. Following HFF lysis, egressed tachyzoites were inoculated onto new HFFs. For mechanical egress, monolayers were dissociated using a cell scraper and passed through a 26G needle thrice.

4.6.b Cryopreservation

HFF and *T. gondii* strains were cryopreserved for long-term storage. *T. gondii* was cryopreserved whilst intracellular. Monolayers were dissociated using a cell scraper and diluted 1:1 in 2× freezing medium and placed in cryovials. Cryovials were incubated at -80°C until frozen then transferred to a liquid nitrogen tank, with the vials occupying either liquid or vapor phase.

Cryovials were thawed at room temperature and contents transferred to complete DMEM before centrifugation for 5 min (240 ×g for HFFs, 500 ×g for *T. gondii*). Supernatant containing freezing medium was aspirated, and pellets resuspended in complete DMEM and cultured per normal.

4.6.c *T. gondii* transfection

Genetic modifications of tachyzoites was achieved through the transfection of plasmids, PCR products, and ssDNA oligos (Soldati and Boothroyd, 1993). 20 μg of plasmid DNA was used for transfections. For CRISPR-skip-in, a 100 μL PCR to amplify repair template was performed and purified using ExtractMe DNA clean-up kit (Blirt) per manufacturer's protocol. For random integration of CbEm plasmids, plasmid DNA was linearised as described above. All DNA to be transfected was mixed in a total volume of 200 μL and precipitated through the addition of 500 μL 100% EtOH and 20 μL 3M NaAc pH5.2 and pelleted through centrifugation 20,000 ×g 10 min. DNA pellets were washed once with 900 μL 70% EtOH, centrifuged again, and air dried in a laminar flow hood. 1×10^7 freshly egressed *T. gondii* tachyzoites were pelleted by centrifugation 500 ×g 5 min and transfected using an Amaxa 4D Nucleofector and 100 μL P3 buffer (Lonza) in 1 mm cuvettes and with electroporation programme FI-158. Tachyzoites were immediately inoculated onto HFFs following electroporation.

4.6.d *T. gondii* strain generation through drug selection

Selection drugs were added 24 h post transfection and continued until regular tachyzoite growth resumed, unless otherwise stated. Once normal growth had resumed, drug-resistant pools were subcloned via 1:3 serial dilution across 96-well plates of HFF monolayers. Following 7 days' culture, plaque formation in HFF monolayers was visually assessed and wells containing single plaques, indicating clonal growth, were subjected to genotypic and phenotypic confirmation via PCR and fluorescence microscopy.

Table 4.6.1: Drug selection regimens used during this study

Drug resistance marker	**Selection**
HXGPRT	78 μM mycophenolic acid in MeOH 230 μM xanthine in 1 M KOH
DHFR-TS	1 μM pyrimethamine in EtOH
CAT	20 mM chloramphenicol in H_2O

4.6.e *T. gondii* strain generation through FACS

For the isolation of transient Cas9-eYFP- expressing or stable CbEm-expressing transgenic lines, FACS was performed. 2 days post transfection, intracellular tachyzoites were mechanically egressed and filtered through a 3 μm filter. Tachyzoite suspensions were run through a FACSAria III and singlet, fluorescent events were sorted into 96-well plates containing HFF monolayers at 1-20 events per well. Following 7 days' culture, plaque formation in HFF monolayers was visually assessed and wells containing single plaques, indicating clonal growth, were subjected to genotypic and phenotypic confirmation via PCR and fluorescence microscopy.

4.6.f AID knockdowns

For the conditional knockdown of mAID-tagged proteins, tachyzoite cultures were supplemented with and maintained under 500 μM IAA (Brown, Long and Sibley, 2018).

4.6.g Jasplakinolide treatment

Jasplakinolide was used to stabilise F-actin. Tachyzoite culture medium was supplemented with 50-200 nM jasplakinolide and further incubated for 30 min prior to fixation with 4% PFA.

4.7 Phenotypic assays

4.7.a Growth assay

Tachyzoite growth through by means of the lytic cycle was assessed by plaque assay (Chaparas and Schlesinger, 1959; Pfefferkorn and Pfefferkorn, 1976). 1,000 freshly egressed tachyzoites were inoculated onto a confluent HFF monolayer in a 6-well plate ± 500 μM IAA and cultured undisturbed for 7 days. Monolayers were washed once with PBS and fixed with -20°C MeOH for 5 min. MeOH was removed and samples allowed to air dry before staining with Hemacolor (Merck) per manufacturer's protocol. The formation of plaques in the HFF monolayer by *T. gondii* tachyzoites was then visually assessed by brightfield microscopy. Samples were imaged using a Leica DMi8 with 10× NA 0.45 objective and Leica DFC9000 GTC sCMOS camera in a stitch-and-tile fashion using LasX software.

4.7.b Replication assay

Tachyzoite replication within a single lytic cycle was assessed by replication assay (Fichera, Bhopale and Roos, 1995). 2×10^6 freshly egressed tachyzoites were inoculated onto a HFF monolayer grown

on a thickness 1.5 13 ⌀ coverslip and allowed to invade for 1 h at normal culture conditions. Uninvaded tachyzoites were removed through triple PBS washing and cultures then supplemented with 500 μM IAA and cultured until stated fixation time point. For fixation, cultures were washed once with PBS, fixed with 4% PFA 20 min, and washed thrice with PBS. IFA labelling thereafter proceeded as described below. Labelled IFAs were visualised and imaged by widefield fluorescence microscopy using a Leica DMi8 equipped with 100× HC PL APO NA1.44 lens and Leica DFC9000 GTC sCMOS camera. The size of a minimum 100 vacuoles was quantified per replicate.

4.8 Immunofluorescence assays

4.8.a IFA labelling

All fixed samples were on thickness 1.5 13 ⌀ coverslips. Samples fixed with 4% PFA were blocked and permeabilised using IFA blocking & permeabilisation buffer 1 or 2. Samples to be labelled with α-centrin were fixed with -20°C MeOH for 5 min, washed thrice with PBS, and blocked with IFA blocking buffer 1 or 2. Both primary and secondary antibodies were diluted in blocking buffer and used at the concentrations given in Table 4.3.5. Samples were incubated with primary antibodies for 1 h in a wet chamber, washed thrice with 0.2% Triton Tx-100 PBS, incubated with secondary antibodies for 45 min in wet chamber, and washed thrice with 0.2% Triton Tx-100 PBS. For mounting, coverslips were washed once with ddH_2O and excess liquid removed before mounting with Fluoromount-G and sealed with nail varnish.

4.8.b Widefield microscopy

Widefield fluorescence microscopy was performed using a Leica DMi8 equipped with 100× HC PL APO NA1.44 lens and Leica DFC9000 GTC 16-bit sCMOS camera controlled by LasX software.

4.8.c Confocal microscopy

Confocal microscopy was performed using an Abberior STED microscope equipped with a 100× UPL SAPO NA 1.45 lens and an APD controlled by Imspector software.

4.8.d STED microscopy

STED microscope was performed using a Nikon eclipse Ti2 equipped with a STEDYCON module (Abberior) and 100× PLAN APO NA 1.45 lens.

4.8.e Image analysis

Micrographs were processed and analysed using FIJI ImageJ. Confocal micrographs were adjusted from 16-bit signed to 16-bit unsigned before further processing. Otsu's thresholding (Otsu, 1979) and intermodes thresholding (Prewitt and Mendelsohn, 1966) were used as indicated. For 3D centroid-to-centroid distance measurements, micrographs were first converted to 8-bit, filtered using a 3D 2 px maximum (3D ImageJ Suite), and Z-max projected. Intermodes thresholding was applied to the projection to obtain a per-image threshold for use with segmentation. For segmentation, a 3D iterative thresholding algorithm was used (3D ImageJ Suite) with the intermodes-determined threshold. Computed segments were manually reviewed and low quality samples, typically with high segment numbers arising from poor signal-to-noise ratio, removed from further analysis. Marker protein to nearest Cen1 segment was computed using 3D distances closest function (3D ImageJ Suite). Number of centrosomes per tachyzoite was quantified through 3D maxima finder function (3D ImageJ Suite). Sum fluorescence intensity of segments was quantified using 3D intensity measure function (3D ImageJ Suite).

4.9 Protein biochemistry

4.9.a Western blotting

For routine western blotting, intracellular tachyzoites were washed once with ice-cold PBS, mechanically egressed, and pelleted by centrifugation 500 ×g, 5 min, 4°C. Pellets were resuspended in 16 μL SDS lysis buffer, incubated on ice for 5 min, and cleared by centrifugation 20,000 ×g, 3 min, 4°C.

For time course KD western blotting, 1.3×10^8 tachyzoites were inoculated onto HFFs and cultured overnight ± 500 μM IAA. At each time point, tachyzoites were mechanically egressed at 4°C, pelleted as above, resuspended in SDS lysis buffer plus 100 units ml^{-1} benzonase at a concentration of 3.85×10^9 tachyzoites ml^{-1}, incubated on ice for 15 min, and cleared by centrifugation 20,000 ×g, 3 min, 4°C. Protein concentration was quantified by Nanodrop spectrophotometry and indicated mass of protein loaded per lane.

Prior to loading, samples were diluted with OrangeG protein loading dye and DTT (final conc. 1× and 100 mM, respectively), and incubated at 95°C for 10 min. SDS-PAGE was performed with 4-20% gradient acrylamide gels. Migrated proteins were transferred to nitrocellulose by wet transfer in

Bjerrum Schafer-Nielson buffer with ice as coolant under 400 mA for 1 h. Transfer efficiency was confirmed by Ponceau S strain. Blots were blocked with 5% milk TBS for 1 h. Blots were incubated with primary antibodies in blocking buffer at 4°C overnight, washed thrice TBS-T 5 min, incubated with secondary antibodies in blocking buffer at room temperature for 45 min, washed thrice TBS-T, washed once TBS, and imaged using Odyssey CLx (Li-Cor).

Western blot images were contrast adjusted and quantified using Image Studio (Li-Cor). For quantification, bounding boxes for bands were autogenerated and manually reviewed, with protein of interest signal intensities normalised to α-aldolase signal intensity.

4.9.b Co-immunoprecipitation & LC-MS analysis

Prior to CoIPs, nuclear proteins were extracted by cell fractionation. 1×10^9 tachyzoites were resuspended in 500 μL swelling buffer plus 0.65% v/v IGEPAL, incubated on ice for 15 min, centrifuged 2,500 ×g, 10 min, 4°C, and the supernatant containing the cytoplasmic fraction removed and retained. The nuclei pellet was washed once with 500 μL swelling buffer, resuspended in 400 μL swelling buffer plus 0.65% v/v IGEPAL and 250 units benzonase, incubated at room temperature for 30 min, supplemented with 250 μL 1 M KCl, incubated 30 min at room temperature, centrifuged 5,000 ×g for 30 min at 4°C. The resulting supernatant containing the nuclear proteins was collected and pellet of insoluble material resuspended in 500 μL 4× OrangeG protein loading dye. Lysate fractions were assessed by western blotting.

For CoIPs, 30 μL α-HA magnetic beads were equilibrated with 400 μL RIPA50. 200 μL soluble nuclear lysate fraction was combined with 400 μL RIPA50 and 1% final v/v IGEPAL. Diluted lysate was added to equilibrated beads and incubated overnight at 4°C on a carousel. Beads were washed thrice for 10 min at 4°C on carousel with 400 μL RIPA50 then washed thrice with 100 μL 50 mM Tris-HCl pH8. 10% beads were resuspended in 4× OrangeG protein loading dye and used for verification of CoIP enrichment by western blot.

Mass spectrometry based proteomic experiments were performed as described previously (Singer *et al.*, 2023) with minor modifications. Briefly, beads were washed thrice with 50 mM NH_4HCO_3 and incubated with 10 ng μL^{-1} trypsin in 1 M urea 50 mM NH_4HCO_3 for 30 min, washed with 50 mM NH_4HCO_3 and the supernatant digested overnight in presence of 1 mM DTT. Digested peptides were alkylated and desalted prior to LC-MS analysis. The peptide mixtures were subjected to nanoRP-LC-MS/MS analysis on an Ultimate 3000 nano chromatography system (Thermo Fisher Scientific) equipped with a

25 cm Aurora column (Ionopticks) and coupled to an Orbitrap Exploris-480 mass spectrometer (Thermo Fisher Scientific).

MaxQuant (Tyanova, Temu and Cox, 2016) v2.0.1.0 was used to identify proteins and quantify by iBAQ with the following parameters: Database Uniprot_UP00000152_Toxoplasmagondii_Me49_20221024-08.04.16.64.fasta; MS tol, 10 ppm; MS/MS tol, 20 ppm Da; Peptide FDR, 0.1; Protein FDR, 0.01 min; Peptide Length, 7; Variable modifications, Oxidation (M); Fixed modifications, Carbamidomethyl (C); Peptides for protein quantitation, razor and unique; Min. peptides, 1; Min. ratio count, 2. Missing values were imputed using a 0.3 wide, downshifted by 3 normal distribution. Identified proteins were considered as interaction partners of the bait if their MaxQuant iBAQ values when compared to the corresponding control (log2(ALP2a) – $\log_2$(Tir1) or $\log_2$(ARP4a) – log2(Tir1)) were ≥ 1 and had an FDR of ≥ 0.05. For display and analysis, the Perseus software (Tyanova *et al.*, 2016) was used. Data has been uploaded to the PRIDE repository (Perez-Riverol *et al.*, 2022) PXD046893.

4.10 Statistical analysis

Data wrangling and statistical analysis was performed using base R and package rstatix v0.7.2 using statistical tests stated in figure legends. All standard deviations are sample standard deviations. Gaussian mixture modelling was performed using package mclust v6.0.0 (Scrucca et al., 2016).

All plots were created using ggplot2 package (v3.4.0) for R. Figures were assembled with Inkscape (v1.3).

5 List of Figures

6 List of Tables

7 List of Abbreviations

3D	3-dimensional
Ac	Acetylation
ADP	Adenosine di-phosphate
AID	Auxin-inducible degron
ALP	Actin-like protein
AP2	Apetala 2
ApiAP2	Apicomplexan AP2 transcription factor family
Ark	Aurora kinase
ARP	Actin-related protein
ATP	Adenosine triphosphate
BLAST	Basic local alignment search tool
BSA	Bovine serum albumin
CAT	Chloramphenicol acetyltransferase
CbEm	Chromobody® mEmerald
CDK	Cyclin-dependant kinase
CHD	Chromo domain helicase DNA-binding
ChIP	Chromatin immunoprecipitation
ChIPseq	Chromatin immunoprecipitation sequencing
CoIP	Co-immunoprecipitation
CRISPR	Clustered regulatory interspaced short palindromic repeats
Crk	Cyclin-related kinase
Cyc	Cyclin
DAPI	4′,6-diamidino-2-phenylindole
DHFR	Dihydrofolate reductase
DHFR-TS	Dihydrofolate reductase-thymidylate synthase
DMEM	Dulbecco's modified Eagle medium
DMSO	Dimethyl sulfoxide
DNA	Deoxyribonucleic acid
dNTP	Deoxynucleotide triphosphate
Drp	Dynamin-related protein
dsDNA	Double stranded DNA
DTT	Dithiothreitol
EDTA	Ethylenediaminetetraacetic acid
EGTA	Ethylene glycol-bis(β-aminoethyl ether)-N,N,N′,N′-tetraacetic acid
EtOH	Ethanol
EuPaGDT	Eukaryotic pathogen sgRNA design tool
FACS	Fluorescence-activated cell sorting
FACS	Fluorescence-activated cell sorting
F-actin	Filamentous actin
FBS	Foetal bovine serum
FDR	False discovery rate
FIJI	FIJI is just ImageJ
G-actin	Globular actin
GAP	Gliding-associated protein
gDNA	Genomic DNA
GFP	Green fluorescent protein
GoI	Gene of interest

H. sapiens	*Homo sapiens*
HA	Haemagglutinin
HDAC	Histone deacetylase
HEPES	4-(2-hydroxyethyl)-1-piperazineethanesulfonic acid
HFF	Human foreskin fibroblast
His	Histidine
HiT	High throughput tagging
HPLC	High pressure liquid chromatography
HSA	Helicase-SANT
HXGPRT	Hypoxanthine-xanthine-guanine phosphoribosyl transferase
IAA	Indole-3-acetic acid
iBAQ	Intensity based absolute quantification
IDR	Inherently disordered region
IFA	Immunofluorescence assay
iKD	Inducible knockdown
IMC	Inner membrane complex
Ino80	Inositol requiring 80
IPTG	Isopropyl ß-D-1-thiogalactopyranoside
ISWI	Imitation switch
KAT	Lysine acetyltransferase
KD	Knockdown
KO	Knockout
LB	Lysogeny broth
LC-MS	Liquid chromatography – mass spectrometry
LED	Light-emitting diode
LIC	Ligation-independent cloning
mAID	Minimal AID domain
MAPK	Mitogen-activated protein kinase
Me	Methylation
MeOH	Methanol
MFI	Mean fluorescence intensity
MOPS	3-(N-morpholino)propanesulfonic acid
MORN	Membrane occupation recognition nexus motif
MPA	Mycophenolic acid
mRNA	Messenger RNA
MTOC	Microtubule organising centre
MUSCLE	MUltiple Sequence Comparison by Log- Expectation
Myo	Myosin
NES	Nuclear export signal
NLS	Nuclear localisation signal
P. falciparum	*Plasmodium falciparum*
PAGE	Polyacrylamide gel electrophoresis
PBS	Phosphate buffered saline
PCR	Polymerase chain reaction
PFA	Paraformaldehyde
Pi	Inorganic phosphate
Plk	Polo-like kinase
PoI	Protein of interest
PRMT	Protein arginine methyltransferase

PTM	Post-translational modification
RIPA	Radioimmunoprecipitation assay buffer
RNA	Ribonucleic acid
RNAPII	RNA polymerase II
RNAseq	RNA sequencing
RoI	Region of interest
S. cerevisiae	*Saccharomyces cerevisiae*
SANT	Swi3, Ada2, N-Cor, and TFIIIB domain
SAR	Taxonomic supergroup: Stramenopiles, Alveolata, and Rhizaria
SDS	Sodium dodecyl sulfate
sgRNA	Small guide RNA
SiR	Silicon rhodamine
siRNA	Small interfering RNA
SLIDE	SANT-like but with indels
SNF	Sucrose non-fermenting
ssDNA	Single stranded DNA
STED	Stimulated emission depletion microscopy
SWI	Switching defective
T. gondii	*Toxoplasma gondii*
TAE	Tris-base, acetic acid, EDTA buffer
TATi	*Trans*-activator trap identified
TBS	Tris buffered saline
Tir	Transport inhibitor response
TS	Temperature sensitive
ULT	Ultra low temperature
UTR	Untranslated region
UV	Ultraviolet
WASp	Wiskott-Aldrich syndrome protein
WT	Wild type
YFP	Yellow fluorescent protein

8 References

A, P. and Weber, S. C. (2019) 'Evidence for and against Liquid-Liquid Phase Separation in the Nucleus.', *Non-coding RNA*, 5(4). doi: 10.3390/ncrna5040050.

Adl, S. M. *et al.* (2019) 'Revisions to the Classification, Nomenclature, and Diversity of Eukaryotes.', *The Journal of eukaryotic microbiology*, 66(1), pp. 4–119. doi: 10.1111/jeu.12691.

Alexander, D. L. *et al.* (2005) 'Identification of the moving junction complex of Toxoplasma gondii: a collaboration between distinct secretory organelles.', *PLoS pathogens*, 1(2), p. e17. doi: 10.1371/journal.ppat.0010017.

Alfert, A., Moreno, N. and Kerl, K. (2019) 'The BAF complex in development and disease.', *Epigenetics & chromatin*, 12(1), p. 19. doi: 10.1186/s13072-019-0264-y.

Almuzzaini, B. *et al.* (2015) 'Nuclear myosin 1 contributes to a chromatin landscape compatible with RNA polymerase II transcription activation.', *BMC biology*, 13, p. 35. doi: 10.1186/s12915-015-0147-z.

Almuzzaini, B. *et al.* (2016) 'In β-actin knockouts, epigenetic reprogramming and rDNA transcription inactivation lead to growth and proliferation defects', *The FASEB Journal*, 30(8), pp. 2860–2873. doi: 10.1096/fj.201600280R.

Alvarez, C. A. and Suvorova, E. S. (2017) 'Checkpoints of apicomplexan cell division identified in Toxoplasma gondii.', *PLoS pathogens*, 13(7), p. e1006483. doi: 10.1371/journal.ppat.1006483.

Amos, B. *et al.* (2022) 'VEuPathDB: the eukaryotic pathogen, vector and host bioinformatics resource center', *Nucleic Acids Research*, 50(D1), pp. D898–D911. doi: 10.1093/nar/gkab929.

Anantharaman, V. and Aravind, L. (2006) 'The NYN domains: novel predicted RNAses with a PIN domain-like fold.', *RNA biology*, 3(1), pp. 18–27. doi: 10.4161/rna.3.1.2548.

Andenmatten, N. *et al.* (2013a) 'Conditional genome engineering in Toxoplasma gondii uncovers alternative invasion mechanisms.', *Nature methods*, 10(2), pp. 125–7. doi: 10.1038/nmeth.2301.

Andenmatten, N. *et al.* (2013b) 'Conditional genome engineering in Toxoplasma gondii uncovers alternative invasion mechanisms.', *Nature methods*, 10(2), pp. 125–7. doi: 10.1038/nmeth.2301.

Anderson-White, B. *et al.* (2012) 'Cytoskeleton assembly in Toxoplasma gondii cell division.', *International review of cell and molecular biology*, 298, pp. 1–31. doi: 10.1016/B978-0-12-394309-5.00001-8.

Antunes, A. V. *et al.* (2023) 'In vitro production of cat-restricted Toxoplasma pre-sexual stages by epigenetic reprogramming', *bioRxiv*, p. 01.16.524187. doi: 10.1101/2023.01.16.524187.

Aramini, J. J., Stephen, C. and Dubey, J. P. (1998) 'Toxoplasma gondii in Vancouver Island cougars (Felis concolor vancouverensis): serology and oocyst shedding.', *The Journal of parasitology*, 84(2), pp. 438–40. Available at: http://www.ncbi.nlm.nih.gov/pubmed/9576522.

Aravind, L. *et al.* (2003) 'Plasmodium biology: genomic gleanings.', *Cell*, 115(7), pp. 771–85. Available at: http://www.ncbi.nlm.nih.gov/pubmed/14697197.

Asakura, S., Taniguchi, M. and Oosawa, F. (1963) 'Mechano-chemical behaviour of F-actin', *Journal of Molecular Biology*, 7(1), pp. 55–69. doi: 10.1016/S0022-2836(63)80018-2.

Aslanidis, C. and de Jong, P. J. (1990) 'Ligation-independent cloning of PCR products (LIC-PCR).', *Nucleic acids research*, 18(20), pp. 6069–74. doi: 10.1093/nar/18.20.6069.

Attias, M., Miranda, K. and De Souza, W. (2019) 'Development and fate of the residual body of Toxoplasma gondii.', *Experimental parasitology*, 196, pp. 1–11. doi: 10.1016/j.exppara.2018.11.004.

Aumeier, C., Polinski, E. and Menzel, D. (2015) 'Actin, actin-related proteins and profilin in diatoms: a comparative genomic analysis.', *Marine genomics*, 23, pp. 133–42. doi:

10.1016/j.margen.2015.07.002.

Avena, J. S. *et al.* (2014) 'Licensing of yeast centrosome duplication requires phosphoregulation of sfi1.', *PLoS genetics*, 10(10), p. e1004666. doi: 10.1371/journal.pgen.1004666.

Baarlink, C. *et al.* (2017) 'A transient pool of nuclear F-actin at mitotic exit controls chromatin organization.', *Nature cell biology*, 19(12), pp. 1389–1399. doi: 10.1038/ncb3641.

Baird, J. K. (2009) 'Malaria zoonoses.', *Travel medicine and infectious disease*, 7(5), pp. 269–77. doi: 10.1016/j.tmaid.2009.06.004.

Balaji, S. *et al.* (2005) 'Discovery of the principal specific transcription factors of Apicomplexa and their implication for the evolution of the AP2-integrase DNA binding domains.', *Nucleic acids research*, 33(13), pp. 3994–4006. doi: 10.1093/nar/gki709.

Bandini, G. *et al.* (2016) 'O-fucosylated glycoproteins form assemblies in close proximity to the nuclear pore complexes of Toxoplasma gondii.', *Proceedings of the National Academy of Sciences of the United States of America*, 113(41), pp. 11567–11572. doi: 10.1073/pnas.1613653113.

Bannas, P., Hambach, J. and Koch-Nolte, F. (2017) 'Nanobodies and Nanobody-Based Human Heavy Chain Antibodies As Antitumor Therapeutics.', *Frontiers in immunology*, 8, p. 1603. doi: 10.3389/fimmu.2017.01603.

Bansal, P. *et al.* (2021) 'Protein kinase TgCDPK7 regulates vesicular trafficking and phospholipid synthesis in Toxoplasma gondii.', *PLoS pathogens*, 17(2), p. e1009325. doi: 10.1371/journal.ppat.1009325.

Barylyuk, K. *et al.* (2020) 'A Comprehensive Subcellular Atlas of the Toxoplasma Proteome via hyperLOPIT Provides Spatial Context for Protein Functions.', *Cell host & microbe*, 28(5), pp. 752-766.e9. doi: 10.1016/j.chom.2020.09.011.

Behnke, M. S. *et al.* (2010) 'Coordinated progression through two subtranscriptomes underlies the tachyzoite cycle of Toxoplasma gondii.', *PloS one*, 5(8), p. e12354. doi: 10.1371/journal.pone.0012354.

Berman, H. M. *et al.* (2000) 'The Protein Data Bank.', *Nucleic acids research*, 28(1), pp. 235–42. doi: 10.1093/nar/28.1.235.

Berry, L. *et al.* (2016) 'The conserved apicomplexan Aurora kinase TgArk3 is involved in endodyogeny, duplication rate and parasite virulence.', *Cellular microbiology*, 18(8), pp. 1106–1120. doi: 10.1111/cmi.12571.

Berry, L. *et al.* (2018) 'Toxoplasma gondii chromosomal passenger complex is essential for the organization of a functional mitotic spindle: a prerequisite for productive endodyogeny.', *Cellular and molecular life sciences : CMLS*, 75(23), pp. 4417–4443. doi: 10.1007/s00018-018-2889-6.

Bevins, S. N. *et al.* (2012) 'Three pathogens in sympatric populations of pumas, bobcats, and domestic cats: implications for infectious disease transmission.', *PloS one*, 7(2), p. e31403. doi: 10.1371/journal.pone.0031403.

Bhandage, A. K. and Barragan, A. (2019) 'Calling in the CaValry-Toxoplasma gondii Hijacks GABAergic Signaling and Voltage-Dependent Calcium Channel Signaling for Trojan horse-Mediated Dissemination.', *Frontiers in cellular and infection microbiology*, 9, p. 61. doi: 10.3389/fcimb.2019.00061.

Bhatti, M. M. *et al.* (2006) 'Pair of unusual GCN5 histone acetyltransferases and ADA2 homologues in the protozoan parasite Toxoplasma gondii.', *Eukaryotic cell*, 5(1), pp. 62–76. doi: 10.1128/EC.5.1.62-76.2006.

Birnbaum, J. *et al.* (2017) 'A genetic system to study Plasmodium falciparum protein function.', *Nature methods*, 14(4), pp. 450–456. doi: 10.1038/nmeth.4223.

El Bissati, K. *et al.* (2016) 'Toxoplasma gondii Arginine Methyltransferase 1 (PRMT1) Is Necessary for Centrosome Dynamics during Tachyzoite Cell Division.', *mBio*, 7(1), pp. e02094-15. doi: 10.1128/mBio.02094-15.

Bjork, K. E., Averbeck, G. A. and Stromberg, B. E. (2000) 'Parasites and parasite stages of free-ranging wild lions (Panthera leo) of northern Tanzania.', *Journal of zoo and wildlife medicine : official publication of the American Association of Zoo Veterinarians*, 31(1), pp. 56–61. doi: 10.1638/1042-7260(2000)031[0056:PAPSOF]2.0.CO;2.

Black, J. C., Van Rechem, C. and Whetstine, J. R. (2012) 'Histone lysine methylation dynamics: establishment, regulation, and biological impact.', *Molecular cell*, 48(4), pp. 491–507. doi: 10.1016/j.molcel.2012.11.006.

Black, M. *et al.* (1995) 'Restriction enzyme-mediated integration elevates transformation frequency and enables co-transfection of Toxoplasma gondii.', *Molecular and biochemical parasitology*, 74(1), pp. 55–63. doi: 10.1016/0166-6851(95)02483-2.

Black, M. W. and Boothroyd, J. C. (1998) 'Development of a stable episomal shuttle vector for Toxoplasma gondii.', *The Journal of biological chemistry*, 273(7), pp. 3972–9. doi: 10.1074/jbc.273.7.3972.

Blangy, A. *et al.* (1995) 'Phosphorylation by p34cdc2 regulates spindle association of human Eg5, a kinesin-related motor essential for bipolar spindle formation in vivo.', *Cell*, 83(7), pp. 1159–69. doi: 10.1016/0092-8674(95)90142-6.

Boeynaems, S. *et al.* (2018) 'Protein Phase Separation: A New Phase in Cell Biology.', *Trends in cell biology*, 28(6), pp. 420–435. doi: 10.1016/j.tcb.2018.02.004.

Bogado, S. S. *et al.* (2014) 'Canonical histone H2Ba and H2A.X dimerize in an opposite genomic localization to H2A.Z/H2B.Z dimers in Toxoplasma gondii.', *Molecular and biochemical parasitology*, 197(1–2), pp. 36–42. doi: 10.1016/j.molbiopara.2014.09.009.

Boudreault, A. A. *et al.* (2003) 'Yeast enhancer of polycomb defines global Esa1-dependent acetylation of chromatin.', *Genes & development*, 17(11), pp. 1415–28. doi: 10.1101/gad.1056603.

Bougdour, A. *et al.* (2009) 'Drug inhibition of HDAC3 and epigenetic control of differentiation in Apicomplexa parasites.', *The Journal of experimental medicine*, 206(4), pp. 953–66. doi: 10.1084/jem.20082826.

Bradley, P. J. *et al.* (2005) 'Proteomic analysis of rhoptry organelles reveals many novel constituents for host-parasite interactions in Toxoplasma gondii.', *The Journal of biological chemistry*, 280(40), pp. 34245–58. doi: 10.1074/jbc.M504158200.

Brameier, M., Krings, A. and MacCallum, R. M. (2007) 'NucPred--predicting nuclear localization of proteins.', *Bioinformatics (Oxford, England)*, 23(9), pp. 1159–60. doi: 10.1093/bioinformatics/btm066.

Brooks, C. F. *et al.* (2011) 'Toxoplasma gondii sequesters centromeres to a specific nuclear region throughout the cell cycle.', *Proceedings of the National Academy of Sciences of the United States of America*, 108(9), pp. 3767–72. doi: 10.1073/pnas.1006741108.

Brown, K. M., Long, S. and Sibley, L. D. (2018) 'Conditional Knockdown of Proteins Using Auxin-inducible Degron (AID) Fusions in Toxoplasma gondii.', *Bio-protocol*, 8(4). doi: 10.21769/BioProtoc.2728.

Brusini, L. *et al.* (2022) 'Composition and organization of kinetochores show plasticity in apicomplexan chromosome segregation.', *The Journal of cell biology*, 221(9). doi: 10.1083/jcb.202111084.

Bryant, J. M. *et al.* (2020) 'Exploring the virulence gene interactome with CRISPR/dCas9 in the human malaria parasite.', *Molecular systems biology*, 16(8), p. e9569. doi: 10.15252/msb.20209569.

Bugyi, B. and Carlier, M.-F. (2010) 'Control of actin filament treadmilling in cell motility.', *Annual review of biophysics*, 39, pp. 449–70. doi: 10.1146/annurev-biophys-051309-103849.

Bunnik, E. M. *et al.* (2019) 'Comparative 3D genome organization in apicomplexan parasites.', *Proceedings of the National Academy of Sciences of the United States of America*, 116(8), pp. 3183–3192. doi: 10.1073/pnas.1810815116.

Calero-Bernal, R. *et al.* (2022) 'Unifying Virulence Evaluation in Toxoplasma gondii: A Timely Task.', *Frontiers in cellular and infection microbiology*, 12, p. 868727. doi:

10.3389/fcimb.2022.868727.

Callebaut, I. *et al.* (2005) 'Prediction of the general transcription factors associated with RNA polymerase II in Plasmodium falciparum: conserved features and differences relative to other eukaryotes.', *BMC genomics*, 6, p. 100. doi: 10.1186/1471-2164-6-100.

Cao, L. *et al.* (2015) 'Negative Regulation of p21Waf1/Cip1 by Human INO80 Chromatin Remodeling Complex Is Implicated in Cell Cycle Phase G2/M Arrest and Abnormal Chromosome Stability.', *PloS one*, 10(9), p. e0137411. doi: 10.1371/journal.pone.0137411.

Cao, T. *et al.* (2016) 'Crystal structure of a nuclear actin ternary complex.', *Proceedings of the National Academy of Sciences of the United States of America*, 113(32), pp. 8985–90. doi: 10.1073/pnas.1602818113.

Cardoso, A. R. *et al.* (2021) 'Genetic Variability of the Functional Domains of Chromodomains Helicase DNA-Binding (CHD) Proteins.', *Genes*, 12(11). doi: 10.3390/genes12111827.

Caridi, C. P. *et al.* (2018) 'Nuclear F-actin and myosins drive relocalization of heterochromatic breaks.', *Nature*, 559(7712), pp. 54–60. doi: 10.1038/s41586-018-0242-8.

Carlier, M. F. (1990) 'Actin polymerization and ATP hydrolysis.', *Advances in biophysics*, 26, pp. 51–73. doi: 10.1016/0065-227x(90)90007-g.

Carlson, M., Osmond, B. C. and Botstein, D. (1981) 'Mutants of yeast defective in sucrose utilization.', *Genetics*, 98(1), pp. 25–40. doi: 10.1093/genetics/98.1.25.

Carruthers, V. B. and Tomley, F. M. (2008) 'Microneme proteins in apicomplexans.', *Sub-cellular biochemistry*, 47, pp. 33–45. doi: 10.1007/978-0-387-78267-6_2.

Cavalier-Smith, T. (1999) 'Principles of protein and lipid targeting in secondary symbiogenesis: euglenoid, dinoflagellate, and sporozoan plastid origins and the eukaryote family tree.', *The Journal of eukaryotic microbiology*, 46(4), pp. 347–66. doi: 10.1111/j.1550-7408.1999.tb04614.x.

Cavalier-Smith, T. (2010) 'Kingdoms Protozoa and Chromista and the eozoan root of the eukaryotic tree.', *Biology letters*, 6(3), pp. 342–5. doi: 10.1098/rsbl.2009.0948.

Chaparas, S. D. and Schlesinger, R. W. (1959) 'Plaque Assay of Toxoplasma on Monolayers of Chick Embryo Fibroblasts.', *Experimental Biology and Medicine*, 102(2), pp. 431–437. doi: 10.3181/00379727-102-25275.

Chen, A. L. *et al.* (2017) 'Novel insights into the composition and function of the Toxoplasma IMC sutures.', *Cellular microbiology*, 19(4). doi: 10.1111/cmi.12678.

Chen, C.-T. *et al.* (2015) 'Compartmentalized Toxoplasma EB1 bundles spindle microtubules to secure accurate chromosome segregation.', *Molecular biology of the cell*, 26(25), pp. 4562–76. doi: 10.1091/mbc.E15-06-0437.

Chen, C.-T. and Gubbels, M.-J. (2013) 'The Toxoplasma gondii centrosome is the platform for internal daughter budding as revealed by a Nek1 kinase mutant.', *Journal of cell science*, 126(Pt 15), pp. 3344–55. doi: 10.1242/jcs.123364.

Chen, C.-T. and Gubbels, M.-J. (2019) 'TgCep250 is dynamically processed through the division cycle and is essential for structural integrity of the Toxoplasma centrosome.', *Molecular biology of the cell*, 30(10), pp. 1160–1169. doi: 10.1091/mbc.E18-10-0608.

Chutani, N. *et al.* (2022) 'Structural and Functional Attributes of Microrchidia Family of Chromatin Remodelers.', *Journal of molecular biology*, 434(14), p. 167664. doi: 10.1016/j.jmb.2022.167664.

Collins, K. A. *et al.* (2005) 'De novo kinetochore assembly requires the centromeric histone H3 variant.', *Molecular biology of the cell*, 16(12), pp. 5649–60. doi: 10.1091/mbc.e05-08-0771.

Courjol, F. and Gissot, M. (2018) 'A coiled-coil protein is required for coordination of karyokinesis and cytokinesis in Toxoplasma gondii.', *Cellular microbiology*, 20(6), p. e12832. doi: 10.1111/cmi.12832.

Curt-Varesano, A. *et al.* (2016) 'The aspartyl protease TgASP5 mediates the export of the Toxoplasma

GRA16 and GRA24 effectors into host cells', *Cellular Microbiology*, 18(2), pp. 151–167. doi: 10.1111/cmi.12498.

Davis, M. W. and Jorgensen, E. M. (2022) 'ApE, A Plasmid Editor: A Freely Available DNA Manipulation and Visualization Program.', *Frontiers in bioinformatics*, 2, p. 818619. doi: 10.3389/fbinf.2022.818619.

Diesh, C. *et al.* (2023) 'JBrowse 2: a modular genome browser with views of synteny and structural variation.', *Genome biology*, 24(1), p. 74. doi: 10.1186/s13059-023-02914-z.

Dobrowolski, J. M., Niesman, I. R. and Sibley, L. D. (1997) 'Actin in the parasite Toxoplasma gondii is encoded by a single copy gene, ACT1 and exists primarily in a globular form.', *Cell motility and the cytoskeleton*, 37(3), pp. 253–62. doi: 10.1002/(SICI)1097-0169(1997)37:3<253::AID-CM7>3.0.CO;2-7.

Donald, R. G. and Roos, D. S. (1993) 'Stable molecular transformation of Toxoplasma gondii: a selectable dihydrofolate reductase-thymidylate synthase marker based on drug-resistance mutations in malaria.', *Proceedings of the National Academy of Sciences of the United States of America*, 90(24), pp. 11703–7. doi: 10.1073/pnas.90.24.11703.

Donald, R. G. and Roos, D. S. (1998) 'Gene knock-outs and allelic replacements in Toxoplasma gondii: HXGPRT as a selectable marker for hit-and-run mutagenesis.', *Molecular and biochemical parasitology*, 91(2), pp. 295–305. doi: 10.1016/s0166-6851(97)00210-7.

van Dooren, G. G. *et al.* (2009) 'An novel dynamin-related protein has been recruited for apicoplast fission in Toxoplasma gondii', *Current biology : CB*. NIH Public Access, 19(4), p. 267. doi: 10.1016/J.CUB.2008.12.048.

Dopie, J. *et al.* (2012) 'Active maintenance of nuclear actin by importin 9 supports transcription.', *Proceedings of the National Academy of Sciences of the United States of America*, 109(9), pp. E544-52. doi: 10.1073/pnas.1118880109.

Dorrell, R. G. and Bowler, C. (2017) 'Secondary Plastids of Stramenopiles', in, pp. 57–103. doi: 10.1016/bs.abr.2017.06.003.

Dubey, J. P. (1977) 'Toxoplasma, Hammondia, Besnotia, Sarcocystis and other tissue cyst-forming coccidia of man and animals', in *Parasitic protozoa III*, pp. 101–137.

Dubey, J. P., Lindsay, D. S. and Speer, C. A. (1998) 'Structures of Toxoplasma gondii tachyzoites, bradyzoites, and sporozoites and biology and development of tissue cysts.', *Clinical microbiology reviews*, 11(2), pp. 267–99. doi: 10.1128/CMR.11.2.267.

Dybas, J. M. *et al.* (2008) 'Computational analysis and experimental validation of gene predictions in Toxoplasma gondii.', *PloS one*, 3(12), p. e3899. doi: 10.1371/journal.pone.0003899.

Egly, J. M. *et al.* (1984) 'Is actin a transcription initiation factor for RNA polymerase B?', *The EMBO journal*, 3(10), pp. 2363–71. doi: 10.1002/j.1460-2075.1984.tb02141.x.

Engelberg, K. *et al.* (2022) 'Proteomic characterization of the Toxoplasma gondii cytokinesis machinery portrays an expanded hierarchy of its assembly and function.', *Nature communications*, 13(1), p. 4644. doi: 10.1038/s41467-022-32151-0.

Euskirchen, G., Auerbach, R. K. and Snyder, M. (2012) 'SWI/SNF chromatin-remodeling factors: multiscale analyses and diverse functions.', *The Journal of biological chemistry*, 287(37), pp. 30897–905. doi: 10.1074/jbc.R111.309302.

Eustermann, S. *et al.* (2018) 'Structural basis for ATP-dependent chromatin remodelling by the INO80 complex.', *Nature*, 556(7701), pp. 386–390. doi: 10.1038/s41586-018-0029-y.

Farhat, D. C. *et al.* (2020) 'A MORC-driven transcriptional switch controls Toxoplasma developmental trajectories and sexual commitment.', *Nature microbiology*, 5(4), pp. 570–583. doi: 10.1038/s41564-020-0674-4.

Farhat, D. C. *et al.* (2021) 'A plant-like mechanism coupling m6A reading to polyadenylation safeguards transcriptome integrity and developmental gene partitioning in Toxoplasma.', *eLife*, 10. doi: 10.7554/eLife.68312.

Farrell, M. and Gubbels, M.-J. (2014) 'The Toxoplasma gondii kinetochore is required for centrosome association with the centrocone (spindle pole).', *Cellular microbiology*, 16(1), pp. 78–94. doi: 10.1111/cmi.12185.

Fenn, S. *et al.* (2011) 'Structural biochemistry of nuclear actin-related proteins 4 and 8 reveals their interaction with actin.', *The EMBO journal*, 30(11), pp. 2153–66. doi: 10.1038/emboj.2011.118.

Fichera, M. E., Bhopale, M. K. and Roos, D. S. (1995) 'In vitro assays elucidate peculiar kinetics of clindamycin action against Toxoplasma gondii.', *Antimicrobial agents and chemotherapy*, 39(7), pp. 1530–7. doi: 10.1128/AAC.39.7.1530.

Fleck, K., Nitz, M. and Jeffers, V. (2021) '"Reading" a new chapter in protozoan parasite transcriptional regulation.', *PLoS pathogens*, 17(12), p. e1010056. doi: 10.1371/journal.ppat.1010056.

Flegr, J. *et al.* (2014) 'Toxoplasmosis--a global threat. Correlation of latent toxoplasmosis with specific disease burden in a set of 88 countries.', *PloS one*, 9(3), p. e90203. doi: 10.1371/journal.pone.0090203.

Foth, B. J. and McFadden, G. I. (2003) 'The apicoplast: a plastid in Plasmodium falciparum and other Apicomplexan parasites.', *International review of cytology*, 224, pp. 57–110. doi: 10.1016/s0074-7696(05)24003-2.

Francia, M. E. *et al.* (2012) 'Cell division in Apicomplexan parasites is organized by a homolog of the striated rootlet fiber of algal flagella.', *PLoS biology*, 10(12), p. e1001444. doi: 10.1371/journal.pbio.1001444.

Francia, M. E. *et al.* (2020a) 'A Homolog of Structural Maintenance of Chromosome 1 Is a Persistent Centromeric Protein Which Associates With Nuclear Pore Components in Toxoplasma gondii.', *Frontiers in cellular and infection microbiology*, 10, p. 295. doi: 10.3389/fcimb.2020.00295.

Francia, M. E. *et al.* (2020b) 'A Homolog of Structural Maintenance of Chromosome 1 Is a Persistent Centromeric Protein Which Associates With Nuclear Pore Components in Toxoplasma gondii.', *Frontiers in cellular and infection microbiology*, 10, p. 295. doi: 10.3389/fcimb.2020.00295.

Frénal, K. *et al.* (2017) 'Myosin-dependent cell-cell communication controls synchronicity of division in acute and chronic stages of Toxoplasma gondii.', *Nature communications*, 8, p. 15710. doi: 10.1038/ncomms15710.

Frenkel, J. K. (1973) 'Toxoplasma In and Around Us', *BioScience*, 23(6), pp. 343–352.

Frenkel, J. K., Dubey, J. P. and Hoff, R. L. (1976) 'Loss of stages after continuous passage of Toxoplasma gondii and Besnoitia jellisoni.', *The Journal of protozoology*, 23(3), pp. 421–4. doi: 10.1111/j.1550-7408.1976.tb03799.x.

Frenkel, J. K., Ruiz, A. and Chinchilla, M. (1975) 'Soil survival of toxoplasma oocysts in Kansas and Costa Rica.', *The American journal of tropical medicine and hygiene*, 24(3), pp. 439–43. doi: 10.4269/ajtmh.1975.24.439.

Fry, A. M. *et al.* (1998) 'C-Nap1, a novel centrosomal coiled-coil protein and candidate substrate of the cell cycle-regulated protein kinase Nek2.', *The Journal of cell biology*, 141(7), pp. 1563–74. doi: 10.1083/jcb.141.7.1563.

Gabler, F. *et al.* (2020) 'Protein Sequence Analysis Using the MPI Bioinformatics Toolkit', *Current Protocols in Bioinformatics*, 72(1). doi: 10.1002/cpbi.108.

Galarneau, L. *et al.* (2000) 'Multiple links between the NuA4 histone acetyltransferase complex and epigenetic control of transcription.', *Molecular cell*, 5(6), pp. 927–37. doi: 10.1016/s1097-2765(00)80258-0.

Gao, Z. *et al.* (2021) 'Liquid-Liquid Phase Separation: Unraveling the Enigma of Biomolecular Condensates in Microbial Cells.', *Frontiers in microbiology*, 12, p. 751880. doi: 10.3389/fmicb.2021.751880.

Gardner, M. J. *et al.* (2002) 'Genome sequence of the human malaria parasite Plasmodium falciparum.', *Nature*, 419(6906), pp. 498–511. doi: 10.1038/nature01097.

Gerace, E., Lo Presti, V. D. M. and Biondo, C. (2019) 'Cryptosporidium Infection: Epidemiology, Pathogenesis, and Differential Diagnosis.', *European journal of microbiology & immunology*, 9(4), pp. 119–123. doi: 10.1556/1886.2019.00019.

Giaimo, B. D. *et al.* (2019) 'The histone variant H2A.Z in gene regulation.', *Epigenetics & chromatin*, 12(1), p. 37. doi: 10.1186/s13072-019-0274-9.

Gissot, M. *et al.* (2007) 'Epigenomic modifications predict active promoters and gene structure in Toxoplasma gondii.', *PLoS pathogens*, 3(6), p. e77. doi: 10.1371/journal.ppat.0030077.

Gissot, M. *et al.* (2012) 'Toxoplasma gondii Chromodomain Protein 1 Binds to Heterochromatin and Colocalises with Centromeres and Telomeres at the Nuclear Periphery', *PLOS ONE*. Public Library of Science, 7(3), p. e32671. doi: 10.1371/JOURNAL.PONE.0032671.

Gkikopoulos, T. *et al.* (2011) 'A role for Snf2-related nucleosome-spacing enzymes in genome-wide nucleosome organization.', *Science (New York, N.Y.)*, 333(6050), pp. 1758–60. doi: 10.1126/science.1206097.

Goldman, M., Carver, R. K. and Sulzer, A. J. (1958) 'Reproduction of Toxoplasma gondii by internal budding.', *The Journal of parasitology*, 44(2), pp. 161–71. Available at: http://www.ncbi.nlm.nih.gov/pubmed/13539708.

Goodson, H. V, Kelley, J. B. and Brawley, S. H. (2021) 'Cytoskeletal diversification across 1 billion years: What red algae can teach us about the cytoskeleton, and vice versa.', *BioEssays : news and reviews in molecular, cellular and developmental biology*, 43(5), p. e2000278. doi: 10.1002/bies.202000278.

Goodwin, L. R. and Picketts, D. J. (2018) 'The role of ISWI chromatin remodeling complexes in brain development and neurodevelopmental disorders.', *Molecular and cellular neurosciences*, 87, pp. 55–64. doi: 10.1016/j.mcn.2017.10.008.

Gordon, J. L. and Sibley, L. D. (2005) 'Comparative genome analysis reveals a conserved family of actin-like proteins in apicomplexan parasites.', *BMC genomics*, 6, p. 179. doi: 10.1186/1471-2164-6-179.

Grant, P. A., Winston, F. and Berger, S. L. (2021) 'The biochemical and genetic discovery of the SAGA complex.', *Biochimica et biophysica acta. Gene regulatory mechanisms*, 1864(2), p. 194669. doi: 10.1016/j.bbagrm.2020.194669.

Griffith, M. B., Pearce, C. S. and Heaslip, A. T. (2022) 'Dense granule biogenesis, secretion, and function in Toxoplasma gondii.', *The Journal of eukaryotic microbiology*, 69(6), p. e12904. doi: 10.1111/jeu.12904.

Gubbels, M.-J. *et al.* (2006) 'A MORN-repeat protein is a dynamic component of the Toxoplasma gondii cell division apparatus.', *Journal of cell science*, 119(Pt 11), pp. 2236–45. doi: 10.1242/jcs.02949.

Gubbels, M.-J. *et al.* (2022) 'Toxoplasma gondii's Basal Complex: The Other Apicomplexan Business End Is Multifunctional.', *Frontiers in cellular and infection microbiology*, 12, p. 882166. doi: 10.3389/fcimb.2022.882166.

Guerra, A. J. *et al.* (2018) 'Structural basis of Toxoplasma gondii perforin-like protein 1 membrane interaction and activity during egress.', *PLoS pathogens*, 14(12), p. e1007476. doi: 10.1371/journal.ppat.1007476.

Haase, R., Dos Santos Pacheco, N. and Soldati-Favre, D. (2022) 'Nanoscale imaging of the conoid and functional dissection of its dynamics in Apicomplexa.', *Current opinion in microbiology*, 70, p. 102226. doi: 10.1016/j.mib.2022.102226.

Habedanck, R. *et al.* (2005) 'The Polo kinase Plk4 functions in centriole duplication.', *Nature cell biology*, 7(11), pp. 1140–6. doi: 10.1038/ncb1320.

Haber, J. E. and Garvik, B. (1977) 'A new gene affecting the efficiency of mating-type interconversions in homothallic strains of Saccharomyces cerevisiae.', *Genetics*, 87(1), pp. 33–50. doi: 10.1093/genetics/87.1.33.

Hara, M. and Fukagawa, T. (2017) 'Critical Foundation of the Kinetochore: The Constitutive Centromere-Associated Network (CCAN).', *Progress in molecular and subcellular biology*, 56, pp. 29–57. doi: 10.1007/978-3-319-58592-5_2.

Harata, M., Mochizuki, R. and Mizuno, S. (1999) 'Two isoforms of a human actin-related protein show nuclear localization and mutually selective expression between brain and other tissues.', *Bioscience, biotechnology, and biochemistry*, 63(5), pp. 917–23. doi: 10.1271/bbb.63.917.

Hartmann, J. *et al.* (2006) 'Golgi and centrosome cycles in Toxoplasma gondii.', *Molecular and biochemical parasitology*, 145(1), pp. 125–7. doi: 10.1016/j.molbiopara.2005.09.015.

Hawkins, L. M. *et al.* (2021) 'Novel CRK-Cyclin Complex Controls Spindle Assembly Checkpoint in Toxoplasma Endodyogeny.', *mBio*, 13(1), p. e0356121. doi: 10.1128/mbio.03561-21.

Hawkins, L. M. *et al.* (2023) 'The Crk4-Cyc4 complex regulates G2 phase of apicomplexan endodyogeny', *bioRxiv*. doi: https://doi.org/10.1101/2023.07.31.551351.

Heaslip, A. T., Nelson, S. R. and Warshaw, D. M. (2016) 'Dense granule trafficking in Toxoplasma gondii requires a unique class 27 myosin and actin filaments.', *Molecular biology of the cell*, 27(13), pp. 2080–9. doi: 10.1091/mbc.E15-12-0824.

Hentzschel, F. *et al.* (2023) 'A non-canonical Arp2/3 complex is essential for Plasmodium DNA segregation and transmission of malaria', *bioRxiv*, p. 2023.10.25.563799. doi: 10.1101/2023.10.25.563799.

Heredero-Bermejo, I. *et al.* (2019) 'TgDrpC, an atypical dynamin-related protein in Toxoplasma gondii, is associated with vesicular transport factors and parasite division', *Molecular Microbiology*. John Wiley & Sons, Ltd, 111(1), pp. 46–64. doi: 10.1111/MMI.14138.

Hildebrand, A. *et al.* (2009) 'Fast and accurate automatic structure prediction with HHpred.', *Proteins*, 77 Suppl 9, pp. 128–32. doi: 10.1002/prot.22499.

Hogan, C. J. *et al.* (2010) 'Fission yeast Iec1-ino80-mediated nucleosome eviction regulates nucleotide and phosphate metabolism.', *Molecular and cellular biology*, 30(3), pp. 657–74. doi: 10.1128/MCB.01117-09.

Hong, D.-P., Radke, J. B. and White, M. W. (2017) 'Opposing Transcriptional Mechanisms Regulate Toxoplasma Development.', *mSphere*, 2(1). doi: 10.1128/mSphere.00347-16.

Hou, H. *et al.* (2010) 'Histone variant H2A.Z regulates centromere silencing and chromosome segregation in fission yeast.', *The Journal of biological chemistry*, 285(3), pp. 1909–18. doi: 10.1074/jbc.M109.058487.

Howe, D. K. and Sibley, L. D. (1995) 'Toxoplasma gondii comprises three clonal lineages: correlation of parasite genotype with human disease.', *The Journal of infectious diseases*, 172(6), pp. 1561–6. doi: 10.1093/infdis/172.6.1561.

Hu, K. *et al.* (2002) 'Daughter cell assembly in the protozoan parasite Toxoplasma gondii.', *Molecular biology of the cell*, 13(2), pp. 593–606. doi: 10.1091/mbc.01-06-0309.

Hu, X. *et al.* (2020) 'Loss of the Conserved Alveolate Kinase MAPK2 Decouples Toxoplasma Cell Growth from Cell Division.', *mBio*, 11(6). doi: 10.1128/mBio.02517-20.

Huang, S. *et al.* (2017) 'Toxoplasma gondii AP2IX-4 Regulates Gene Expression during Bradyzoite Development.', *mSphere*, 2(2). doi: 10.1128/mSphere.00054-17.

Hunt, A. *et al.* (2019) 'Differential requirements for cyclase-associated protein (CAP) in actin-dependent processes of Toxoplasma gondii.', *eLife*, 8. doi: 10.7554/eLife.50598.

Hurley, J. H. (1996) 'The sugar kinase/heat shock protein 70/actin superfamily: implications of conserved structure for mechanism.', *Annual review of biophysics and biomolecular structure*, 25, pp. 137–62. doi: 10.1146/annurev.bb.25.060196.001033.

Huynh, M.-H. and Carruthers, V. B. (2009) 'Tagging of endogenous genes in a Toxoplasma gondii strain lacking Ku80.', *Eukaryotic cell*, 8(4), pp. 530–9. doi: 10.1128/EC.00358-08.

Iyer, L. M. *et al.* (2008) 'Comparative genomics of transcription factors and chromatin proteins in parasitic protists and other eukaryotes.', *International journal for parasitology*, 38(1), pp. 1–

31. doi: 10.1016/j.ijpara.2007.07.018.
Janouskovec, J. *et al.* (2010) 'A common red algal origin of the apicomplexan, dinoflagellate, and heterokont plastids.', *Proceedings of the National Academy of Sciences of the United States of America*, 107(24), pp. 10949–54. doi: 10.1073/pnas.1003335107.
Jeffers, V. and Sullivan, W. J. (2012) 'Lysine acetylation is widespread on proteins of diverse function and localization in the protozoan parasite Toxoplasma gondii.', *Eukaryotic cell*, 11(6), pp. 735–42. doi: 10.1128/EC.00088-12.
Kabsch, W. and Holmes, K. C. (1995) 'The actin fold.', *FASEB journal : official publication of the Federation of American Societies for Experimental Biology*, 9(2), pp. 167–74. doi: 10.1096/fasebj.9.2.7781919.
Kafsack, B. F. C. *et al.* (2009) 'Rapid Membrane Disruption by a Perforin-Like Protein Facilitates Parasite Exit from Host Cells', *Science*, 323(5913), pp. 530–533. doi: 10.1126/science.1165740.
Kahana, J. A. *et al.* (1998) 'The yeast dynactin complex is involved in partitioning the mitotic spindle between mother and daughter cells during anaphase B.', *Molecular biology of the cell*, 9(7), pp. 1741–56. doi: 10.1091/mbc.9.7.1741.
Kapitein, L. C. *et al.* (2005) 'The bipolar mitotic kinesin Eg5 moves on both microtubules that it crosslinks.', *Nature*, 435(7038), pp. 114–8. doi: 10.1038/nature03503.
Kato, H. *et al.* (2013) 'A conserved mechanism for centromeric nucleosome recognition by centromere protein CENP-C.', *Science (New York, N.Y.)*, 340(6136), pp. 1110–3. doi: 10.1126/science.1235532.
van Kempen, M. *et al.* (2023) 'Fast and accurate protein structure search with Foldseek.', *Nature biotechnology*. doi: 10.1038/s41587-023-01773-0.
Kensche, P. R. *et al.* (2016) 'The nucleosome landscape of Plasmodium falciparum reveals chromatin architecture and dynamics of regulatory sequences.', *Nucleic acids research*, 44(5), pp. 2110–24. doi: 10.1093/nar/gkv1214.
Kessler, H. *et al.* (2008) 'Microneme protein 8--a new essential invasion factor in Toxoplasma gondii.', *Journal of cell science*, 121(Pt 7), pp. 947–56. doi: 10.1242/jcs.022350.
Khelifa, A. S. *et al.* (2021) 'TgAP2IX-5 is a key transcriptional regulator of the asexual cell cycle division in Toxoplasma gondii.', *Nature communications*, 12(1), p. 116. doi: 10.1038/s41467-020-20216-x.
Kim, J. H. *et al.* (2011) 'High cleavage efficiency of a 2A peptide derived from porcine teschovirus-1 in human cell lines, zebrafish and mice.', *PloS one*, 6(4), p. e18556. doi: 10.1371/journal.pone.0018556.
Kim, K., Soldati, D. and Boothroyd, J. C. (1993) 'Gene replacement in Toxoplasma gondii with chloramphenicol acetyltransferase as selectable marker.', *Science (New York, N.Y.)*, 262(5135), pp. 911–4. doi: 10.1126/science.8235614.
Kissinger, J. C. *et al.* (2003) 'ToxoDB: accessing the Toxoplasma gondii genome.', *Nucleic acids research*, 31(1), pp. 234–6. doi: 10.1093/nar/gkg072.
Klare, K. *et al.* (2015) 'CENP-C is a blueprint for constitutive centromere-associated network assembly within human kinetochores.', *The Journal of cell biology*, 210(1), pp. 11–22. doi: 10.1083/jcb.201412028.
Klein-Brill, A. *et al.* (2019) 'Dynamics of Chromatin and Transcription during Transient Depletion of the RSC Chromatin Remodeling Complex.', *Cell reports*, 26(1), pp. 279-292.e5. doi: 10.1016/j.celrep.2018.12.020.
Konstantinovic, N. *et al.* (2019) 'Treatment of toxoplasmosis: Current options and future perspectives.', *Food and waterborne parasitology*, 15, p. e00036. doi: 10.1016/j.fawpar.2019.e00036.
Koreny, L. *et al.* (2021) 'Molecular characterization of the conoid complex in Toxoplasma reveals its conservation in all apicomplexans, including Plasmodium species.', *PLoS biology*, 19(3), p. e3001081. doi: 10.1371/journal.pbio.3001081.

Koreny, L. *et al.* (2023) 'Stable endocytic structures navigate the complex pellicle of apicomplexan parasites.', *Nature communications*, 14(1), p. 2167. doi: 10.1038/s41467-023-37431-x.

Korn, E. D., Carlier, M. F. and Pantaloni, D. (1987) 'Actin polymerization and ATP hydrolysis.', *Science (New York, N.Y.)*, 238(4827), pp. 638–44. doi: 10.1126/science.3672117.

Kremer, K. *et al.* (2013) 'An overexpression screen of Toxoplasma gondii Rab-GTPases reveals distinct transport routes to the micronemes.', *PLoS pathogens*, 9(3), p. e1003213. doi: 10.1371/journal.ppat.1003213.

Krietenstein, N. *et al.* (2016) 'Genomic Nucleosome Organization Reconstituted with Pure Proteins.', *Cell*, 167(3), pp. 709-721.e12. doi: 10.1016/j.cell.2016.09.045.

Krippner, S. *et al.* (2020) 'Postmitotic expansion of cell nuclei requires nuclear actin filament bundling by α-actinin 4.', *EMBO reports*, 21(11), p. e50758. doi: 10.15252/embr.202050758.

Krishna, R. *et al.* (2015) 'A large-scale proteogenomics study of apicomplexan pathogens-Toxoplasma gondii and Neospora caninum.', *Proteomics*, 15(15), pp. 2618–28. doi: 10.1002/pmic.201400553.

Krogan, N. J. *et al.* (2003) 'A Snf2 family ATPase complex required for recruitment of the histone H2A variant Htz1.', *Molecular cell*, 12(6), pp. 1565–76. doi: 10.1016/s1097-2765(03)00497-0.

Kudryashov, D. S. and Reisler, E. (2013) 'ATP and ADP actin states.', *Biopolymers*, 99(4), pp. 245–56. doi: 10.1002/bip.22155.

Lamarque, M. *et al.* (2011) 'The RON2-AMA1 interaction is a critical step in moving junction-dependent invasion by apicomplexan parasites.', *PLoS pathogens*, 7(2), p. e1001276. doi: 10.1371/journal.ppat.1001276.

Längst, G. and Manelyte, L. (2015) 'Chromatin Remodelers: From Function to Dysfunction.', *Genes*, 6(2), pp. 299–324. doi: 10.3390/genes6020299.

Lee, D. S. W., Strom, A. R. and Brangwynne, C. P. (2022) 'The mechanobiology of nuclear phase separation.', *APL bioengineering*, 6(2), p. 021503. doi: 10.1063/5.0083286.

de Leon, J. C. *et al.* (2013) 'A SAS-6-like protein suggests that the Toxoplasma conoid complex evolved from flagellar components.', *Eukaryotic cell*, 12(7), pp. 1009–19. doi: 10.1128/EC.00096-13.

Lesage, K. M. *et al.* (2018) 'Cooperative binding of ApiAP2 transcription factors is crucial for the expression of virulence genes in Toxoplasma gondii.', *Nucleic acids research*, 46(12), pp. 6057–6068. doi: 10.1093/nar/gky373.

Leung, J. M. *et al.* (2017) 'Stability and function of a putative microtubule-organizing center in the human parasite Toxoplasma gondii.', *Molecular biology of the cell*, 28(10), pp. 1361–1378. doi: 10.1091/mbc.E17-01-0045.

Li, J. *et al.* (2019) 'Single-Molecule Nanoscopy Elucidates RNA Polymerase II Transcription at Single Genes in Live Cells.', *Cell*, 178(2), pp. 491-506.e28. doi: 10.1016/j.cell.2019.05.029.

Li, W. *et al.* (2022) 'A splitCas9 phenotypic screen in Toxoplasma gondii identifies proteins involved in host cell egress and invasion.', *Nature microbiology*, 7(6), pp. 882–895. doi: 10.1038/s41564-022-01114-y.

Lim, L. and McFadden, G. I. (2010) 'The evolution, metabolism and functions of the apicoplast.', *Philosophical transactions of the Royal Society of London. Series B, Biological sciences*, 365(1541), pp. 749–63. doi: 10.1098/rstb.2009.0273.

Liu, C., Zhu, R. and Mao, Y. (2018) 'Nuclear Actin Polymerized by mDia2 Confines Centromere Movement during CENP-A Loading.', *iScience*, 9, pp. 314–327. doi: 10.1016/j.isci.2018.10.031.

Liu, H. *et al.* (2020) 'Actin-related protein Arp4 regulates euchromatic gene expression and development through H2A.Z deposition in blood-stage Plasmodium falciparum.', *Parasites & vectors*, 13(1), p. 314. doi: 10.1186/s13071-020-04139-6.

Liu, Z. *et al.* (2017) 'Systematic comparison of 2A peptides for cloning multi-genes in a polycistronic vector.', *Scientific reports*, 7(1), p. 2193. doi: 10.1038/s41598-017-02460-2.

Llinás, M. and DeRisi, J. L. (2004) 'Pernicious plans revealed: Plasmodium falciparum genome wide expression analysis.', *Current opinion in microbiology*, 7(4), pp. 382–7. doi: 10.1016/j.mib.2004.06.014.

Lorestani, A. *et al.* (2010) 'A Toxoplasma MORN1 null mutant undergoes repeated divisions but is defective in basal assembly, apicoplast division and cytokinesis.', *PloS one*, 5(8), p. e12302. doi: 10.1371/journal.pone.0012302.

Lou, J. *et al.* (2023) 'Single cell expression and chromatin access of the Toxoplasma gondii lytic cycle identifies AP2XII-8 as an essential pivotal controller of a ribosome regulon', *bioRxiv*. doi: https://doi.org/10.1101/2023.10.06.561197.

Ma, J. *et al.* (2017) 'Super-resolution mapping of scaffold nucleoporins in the nuclear pore complex.', *Journal of cell science*, 130(7), pp. 1299–1306. doi: 10.1242/jcs.193912.

Madeira, F. *et al.* (2022) 'Search and sequence analysis tools services from EMBL-EBI in 2022.', *Nucleic acids research*, 50(W1), pp. W276–W279. doi: 10.1093/nar/gkac240.

Maenz, M. *et al.* (2014) 'Ocular toxoplasmosis past, present and new aspects of an old disease.', *Progress in retinal and eye research*, 39, pp. 77–106. doi: 10.1016/j.preteyeres.2013.12.005.

Matsuzaki, M. *et al.* (2001) 'Large amounts of apicoplast nucleoid DNA and its segregation in Toxoplasma gondii.', *Protoplasma*, 218(3–4), pp. 180–91. doi: 10.1007/BF01306607.

Mayor, T. *et al.* (2002) 'The mechanism regulating the dissociation of the centrosomal protein C-Nap1 from mitotic spindle poles.', *Journal of cell science*, 115(Pt 16), pp. 3275–84. doi: 10.1242/jcs.115.16.3275.

Mayr, C. (2019) 'What Are 3' UTRs Doing?', *Cold Spring Harbor perspectives in biology*, 11(10). doi: 10.1101/cshperspect.a034728.

Mazumdar, J. *et al.* (2006) 'Apicoplast fatty acid synthesis is essential for organelle biogenesis and parasite survival in Toxoplasma gondii.', *Proceedings of the National Academy of Sciences of the United States of America*, 103(35), pp. 13192–7. doi: 10.1073/pnas.0603391103.

Meissner, M., Schlüter, D. and Soldati, D. (2002) 'Role of Toxoplasma gondii myosin A in powering parasite gliding and host cell invasion.', *Science (New York, N.Y.)*, 298(5594), pp. 837–840. doi: 10.1126/science.1074553.

Meissner, M. and Soldati, D. (2005) 'The transcription machinery and the molecular toolbox to control gene expression in Toxoplasma gondii and other protozoan parasites.', *Microbes and infection*, 7(13), pp. 1376–84. doi: 10.1016/j.micinf.2005.04.019.

Melak, M., Plessner, M. and Grosse, R. (2017) 'Actin visualization at a glance.', *Journal of cell science*, 130(3), pp. 525–530. doi: 10.1242/jcs.189068.

Melatti, C. *et al.* (2019) 'A unique dynamin-related protein is essential for mitochondrial fission in Toxoplasma gondii.', *PLoS pathogens*, 15(4), p. e1007512. doi: 10.1371/journal.ppat.1007512.

Minoda, A. *et al.* (2005) 'BAF53/Arp4 homolog Alp5 in fission yeast is required for histone H4 acetylation, kinetochore-spindle attachment, and gene silencing at centromere.', *Molecular biology of the cell*, 16(1), pp. 316–27. doi: 10.1091/mbc.e04-06-0519.

Mizuguchi, G. *et al.* (2004a) 'ATP-driven exchange of histone H2AZ variant catalyzed by SWR1 chromatin remodeling complex.', *Science (New York, N.Y.)*, 303(5656), pp. 343–8. doi: 10.1126/science.1090701.

Mizuguchi, G. *et al.* (2004b) 'ATP-driven exchange of histone H2AZ variant catalyzed by SWR1 chromatin remodeling complex.', *Science (New York, N.Y.)*, 303(5656), pp. 343–8. doi: 10.1126/science.1090701.

Monahan, B. J. *et al.* (2008) 'Fission yeast SWI/SNF and RSC complexes show compositional and functional differences from budding yeast.', *Nature structural & molecular biology*, 15(8), pp. 873–80. doi: 10.1038/nsmb.1452.

Mondragon, R. *et al.* (1998) 'Genotypic analysis of Toxoplasma gondii isolates from pigs.', *The Journal*

of parasitology, 84(3), pp. 639–41. Available at: http://www.ncbi.nlm.nih.gov/pubmed/9645877.

Montano, H. *et al.* (2023) 'TgTKL4 Is a Novel Kinase That Plays an Important Role in Toxoplasma Morphology and Fitness.', *mSphere*, 8(2), p. e0064922. doi: 10.1128/msphere.00649-22.

Morlon-Guyot, J. *et al.* (2014) 'The Toxoplasma gondii calcium-dependent protein kinase 7 is involved in early steps of parasite division and is crucial for parasite survival.', *Cellular microbiology*, 16(1), pp. 95–114. doi: 10.1111/cmi.12186.

Morlon-Guyot, J. *et al.* (2017) 'Towards a molecular architecture of the centrosome in Toxoplasma gondii.', *Cytoskeleton (Hoboken, N.J.)*, 74(2), pp. 55–71. doi: 10.1002/cm.21353.

Morrissette, N. S. and Sibley, L. D. (2002) 'Disruption of microtubules uncouples budding and nuclear division in Toxoplasma gondii.', *Journal of cell science*, 115(Pt 5), pp. 1017–25. doi: 10.1242/jcs.115.5.1017.

Muir, K. W. *et al.* (2020) 'The structure of the cohesin ATPase elucidates the mechanism of SMC-kleisin ring opening.', *Nature structural & molecular biology*, 27(3), pp. 233–239. doi: 10.1038/s41594-020-0379-7.

Muller, J. *et al.* (2005) 'Sequence and comparative genomic analysis of actin-related proteins.', *Molecular biology of the cell*, 16(12), pp. 5736–48. doi: 10.1091/mbc.e05-06-0508.

Murakami, K. *et al.* (2010) 'Structural basis for actin assembly, activation of ATP hydrolysis, and delayed phosphate release.', *Cell*, 143(2), pp. 275–87. doi: 10.1016/j.cell.2010.09.034.

Nagai, S. *et al.* (2017) 'Chromatin potentiates transcription.', *Proceedings of the National Academy of Sciences of the United States of America*, 114(7), pp. 1536–1541. doi: 10.1073/pnas.1620312114.

Naguleswaran, A. *et al.* (2010) 'Toxoplasma gondii lysine acetyltransferase GCN5-A functions in the cellular response to alkaline stress and expression of cyst genes.', *PLoS pathogens*, 6(12), p. e1001232. doi: 10.1371/journal.ppat.1001232.

Nair, S. C. *et al.* (2011) 'Apicoplast isoprenoid precursor synthesis and the molecular basis of fosmidomycin resistance in Toxoplasma gondii.', *The Journal of experimental medicine*, 208(7), pp. 1547–59. doi: 10.1084/jem.20110039.

Nardelli, S. C. *et al.* (2013) 'The histone code of Toxoplasma gondii comprises conserved and unique posttranslational modifications', *mBio*. American Society for Microbiology1752 N St., N.W., Washington, DC, 4(6), pp. 922–935. doi: 10.1128/MBIO.00922-13/SUPPL_FILE/MBO006131681S1.DOCX.

Nardelli, S. C. *et al.* (2022) 'Genome-wide localization of histone variants in Toxoplasma gondii implicates variant exchange in stage-specific gene expression.', *BMC genomics*. Springer Science and Business Media LLC, 23(1), p. 128. doi: 10.1186/s12864-022-08338-6.

Nardozzi, J. D., Lott, K. and Cingolani, G. (2010) 'Phosphorylation meets nuclear import: a review.', *Cell communication and signaling : CCS*, 8, p. 32. doi: 10.1186/1478-811X-8-32.

Naumov, A. *et al.* (2017) 'The Toxoplasma centrocone houses cell cycle regulatory factors', *mBio*. American Society for Microbiology, 8(4). doi: 10.1128/MBIO.00579-17/SUPPL_FILE/MBO001173443SD2.XLSX.

Naumov, A. V *et al.* (2022) 'Restriction Checkpoint Controls Bradyzoite Development in Toxoplasma gondii.', *Microbiology spectrum*, 10(3), p. e0070222. doi: 10.1128/spectrum.00702-22.

Nehlig, A. *et al.* (2017) 'Regulation of end-binding protein EB1 in the control of microtubule dynamics.', *Cellular and molecular life sciences : CMLS*, 74(13), pp. 2381–2393. doi: 10.1007/s00018-017-2476-2.

Nicolle, C. and Manceaux, L. H. (1908) 'Sur une infection a corps de Leishman (ou organismes voisons) du gondi', *Comptes rendus de l'Académie des Sciences*, 147, p. 736.

Nicolle, C. and Manceaux, L. H. (2009) 'On a leishman body infection (or related organisms) of the gondi. 1908.', *International journal for parasitology*, 39(8), pp. 863–4. doi:

10.1016/j.ijpara.2009.02.001.
Nishi, M. *et al.* (2008) 'Organellar dynamics during the cell cycle of Toxoplasma gondii.', *Journal of cell science*, 121(Pt 9), pp. 1559–68. doi: 10.1242/jcs.021089.
Nishimura, K. *et al.* (2009) 'An auxin-based degron system for the rapid depletion of proteins in nonplant cells.', *Nature methods*, 6(12), pp. 917–22. doi: 10.1038/nmeth.1401.
O'Shaughnessy, W. J. *et al.* (2020) 'Loss of a conserved MAPK causes catastrophic failure in assembly of a specialized cilium-like structure in Toxoplasma gondii.', *Molecular biology of the cell*, 31(9), pp. 881–888. doi: 10.1091/mbc.E19-11-0607.
O'Shaughnessy, W. J. *et al.* (2023) 'Toxoplasma ERK7 protects the apical complex from premature degradation.', *The Journal of cell biology*, 222(6). doi: 10.1083/jcb.202209098.
Ogiwara, H. *et al.* (2007) 'Actin-related protein Arp4 functions in kinetochore assembly.', *Nucleic acids research*, 35(9), pp. 3109–17. doi: 10.1093/nar/gkm161.
Olave, I. *et al.* (2002) 'Identification of a polymorphic, neuron-specific chromatin remodeling complex.', *Genes & development*, 16(19), pp. 2509–17. doi: 10.1101/gad.992102.
Ollion, J. *et al.* (2013) 'TANGO: a generic tool for high-throughput 3D image analysis for studying nuclear organization.', *Bioinformatics (Oxford, England)*, 29(14), pp. 1840–1. doi: 10.1093/bioinformatics/btt276.
Olson, E. N. and Nordheim, A. (2010) 'Linking actin dynamics and gene transcription to drive cellular motile functions.', *Nature reviews. Molecular cell biology*, 11(5), pp. 353–65. doi: 10.1038/nrm2890.
Oma, Y. and Harata, M. (2011) 'Actin-related proteins localized in the nucleus: from discovery to novel roles in nuclear organization.', *Nucleus (Austin, Tex.)*, 2(1), pp. 38–46. doi: 10.4161/nucl.2.1.14510.
Otsu, N. (1979) 'A Threshold Selection Method from Gray-Level Histograms', *IEEE Transactions on Systems, Man, and Cybernetics*, 9(1), pp. 62–66. doi: 10.1109/TSMC.1979.4310076.
Ouologuem, D. T. and Roos, D. S. (2014) 'Dynamics of the Toxoplasma gondii inner membrane complex.', *Journal of cell science*, 127(Pt 15), pp. 3320–30. doi: 10.1242/jcs.147736.
Ovciarikova, J. *et al.* (2017) 'Mitochondrial behaviour throughout the lytic cycle of Toxoplasma gondii.', *Scientific reports*, 7(2), p. 42746. doi: 10.1038/srep42746.
Painter, H. J., Campbell, T. L. and Llinás, M. (2011) 'The Apicomplexan AP2 family: integral factors regulating Plasmodium development.', *Molecular and biochemical parasitology*, 176(1), pp. 1–7. doi: 10.1016/j.molbiopara.2010.11.014.
Palme, J., Hochreiter, S. and Bodenhofer, U. (2015) 'KeBABS: an R package for kernel-based analysis of biological sequences', *Bioinformatics*, 31(15), pp. 2574–2576. doi: 10.1093/bioinformatics/btv176.
Papamichos-Chronakis, M. *et al.* (2011) 'Global regulation of H2A.Z localization by the INO80 chromatin-remodeling enzyme is essential for genome integrity.', *Cell*, 144(2), pp. 200–13. doi: 10.1016/j.cell.2010.12.021.
Pasquarelli, R. R. *et al.* (2023) 'Identification of IMC43, a novel IMC protein that collaborates with IMC32 to form an essential daughter bud assembly complex in Toxoplasma gondii.', *PLoS pathogens*, 19(10), p. e1011707. doi: 10.1371/journal.ppat.1011707.
Peng, D. and Tarleton, R. (2015) 'EuPaGDT: a web tool tailored to design CRISPR guide RNAs for eukaryotic pathogens.', *Microbial genomics*, 1(4), p. e000033. doi: 10.1099/mgen.0.000033.
Perez-Riverol, Y. *et al.* (2022) 'The PRIDE database resources in 2022: a hub for mass spectrometry-based proteomics evidences.', *Nucleic acids research*, 50(D1), pp. D543–D552. doi: 10.1093/nar/gkab1038.
Periz, J. *et al.* (2017) 'Toxoplasma gondii F-actin forms an extensive filamentous network required for material exchange and parasite maturation.', *eLife*, 6. doi: 10.7554/eLife.24119.
Periz, J. *et al.* (2019) 'A highly dynamic F-actin network regulates transport and recycling of

micronemes in Toxoplasma gondii vacuoles.', *Nature communications*, 10(1), p. 4183. doi: 10.1038/s41467-019-12136-2.

Pfefferkorn, E. R. and Pfefferkorn, L. G. (1976) 'Toxoplasma gondii: Isolation and preliminary characterization of temperature-sensitive mutants', *Experimental Parasitology*, 39(3), pp. 365–376. doi: 10.1016/0014-4894(76)90040-0.

Pieperhoff, M. S. *et al.* (2015) 'Conditional U1 gene silencing in Toxoplasma gondii', *PLoS ONE*, 10(6). doi: 10.1371/journal.pone.0130356.

Plessner, M. *et al.* (2015) 'Nuclear F-actin formation and reorganization upon cell spreading.', *The Journal of biological chemistry*, 290(18), pp. 11209–16. doi: 10.1074/jbc.M114.627166.

Poch, O. and Winsor, B. (1997) 'Who's who among the Saccharomyces cerevisiae actin-related proteins? A classification and nomenclature proposal for a large family.', *Yeast (Chichester, England)*, 13(11), pp. 1053–8. doi: 10.1002/(SICI)1097-0061(19970915)13:11<1053::AID-YEA164>3.0.CO;2-4.

Pollard, T. D. (2007) 'Regulation of actin filament assembly by Arp2/3 complex and formins.', *Annual review of biophysics and biomolecular structure*, 36, pp. 451–77. doi: 10.1146/annurev.biophys.35.040405.101936.

Pollard, T. D. and Cooper, J. A. (2009) 'Actin, a central player in cell shape and movement.', *Science (New York, N.Y.)*, 326(5957), pp. 1208–12. doi: 10.1126/science.1175862.

Pospich, S. *et al.* (2017) 'Near-atomic structure of jasplakinolide-stabilized malaria parasite F-actin reveals the structural basis of filament instability.', *Proceedings of the National Academy of Sciences of the United States of America*, 114(40), pp. 10636–10641. doi: 10.1073/pnas.1707506114.

Pray-Grant, M. G. *et al.* (2005) 'Chd1 chromodomain links histone H3 methylation with SAGA- and SLIK-dependent acetylation.', *Nature*, 433(7024), pp. 434–8. doi: 10.1038/nature03242.

Prewitt, J. M. S. and Mendelsohn, M. L. (1966) 'THE ANALYSIS OF CELL IMAGES*', *Annals of the New York Academy of Sciences*, 128(3), pp. 1035–1053. doi: 10.1111/j.1749-6632.1965.tb11715.x.

Qu, K. *et al.* (2022) 'Structure of the NuA4 acetyltransferase complex bound to the nucleosome.', *Nature*, 610(7932), pp. 569–574. doi: 10.1038/s41586-022-05303-x.

Radke, J. B. *et al.* (2013) 'ApiAP2 transcription factor restricts development of the Toxoplasma tissue cyst.', *Proceedings of the National Academy of Sciences of the United States of America*, 110(17), pp. 6871–6. doi: 10.1073/pnas.1300059110.

Radke, J. B. *et al.* (2018) 'Transcriptional repression by ApiAP2 factors is central to chronic toxoplasmosis.', *PLoS pathogens*, 14(5), p. e1007035. doi: 10.1371/journal.ppat.1007035.

Radke, J. R. *et al.* (2001) 'Defining the cell cycle for the tachyzoite stage of Toxoplasma gondii.', *Molecular and biochemical parasitology*, 115(2), pp. 165–75. doi: 10.1016/s0166-6851(01)00284-5.

Radke, J. R. *et al.* (2005) 'The transcriptome of Toxoplasma gondii.', *BMC biology*, 3, p. 26. doi: 10.1186/1741-7007-3-26.

Ralph, S. A. *et al.* (2004) 'Tropical infectious diseases: metabolic maps and functions of the Plasmodium falciparum apicoplast.', *Nature reviews. Microbiology*, 2(3), pp. 203–16. doi: 10.1038/nrmicro843.

Rocchetti, A., Hawes, C. and Kriechbaumer, V. (2014) 'Fluorescent labelling of the actin cytoskeleton in plants using a cameloid antibody.', *Plant methods*, 10, p. 12. doi: 10.1186/1746-4811-10-12.

Roos, D. S. *et al.* (1997) 'Tagging genes and trapping promoters in Toxoplasma gondii by insertional mutagenesis.', *Methods (San Diego, Calif.)*, 13(2), pp. 112–22. doi: 10.1006/meth.1997.0504.

Ryan, M. D., King, A. M. and Thomas, G. P. (1991) 'Cleavage of foot-and-mouth disease virus polyprotein is mediated by residues located within a 19 amino acid sequence.', *The Journal of general*

virology, 72 (Pt 11, pp. 2727–32. doi: 10.1099/0022-1317-72-11-2727.

Ryan, U. *et al.* (2016) 'It's official - Cryptosporidium is a gregarine: What are the implications for the water industry?', *Water research*, 105, pp. 305–313. doi: 10.1016/j.watres.2016.09.013.

Sabin, A. B. (1941) 'Toxoplasmic encephalitis in children', *JAMA : the journal of the American Medical Association*, 116(9), pp. 801–807.

Saeij, J. P. J. *et al.* (2007) 'Toxoplasma co-opts host gene expression by injection of a polymorphic kinase homologue.', *Nature*, 445(7125), pp. 324–7. doi: 10.1038/nature05395.

Saeij, J. P. J., Boyle, J. P. and Boothroyd, J. C. (2005) 'Differences among the three major strains of Toxoplasma gondii and their specific interactions with the infected host.', *Trends in parasitology*, 21(10), pp. 476–81. doi: 10.1016/j.pt.2005.08.001.

Saksouk, N. *et al.* (2005) 'Histone-modifying complexes regulate gene expression pertinent to the differentiation of the protozoan parasite Toxoplasma gondii.', *Molecular and cellular biology*, 25(23), pp. 10301–14. doi: 10.1128/MCB.25.23.10301-10314.2005.

Sali, A. *et al.* (1995) 'Evaluation of comparative protein modeling by MODELLER.', *Proteins*, 23(3), pp. 318–26. doi: 10.1002/prot.340230306.

Saraf, A. *et al.* (2016) 'Dynamic and Combinatorial Landscape of Histone Modifications during the Intraerythrocytic Developmental Cycle of the Malaria Parasite.', *Journal of proteome research*, 15(8), pp. 2787–801. doi: 10.1021/acs.jproteome.6b00366.

Sautel, C. F. *et al.* (2007) 'SET8-mediated methylations of histone H4 lysine 20 mark silent heterochromatic domains in apicomplexan genomes.', *Molecular and cellular biology*, 27(16), pp. 5711–24. doi: 10.1128/MCB.00482-07.

Schindelin, J. *et al.* (2012) 'Fiji: an open-source platform for biological-image analysis', *Nature Methods*, 9(7), pp. 676–682. doi: 10.1038/nmeth.2019.

Schmitz, S. *et al.* (2005) 'Malaria parasite actin filaments are very short.', *Journal of molecular biology*, 349(1), pp. 113–25. doi: 10.1016/j.jmb.2005.03.056.

Scrucca, L. *et al.* (2016) 'mclust 5: Clustering, Classification and Density Estimation Using Gaussian Finite Mixture Models.', *The R journal*, 8(1), pp. 289–317. Available at: http://www.ncbi.nlm.nih.gov/pubmed/27818791.

Sehnal, D. *et al.* (2021) 'Mol* Viewer: modern web app for 3D visualization and analysis of large biomolecular structures.', *Nucleic acids research*, 49(W1), pp. W431–W437. doi: 10.1093/nar/gkab314.

Severo, V. *et al.* (2022) 'Previously Unidentified Histone H1-Like Protein Is Involved in Cell Division and Ribosome Biosynthesis in Toxoplasma gondii.', *mSphere*, 7(6), p. e0040322. doi: 10.1128/msphere.00403-22.

Sheffield, H. G. and Melton, M. L. (1968) 'The fine structure and reproduction of Toxoplasma gondii.', *The Journal of parasitology*, 54(2), pp. 209–26. Available at: http://www.ncbi.nlm.nih.gov/pubmed/5647101.

Sheiner, L. *et al.* (2010) 'Toxoplasma gondii transmembrane microneme proteins and their modular design.', *Molecular microbiology*, 77(4), pp. 912–29. doi: 10.1111/j.1365-2958.2010.07255.x.

Shen, B. *et al.* (2017) 'Development of CRISPR/Cas9 for Efficient Genome Editing in Toxoplasma gondii.', *Methods in molecular biology (Clifton, N.J.)*, 1498, pp. 79–103. doi: 10.1007/978-1-4939-6472-7_6.

Shen, X. *et al.* (2000) 'A chromatin remodelling complex involved in transcription and DNA processing.', *Nature*, 406(6795), pp. 541–4. doi: 10.1038/35020123.

Sidik, S. M. *et al.* (2016) 'A Genome-wide CRISPR Screen in Toxoplasma Identifies Essential Apicomplexan Genes.', *Cell*, 166(6), pp. 1423-1435.e12. doi: 10.1016/j.cell.2016.08.019.

Simon, C. S. *et al.* (2021) 'An extended DNA-free intranuclear compartment organizes centrosome microtubules in malaria parasites.', *Life science alliance*, 4(11). doi: 10.26508/lsa.202101199.

Sindikubwabo, F. *et al.* (2017) 'Modifications at K31 on the lateral surface of histone H4 contribute to

genome structure and expression in apicomplexan parasites.', *eLife*, 6. doi: 10.7554/eLife.29391.

Singer, M. *et al.* (2023) 'A central CRMP complex essential for invasion in Toxoplasma gondii.', *PLoS biology*, 21(1), p. e3001937. doi: 10.1371/journal.pbio.3001937.

Smith, A. T. *et al.* (2005) 'MYST family histone acetyltransferases in the protozoan parasite Toxoplasma gondii.', *Eukaryotic cell*, 4(12), pp. 2057–65. doi: 10.1128/EC.4.12.2057-2065.2005.

Smith, T. A. *et al.* (2022) 'Screening the Toxoplasma kinome with high-throughput tagging identifies a regulator of invasion and egress.', *Nature microbiology*, 7(6), pp. 868–881. doi: 10.1038/s41564-022-01104-0.

Soldati, D. and Boothroyd, J. C. (1993) 'Transient transfection and expression in the obligate intracellular parasite Toxoplasma gondii.', *Science (New York, N.Y.)*, 260(5106), pp. 349–52. Available at: http://www.ncbi.nlm.nih.gov/pubmed/8469986.

Splendore, A. (1908) 'Un nuovo protozoa parassita deconigli incontrato nelle lesioni anatomiche d'une malattia che ricorda in molti punti il Kala-azar dell'uoma. Nota preliminare pel', *Revista do Instituto de Medicina Tropical de Sao Paulo*, 3, pp. 109–112.

Splendore, A. (2009) 'A new protozoan parasite in rabbits.', *International journal for parasitology*, 39(8), pp. 861–2. doi: 10.1016/j.ijpara.2009.02.002.

Srivastava, S. *et al.* (2023) 'Toxoplasma gondii AP2XII-2 Contributes to Transcriptional Repression for Sexual Commitment.', *mSphere*, 8(2), p. e0060622. doi: 10.1128/msphere.00606-22.

Srivastava, S., White, M. W. and Sullivan, W. J. (2020) 'Toxoplasma gondii AP2XII-2 Contributes to Proper Progression through S-Phase of the Cell Cycle.', *mSphere*, 5(5). doi: 10.1128/mSphere.00542-20.

Stortz, J. F. *et al.* (2019) 'Formin-2 drives polymerisation of actin filaments enabling segregation of apicoplasts and cytokinesis in Plasmodium falciparum.', *eLife*, 8. doi: 10.7554/eLife.49030.

Strassert, J. F. H. *et al.* (2021) 'A molecular timescale for eukaryote evolution with implications for the origin of red algal-derived plastids.', *Nature communications*, 12(1), p. 1879. doi: 10.1038/s41467-021-22044-z.

Sullivan, W. J. *et al.* (2003) 'Molecular cloning and characterization of an SRCAP chromatin remodeling homologue in Toxoplasma gondii.', *Parasitology research*, 90(1), pp. 1–8. doi: 10.1007/s00436-002-0814-1.

Suvorova, E. S. *et al.* (2012) 'Nuclear actin-related protein is required for chromosome segregation in Toxoplasma gondii.', *Molecular and biochemical parasitology*, 181(1), pp. 7–16. doi: 10.1016/j.molbiopara.2011.09.006.

Suvorova, E. S. *et al.* (2015) 'A novel bipartite centrosome coordinates the apicomplexan cell cycle.', *PLoS biology*, 13(3), p. e1002093. doi: 10.1371/journal.pbio.1002093.

Takeshima, H. *et al.* (2000) 'Junctophilins: a novel family of junctional membrane complex proteins.', *Molecular cell*, 6(1), pp. 11–22. doi: 10.1016/s1097-2765(00)00003-4.

Toenhake, C. G. *et al.* (2018) 'Chromatin Accessibility-Based Characterization of the Gene Regulatory Network Underlying Plasmodium falciparum Blood-Stage Development.', *Cell host & microbe*, 23(4), pp. 557-569.e9. doi: 10.1016/j.chom.2018.03.007.

Tomasina, R. *et al.* (2022) 'Separate To Operate: the Centriole-Free Inner Core of the Centrosome Regulates the Assembly of the Intranuclear Spindle in Toxoplasma gondii.', *mBio*, p. e0185922. doi: 10.1128/mbio.01859-22.

Torgerson, P. R. and Mastroiacovo, P. (2013) 'The global burden of congenital toxoplasmosis: a systematic review.', *Bulletin of the World Health Organization*, 91(7), pp. 501–8. doi: 10.2471/BLT.12.111732.

Tosetti, N. *et al.* (2019a) 'Three F-actin assembly centers regulate organelle inheritance, cell-cell communication and motility in Toxoplasma gondii.', *eLife*, 8. doi: 10.7554/eLife.42669.

Tosetti, N. *et al.* (2019b) 'Three F-actin assembly centers regulate organelle inheritance, cell-cell

communication and motility in Toxoplasma gondii.', *eLife*, 8. doi: 10.7554/eLife.42669.

Tosetti, N. *et al.* (2020) 'Essential function of the alveolin network in the subpellicular microtubules and conoid assembly in Toxoplasma gondii.', *eLife*, 9. doi: 10.7554/eLife.56635.

Treeck, M. *et al.* (2011) 'The phosphoproteomes of Plasmodium falciparum and Toxoplasma gondii reveal unusual adaptations within and beyond the parasites' boundaries.', *Cell host & microbe*, 10(4), pp. 410–9. doi: 10.1016/j.chom.2011.09.004.

Tsopoulidis, N. *et al.* (2019) 'T cell receptor-triggered nuclear actin network formation drives CD4+ T cell effector functions.', *Science immunology*, 4(31). doi: 10.1126/sciimmunol.aav1987.

Tyanova, S. *et al.* (2016) 'The Perseus computational platform for comprehensive analysis of (prote)omics data.', *Nature methods*, 13(9), pp. 731–40. doi: 10.1038/nmeth.3901.

Tyanova, S., Temu, T. and Cox, J. (2016) 'The MaxQuant computational platform for mass spectrometry-based shotgun proteomics.', *Nature protocols*, 11(12), pp. 2301–2319. doi: 10.1038/nprot.2016.136.

Tyler, J. S. and Boothroyd, J. C. (2011) 'The C-terminus of Toxoplasma RON2 provides the crucial link between AMA1 and the host-associated invasion complex.', *PLoS pathogens*, 7(2), p. e1001282. doi: 10.1371/journal.ppat.1001282.

Uchiumi, T., Longo, D. L. and Ferris, D. K. (1997) 'Cell cycle regulation of the human polo-like kinase (PLK) promoter.', *The Journal of biological chemistry*, 272(14), pp. 9166–74. doi: 10.1074/jbc.272.14.9166.

Varadi, M. *et al.* (2022) 'AlphaFold Protein Structure Database: massively expanding the structural coverage of protein-sequence space with high-accuracy models', *Nucleic Acids Research*, 50(D1), pp. D439–D444. doi: 10.1093/nar/gkab1061.

Verhoef, J. M. J., Meissner, M. and Kooij, T. W. A. (2021) 'Organelle Dynamics in Apicomplexan Parasites.', *mBio*, 12(4), p. e0140921. doi: 10.1128/mBio.01409-21.

Viita, T. *et al.* (2019) 'Nuclear actin interactome analysis links actin to KAT14 histone acetyl transferase and mRNA splicing.', *Journal of cell science*, 132(8). doi: 10.1242/jcs.226852.

Vonlaufen, N. *et al.* (2010) 'MYST family lysine acetyltransferase facilitates ataxia telangiectasia mutated (ATM) kinase-mediated DNA damage response in Toxoplasma gondii.', *The Journal of biological chemistry*, 285(15), pp. 11154–61. doi: 10.1074/jbc.M109.066134.

Wagner, M. *et al.* (2023) 'The SUN-like protein TgSLP1 is essential for nuclear division in the apicomplexan parasite Toxoplasma gondii.', *Journal of cell science*. doi: 10.1242/jcs.260337.

Waldman, B. S. *et al.* (2020) 'Identification of a Master Regulator of Differentiation in Toxoplasma.', *Cell*. doi: 10.1016/j.cell.2019.12.013.

Walker, R., Gissot, M., Croken, M. M., *et al.* (2013) 'The Toxoplasma nuclear factor TgAP2XI-4 controls bradyzoite gene expression and cyst formation.', *Molecular microbiology*, 87(3), pp. 641–55. doi: 10.1111/mmi.12121.

Walker, R., Gissot, M., Huot, L., *et al.* (2013) 'Toxoplasma transcription factor TgAP2XI-5 regulates the expression of genes involved in parasite virulence and host invasion.', *The Journal of biological chemistry*, 288(43), pp. 31127–38. doi: 10.1074/jbc.M113.486589.

Waller, R. F. and McFadden, G. I. (2005) 'The apicoplast: a review of the derived plastid of apicomplexan parasites.', *Current issues in molecular biology*, 7(1), pp. 57–79. Available at: http://www.ncbi.nlm.nih.gov/pubmed/15580780.

Wang, C. *et al.* (2021) 'Internal daughter formation of Toxoplasma gondii tachyzoites is coordinated by transcription factor TgAP2IX-5.', *Cellular microbiology*, 23(3), p. e13291. doi: 10.1111/cmi.13291.

Wang, R.-J. *et al.* (2018) 'Widespread occurrence of Cryptosporidium infections in patients with HIV/AIDS: Epidemiology, clinical feature, diagnosis, and therapy.', *Acta tropica*, 187, pp. 257–263. doi: 10.1016/j.actatropica.2018.08.018.

Watzlowik, M. T. *et al.* (2021) 'Peculiarities of Plasmodium falciparum Gene Regulation and Chromatin

Structure.', *International journal of molecular sciences*, 22(10). doi: 10.3390/ijms22105168.

Wei, Y. *et al.* (1998) 'Phosphorylation of histone H3 at serine 10 is correlated with chromosome condensation during mitosis and meiosis in Tetrahymena.', *Proceedings of the National Academy of Sciences of the United States of America*, 95(13), pp. 7480–4. doi: 10.1073/pnas.95.13.7480.

Wei, Y. *et al.* (1999) 'Phosphorylation of histone H3 is required for proper chromosome condensation and segregation.', *Cell*, 97(1), pp. 99–109. doi: 10.1016/s0092-8674(00)80718-7.

Weiss, L. M. and Kim, K. (2020) *Toxoplasma Gondii The model apicomplexan - perspectives and methods*. 3rd editio.

White, M. W., Radke, J. R. and Radke, J. B. (2014) 'Toxoplasma development - turn the switch on or off?', *Cellular microbiology*, 16(4), pp. 466–72. doi: 10.1111/cmi.12267.

Whitelaw, J. A. *et al.* (2017) 'Surface attachment, promoted by the actomyosin system of Toxoplasma gondii is important for efficient gliding motility and invasion.', *BMC biology*, 15(1), p. 1. doi: 10.1186/s12915-016-0343-5.

Whitelaw, J. A. (2017) *The dynamic nature and functions of actin in Toxoplasma gondii*. University of Glasgow. Available at: http://theses.gla.ac.uk/8072/.

Wickham, H. (2009) *ggplot2*. New York, NY: Springer New York. doi: 10.1007/978-0-387-98141-3.

Williamson, D. H. *et al.* (2001) 'The in vivo conformation of the plastid DNA of Toxoplasma gondii: implications for replication.', *Journal of molecular biology*, 306(2), pp. 159–68. doi: 10.1006/jmbi.2000.4385.

Wilson, B. G. and Roberts, C. W. M. (2011) 'SWI/SNF nucleosome remodellers and cancer.', *Nature reviews. Cancer*, 11(7), pp. 481–92. doi: 10.1038/nrc3068.

World malaria report (2022). Geneva.

Xia, J. *et al.* (2021) 'Third-generation sequencing revises the molecular karyotype for Toxoplasma gondii and identifies emerging copy number variants in sexual recombinants.', *Genome research*, 31(5), pp. 834–851. doi: 10.1101/gr.262816.120.

Xu, P. *et al.* (2016) 'The NuA4 Core Complex Acetylates Nucleosomal Histone H4 through a Double Recognition Mechanism', *Molecular Cell*, 63(6), pp. 965–975. doi: 10.1016/j.molcel.2016.07.024.

Yakubu, R. R. *et al.* (2017) 'Comparative Monomethylarginine Proteomics Suggests that Protein Arginine Methyltransferase 1 (PRMT1) is a Significant Contributor to Arginine Monomethylation in Toxoplasma gondii.', *Molecular & cellular proteomics : MCP*, 16(4), pp. 567–580. doi: 10.1074/mcp.M117.066951.

Yang, C. *et al.* (2023) 'The protein phosphatase PPKL is a key regulator of daughter parasite development in Toxoplasma gondii.', *bioRxiv : the preprint server for biology*. doi: 10.1101/2023.06.13.544803.

Zhu, S., Shapiro, K. and VanWormer, E. (2022) 'Dynamics and epidemiology of Toxoplasma gondii oocyst shedding in domestic and wild felids.', *Transboundary and emerging diseases*, 69(5), pp. 2412–2423. doi: 10.1111/tbed.14197.

Zimmermann, L. *et al.* (2018) 'A Completely Reimplemented MPI Bioinformatics Toolkit with a New HHpred Server at its Core', *Journal of Molecular Biology*, 430(15), pp. 2237–2243. doi: 10.1016/j.jmb.2017.12.007.

9 Eidesstattliche Erklärung

Ich versichere hiermit an Eides statt, dass die vorgelegte Dissertation von mir selbständig und ohne unerlaubte Hilfe angefertigt wurde. Des Weiteren erkläre ich, dass die Dissertation nicht ganz oder in wesentlichen Teilen einer anderen Prüfungskommission vorgelegt ist und, dass ich mich anderweitig einer Doktorprüfung ohne Erfolg nicht unterzogen habe.

Matthew Gow
Hamburg, den 12. Juni 2024